UNIVERSITY OF SOUTHAMPTON

DEPARTMENT OF ELECTRONICS

WAVELENGTH-DEPENDENT EFFECTS IN OPTICAL-FIBRE WAVEGUIDES

by

ARTHUR HAROLD HARTOG

A thesis submitted for the degree of
Doctor of Philosophy
May 1981.

UNIVERSITY OF SOUTHAMPTON

ABSTRACT

FACULTY OF ENGINEERING & APPLIED SCIENCE

ELECTRONICS

Doctor of Philosophy

WAVELENGTH-DEPENDENT EFFECTS IN OPTICAL FIBRE WAVEGUIDES

by Arthur Harold Hartog

The determination of the wavelength-dependence of several major characteristics of optical fibre waveguides is discussed.

A laser system is described which allows many types of measurement to be made in optical fibres over the wavelength range 0.45-2.6μm. The source consists of a flash-lamp pumped dye laser, followed by a $LiNbO_3$ temperature-tuned optical parametric oscillator. The pulse width is determined by an electro-optic modulator and may be varied from 0.5 ns to 1μs. Widely tunable, short duration pulses of several hundred watts peak power are thus available for time domain measurements in optical fibres.

The wavelength-dependence of the material dispersion parameter of several glass compositions is measured using a pulse-delay technique. It is shown that the material dispersion of phosphosilicate and silica fibres is much the same as that of silica in bulk form. In contrast, the material dispersion of germanosilicate glasses varies with their composition. In all cases, it is shown directly that the material dispersion parameter falls to zero at a wavelength in the region of 1.27-1.36μm. The technique is similarly applicable to the determination of the chromatic dispersion of single-mode fibres.

Measurements of the wavelength-dependence of intermodal dispersion in multimode fibres are presented and compared with values calculated from the refractive-index profiles of the fibres. It is shown that minor imperfections of the profiles substantially reduce the fibre bandwidth. Moreover the length-dependence of the profile strongly influences the bandwidth/wavelength function.

The stability of the pulse delay in optical fibres is assessed for variations of both stress and temperature by means of measurements of pulse transit-times in unjacketed silica-based fibres. The data obtained is used to interpret variations of time delay observed in jacketed fibres. It is shown that the application of close-fitting plastic cabling materials results in residual stress on the fibre which varies with temperature, humidity and other environmental parameters.

The backscatter technique is used to investigate the length- and wavelength-dependence of fibre losses with the aid of a new two-channel scheme for waveform analysis. Good agreement is obtained with conventional spectral attenuation measurements. Comparison of length-dependent losses measured at different wavelengths shows a strong axial variation of OH^- impurity content.

ACKNOWLEDGEMENTS

I would like to thank Professor W.A. Gambling for supervising the project, for his comments on the manuscript of the thesis and for providing an atmosphere conducive to stimulating research.

I have much benefited from the comments, help and experience of my colleagues in the Optical Communications and Non-linear Optics groups during the whole of the project. Special thanks are due to David Payne for many suggestions and criticisms of the work, to Mike Adams for many enlightening discussions and his contribution to the theoretical side of the project, and to Francis Sladen for much advice and for his detailed measurements of fibre profile data. I have had the great good fortune of being able to share the work described in chapters 5 and 6 with Allen Conduit, whose collaboration I much appreciated.

I am grateful to Steve Norman, Chris Hamond, Howard Ward, Bob Mansfield, Max Hadley and Eleanor Tarbox for supplying many of the fibres used in the experiments and for much information about the fabrication processes used.

I would also like to thank Michel Eve and Raman Kashyap of the British Post Office (now British Telecom) for their collaboration in some of the bandwidth measurements, and for the loan of fibres.

Many thanks are due to Sue Long and Anne Owens for typing the thesis, to Jan Ditchfield and Nicki Pink for typing the manuscripts of publications and to Chris Nash for providing most of the drawings.

I gratefully acknowledge the help of Roy Came and Mike Carrington and other members of the mechanical workshop for their advice and their accurate machining of many parts needed for the experiments.

Finally, I would like to thank the University of Southampton for the provision of a Research Studentship.

CONTENTS

CONTENTS (Cont'd.)

CONTENTS (Cont'd.)

CONTENTS (Cont'd.)

CONTENTS (Cont'd.)

CONTENTS (Cont'd.)

CHAPTER 1 - INTRODUCTION

1.1 BACKGROUND

The use of glass fibres as a transmission medium for optical communications was proposed in 1966 by Kao and Hockham[1]. This suggestion must have seemed somewhat speculative since, at that time, fibre losses were of the order of 1000dB/km. It was estimated that optical fibre communications would be practicable if the attenuation of the fibres could be reduced to 20dB/km or less. This figure was achieved in 1970[2] and, after many refinements in the fabrication processes, a fibre with an attenuation of 0.15dB/km has recently been produced[3].

Fibres such as this will, in the near future, allow the design of communication systems with repeater spacings greater than 100 km. It is possible that the bandwidth of the fibre will be a limitation on the capacity of such systems, or on the repeater spacing.

1.1.1 Bandwidth of Optical Fibres

A major part of the present study is concerned with the investigation of the mechanisms which limit the bandwidth of an optical fibre link. It is important to characterise the various effects separately, in order to acquire some insight into the fundamental processes which are involved, and hence to allow the design of optical fibre communication systems with maximum information-carrying capacity.

One is concerned here with the pulse broadening which accompanies propagation in optical fibres, and which falls into two categories, namely intramodal (or "chromatic" dispersion) and intermodal dispersion.

The latter effect occurs only in multimode fibres, i.e. fibres of sufficiently large dimensions to carry light in many different electro-magnetic field patterns, or modes. It originates from

differences in group velocity between the modes and is almost independent of the linewidth of the source. Intermodal dispersion can be minimised by a suitable design of the refractive-index profile[4,5]. In principle, an r.m.s. pulse broadening of approximately 30ps/km can be achieved[4,5] in a fibre having a numerical aperture of 0.25. The optimum profile does, however, depend on the dispersive properties of the core and cladding, and thus varies with wavelength, an effect known as 'profile dispersion'[5]. A graded-index multimode fibre can therefore have a very high bandwidth at one wavelength and a much lower bandwidth at another. Conversely, the wavelength at which such a fibre has minimal intermodal dispersion is a function of the refractive-index profile. The operating wavelength is therefore an important parameter which must be taken into account in the fabrication of an optical fibre.

Intramodal dispersion, on the other hand, is the variation of the propagation delay of each mode with wavelength. Since all practical sources have a finite linewidth, a fibre is normally excited simultaneously by light consisting of a range of wavelengths. The various spectral components travel with different group velocities and thus arrive at the detector delayed with respect to each other. The pulse is thus broadened and the information-carrying capacity of the fibre reduced. The transit time τ at wavelength λ may be related to that at λ_o by a Taylor series of the form:

$$\tau(\lambda) = \tau(\lambda_o) + \Delta\lambda \frac{d\tau}{d\lambda} + \frac{(\Delta\lambda)^2}{2!} \frac{d^2\tau}{d\lambda^2} + \ldots \qquad (1.1)$$

where $\Delta\lambda = \lambda - \lambda_o$.

To a first approximation, therefore, the intramodal broadening $\Delta\tau = \tau(\lambda) - \tau(\lambda_o)$ resulting from a linewidth $\Delta\lambda$ is given by

$$\Delta\tau = \Delta\lambda \frac{d\tau}{d\lambda} \qquad (1.2)$$

Intramodal dispersion can be reduced either by using sources having narrow linewidths or by operating the optical link in a wavelength

region where the derivative $\frac{d\tau}{d\lambda}$ is small. Intramodal dispersion is the only pulse broadening mechanism in single mode fibres; in multimode fibres with near-optimal profiles, it can also be a limitation on the fibre bandwidth [6,7].

Intramodal broadening is commonly subdivided into material dispersion and waveguide dispersion[5], although in many cases of practical importance these effects are strongly inter-related. It has recently been shown [8,9] that the variation with wavelength of the difference between the refractive index of the core and that of the cladding also contributes to intramodal dispersion.

The properties of all waveguide modes are sensitive to the ratio a/λ of the core radius to the wavelength of the propagated light. A change in wavelength thus usually results in a variation of the pulse transit time of each mode simply from a geometric scaling of the core size to the wavelength. This form of dispersion, which is very important in the design of single mode fibres is known as waveguide dispersion. In multimode fibres, waveguide dispersion is dominated by other effects, namely intermode dispersion and material dispersion.

Material dispersion is an effect which occurs even in the absence of a waveguide structure; it is caused by the variation of the refractive index of the glass with wavelength. The transit time τ of a pulse in a medium of refractive index n is given by:

$$\tau = \frac{L}{c} \left(n - \lambda \frac{dn}{d\lambda}\right) = \frac{L}{c} N \qquad (1.3)$$

where $N = n - \lambda \frac{dn}{d\lambda}$ is the group index, L the fibre length and c the speed of light in free space. Since the pulse delay is proportional, to first order, to the group index, it is clear that the wavelength-dispersive properties of the materials which the fibre is made from will contribute to intramodal broadening. The material dispersion parameter $M(\lambda)$ is defined as the derivative with respect to wavelength of the normalised pulse delay, ignoring any waveguide effects:

$$M(\lambda) = \frac{1}{L}\frac{d\tau}{d\lambda} = \frac{1}{c}\frac{dN}{d\lambda} = -\frac{\lambda}{c}\frac{d^2n}{d\lambda^2} \qquad (1.4)$$

As an example of the importance of material dispersion, let us consider an optical link driven by a GaAs light-emitting diode operating at a wavelength of 0.82 μm and having an r.m.s. full spectral width of 40 nm. In silica, the material dispersion parameter at 0.82 μm is ∿ 100 ps nm^{-1} km^{-1} and intramodal broadening is thus approximately 4 ns km^{-1}, which is well in excess of the intermodal dispersion found in good-quality graded-index fibres. In a case such as this, the bandwidth of the fibre link is limited by material dispersion .

Fortunately, the material dispersion parameter of silica-based glasses is negligible at a wavelength near 1.3 μm. The operation of optical links in this wavelength region was proposed a few years ago[10]; at that time, however, there existed no suitable semiconductor sources or low-noise detectors. In addition, when the present work was undertaken very little data concerning material dispersion in glasses used for fibre-fabrication was available to designers.

Much of the work to be described in the thesis is concerned with the determination of the various contributions to pulse broadening, particularly in multimode fibres, and the investigation of their wavelength dependence.

1.1.2 Fibre Strength

The tensile strength of optical fibres has become very important now that optical cables are being put to practical use in many communications systems. The breaking of a fibre during installation or during the life of the cable would almost certainly lead to a loss in transmission and must therefore be avoided. A fibre with a pristine surface is immensely strong. To preserve that intrinsic tensile strength, the surface must be protected. Thus polymer coatings are normally applied to the fibres during the drawing process and further extrusions of close-fitting plastic jacketing materials are often carried out during the cabling. In this way, fibres

capable of withstanding extensions of about 1% without breaking can now be produced routinely.

The application of coating materials can however result in permanent stresses being applied to the fibres by their jackets, for instance because of the difference in expansion coefficients of silica and most plastics. These stresses can have detrimental effects on the performance of the fibre, such as increased microbending loss. A technique for estimating the stress applied to a fibre by the jacket from the observation of the pulse transit time was developed in the course of the present work and is described in the thesis.

1.1.3 Attenuation of optical fibres

Another very important property of optical fibres is their attenuation. Attenuation has a direct influence on the repeater spacing in optical communication systems. Reducing the loss of optical waveguides has always been - and is likely to remain - one of the main research objectives in the area of fibre fabrication. A number of measurement techniques have been developed[11] in order to separate the various contributions to fibre attenuation and thus assess the effect of modifications to the fabrication processes.

One technique which has attracted much attention recently is the backscattering method[12,13]. The latter relies on the minute fraction of energy of an optical pulse travelling in a fibre, which is continuously scattered by microscopic inhomogeneities in the glass. A proportion of this scattered light is trapped by the fibre, and guided back to the launching end where it may be detected. The backscatter signal is in the form of a decaying pulse, since the returned power decreases as the forward-travelling energy is attenuated by propagation in the fibre. The rate of decay is a direct measure of the local fibre attenuation at a point determined by the round-trip pulse transit-time.

The backscatter technique allows localised fluctuations of attenuation to be resolved and is thus useful in the location of

faults in optical cables and in the identification of sections of poor quality. In addition, the nature of the defect causing a localised increase in attenuation can often be identified from the shape of the backscatter return. The technique is nondestructive and requires access to one end of the fibre only; it thus has a clear application in field measurements.

Part of the thesis is devoted to the backscatter technique and in particular to spectral measurements of fibre attenuation.

1.2 CONTENTS OF THE THESIS

1.2.1 Presentation

Several quite separate aspects of light propagation in optical fibres have been studied and are discussed in the thesis. Thus the main body of the thesis consists of four chapters describing measurements of material dispersion (Chapter 3), of intermodal dispersion (Chapter 4), of the effect of stress and temperature on pulse transit time (Chapter 5) and of fibre attenuation using the backscattering technique (Chapter 6). Each of these chapters is intended to be independent, although they rely on Chapter 2 for a description of the equipment used in most of the experimental work.

Each chapter consists of an introduction to the specific topic and a section giving a theoretical background, followed by a description of the work, the results, a discussion and a summary.

The main results of the work and the most important conclusions have been drawn together in Chapter 7, where some suggestions for further work have also been given.

1.2.2 Development of a tunable laser system for measurements in optical fibres

Chapter 2 consists of a description of the laser system which

was developed in the course of the present study and which allows many properties of optical fibres to be investigated over a wide range of wavelengths. This fibre test facility was unique when it was first established in 1976 and 1977. Alternative techniques have been implemented in other laboratories since the present work began[14,15]. Nevertheless, through continuous refinement of both the equipment and of the experimental procedures, the dye-laser system which is described in chapter 2 remains one of the most useful research tools of its kind. This equipment was used in most of the experimental work presented in the thesis.

1.2.3 Measurements of material dispersion by a pulse delay technique

Measurements of the variation of material dispersion with wavelength in optical fibres are presented in chapter 3. The material dispersion parameter is deduced from the wavelength-dependence of the pulse transit-time in multimode fibres measured using the dye-laser system. The technique is convenient and sensitive. Several glass-compositions commonly used in the fabrication of optical fibres have been investigated. It is shown that the material dispersion of phosphosilicate fibres is not significantly different from that of pure silica. In contrast, the addition of germania to silica substantially alters the material dispersion and causes an increase in the wavelength of zero material dispersion with increasing concentration of additive.

The pulse-delay technique can also be used to determine the chromatic dispersion of single-mode fibres[16]. The dispersion measured in this way is a function not only of the dispersive properties of the core and cladding material, but also of the core radius, the numerical aperture and the refractive index profile[8]. Measurements of pulse delay as a function of wavelength can assist in the development[17]of single-mode fibres with minimum dispersion at the wavelength, 1.55 μm, where the losses of silicate fibres are lowest[3]. Preliminary measurements of chromatic dispersion in single-mode fibres are included in chapter 3.

1.2.4 Measurements of intermodal dispersion as a function of wavelength

Wavelength-dependent measurements of intermodal dispersion, described in Chapter 4, clearly demonstrate the profile dispersion[5] effect. Measurements of refractive-index profile[18] and of the profile-dispersion parameter[19] performed by my colleague, Dr. F.M.E. Sladen, allow predictions to be made of the variation of bandwidth with wavelength. The difficulties which were experienced in correlating the latter calculations with measured values of intermodal dispersion have underscored the sensitivity of fibre bandwidths to the refractive-index profile. The importance of seemingly minor perturbations in the index-profile has perhaps not been fully appreciated until recently[20-22]. The work described in Chapter 4 clearly shows that small errors in the index-profile of a multimode fibre have a very severe effect on the intermodal dispersion, particularly at the optimum operating wavelength.

1.2.5 Effect of stress and temperature on pulse transit time

Chapter 5 is concerned with the variation of pulse delay in optical fibres with stress and temperature.

During the fabrication of an optical cable, stresses are inevitably applied to the fibre, and a proportion of these are likely to remain throughout the life of the cable. Externally-applied stress is usually undesirable since it can lead to increased microbending loss or premature failure of the fibre through static fatigue. A technique has been invented[23], which allows cable designers to test the residual longitudinal stress applied to a cabled fibre from the observation of the pulse transit-time.

The pulse transit-time in an optical fibre is slightly sensitive to stress via both the elongation and the stress-optical effect. The sensitivity of pulse delay to longitudinal stress was accurately calibrated using a specially-developed experimental arrangement. With this information, any pulse-delay variation observed

during the cabling of a fibre can be related to the forces which are causing it. Temperature variations can be allowed for, using a coefficient which was also measured in the course of this study.

The pulse-delay technique has been used[23] to determine the residual stress applied by a secondary plastic coating under various environmental conditions, and in particular as a function of temperature. These measurements provide a good diagnosis of the behaviour of the plastic coatings and thus may find use in the testing of optical cables designed for harsh environments.

1.2.6 Measurements of fibre attenuation by the backscattering method

Chapter 6 describes wavelength-dependent attenuation measurements using the backscatter technique[12,13]. The major reason for the active interest in the backscattering method lies in its ability to resolve localised fluctuations of attenuation. This, coupled with the tunability provided by the dye-laser system, allows the length-dependence of impurity concentration to be accurately determined. Thus the variation of OH ion content has been measured[24] along a 1.5 km section of fibre by comparing the loss at 0.946 μm (at the peak wavelength of the absorption line) with that at 0.906 μm and 1.006 μm.

The intrinsic instability of the laser source has motivated the development of a new experimental arrangement[25] for the measurement of the backscattered signal. The backscatter waveform is sampled on each pulse at two points which are slightly separated in time and which can be sited so as to examine any point on the fibre. The ratio of these two samples gives directly the attenuation of the section of fibre corresponding to the difference in sampling time. In this way, the measurement is insensitive to fluctuations in pulse energy, detector sensitivity or amplifier gain, since each ratio is automatically source-compensated.

This two-channel technique would appear to be ideally suited for field instruments, particularly if these are to be controlled

by a microprocessor. It has been estimated that such an instrument using a pulsed semiconductor laser is likely to be able to measure the loss of a section of fibre to within 0.1 dB/km, with up to 26 dB insertion loss (in each direction) between the source and the portion of fibre to be characterised. This figure for the allowable insertion loss is far in excess of the capability of existing instruments in which a single sampling gate is scanned along the entire duration of the backscatter signal.

REFERENCES TO CHAPTER 1

[1] K.C. KAO and G.A. HOCKHAM: 'Dielectric-fibre surface waveguides for optical frequencies.' Proc. I.E.E., 1966, *113*, pp. 1151-1158.

[2] F.P. KAPRON, D.B. KECK and R.D. MAURER: "Radiation losses in glass optical waveguides.' *Appl. Phys. Lett.*, 1970, *17*, pp. 423-425.

[3] H. MATSUMURA (private communication). The lowest value of attenuation to be found in the literature is 0.2 dB km^{-1} and is reported in:

T. MIYA, Y. TERUNUMA, T. HOSAKA and T. MIYASHITA: 'Ultimate low-loss single-mode fibre at 1.55 μm.' *Electron. Lett.*, 1979, 15(4), pp. 106-108.

[4] D. GLOGE and E.A.J. MARCATILI: 'Multimode theory of graded-core fibres.' *Bell Syst. Tech. J.*, 1973, *52*, pp. 1563-1578.

[5] R. OLSHANSKY and D.B. KECK: 'Pulse broadening in graded-index optical fibers.' *Appl. Opt.*, 1976, *15*, pp. 483-491.

[6] M.J. ADAMS, D.N. PAYNE, F.M.E. SLADEN and A.H. HARTOG: 'Optimum operating wavelength for chromatic equalisation in multimode optical fibres.' *Electron. Lett.*, 1978, *14*, pp. 64-65.

[7] W.M. MUSKA, T. LI, T.P. LEE and A.G. DENTAI: 'Material-dispersion-limited operation of high-bit-rate optical-fibre data links using l.e.d.s.' *Electron. Lett*, 1977, *13*, pp. 605-606.

[8] W.A. GAMBLING, H. MATSUMURA and C.M. RAGDALE: 'Mode dispersion, material dispersion and profile dispersion in graded-index single-mode fibres.' *I.E.E. J. Microwaves, Optics and Antennas* 1979, *3* (6), pp. 239-246. (This work was first presented in an invited paper at the fourth European conference on optical communication, Genoa, 1978)

[9] K. JURGENSEN: 'Dispersion minimum of monomode fibres.' *Appl. Opt.* 1979, *18*, pp. 1259-1261.

[10] D.N. PAYNE and W.A. GAMBLING: 'Zero material dispersion in optical fibres.' *Electron. Lett.*, 1975, *11*, pp. 176-178.

[11] J.E. MIDWINTER: '*Optical fibers for transmission.*' Wiley, New York, 1979.

[12] F.P. KAPRON, R.D. MAURER and M.P. TETER: 'Theory of backscattering effects in waveguides.' *Appl. Opt.*, 1972, *11*, pp. 1352-1356.

[13] M.K. BARNOSKI, M.D. ROURKE, S.M. JENSEN and R.T. MELVILLE: 'Optical time domain reflectometer.' *Appl. Opt.*, 1977, *16*, pp. 2375-2379.

[14] L.G. COHEN and CHINLON LIN: 'A universal fiber-optic (UFO) measurement system based on a near IR fiber Raman laser.' *IEEE J. Quantum Electron.*, 1978, *QE-14*, pp. 855-859.

[15] A. SUGIMURA and K. DAIKOKU: 'Wavelength dispersion of optical fibers directly measured by 'difference method' in the 0.8 - 1.6 μm range.' *Rev. Sci. Instrum*, 1979, *50(3)*, pp. 343-346.

[16] C. LIN, L.G. COHEN, W.G. FRENCH and H.M. PRESBY: 'Measuring dispersion in single-mode fibers in the 1.1 - 1.3 μm spectral region - a pulse synchronisation technique.' Proc. Optical Communication Conference, Amsterdam, September 1979.

[17] L.G. COHEN, CHINLON LIN, and W.G. FRENCH: 'Tailoring zero chromatic dispersion into the 1.5 - 1.6 μm low-loss spectral region of single-mode fibres.' *Electron. Lett.*, 1979, *15(12)*, pp. 334-335.

[18] F.M.E. SLADEN, D.N. PAYNE and M.J. ADAMS: 'Determination of optical fibre refractive index profiles by a near-field scanning technique.' *Appl. Phys. Lett.*, 1976, *28 (15)*, pp. 255-258.

[19] F.M.E. SLADEN, D.N. PAYNE and M.J. ADAMS: 'Definitive profile-dispersion data for germania-doped silica fibres over an extended wavelength range.' *Electron. Lett.*, 1979, *15*, pp. 469-470.

[20] R. OLSHANSKY: 'Pulse broadening caused by deviations from the optimal index profile.' *Appl. Opt.*, 1976, *15(3)*, pp. 782-788.

[21] D. MARCUSE: 'Calculation of bandwidth from index profiles of optical fibres. 1: Theory.' *Appl. Opt.*, 1979, *18(12)*, pp. 2073-2080.

22 J.J. RAMSKOV HANSEN and E. NICOLAISEN: 'Propagation in graded-index fibers : comparison between experiment and three theories.' *Appl. Opt.*, 1978, *17*, pp. 2831-2835.

23 A.J. CONDUIT, A.H. HARTOG and D.N. PAYNE: 'Residual stress diagnosis in jacketed optical fibres by a pulse delay technique.' Proceedings 5th Conference on Optical Communication Amsterdam, 1979, pp. 8.2.1 - 4.

24 A.J. CONDUIT, A.H. HARTOG, and D.N. PAYNE: 'Spectral- and length-dependent losses in optical fibres investigated by a two-channel backscatter technique.' *Electron. Lett.*, 1980, *16*, pp. 77-78.

25 A.J. CONDUIT, J.L. HULLETT, A.H. HARTOG and D.N. PAYNE: 'An optimised technique for backscatter attenuation measurements in optical fibres.' *Opt. & Quant. Electron.*, 1980, *11*, pp. 169-178.

CHAPTER 2 - TUNABLE LASER SYSTEM

2.1 INTRODUCTION

The dye laser system described here was designed to meet a requirement, common to several experiments discussed in this thesis, for very short (< 1 ns) optical pulses tunable over a wide wavelength range. Moreover, the installation and operation of this equipment represents a significant part of the work presented in the thesis.

The dye-laser system was unique when first operated, and possibly still is. It is an extremely powerful tool for the investigation of certain aspects of light propagation in optical fibres. In addition, its characteristics have largely dictated the way in which the experiments to be discussed were carried out.

The system is designed to measure pulse delay and pulse broadening as a function of wavelength. The requirements which this imposes on the experimental apparatus are first discussed and the equipment is then described in detail. The performance is summarised in section 2.4.

2.2 REQUIREMENTS

2.2.1 Tunability

Tunability is a fairly obvious necessity for wavelength-dependent measurements. A system which could be tuned over the range 0.8 to 1.6 μm would cover all the operating wavelengths envisaged to date for silica-based fibres. This is a minimum requirement, and a wider tuning-range is a considerable advantage for the investigation of the fundamental properties of glasses from which fibres are made. For instance, the value of the material dispersion parameter inferred from the measured variation of pulse delay with wavelength (see chapter 3) is not accurate within approximately 100 nm from either extremity of the wavelength range. Thus the measurements should, ideally, cover

the region of at least 0.7 - 1.7 μm.

It is also important that such quantities as linewidth, pulse width, or peak power should not vary much with the operating wavelength.

2.2.2 Bandwidth

The modulation bandwidth of the apparatus (including the source) is most important in pulse-broadening measurements and it should, ideally, be at least as large as that of the fibres. The pulse duration should therefore be as short as possible and, for good graded-index fibres, pulsewidths well under 1 ns are required. This places a similar demand on the detectors and oscilloscopes which are used to record the optical signals.

2.2.3 Linewidth

A narrow linewidth is useful since, in multimode fibres, it permits the independent measurement of intermodal and material dispersions. A linewidth of 0.5 nm or less is usually adequate.

2.2.4 Beam quality and stability

There are several experiments, such as the launching of selected modes of a multimode fibre, or any work involving single-mode fibres, where it is helpful if the laser operates in the lowest-order transverse mode. The TEM_{00} mode couples most efficiently into single-mode fibres and allows a small portion of the mode spectrum to be excited in multimode fibres.

It is often found in multimode lasers that the distribution of power amongst the modes fluctuates. This is particularly the case with pulsed lasers, where the distributions of bright spots in the near-field is observed to change between consecutive shots. Such fluctuations are troublesome since they can cause variations in

launching conditions and in the energy contained in successive pulses. This may lead, in turn, to longer averaging times in experiments, such as the determination of fibre attenuation by the backscatter technique, where weak signals must be extracted from noise using boxcar integrators.

Pulse amplitude fluctuations also originate in the laser itself, particularly when the pump radiation is produced by a flash lamp.

2.2.5 Power

High power is an advantage since it relaxes the requirements for sensitive, and low-noise, detectors. This is an important consideration at wavelengths longer than 1.1 μm for which germanium detectors (which produce more noise than silicon devices) must be used.

A high-power source also increases the sensitivity of certain experiments by enabling longer fibres to be measured, since a larger insertion loss can be tolerated.

2.2.6 Pulse repetition rate

If the pulse repetition rate is greater than about 500 Hz, then a sampling oscilloscope can be used, which has the virtue of giving a wider bandwidth to the system. Real-time, commercially-available, oscilloscopes were, until recently, limited to a bandwidth of 500 MHz. Even when a real-time oscilloscope is used and where measurements are made on very few pulses, a repetition frequency of 5 Hz or more is an advantage. Thus, the laser beams are then quasi-continuous and optical alignments are greatly facilitated.

If signal averaging is considered a high repetition rate is again an advantage since the integration time is reduced, and the effects of long-term offset-drift are less severe.

2.3 DESCRIPTION OF THE EQUIPMENT

2.3.1 Outline

A block diagram of the system is shown in figure 2.1.

A flash-lamp-pumped dye-laser followed by a $LiNbO_3$ parametric oscillator produces optical pulses in the wavelength range 0.4 - 2.6 μm. The output of this source has been tailored to very short duration (< 1 ns) pulses by an electro-optic modulator. The latter comprises a polariser and a Pockels cell driven by a high-voltage pulse generator having a fast rise time.

High-power, tunable and narrow-linewidth optical pulses are thus available for launching into the fibres under the test. At the output of the fibres, the light is detected using a germanium avalanche photodiode. The electrical signal thus obtained is displayed on a real-time oscilloscope.

2.3.2 Dye-laser

The dye-laser is a Chromatix CMX-4 laser pumped by a flash lamp and incorporates a continuous flow of dye. By changing dyes, the laser can cover the entire visible spectrum from 0.4 μm to 0.8 μm.

When the laser is used to pump the optical parametric oscillator, the dye used is a solution of rhodamine 6G in 1:1 water/methanol or in 4% amonyx and 96% water. The energy output and tuning range with these solvents are, respectively: 10 mJ, 580-620 nm and 6 mJ, 595-635 nm. Although it curtails the dye lifetime, the second solvent provides better pulse-to-pulse amplitude stability.

Other dyes which have been used in the present work include Coumarin 102, which covers the wavelength region 485-515 nm and Oxazine 170 for the range 700-740 nm.

The pulse repetition rate can be varied up to 25 pulses/s. The

pulse duration is approximately 1 μs. With well-aligned mirrors, and using Rhodamine 6G in amonyx/water, pulse-to-pulse amplitude fluctuations are generally less than ± 5%.

The linewidth of the dye-laser is normally ∿0.1 nm at 0.6 μm but can be reduced to 0.01 nm with the help of an intracavity Fabry-Perot etalon.

2.3.3 Optical Parametric Oscillator (O.P.O.)

Most of the wavelength range attainable with this laser system is provided by the lithium niobate parametric oscillator, which is pumped at a wavelength of about 0.6 μm by the CMX-4 dye-laser.

The O.P.O. is tunable from 0.76 μm to 2.6 μm, although several mirror-changes are required to do so. Energy at two wavelengths, that of the signal, λ_s, and the idler, λ_i, is generated in the parametric oscillator. The signal and idler wavelengths are related to the wavelength λ_p of the dye-laser by:

$$\frac{1}{\lambda_p} = \frac{1}{\lambda_s} + \frac{1}{\lambda_i} \quad \text{where } \lambda_s < \lambda_i$$

i.e. the energy of a signal photon plus that of an idler photon is equal to the energy of a pump photon. The output wavelengths (signal and idler) are determined by the phase-matching condition: the signal travels, as an extraordinary wave in the birefringent crystal, at the same phase velocity as the pump power in the ordinary polarisation. The O.P.O. can therefore be tuned either by adjusting the pump wavelength, or by altering the temperature, and hence the birefringence, of the crystal. Thus variation of the pump wavelength produces fine tuning of the O.P.O., while major changes in output wavelength are achieved by altering the temperature of the crystal, which is contained in an oven.

Degeneracy is the operating condition where $\lambda_s = \lambda_i = 2\,\lambda_p \equiv \lambda_d$. It is well known that near degeneracy, the output linewidth of

parametric oscillators increases dramatically, and that their operation becomes somewhat unstable. In our case, λ_d is in the range: 1.18 μm - 1.26 μm, which is near the region of zero material dispersion in high-silica glasses. Fortunately, by judicious control of crystal temperature and pump wavelength, it is possible to cover the entire wavelength range of the O.P.O. with a maximum linewidth of 1 nm. As the device is tuned away from degeneracy, the linewidth reduces to a minimum of about 0.2 nm.

The O.P.O. is rather like a laser cavity in that it comprises an amplifying medium (the $LiNbO_3$ crystal) and two mirrors. It oscillates when the gain due to parametric conversion in the crystal overcomes the losses of the cavity. The O.P.O. is designed so that only energy at the idler wavelength is used to provide optical feedback, and hence enable the oscillation to take place. Thus when power at the signal wavelength is needed, mirrors reflecting 100% at the idler wavelength may be installed in the cavity and their use approximately doubles the useful output-energy. Conversely, when power at the idler wavelength is required, the signal wave is also present in the output. When the O.P.O. is operated near degeneracy, then an edge-filter, with very sharp cut-off characteristics is required to separate the two waves.

The energy per pulse in the O.P.O. output decreases from 0.5 mJ to 0.2 mJ as the wavelength is tuned from 0.8 μm to 2.0 μm. The maximum pulse repetition rate is 12.5 pps and the pulse duration is approximately 1 μs.

2.3.4 Pulse-slicer

The dye-laser and the parametric oscillator produce pulses of approximately 1 μs duration, which are far too long for dispersion measurements in optical fibres. The function of the pulse-slicer is, therefore, to extract one pulse of very short duration (< 1 ns) from the output of either source. The pulse-slicer consists of a high-speed modulator driven by a high-voltage pulse-generator. The electro-optic modulator is only effective with a linearly-polarised

input beam. Since the outputs of the dye-laser and the O.P.O. are highly-polarised, but in directions orthogonal to one another, these sources cannot normally be modulated simultaneously.

2.3.4.1 Modulator

Referring to figure 2.1, the modulator consists of a Pockels cell and a prism-polariser. The Pockels cell is aligned so as not to affect the polarisation of the light it transmits when no voltage is present. After travelling through the Pockels cell, the optical beam reaches the polariser. The latter is orientated so as to reject the light. The modulator, or optical gate is thus normally closed and it rejects more than 99.9% of incoming light, provided that the latter is suitably polarised.

If a large voltage, V, is present, the Pockels cell exhibits electrically-controlled birefringence and rotates the polarisation of the light travelling through it. A proportion of the incident power is thus allowed through the polariser. The transmission, T, of the optical gate is given by:

$$T = \sin^2\left(\frac{\pi}{2}\,\frac{V}{V_{\lambda/2}}\right)$$

The half-wave voltage $V_{\lambda/2}$ is proportional to the wavelength of the modulated light. The value $V_{\lambda/2}$ = 5 kV at 633 nm was measured on the device used in the system.

The active element in the Pockels cell is a KD*P (deuterated potassium dihydrogen phosphate) crystal which transmits light at wavelengths shorter than 1.8 μm. The device is designed to appear (electrically) as an ordinary 50 Ω transmission line. Thus high-voltage pulses are transmitted with little distortion and their temporal width determines the duration of the optical pulse, within the limitations introduced by the speed of the modulator itself.

The Pockels cell used in the present work (Lasermetrics model 1080)

was probably the fastest commercially-available device of its type at the time it was purchased. The rise-time of similar models has been measured by workers at Lawrence Livermore Laboratory[1] with a streak-camera, giving a value of 250 ps.

In a similar experiment I used a reed-delay pulse generator to drive the pulse-slicer, and modulated a 50 mW cw He-Ne laser. The resultant pulses were detected with a silicon avalanche photodiode, fed to a sampling oscilloscope and averaged in a slow-scanning boxcar integrator. The resultant noise-free optical output was compared with the electrical input pulse-shape and gave the same figure of 250 ps for the modulator rise-time. The rise-time is almost certainly limited by minor electrical mismatches in the transmission-line modulator.

The rise-time of the modulator sets a lower limit on the width of the optical pulses which can be produced. In practice, a greater pulse width is obtained since it also depends on the rise-time of the high voltage pulse generator and on the arrangement of the electrical signal path.

2.3.4.2 Spark-gap

Spark-gaps are the only devices capable of producing voltage pulses with amplitudes greater than 10 kV, and having rise-times less than 0.5 ns. A spark-gap is a chamber filled with a gas, such as nitrogen, at high pressure and containing two electrodes. The latter are separated by a gap d (of the order of 1 - 4 mm) and they are biased with a large potential difference. The voltage V_b which the gap withstands without breaking down depends upon the inter-electrode spacing d, and the pressure and nature of the gas.

The usual way to operate a spark-gap is to bias the device very near to the breakdown voltage V_b, and to trigger the gap at the appropriate time. The gap breaks down by avalanche multiplication of ions in the inter-electrode spacing. The process relies on the presence of at least one ion in the region of high electric-field and

is thus statistical in nature. After initiation of the breakdown, the gap switches extremely rapidly (a few hundred picoseconds) to a state of low impedance, which requires, typically, a current of 1 mA for it to be maintained. If the current is switched off, the device returns to a state of high impedance. The spark-gap thus delivers a high-voltage pulse, the leading edge of which corresponds to the breakdown of the device.

The most common ways of triggering spark-gaps are:

a) to illuminate the inter-electrode region with a flux of ions, or ionising radiation[2],
b) to increase abruptly the applied voltage beyond V_b or,
c) to focus a high-power laser between the electrodes[3].

In the latter case the electric field of the laser beam adds to that created by the high-voltage bias so that the dielectric strength of the gap is exceeded. Laser triggering provides extremely reliable and fast switching. Moreover it is immune from the problems encountered with electrical triggering, of interference between the trigger line and the output line. Unfortunately the power available from the CMX-4 dye-laser is not sufficient to operate a laser triggered spark-gap reliably and thus electrical triggering must be used. Two commercial spark-gaps were tried and both were unsatisfactory.

The first device (fig. 2.2) was a laser-triggered spark-gap modified for electrical triggering by incorporation of a third, trigger, electrode. The intrinsically fast rise-time of the laser-triggered device was severely degraded by electrical reflections from impedance mismatches at the trigger electrode. The gap was biased via a length of 50 Ω high-voltage coaxial cable and discharged into a 50 Ω load. This arrangement ensures that a single, rectangular pulse is delivered. It has, however, the disadvantage, that the amplitude of the output pulse is only half that of the charging voltage. In view of the dielectric strength of the connectors and

cables used in the system, the output voltage was limited to $\approx$8 kV, and this reduced the efficiency of the optical gate. Moreover, the triggering of the device was rather erratic and its rise time was too long ($\sim$ 1.2 ns).

A replacement gap was then tried. In this device the spark-gap is mounted directly onto a Blumlein charging circuit (fig. 2.3). In this way, impedance mismatches at the connections between the charging circuit, the spark-gap and the output transmission line can be minimised. The coaxial electrode configuration and the improved design results in very reliable triggering (better than 99.9%). Because the Blumlein charging circuit is employed, the output-pulse amplitude is almost equal to the charging voltage, and thus the device can produce 15 kV pulses.

Unfortunately, the rise-time of the Blumlein-based spark-gap is approximately 1.4 ns. From measurements using a time-domain reflectometer, this relatively slow rise-time can be attributed to an incorrect design of the Blumlein charging circuit, the impedance of which is too low.

The performance of the two devices described so far is adequate for pulse-delay measurements, where the pulse-width is not critical. For pulse-broadening measurements, however, very narrow pulses are essential. Since it was becoming increasingly obvious that the supplier could not meet its specifications, I decided to design my own spark-gap (fig. 2.4) which was used subsequently whenever very short pulses were required.

Following the work of Fletcher[2], and Michon et al[4], a pulse-sharpening spark-gap was built. This type of spark-gap is supplied, not with a d.c. potential, but with a high-voltage pulse which is transmitted, with a much faster rise-time.

The device built for the present work has a coaxial structure with a characteristic impedance of 50 Ω. When ionised, it therefore approximates an ordinary transmission line. In the middle portion of

the device, the inner conductor is replaced by two tungsten electrodes. The inter-electrode separation can be adjusted to optimise the performance of the spark-gap while it is in operation. The gap is normally filled with dry nitrogen at atmospheric pressure.

The electrode spacing is adjusted so that the spark-gap breaks down at a very low voltage. Thus if a slowly-rising high-voltage wave is applied to the input electrode, the spark-gap is almost immediately over-volted. For a short time, which corresponds to the formation of a conductive path between the electrodes, no output is produced. The delay has two origins[5], namely the statistical time taken for a charged particle to appear in the high-field inter-electrode region and the time taken for the avalanche multiplication of ions to form a conductive path in the gas. The intrinsic turn-on delay of the device, which depends on the electrode spacing, is adjusted to allow the input waveform to reach its maximum. When the spark-gap then switches, a high-voltage pulse with an extremely fast rise-time is launched down the output cable.

Figure 2.5 shows the output waveform of the spark-gap, displayed on a Tektronix 7104 oscilloscope. Note that the rise-time shown in fig. 2.5 is entirely limited by the 1 GHz bandwidth of the oscilloscope. It is concluded, from fig. 2.5, that this pulse-sharpening gap can produce pulses with rise-times of the order of 200 ps. The spark-gap has been used for 18 months with no degradation in its performance.

2.3.4.3 Electrical arrangement

The output of the spark-gap is a pulse of several tens of nanoseconds duration having a fast rise-time. The leading edge of the pulse is used to switch the optical gate on and off. The electrical arrangement is shown in figure 2.6. A short circuit is placed in series with the Pockels cell at a distance ℓ_{sc} from the KD*P crystal. The high-voltage wave originating at the spark-gap arrives at the Pockels cell, turns the optical gate on, and proceeds to the short-circuit. A reflected wave (of opposite polarity) is launched back towards the crystal and cancels the incident wave. The

optical gate is thus closed at a time $\tau = \frac{2\ell_{sc}}{v_g}$, where $v_g \approx 2 \times 10^8 \text{ m s}^{-1}$, after it is opened. The pulse duration can therefore be adjusted via the distance ℓ_{sc} which separates the short circuit from the electro-optic crystal. The shortest available pulse-duration is limited by the rise-times of the spark-gap and the Pockels cell. Figure 2.7 shows an oscilloscope trace of an optical pulse produced using the pulse-sharpening gap and a transmission line length ℓ_{sc} of 3.5 cm. The pulse width is 850 ps and is limited:

a) by the rise-time of the oscilloscope, and
b) by the rise-time of the Pockels cell and the detector.

The oscillation shown on the photograph is caused by ringing in the oscilloscope.

As the trailing edge of the high voltage pulse reaches the crystal, the reflected wave is no longer cancelled by the incident wave, and a second optical pulse is produced. Although this is normally of little consequence, the second pulse can be gated out, if necessary, with a second Pockels cell.

The short-circuit used here has in fact a finite resistance of about 0.1 Ω, and provides a trigger signal for electronic instrumentation.

2.4 PERFORMANCE OF THE SYSTEM

Table 2.1 summarises the performance of the dye-laser and O.P.O. system. Each component is entered as a separate line and, where relevant, its performance is indicated in the appropriate column. The final line takes into account the way all the components work together and the limitations, or enhancement, brought by each part to the system as a whole.

The dye-laser system has the widest tuning range reported in the optical fibre literature[6-8]. In addition, the O.P.O. is easily and rapidly tuned by adjustment of either the dye-laser wavelength or

the temperature of the crystal. This characteristic makes the parametric oscillator much more convenient to use than one which is temperature-tuned only.

The low pulse-repetition rate is the major drawback of the system, since it precludes the use of a sampling oscilloscope. Although, real-time oscilloscopes with 1 GHz bandwidth and 10 mV/div sensitivity are now commercially available, the dye-laser system is limited by the 500 MHz bandwidth of the transient-digitiser presently used. The low repetition rate also makes the use of boxcar integrators much more difficult.

The oscilloscope used in the measurements to be described is a Tektronix R 7912 transient digitiser. This instrument has a bandwidth of 500 MHz and a sensitivity of 10 mV/division. The R 7912 has the ability to acquire a single pulse and display it very brightly either on a television monitor or a storage monitor. This feature is extremely useful when a low repetition laser is used.

The linewidths of the laser and O.P.O. vary with wavelength. It has been estimated, however, that in most multimode fibres, the pulse broadening is heavily dominated by intermodal dispersion. Thus measurements of pulse broadening and pulse-delay in multimode fibres clearly separate the intermodal and intramodal contributions to pulse dispersion. In particular, it is not necessary to account for the linewidth of the laser or O.P.O. in measurements of intermodal broadening.

The peak power available ($\sim$ 100 W at 0.9 μm) is very high by comparison to most other measurement systems. In contrast to, for instance, the fibre-Raman source[7], the pulse energy is concentrated in a very narrow spectral range. No power is lost, therefore, by wavelength filtering which is used in other tunable systems[6,7] to reduce the linewidth.

In summary, the dye-laser system is somewhat limited by its low pulse repetition rate. Its wide tunability, high spectral

brightness and large peak power make it, however, an extremely useful and versatile source for optical fibre measurements.

2.5 REFERENCES TO CHAPTER 2

[1] B.C. JOHNSON, K.R. GUINN, W.E. MARTIN and Wm. D. FOUNTAIN. 'Optical rise-time measurements on KD*P transmission-line Pockels cells.' *J. Appl. Phys.*, 1978, *49*(1), pp. 75-80.

[2] R.C. FLETCHER. 'Production and measurement of ultra-high-speed impulses.' *Rev. Sci. Instrum.*, 1949, *20*(12), pp. 861-869.

[3] L.L. STEINMETZ. 'Laser-triggered spark-gap.' *Rev. Sci. Instrum.*, 1968, *39*(6), pp. 904-909.

[4] M. MICHON, H. GUILLET, D. Le GOFF and S. RAYNOUD. 'A subnanosecond rise-time electro-optic shutter for use in a laser system.' *Rev. Sci. Instrum.*, 1969, *40*, pp. 263-265.

[5] F. LLEWELLYN-JONES and E.T. de la PERRELLE. 'Field emission of electrons in discharges.' *Proc. Roy. Soc. A*, 1953, *216*, pp. 267-279.

[6] M. HORIGUCHI, Y. OHMORI, and T. MIYA. 'Evaluation of material dispersion using a nanosecond pulse radiator.' *Appl. Opt.*, 1979, *18*, pp. 2223-2228.

[7] L.G. COHEN and CHINLON LIN. 'A universal fiber-optic (UFO) measurement system based on a near-IR fiber Roman laser.' *IEEE J. Quant. Electron.*, 1978, QE-14, pp. 855-859.

[8] A. SUGIMURA and K. DAIKOKU. 'Wavelength dispersion of optical fibers directly measured by "difference method" in the 0.7 - 1.6 μm range.' *Rev. Sci. Instrum.*, 1979, *50*(3), pp. 343-346.

Table 2.1

Performance of the dye-laser system and of its components

property / component	tuning range (μm)	pulse duration (FWHM)	linewidth (nm)	output power (W)	maximum pulse repetition frequency (Hz)
dye-laser	0.4-0.8	∿ 1 μs	0.01-0.1	6×10^3	25
O.P.O.	0.76-2.6	∿ 1 μs	0.2-1	200-500	12.5
Spark gap	-	risetime : 0.2 ns	-	-	> 25
Pockels cell	0.4-1.8	risetime : 0.25 ns	-	∿ 100 W	-
detector	0.4-1.9	risetime : ∿ 0.25 ns	-	-	-
oscilloscope	-	0.7 ns	-	-	-
laser system	0.4-1.9 μm	0.8-0.85 ns	0.02-1 nm	100 W	12.5 Hz
limiting factors	transmission of KD*P crystal	1/ oscilloscope 2/ detector	Degeneracy of the O.P.O.	1/ damage to $LiNbO_3$ crystal 2/ efficiency of pulse slicer	damage to $LiNbO_3$ crystal and design of dye-laser

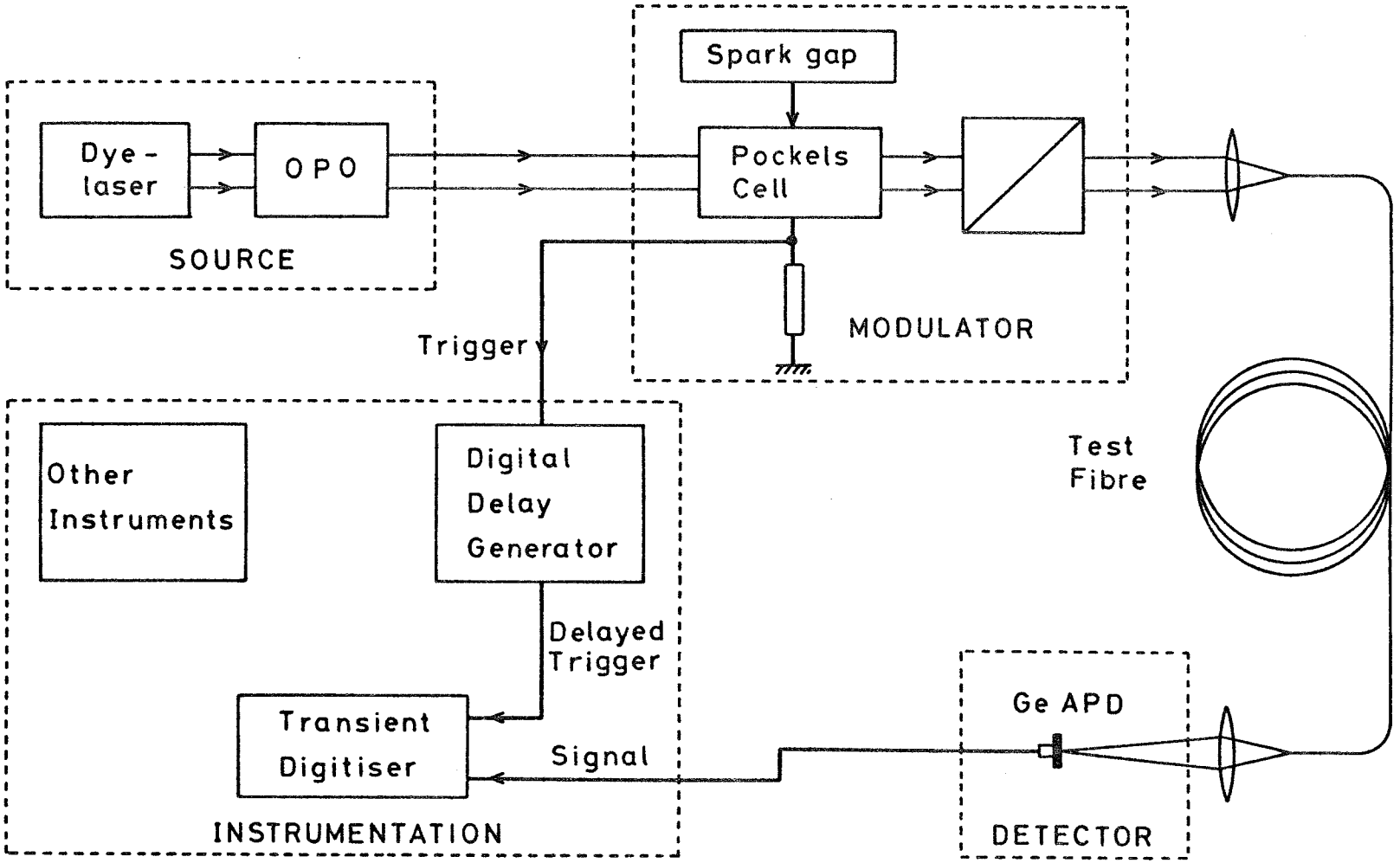

Figure 2.1: Schematic diagram of the tunable dye-laser system

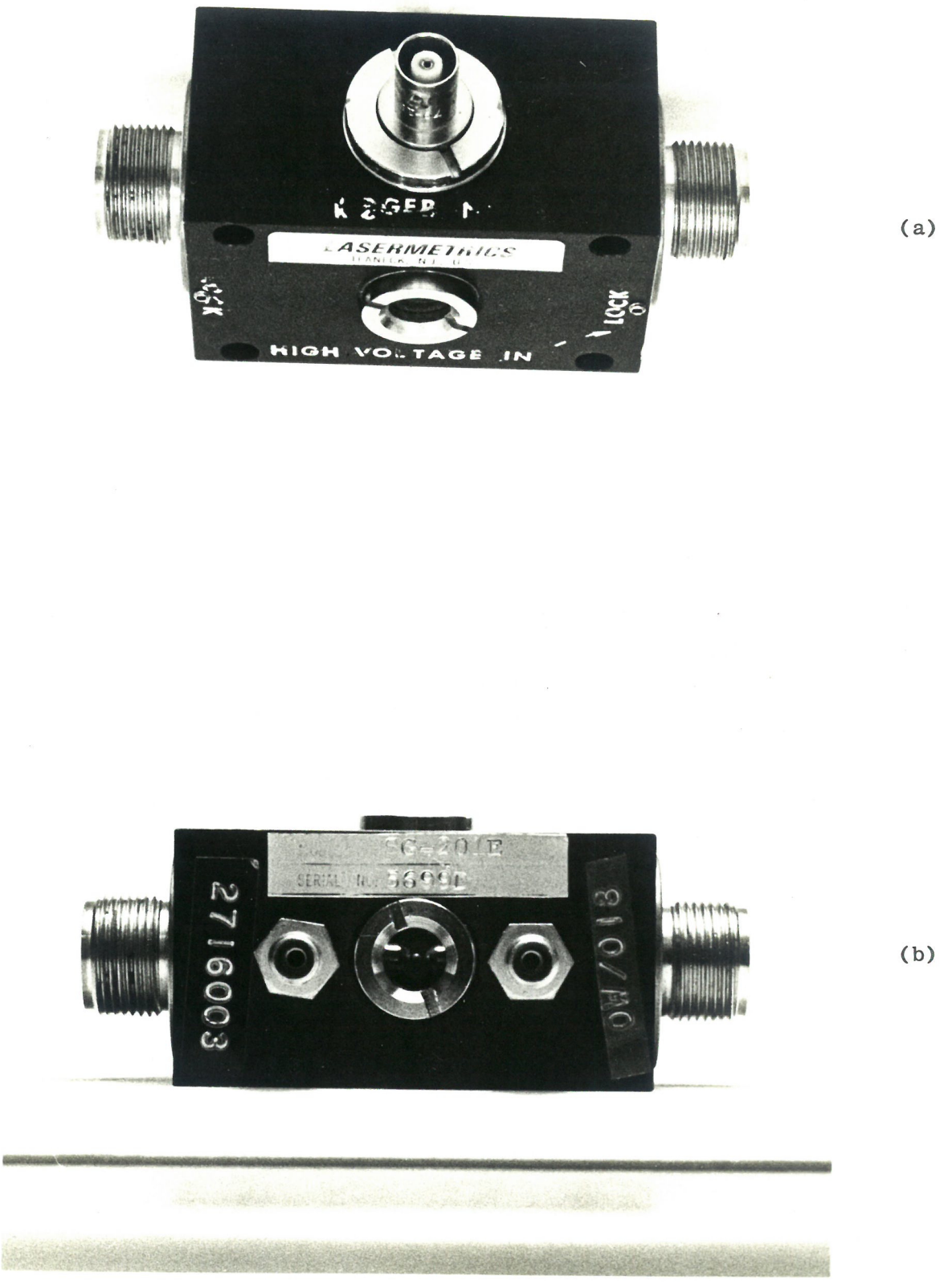

(a)

(b)

Figure 2.2. Two views of the modified laser-triggered spark-gap showing (a) the three high-voltage connectors, and (b) the gas fittings and, through the side viewing port, the three electrodes.

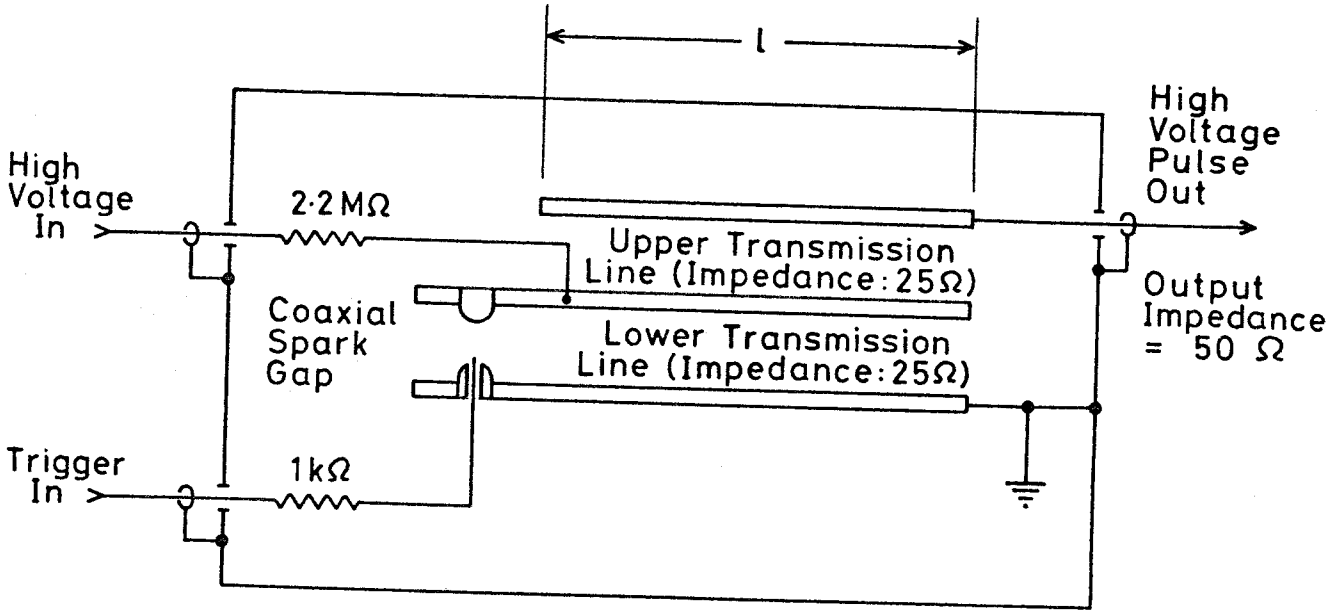

Figure 2.3 : Internal electrical arrangement of the Blumlein-based spark-gap.

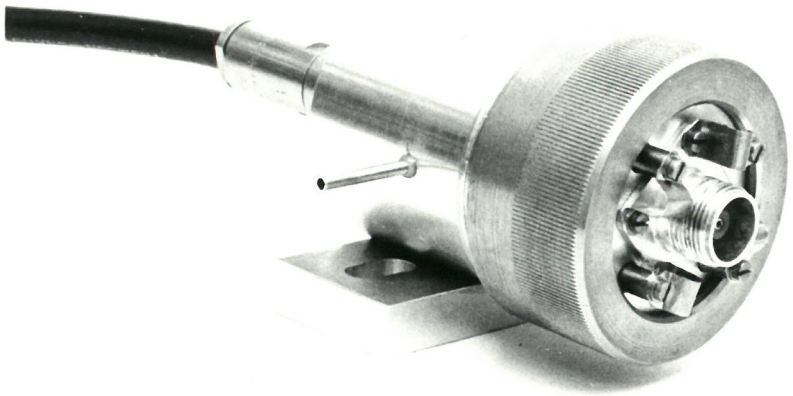

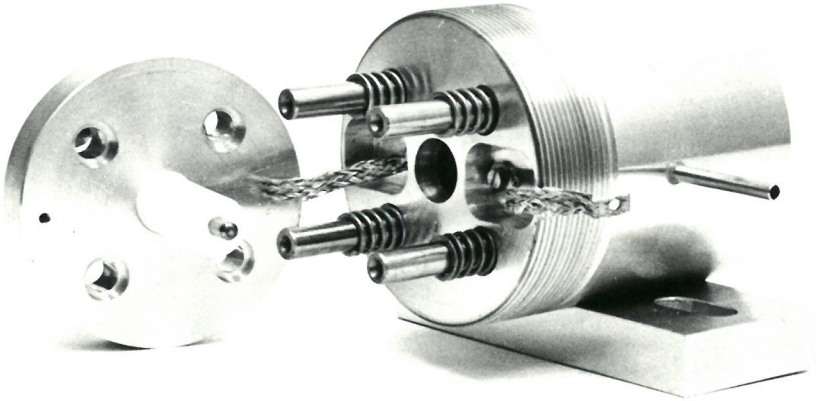

Figure 2.4. The pulse-sharpening spark gap:
(a) assembled
(b) taken apart to reveal the internal structure

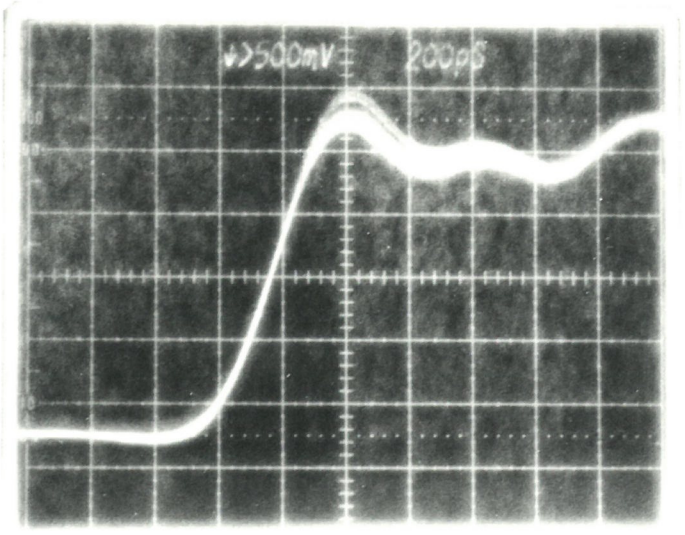

Figure 2.5. Leading edge of the electrical output of the pulse-sharpening spark gap. The horizontal scale is 200 ps/div and the oscilloscope has a nominal bandwidth of 1 GHz.

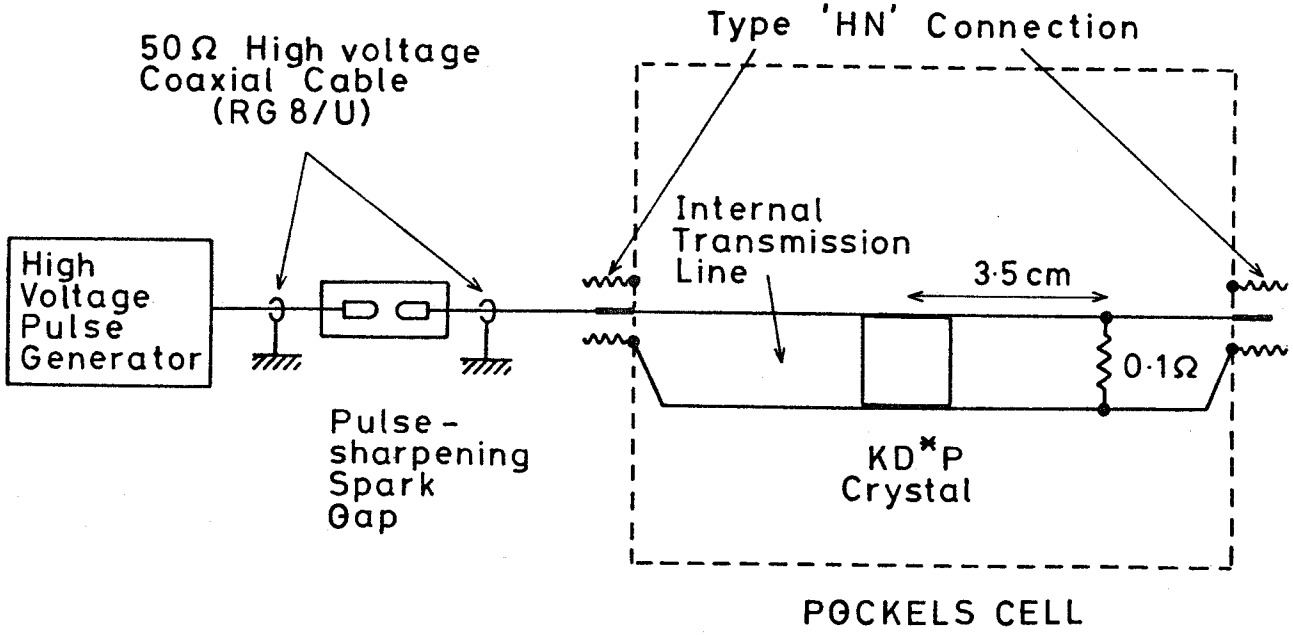

Figure 2.6 : Electrical arrangement of the pulse-forming network driving the electro-optic modulator.

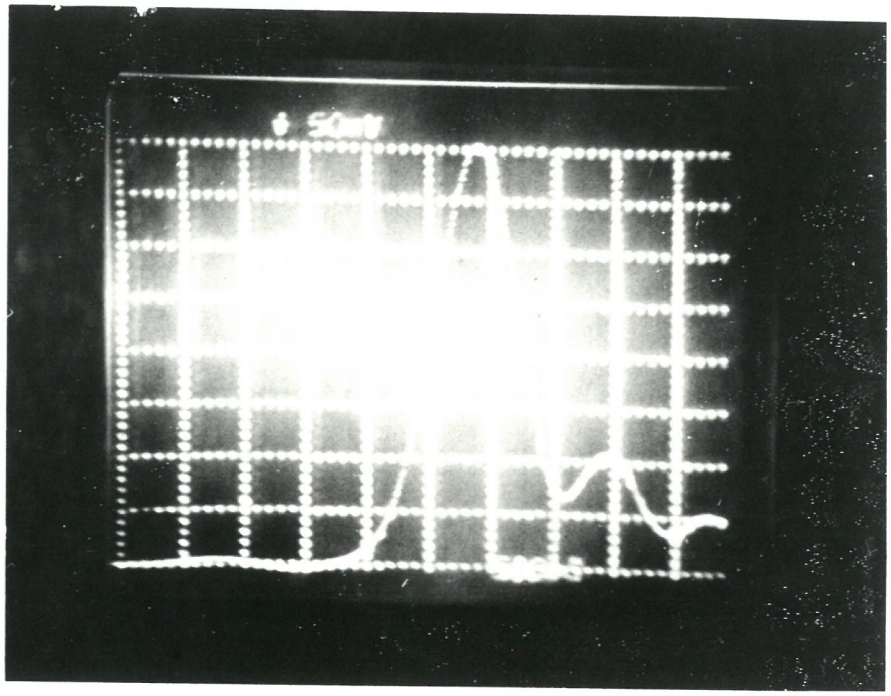

Figure 2.7. Optical pulse produced using the pulse-slicing arrangement shown in figure 2.6 The oscilloscope used to display the pulse is a R 7912 transient digitiser having a bandwidth of 500 MHz. The horizontal scale is 500 ps/div.

CHAPTER 3 - MEASUREMENT OF THE MATERIAL DISPERSION PARAMETER IN OPTICAL FIBRES

3.1 INTRODUCTION

As pointed out in chapter 1, the bandwidth of a multimode fibre is primarily limited by two effects, namely intermode dispersion and material dispersion. The latter type of dispersion is a result of the variation of pulse-delay with wavelength and originates in the frequency-dependence of the refractive index of the glass. Pulse broadening, in this case, occurs when the source carries power in a finite range of wavelengths, since each spectral component has a different propagation velocity. Note that modulation of the source will also broaden the spectrum entering the fibre; this effect is, however, normally negligible compared with the linewidth of unmodulated semiconductor sources.

In principle, the degradation of bandwidth caused by material dispersion can be reduced by using a source with sufficiently narrow spectral width. For instance a light-emitting diode operating at the wavelength 0.85μm would, typically, have a spectral width (full width at half-maximum) of about 40nm[1]. In a germania-doped silica fibre, with a numerical aperture of 0.25, material dispersion acting on such a linewidth would lead to a pulse broadening of 4.3ns km^{-1}. In the same fibre, the output of a semiconductor laser, with a spectral width of 2nm[1,2] would be broadened by 0.21ns km^{-1}, while that of a distributed feedback laser[3] might experience a pulse spreading of only 3ps km^{-1}. Light-emitting diodes are, however, still very attractive for communications systems, because they are cheaper and more reliable than are semiconductor lasers. Furthermore, the emission wavelength of narrow-linewidth devices (e.g. single-mode lasers) has been shown to vary, or 'chirp',[4] and broaden[5] during pulses: these devices can therefore have relatively wide dynamic spectral widths.

An alternative approach is to choose an operating wavelength such that the material dispersion of the glass is negligible[6]. It has

been predicted from refractive-index measurements on bulk samples[7], that material dispersion in fused silica is zero at the wavelength of 1.27μm. Operating at this wavelength can lead to substantial improvements in the information-carrying capacity of fibre systems, particularly if these are driven with l.e.d. sources. It is therefore important, for the design of high-capacity systems, to know the equivalent optimum wavelength in other materials of practical importance, such as germanosilicate or phosphosilicate glasses. In addition, a knowledge of the magnitude of material dispersion at other wavelengths enables the power penalties[8] incurred by not operating at the optimum wavelength to be calculated.

Material dispersion is also an important factor in the design of single-mode fibres. In this type of fibre, all dispersion mechanisms (material, waveguide, and profile dispersion) are related to the variation of pulse delay with wavelength. This variation is a result of changes in refractive index and in the normalised frequency, V, of the waveguide. Of these effects, material dispersion normally dominates, though the waveguide can be designed in such a way that the remaining forms of dispersion substantially alter the wavelength-dependence of chromatic dispersion[9,10]. Thus, the general trend of the chromatic dispersion is set by the material properties of the glasses, but is usually altered to some extent by the waveguide design.

It is clear, therefore, that material dispersion is an important parameter in the design of both multimode and single-mode optical communications systems. When the study described below began, the material dispersion parameter was not accurately known. The work presented in this chapter is therefore concerned with the determination of the value of the material dispersion parameter in optical fibres. Further points of interest include the effect of the thermal history of the glass on its dispersive properties and how the latter are affected by the glass composition and operating wavelength. The influence of the waveguide structure on the measurements is also

examined.

The most important aspect of the work to follow, is probably the determination of the material dispersion parameter and of the wavelength of zero material dispersion as a function of glass-composition for the two most common core dopants for silica-based fibres, namely germania and phosphorous pentoxide.

3.2 THEORY

3.2.1 Mode Transit Time in Step-index Optical Fibres

This section deals, for simplicity, mainly with the special case of step-index fibres. This type of fibre was used wherever possible in the experimental work on material dispersion. Many of the results have, however, general validity, or can easily be extended to graded-index fibres.

We consider a cylindrical fibre with core radius a and refractive indices n_1 and n_2 in the core and cladding, respectively, with $n_1 > n_2$. In general, such a dielectric waveguide will support a number of modes each having characteristic properties such as the distribution of power or group velocity.

The eigenvalue u, of a mode is given by[11]

$$u^2 = a^2(k^2n_1^2 - \beta^2) \qquad (3.1)$$

where β is the longitudinal propagation constant and depends on the core size, the refractive-index profile $n_1(r)$ and the mode number. The wavenumber k is given by $k=2\pi/\lambda$ where λ is the wavelength in free space.

The normalised frequency V, where

$$V = ak(n_1^2-n_2^2)^{1/2} \qquad (3.2)$$

is a measure of the number of modes which can propagate. The propagation constants of the guided modes are restricted to the range:

$$k\, n_2 < \beta < k n_1 \tag{3.3}$$

with the consequence that u is always less than V for guided modes. The group delay of the mode $\tau_{\nu\mu}$ is given by

$$\tau_{\nu\mu} = \frac{L}{c}\frac{d\beta}{dk} = \frac{L}{c} N_{\nu\mu} \tag{3.4}$$

where $N_{\nu\mu}$ is the effective group index. The mode numbering is described in reference 11. In step-index fibres, $N_{\nu\mu}$ is related to the waveguide parameters by[12]:

$$n_{\nu\mu} N_{\nu\mu} = n_1 N_1 \Gamma + n_2 N_2 (1-\Gamma) \tag{3.5}$$

where $n_{\nu\mu}$ is the effective phase index, and N_1 and N_2 are the group indices in the core and the cladding regions. These quantities are related to those already defined by the relations:

$$n_{\nu\mu} = \beta/k \tag{3.6}$$

and

$$N_i = n_i - \lambda \frac{dn_i}{d\lambda} \; ; \quad i = 1,2 \tag{3.7}$$

Γ is the power confinement factor and is equal to the proportion of the power carried by a mode which travels in the core region. Γ varies from 0 (for modes at cut-off) to ~1 for modes very far from cut-off. For illustration, Γ is plotted as a function of V-value for a few low-order modes of a step-index fibre (figure 3.1). We note, that, for a given V, higher-order modes are near to cut-off, so that Γ is very low, while most of the power of low-order modes is confined to the core region.

The effective phase index n can be written in terms of the refractive indices n_1 and n_2 as [12]

$$n = \left[n_1^2\, b + n_2^2\, (1-b)\right]^{1/2} \qquad (3.8)$$

where $b = 1 - u^2/V^2$ is the normalised propagation constant which lies between 0 and 1 in a similar manner to Γ (fig. 3.2). The quantities b and Γ are compared, for the lowest-order mode, in fig. 3.3, where it will be noticed that Γ is always greater than b.

These two waveguide parameters are related by

$$\Gamma = b + \tfrac{1}{2}\, V \frac{db}{dV}. \qquad (3.9)$$

From equation 3.8, the ratios $\frac{n}{n_1}$ and $\frac{n}{n_2}$ are approximated by:

$$\frac{n}{n_1} \simeq 1 - \Delta(1-b) \qquad (3.10)$$

and

$$\frac{n}{n_2} \simeq 1 + \Delta b \qquad (3.11)$$

where the relative index-difference Δ is given by:

$$\Delta = \frac{n_1 - n_2}{n_2} \qquad (3.12)$$

Δ is normally of order 1% in fibres used for optical communications and therefore the relations 3.10 and 3.11 where terms of order Δ^2 and higher have been neglected are quite accurate.

Substituting equations 3.5, 3.10 and 3.11 into equation 3.4 gives the following expression for the group delay of mode ν, μ:

$$\tau_{\nu\mu} = \frac{L}{c}\left[N_1\, \Gamma\, \{1 + \Delta(1 - b)\} + N_2\, (1 - \Gamma)\, (1 + \Delta b)\right] \qquad (3.13)$$

This relation shows explicitly the dependence of group delay on material parameters (N_1, N_2 and Δ) and waveguide parameters (Γ and b). All of these parameters are functions of wavelength. Thus N_1, N_2 and Δ, depend on the dispersive properties of the materials from which the fibre is made whilst the changes in the waveguide parameters

Γ and b originate in the variation of V- value with wavelength.

3.2.2 First-order Material Dispersion

In multimode fibres, a large majority of modes are far from cut-off. As a result, most of the power is carried in the core region and, from figure 3.1 and reference 11, the Γ and b parameters of many modes lie near 1. With the approximation $\Gamma \simeq b \simeq 1$, equation 3.13 is much simplified, and the pulse transit-time is given by:

$$\tau(\lambda) = \frac{L}{c} N_1(\lambda) \qquad (3.14)$$

Equation 3.14 states that the pulse delay in a multimode fibre is almost independent of the properties of the cladding and that the pulse travels more or less as if it were simply in a medium of refractive index n_1.

Sources having a spectral power distribution $S(\lambda)$ are often described by their mean wavelength λ_c and their r.m.s. spectral widths σ_s which are defined [13] as:

$$\lambda_c = \int_o^\infty S(\lambda)\ \lambda d\lambda \qquad (3.15a)$$

and

$$\sigma_s = \left[\int_o^\infty (\lambda-\lambda_c)^2\ S(\lambda)\ d\lambda\right]^{1/2} \qquad (3.15b)$$

when the total power is normalised to unity i.e.:

$$\int_o^\infty S(\lambda)\ d\lambda = 1 \qquad (3.15c)$$

The pulse broadening σ_M caused by material dispersion is obtained by expanding equation 3.14 in a Taylor series about λ_c:

$$\sigma_M = \sigma_s \frac{d\tau(\lambda_c)}{d\lambda} + \frac{\sigma_s^2}{2!} \frac{d^2\tau(\lambda_c)}{d\lambda^2} + \frac{\sigma_s^3}{3!} \frac{d^3\tau(\lambda_c)}{d\lambda^3} + \ldots \qquad (3.16)$$

In many cases of practical importance, it is found that equation 3.16 is dominated by the first term $\sigma_s \frac{d\tau}{d\lambda}$. From equations 3.14 and 3.7 it is found that:

$$\frac{d\tau(\lambda)}{d\lambda} = -\frac{L}{c} \lambda \frac{d^2 n_1}{d\lambda^2} \tag{3.17}$$

Thus if the material dispersion parameter M_1 for the glass forming the core is defined as:

$$M_1(\lambda) = -\frac{\lambda}{c} \frac{d^2 n_1}{d\lambda^2} \tag{3.18}$$

the pulse broadening caused by material dispersion is given to first order by:

$$\sigma_M = M_1(\lambda_c)\, \sigma_s\, L \tag{3.19}$$

Material dispersion therefore increases linearly with the length of the fibre and with the spectral width of the source. It is also proportional to a parameter M_1 which describes the dependence of material dispersion upon the operating wavelength and the characteristics of the transmission medium.

3.2.3 Refractive-index of Optical Glasses

Potential fibre materials are, of necessity, highly transparent in the vicinity of the operating wavelength. This, in practice, means that the region of transmission lies somewhere between the electronic absorption bands (in the ultra-violet) and the vibrational absorption bands (in the infra-red). The absorption bands must be well-separated from the operating wavelength and therefore the intrinsic absorption of the material is low. However, the absorption bands still exert considerable influence on the refractive index in the transparent region via the Kramers-Kronig relation[14]. Thus the refractive-index tends to decrease monotonically from the ultra-violet region to the infra-red as shown schematically in figure 3.4.

The refractive-index can be approximated by the Sellmeier equation which represents each absorption band by a single resonance and neglects the residual absorbance in the transparent region:

$$n^2 - 1 = \sum_i \frac{A_i \lambda^2}{\lambda^2 - \ell_i^2} \qquad (3.20)$$

Here A_i and ℓ_i represent the equivalent oscillator strengths and wavelengths, respectively. The positions ℓ_i of these absorption bands are dictated by the atomic weight of the elements in the glass molecule, their spatial arrangements and the nature of the chemical bonds. The values of the coefficients A_i and ℓ_i which have been published for various materials are usually obtained, however, by a least-squares fit[15] of equation 3.20 to measured refractive index data and thus only have a qualitative physical interpretation. Nevertheless, it is often found that ℓ_i coefficients do correspond to the position of an absorption band. In addition, the Sellmeier equation is a very useful means of interpolating refractive index data. As a specific instance, let us take the case of fused silica in bulk form. It has been found[7] that measured values of the refractive-index can be fitted accurately by a three-term Sellmeier equation with two ultra-violet lines (at 0.11 μm and 0.06 μm) and one infra-red line (at 9.9 μm).

As a result of the existence of electronic and vibrational absorption bands, the refractive-index/wavelength function in general has a point of inflection in the transparent region, i.e. there exists a wavelength at which the second derivative $\frac{d^2n}{d\lambda^2}$ of refractive index is zero. At this point, as illustrated in figure 3.4, the transit time of an optical pulse does not vary with wavelength and therefore the first-order material-dispersion parameter is zero. Operation at this wavelength can result in major improvements in the bandwidth of an optical fibre.

3.2.4 Higher-order Material Dispersion

In Section 3.2.2 it is shown that the pulse broadening due to material dispersion is, to a first approximation, proportional to the derivative of pulse delay with wavelength. It is clear that near the wavelength of zero material dispersion, higher-order terms in the Taylor expansion of equation 3.14 must be considered.

The importance of the higher derivatives of $\tau(\lambda)$ was pointed out by Kapron[16], who showed that they lead to an ultimate limitation of the information-carrying capacity of single-mode fibres. The values of the first two derivatives of $\tau(\lambda)$ (which appear in the RHS of equation 3.16) are plotted as a function of wavelength in figure 3.5. The data were obtained from measurements of the refractive index of pure silica[7]. Note that at most wavelengths, for typical source spectral widths (σ_s < 50 nm), first-order material dispersion dominates, except in the vicinity of 1272 nm, where $\frac{d\tau}{d\lambda}$ vanishes. In the latter wavelength region the second-order term becomes the major contribution to material dispersion. The contribution of the third derivative $\frac{d^3\tau}{d\lambda^3}$ is small compared with that of the first two derivatives at all wavelengths.

Since second-order material dispersion is proportional to source linewidth squared, it can only be compared to the first-order term for a specific spectral width. Figure 3.6 therefore gives the effective material dispersion parameter as a function of wavelength, for a number of source spectral widths. The effective material dispersion parameter is defined as the ratio of intramodal broadening to source linewidth. At the wavelength of zero material dispersion λ_o, these curves are equal to the contribution of the second term in equation 3.16. With departure from λ_o all curves tend towards the dotted lines which represent the absolute value of the first-order material-dispersion parameter.

Second-order chromatic dispersion is particularly important in very long, high bit-rate links using light-emitting diodes and operating at the wavelength of zero material dispersion. Light-emitting diodes

for this wavelength region exhibit very wide spectral widths[17, 18] (with full r.m.s. spectral widths $2\sigma_s$ as large as 80 - 100 nm), which can lead to intramodal dispersion ($2\sigma_m$) as large as 300 ps/km at the optimum wavelength. This value is roughly equivalent to the intermodal pulse broadening in the best presently available multimode fibres and the bandwidth of the fibre is thus limited by material dispersion[18]. In addition, if we consider the length-dependence of both dispersion mechanisms, we find that intramodal broadening is linear with fibre length. On the other hand, if mode-coupling is present[19], or if fibres with slightly different profiles are jointed to form a long link[20], intermode dispersion does not increase as fast as if its length-dependence were linear. In such circumstances, intramodal dispersion may well dominate even at the wavelength of zero material dispersion.

A further effect which must be considered in relation to pulse-broadening in long links, is the spectral filtering of the source by the fibre. The attenuation/wavelength function of ultra-low-loss fibres appears to reveal regions where the loss is low, and relatively independent of wavelength. Stewart[21] has pointed out, however, that the transmission of long fibre links has only relatively narrow spectral windows, since small differences in attenuation between neighbouring wavelengths may be multiplied by large fibre lengths and result in markedly different values of transmission. Thus the effective linewidth of a source and particularly of an l.e.d. measured at the fibre output is more a function of the fibre than of the source and is usually narrower than if it were measured at the launching end. In addition, the peak wavelength may also be dictated by the fibre transmission.

3.3. MEASUREMENT OF THE MATERIAL-DISPERSION PARAMETER

The following three equations (which have been introduced in section 3.2) can be used as a basis for the measurement of the material-dispersion parameter M_1:

$$M_1 = -\frac{\lambda}{c}\frac{d^2 n_1}{d\lambda^2} \qquad (a)$$

$$\sigma_M = M_1 \sigma_s L \qquad (b)$$

and

$$M_1(\lambda) = \frac{1}{L}\frac{d\tau}{d\lambda} = \frac{1}{c}\frac{dN_1}{d\lambda} \qquad (c)$$

As suggested by equation (a), the material dispersion parameter may be deduced from wavelength-dependent measurements of the phase index n_1 by two successive differentiations[7,22-24]. Another approach (b) is to measure the pulse-broadening caused by material dispersion directly.[25]

A third possibility (c) is to measure the variation of pulse delay[26-30] with wavelength and to obtain the material dispersion parameter by differentiation. The three methods are outlined and briefly discussed in subsection 3.3.1. The pulse-delay technique, which was used in the present study is then described in detail in the rest of this chapter.

3.3.1 Review of Techniques for Material-dispersion Measurements

3.3.1.1 The bulk-sample method

The refractive-index of prism-shaped glass samples can be measured very accurately (a few parts in 10^6) using the minimum deviation method[7]. If a number of such measurements are made using the principal spectral lines of common vapour lamps and the results are least-squares fitted to a three-term Sellmeier equation,[15] then the material-dispersion parameter can be deduced by two successive differentiations. The advantages of the bulk-sample method are:

(a) The composition of the glass can be determined by wet chemical analysis.

(b) The material dispersion of a new glass can be evaluated before samples are available having sufficient purity to enable direct measurements in long fibres. This may, however, be of dubious

value since the impurities which cause the high attenuation could also distort the wavelength-dependence of refractive-index through anomalous dispersion[14].

(c) The method is not affected by effects which might occur in waveguides, such as waveguide dispersion, material dispersion in the cladding or differential mode attenuation.

(d) Material dispersion can be measured in cladding glasses. This is a major advantage of the bulk-sample method since neither of the other techniques can easily be used to examine cladding materials.

The bulk-sample method was not used in the present work, however, because it does have a few important drawbacks:

(a) It requires much careful sample-preparation; the glass must be very homogeneous and the surfaces must be flat and highly polished.

(b) The glasses used for optical fibres are often made by the c.v.d. process and may be difficult to obtain in bulk form.

(c) The refractive-index could be affected by the thermal history[31] and the stress levels in the sample[32]. An optical fibre is cooled from above 2000°C to room temperature in less than one second, whereas glass in bulk form cools much more slowly, even if it is deliberately chilled. Moreover, the difference in expansion coefficients between the core- and cladding-glasses causes a high level of stress[32] which inevitably modifies the refractive-index, via the stress-optical effect, and could also affect the dispersion of the glass in fibre form. It is therefore felt that measurements on bulk samples may not accurately reflect the effects which take place in a fibre and that measurements directly on fibres are thus essential.

(d) The material dispersion parameter is inferred by differentiating the refractive-index data twice and thus a very high degree of experimental accuracy is required. A very wide wavelength range is also necessary if the wavelength of zero material dispersion is to be determined with adequate precision.

3.3.1.2 The 'direct' technique

Tanifuji and Ikeda[25] have reported a frequency-domain technique for the determination of material dispersion in fibres. They measure the baseband frequency response $P_o(z, \omega)$ of their fibres with an l.e.d. of broad spectral width and repeat the measurement, having filtered their source with a narrow-band interference-filter. The material dispersion is inferred from the ratio $P_2(z, \omega) = P_o/P_1$ of the two transfer functions thus obtained.

The method consists essentially of a deconvolution of the intermodal dispersion from the measured fibre bandwidth. The fundamental assumption is that intermodal broadening is independent of source linewidth. Olshansky and Keck[13] have shown that this is true to first order only. In addition, detailed knowledge of the spectral response of the source at each wavelength is required, as is some means of altering the linewidth without shifting the centre wavelength. The inference of material dispersion from the baseband frequency response is complex unless assumptions regarding the spectral distribution of the source are made[25] and these assumptions may compromise the accuracy of the procedure.

Finally the method is fundamentally inaccurate. Thus results obtained on graded-index fibres cannot be interpreted in terms of the properties of the core and cladding materials since the power travels in a range of glass compositions. The mean composition, and hence the measured group index, depends on the excitation conditions, and is thus rather poorly defined. The use of step-index fibres removes this limitation, but the accuracy is then inevitably degraded since the intermode dispersion becomes much greater than material dispersion. Thus at the -3dB frequency of $P_2(z, \omega)$, which represents the limitation to bandwidth caused by material dispersion, the baseband signal may be reduced by up to -20 or -30dB relatively to its value at zero frequency. Any errors in P_o or P_1 are therefore multiplied by the ratio P_2/P_o, i.e. 20 to 30 dB.

In spite of these drawbacks, the method is interesting and it may be useful for measuring material dispersion in, for instance, links driven with l.e.d.'s and which are already installed. However, it is not applicable to the systematic study of the wavelength-dependence of material dispersion in many types of glass.

3.3.1.3 The pulse-delay technique

In multimode fibres, the pulse-propagation delay is, to a very good approximation[33], proportional to the group index N_1 of the fibre core. Thus measurements over a wide range of wavelengths will enable the material dispersion parameter to be found from the slope of the pulse delay/wavelength curve.

The technique is very accurate and the results are easily processed to obtain the material dispersion parameter. In addition, neither the linewidth of the source nor the pulse shape are critical to the measurement. Moreover, waveguide effects cause only small uncertainties in the measured dispersion, provided that a fibre with a sufficiently large V-value is chosen (see sec. 3.3.4). Finally, the data is taken directly on fibre samples and the chilled state of the glass is reflected in the resulting values of dispersion. The errors which might occur in measurements on bulk-samples and which arise from the thermal history of the glasses are thus avoided.

The main disadvantages of the pulse-delay technique are that fibres with low losses are required and that it is difficult to measure the dispersion of cladding materials. The technique was, however, used in the present work because it is much better suited to a systematic study of material dispersion than the 'direct' technique and it appeared to be more reliable and accurate than the bulk-sample method.

3.3.2 Determination of the Material Dispersion Parameter by a Pulse-delay Technique

Several experimental arrangements based on the pulse-delay method have been devised here, at Southampton, and elsewhere. The implementation of the technique on the dye-laser/O.P.O. system is discussed in the present sub-section and a brief description of other possible arrangements is then given.

3.3.2.1 Implementation using the dye-laser/O.P.O. system

The dye-laser system already discussed in Chapter 2 forms the basis of the experiment, the arrangement of which is sketched in figure 3.7. The optical parametric oscillator (O.P.O.) is pumped by the dye-laser and produces pulses of 1 μs duration in the wavelength region: 0.76 - 2.6 μm. The output of the dye-laser itself can be tuned to any wavelength in the visible spectrum. The electro-optic shutter reduces the pulse width to approximately 1 ns at half-height. Launching into the fibre is effected by a lens of long focal length (10cm) in order to ensure that the power is carried predominantly by low-order modes. At the fibre output, the pulse is detected by a Ge avalanche photodiode, and the signal is fed to the transient digitiser.

The high-voltage pulse which activates the optical shutter also triggers the time-delay generator. The latter provides a pulse which is delayed with respect to the triggering event by a time corresponding to the propagation delay of the fibre. Thus the time-base of the transient digitiser is triggered as the optical pulse emerges from the fibre; the signal can therefore be displayed with a very fast sweep-speed(0.5 or 1.0 ns/div) and its time-position determined with high accuracy.

The O.P.O. is tuned after each measurement and the whole process is repeated at wavelength intervals of, typically, 5nm over

as wide a spectral range as possible. The latter is usually limited by the attenuation of the fibre but in a low-loss germania-doped fibre, the region 0.6 - 1.8 μm can usually be covered. Beyond 1.8 μm, the transmission of the Pockels cell and the response of the germanium detector decrease rapidly.

There are two main limitations to the accuracy of this technique, namely drift and jitter. The latter is caused primarily by fluctuations in pulse amplitude and rise-time at the output of the spark-gap which indirectly triggers the oscilloscope. The variation in the position of the leading edge of the optical pulse is approximately ± 300 ps. The problem is alleviated to some extent by the use of the storage monitor on the transient-digitiser. The position of a number of pulses is averaged by eye and the resolution is thus improved. It is found that the standard deviation of the readings taken in this way is ∿ 150 ps.

Drift is a much more serious problem since it is a systematic error. The variation of pulse-delay over the entire wavelength-range is less than 2% of the total transit-time, i.e. ∿ 80ns in 5000 ns for a 1km fibre. Thus drift should be kept below 500 ps and the relative stability should therefore be better than 1 part in 10^4. It must be remembered in this context, that the time delay data must be differentiated, a procedure which tends to enhance experimental errors.

Delay drift plagued the early measurements and its origins were therefore carefully investigated. The two main sources of drift arise in the fibre itself and in the instrumentation. The latter type of drift is common to most experiments and is caused by variations in the characteristics of electronic components due, for example, to temperature changes. The first precaution taken was to calibrate the insertion delay of the digital delay-generator (Berkeley Nucleonics Corp., Model 7030) with a time-interval counter after each measurement. It was found that the other instruments do not drift significantly

once they have warmed up. A more definitive cure is described in Section 3.3.2.2.

The drift in the fibre arises because the group delay is sensitive to stress via the elongation and via the stress-optical effect which induce changes in, respectively, the length and the refractive index of the waveguide. Temperature changes also affect the time delay mainly through changes in refractive-index. The resulting stability problems have been investigated in detail[34] and are described in Chapter 5.

The temperature dependence of pulse-delay was found to be 35.7 $ps.km^{-1}K^{-1}$ [34]. This is sufficient to cause a measurable drift, as a 10 K temperature change throughout a day is not uncommon in the laboratory. Moreover, the fibres are subjected to a varying amount of longitudinal stress resulting from the thermal expansion of the plastic drums which they are wound on. This in turn causes variations in pulse-delay.

The sensitivity of pulse transit-time to temperature is eliminated by placing the fibre, still wound on its drum, in a commercial freezer. This causes the drum to contract and the fibre to become loose since the expansion coefficient of fused silica is negligible in comparison to that of most plastics. The pulse-delay is thus no longer affected by stress; moreover, the temperature is stabilised and therefore no longer causes the refractive-index to fluctuate.

3.3.2.2 Refinements in the measurement technique

The optical arrangement shown in figure 3.7 has been modified recently and as a result the sensitivity and, more importantly the stability, of the pulse-delay measurement are improved. Unfortunately, the insertion loss is also increased and, as a result, the wavelength range can be reduced. Figure 3.8 shows the modified experimental arrangement. The laser pulse passes through a 50% beamsplitter and

and is launched into a ∿ 25m section of fibre which is butted against the fibre to be measured. The butt-joint consists of a pair of accurately-aligned v-shaped grooves, one of which is mounted on an x-y-z translation stage. There is no index-matching fluid and a Fresnel reflection amounting to 8% of the incident power is therefore sent back from the joint to the launching end where it is directed onto the detector by the beamsplitter. This pulse provides a time-reference corresponding to the entry of the remaining 92% of the pulse-energy into the test fibre. An aluminium mirror is butted against the far end of the test fibre, which is held in a special jig. The bulk of the power is thus reflected back down the fibre and eventually reaches the avalanche photodiode. The arrival time of the reference pulse and that returned from the mirror are measured using the digital-delay generator and the transient digitiser. The difference between these readings gives twice the pulse-delay in the fibre.

This experimental procedure eliminates the effect of trigger-delay drifts in the electronic equipment since these are common to both measurements. For the same reason, the material dispersion of the short, launch fibre is of no importance. Note that the launch fibre serves as a delay-line and prevents the reference pulse from reaching the oscilloscope before the minimum insertion-delay of the instruments (∿ 150ns) has elapsed.

The back-reflection technique improves the sensitivity of the experiment, since the effective fibre-length is doubled. A further considerable advantage is that the pulse transit-time which is measured applies to a well-defined section of fibre, namely from the butt-coupler to the aluminium mirror. Thus the absolute pulse-delay of the fibre is determined, in addition to the relative delay at various wavelengths. By contrast, when the arrangement of fig. 3.7 is used, uncalibrated delays are added to the result and must be compensated for by a tedious and inaccurate procedure. If, therefore, the length of the fibre is accurately known, the group-index may be deduced. This information is of great interest, since it allows

refractive-index comparisons between fibre- and bulk-sample measurements to be made. Thereby, some insight is gained into the influence of the thermal history of the sample on its refractive index. Ideally, the launch fibre should be taken from the test fibre, or from one with similar characteristics to ensure high efficiency and low mode conversion at the joint. The quality of the fibre end is important for the same reason. The well-known method of scratching the fibre with a sharp blade and bending it under tension was found to give satisfactory results as confirmed by observation of the far-field pattern.

The increased insertion loss is a drawback of the back-reflection technique. The beamsplitter attenuates the signal by at least 6dB, and the efficiency of the aluminium mirror is approximately 80%. In addition, the attenuation of the fibre itself is effectively doubled.

The arrangement shown in figure 3.9 can be used if the attenuation is too large to allow two passes through the fibre. It is also very useful for measurements on single-mode fibres,where it is usually difficult to launch efficiently back into the fibre the light emerging at the remote end.

Referring to fig. 3.9, the laser pulse is sampled by a 10% beamsplitter which directs a portion of the power into a section of graded-index fibre, the function of which is purely to delay the optical signal;graded-index fibres are very good delay lines, with delay x bandwidth products greater than 5000. The output of the delay-line is detected by the germanium photodiode and fed to the oscilloscope. The portion of the pulse which is transmitted by the beamsplitter is launched into the fibre under test. At the output of this fibre, the pulse is collimated, travels again through the beamsplitter and is launched into the fibre delay-line. The detector thus receives the reference pulse and the pulse which has travelled through the test fibre. The time-separation of these signals is given by the sum of the pulse delay in the test fibre and the small insertion delay of the non-common optical path in air. The latter delay is normally of the order of 1.2 ns and can be calibrated very accurately.

This arrangement is somewhat more complex and difficult to align than the back-reflection layout. It has, however, much less insertion loss and the same stability.

Recently the time delay-generator was replaced by a Hewlett-Packard time-synthesiser (model 5395A). The timing of this instrument is controlled by a quartz crystal oscillator and has extremely good long-term stability ($\sim$ 1 part in 10^9 per day). It is therefore no longer necessary to calibrate the insertion delay of the instrument after each reading.

3.3.2.3 Other implementations of the pulse-delay technique

All of the experimental arrangements described below are designed for the measurement of material dispersion or of chromatic dispersion from the wavelength dependence of pulse delay. The main differences between the methods lie in the technique used for the determination of pulse delay.

(a) The two-pulse technique

The problem of pulse jitter and delay drift has already been mentioned and it has been shown that the use of a time reference greatly improves the stability of pulse-delay measurements. An alternative method is to use a wavelength reference[26,27]. In this case two pulses at different wavelengths are launched into the fibre and the delay-difference between them is measured at the output. One wavelength is held constant and provides a reference, while the other is tuned to cover a wide wavelength range. Both jitter and drift are eliminated, since they affect both pulses in an identical manner.

This technique has been implemented with the dye-laser system. In this experiment the O.P.O. was tuned and the wavelength of the dye-laser was held constant to provide a reference.

The oscilloscope traces of figure 3.10 show the result of the measurement at several wavelengths. In each photograph, the right-hand pulse is generated by the dye-laser, at the wavelength 0.606μm. The left-hand pulse is emitted by the O.P.O. and is at a different wavelength in each picture. The output of the dye-laser and of the O.P.O. are gated simultaneously by the Pockels cell. The separation between the pulses at the two wavelengths is a vivid demonstration of the material dispersion phenomenon. As the O.P.O. is tuned to longer wavelengths, the delay between the pulses increases until the wavelength of zero material dispersion, in this case 1272 nm, is reached and, thereafter, the separation decreases again. A large number of similar photographs are normally taken over as wide a wavelength range as possible. The variation of group delay with wavelength is thus determined, relative to the delay at 0.606μm.

The output-wavelength and state of polarisation of the dye-laser and the O.P.O. are different. As a result, a high insertion loss is suffered when both beams are pulse-sliced simultaneously, since several optical components must be added in order to rotate the polarisation of the dye-laser beam without affecting that of the infrared light. In addition, there are a number of critical alignments of optical components which require adjustment after each mirror change on the O.P.O. In spite of the increased complexity of the experiment, the resolution is not as high as that achieved by measuring absolute pulse transit time. It would appear that the accuracy of the two-pulse technique in its present form is limited by the linearity of the time-base of the oscilloscope. This technique was therefore not pursued any further during the present study.

(b) The 'difference' method

This technique was reported by Daikoku and Sugimura[35]. The output of a temperature tunable O.P.O. is sinusoidally modulated at a frequency of 840MHz, and transmitted through the fibre. The phase of the modulation at the fibre output is directly related to the group-delay. Thus, if the excitation wavelength is changed, the

phase of the photo-detector signal is shifted. The phase shift is measured by displaying the input and output modulation signals on a sampling oscilloscope as a Lissajous figure, the shape of which is adjusted using a variable delay-line. The accuracy on the difference in group delay of pulses at two neighbouring wavelengths is claimed to be excellent. It must be pointed out, however, that the variance of the dispersion results[36] published so far appears to be greater than is normally observed in measurements on the dye-laser system.

The method has been used for single-mode fibres only, though there is no intrinsic reason why it cannot be applied to multimode fibres. The bandwidth of step-index multimode fibres might limit the applicability of the technique to material-dispersion measurements.

(c) The pulse-synchronisation technique

The dispersion-tuned Raman-fibre-laser[37] has led to a very elegant technique for measuring chromatic dispersion in single-mode fibres. A continuous train of pulses generated by a mode-locked Nd: YAG laser is launched into a single-mode fibre. The power-density in such a fibre causes multiple order stimulated Raman scattering. The gain of the frequency-shifted Stokes signals can be sufficient for oscillation to occur if the fibre is placed in a resonator cavity. The Stokes outputs are separated with prisms and each is provided with an independent feedback mirror. A Stokes signal has maximum gain when the duration of one of its cavity round-trips is an integral multiple of the pulse repetition frequency. If this is the case, pump and Stokes pulses coincide at the launching end of the fibre. In the absence of any other tuning mechanism, the wavelength which is generated corresponds to the peak of the gain curve. The fibre-Raman laser is thus tuned by altering the position of the output mirrors, which modifies the duration of a cavity round-trip. Conversely, the tuning curve of the device is a direct measure of the pulse-delay as a function of wavelength, since the mirror position is related to the pulse transit-time in the fibre at a given wavelength.

The method is extremely accurate since a translation of a mirror by, say, 3mm will lead to a change in pulse-delay of only 10 ps for a single pass and the results shown in reference 37 show very little scatter. It may well be that in this experiment, the accuracy is limited by the determination, not of the pulse delay, but of the peak wavelength of the Stokes signal since the output linewidth may be rather broad. The technique is unfortunately limited to single-mode fibres, which in addition should have very low loss. For fibres with even a moderate OH^- absorption band at 1.4μm, the wavelength range does not extend much beyond 1.3μm[38].

3.3.3 Analysis of Pulse-delay Data

3.3.3.1 Inference of the material dispersion parameter

The group delay in a multimode step-index fibre is given by:

$$\tau(\lambda) = \frac{L}{c}\left[n_1(\lambda) - \lambda \frac{dn_1(\lambda)}{d\lambda}\right] \qquad \text{(cf. equ. 3.14)}$$

Since the wavelength-dependence of refractive index is accurately modelled by a three-term Sellmeier equation (see sub-section 3.2.3), the function $\tau(\lambda)$ can be described by an expression incorporating the terms of the Sellmeier equation and their derivatives. Such an expression is however rather complex. Moreover the coefficients A_i and ℓ_i cannot be obtained by least-squares fitting pulse-delay data.

The ℓ_i coefficients (which have dimensions of length) are markedly different from the values of wavelength of interest (0.6μm to 1.8μm). As a result, a series expansion of equation 3.20 and its derivative is likely to be accurate with a moderate number of terms. It turns out that this leads to even-order, positive and negative powers of wavelength only and, retaining terms to the fourth power, the wavelength-dependence of pulse-delay may thus be modelled by an expression of the form:

$$\tau(\lambda) = a_{-4}\,\lambda^{-4} + a_{-2}\,\lambda^{-2} + a_o + a_2\lambda^2 + a_4\lambda^4 \qquad (3.21)$$

Although coefficients a_{-4} to a_4 are not directly related to the Sellmeier coefficients, a_{-2} and a_{-4} originate from the u.v. lines, and a_2 and a_4 from the infra-red line; a_o is determined by a combination of all three absorption bands. The coefficients a_{-4} to a_4 can readily be estimated from the measured values τ_i of pulse delay at wavelengths λ_i by least-squares fitting and are the solution of the following set of simultaneous equations.

$$\begin{bmatrix} \Sigma\lambda_i^{-8} & \Sigma\lambda_i^{-6} & \Sigma\lambda_i^{-4} & \Sigma\lambda_i^{-2} & n \\ \Sigma\lambda_i^{-6} & \Sigma\lambda_i^{-4} & \Sigma\lambda_i^{-2} & n & \Sigma\lambda^2 \\ \Sigma\lambda_i^{-4} & \Sigma\lambda_i^{-2} & n & \Sigma\lambda_i^{2} & \Sigma\lambda_i^{4} \\ \Sigma\lambda_i^{-2} & n & \Sigma\lambda_i^{2} & \Sigma\lambda_i^{4} & \Sigma\lambda_i^{6} \\ n & \Sigma\lambda_i^{2} & \Sigma\lambda_i^{4} & \Sigma\lambda_i^{6} & \Sigma\lambda_i^{8} \end{bmatrix} \begin{bmatrix} a_{-4} \\ a_{-2} \\ a_o \\ a_2 \\ a_4 \end{bmatrix} = \begin{bmatrix} \Sigma\tau_i\lambda_i^{-4} \\ \Sigma\tau_i\lambda_i^{-2} \\ \Sigma\tau_i \\ \Sigma\tau_i\lambda_i^{2} \\ \Sigma\tau_i\lambda_i^{4} \end{bmatrix} \qquad (3.22)$$

where the summation extends over all pairs of values (λ_i, τ_i). Note that the 5 x 5 matrix (which will be referred to as $[M]$) in the LHS of equation (3.22) is symmetric about the descending diagonal and independent of the measured time delays.

The material dispersion parameter $M_1(\lambda)$ and the wavelength of zero material dispersion λ_o can be calculated from the fitted coefficients.

It is important to evaluate the accuracy of this fitting procedure to ensure that the results are valid. Pulse-delay values for pure silica were therefore calculated from published Sellmeier

coefficients[7] and processed using equation (3.22). Sixty pairs of values in the spectral range 550nm - 1750nm were used in this simulation which therefore covered much the same wavelength region as the experimental data. It was found that values of $\tau(\lambda)$ calculated from the fitted coefficients and those obtained directly from the Sellmeier equation agreed to within 1ps km^{-1} while, for the material dispersion parameter, the corresponding figure is 0.2ps nm^{-1} km^{-1}. The wavelengths of zero material dispersion given by the two methods differed by 0.03 nm. The accuracy of the series expansion naturally improves if more terms are included. The four-term expansion, however, provides adequate accuracy for the analysis of experimental data, since the scatter of the latter is at least one order of magnitude greater than the error introduced by the fitting procedure. On the other hand, it might be necessary to take further terms into account if the wavelength - range were extended, or the accuracy of the pulse-delay measurement improved.

3.3.3.2 Error analysis

The least-squares fitting procedure described in the previous section serves two main functions. Firstly, it extracts the useful information from the results of an entire wavelength scan and presents it in the form of a small number of coefficients. A simple, analytic expression for the wavelength dependence of group delay or material dispersion is thus provided.

Secondly, the fitting procedure reduces the influence of scatter in the pulse-delay measurements on the estimate of material dispersion. The assumption is made that the pulse-delay varies only slowly with wavelength and this is reflected in the form of the fitting function. Any rapid variations of pulse-delay with wavelength are therefore interpreted as random experimental errors. These non-systematic errors should, in principle, average to zero and the individual transit-time measurements are thus effectively smoothed. The fitted values obtained from the coefficients a_{-4} to a_4 are therefore more accurate

than the individual data, provided that a sufficiently large number of readings are taken.

The object of the present analysis is to estimate confidence intervals for the group delay, the material dispersion parameter and the wavelength of zero material dispersion.

From equation 3.21, the variance of $\tau(\lambda)$ may be written as:

$$\begin{aligned}\text{var}\,[\tau(\lambda)] = {} & \text{var}\,(a_{-4})\,\lambda^{-8} + 2\,\text{cov}\,(a_{-4}, a_{-2})\,\lambda^{-6} \\ & + [\text{var}\,(a_{-2}) + 2\,\text{cov}\,(a_{-4}, a_o)]\,\lambda^{-4} \\ & + 2[\text{cov}(a_{-4}, a_2) + \text{cov}(a_{-2}, a_o)]\,\lambda^{-2} + \text{var}(a_o) + 2\text{cov}(a_{-4}, a_4) \\ & + 2\,\text{cov}(a_{-2}, a_2) + 2[\text{cov}(a_4, a_{-2}) + \text{cov}(a_2, a_o)]\,\lambda^{2} \\ & + [\text{var}\,(a_2) + 2\,\text{cov}(a_4, a_o)]\,\lambda^{4} + 2\,\text{cov}(a_4, a_2)\,\lambda^{6} \\ & + \text{var}\,(a_4)\,\lambda^{8} \end{aligned} \tag{3.23}$$

Guest[39] has shown that for a number of functions, including that defined in equation 3.21, the variances and covariances of the fitted coefficients are proportional to the elements of the inverse of matrix $[M]$ which we shall refer to as $[\chi]$. Thus the variances of the fitted coefficients are proportional to the diagonal elements of $[\chi]$:

$$\left.\begin{aligned} \text{var}\,(a_{-4}) &= \chi_{11}\,.R^2 \\ \text{var}\,(a_{-2}) &= \chi_{22}\,.R^2 \\ \text{var}\,(a_o) &= \chi_{33}\,.R^2 \\ \text{var}\,(a_2) &= \chi_{44}\,.R^2 \\ \text{var}\,(a_4) &= \chi_{55}\,.R^2 \end{aligned}\right\} \tag{3.24}$$

Here R is the mean residual and is defined as:

$$(n-6)\ R^2 = \sum_{i=1}^{n} \left[\tau_i - (a_{-4}\,\lambda_i^{-4} + a_{-2}\,\lambda_i^{-2} + a_o + a_2\lambda_i^2 + a_4\lambda_i^4)\right]^2 \quad (3.25)$$

where n is the number of pairs of values (τ_i, λ_i) which $\tau(\lambda)$ has been fitted to. R is an estimate of the scatter of the readings and is normally in the range 100-300ps.

Similarly, the covariances of the coefficients a_{-4} to a_4 are given by:

$$\begin{aligned}
&\text{cov}\,(a_o, a_{-4}) = \text{cov}(a_{-4}, a_o) = \chi_{1,3}\,.R^2 \\
&\text{cov}\,(a_o, a_{-2}) = \text{cov}(a_{-2}, a_o) = \chi_{3,2}\,.R^2 \\
&\ldots\ldots \qquad\qquad (3.26) \\
&\ldots\ldots \\
&\text{cov}\,(a_2, a_4) = \text{cov}(a_4, a_2) = \chi_{4,5}\,.R^2
\end{aligned}$$

The variance of the fitted function $\tau(\lambda)$ may thus be evaluated at any wavelength from the mean residual R and the elements of the matrix $[\chi]$. In addition, the variance of the inferred value of material dispersion $M_1(\lambda)$ can be calculated from an expression similar to the right-hand side of equation 3.23. In particular, the variance of $M_1(\lambda)$ at the wavelength λ_o of zero material dispersion, in conjunction with $\frac{dM_1}{d\lambda}$ (which can be calculated from the fitted coefficients) yields an estimate of the accuracy of λ_o.

A typical plot of the standard deviation of $\tau(\lambda)$ and $M_1(\lambda)$ normalised to the mean residual is shown in fig. 3.11. The readings were made in the wavelength-regions: 590-630nm and 800-1820nm in intervals of 5nm. The standard deviation of $\tau(\lambda)$ over the range 600-1800nm is about one order of magnitude less than the mean residual and this demonstrates the ability of the fitting procedure to smooth the data. At the edges of the wavelength range of the data, however, the uncertainty in $\tau(\lambda)$ increases. It is therefore important

that as wide a wavelength region as possible be covered, in order that the useful, central part of the scan include all the wavelengths of interest. The extrapolation of $\tau(\lambda)$ outside the wavelength range 600-1800nm is clearly inaccurate. The standard deviation of M_1 is of the order of 10^{-3} x R (in units of ps. nm^{-1}) for this set of data. We note, however that the spectral region over which $M_1(\lambda)$ is accurately estimated is narrower by about 200nm than the wavelength range over which measurements were made.

This error analysis gives a measure of the self-consistency of the data; it does not reveal the presence of systematic errors in the measurement which could be caused, for instance, by drift in the timing circuitry, or by differential mode attenuation in the vicinity of impurity absorption bands. Further calculations have shown that the sensitivity of the fitted function $\tau(\lambda)$ to a measurement error is greatest near the ends of the wavelength range. Systematic errors are thus particularly to be avoided at these wavelengths.

3.3.4 Influence of Waveguide Effects on Pulse-delay Measurements of Material Dispersion

The technique for the measurement of material dispersion which has been described in Sec. 3.3.2 is based on the determination of the pulse transit-time in a multimode fibre as a function of wavelength. It is then assumed that the chromatic dispersion thus found is equal to the material dispersion of the glass forming the fibre core, i.e. that the transit-time is unaffected by the waveguide structure. It has been suggested[9], however, that this approximation is not valid, and that it is the origin of the discrepancy[40] between measurements on bulk samples[24] and on step-index multimode fibres[29].

The purpose of the present sub-section is, therefore, to clarify this point by modelling the pulse-delay experiment and evaluating the influence of the waveguide structure on the predicted values of material dispersion. As suggested in reference 9, the

chromatic dispersion of any individual mode of the fibre may be calculated and compared with the pure material dispersion in the core region. We shall show, however, that the dispersion of individual modes does not, by itself, accurately describe the total chromatic dispersion of pulses containing power in many modes, i.e. that the dispersive behaviour of the individual modes is quite different from that of their temporal envelope. Therefore, the pulse transit-time is calculated as a function of wavelength by combining the group delay of all propagating modes. The chromatic dispersion is then evaluated and the effect of the waveguide structure is assessed.

3.3.4.1 Chromatic dispersion of individual modes in multimode, step-index fibres

The relationship between the parameters of a step-index dielectric waveguide and the group delay per unit length of its modes is described by equations 3.4 and 3.5 which may be rewritten as:

$$\tau_{\nu\mu} = \frac{1}{c}\left[\Gamma_{\nu\mu}\frac{n_1}{n_{\nu\mu}}N_1 + (1-\Gamma_{\nu\mu})\frac{n_2}{n_{\nu\mu}}N_2\right] \qquad (3.27)$$

where all the terms are defined in sec. 3.2.

Equation 3.27 includes the effect of material dispersion in both core and cladding via the wavelength dependence of the group indices N_1 and N_2. Waveguide dispersion $-(V/\lambda)d\tau_{\nu\mu}/dV$ is also represented by the sensitivity of Γ and n to V-value. Finally, profile dispersion (usually defined as $(n_1/N_1).(\lambda/\Delta).(d\Delta/d\lambda)$) is implicit through $n_1/n \simeq 1 + \Delta(1-b)$ and $n_2/n \simeq 1 - \Delta b$, where $\Delta = (n_1 - n_2)/n_2$. Recent publications on light propagation in single-mode fibres[9, 10] have shown that each of these forms of dispersion can have a significant effect on the wavelength of zero chromatic dispersion.

Equation 3.27 may be used to obtain the variation of group delay with wavelength λ for any individual mode in the fibre. If these results are processed separately in the same way as experimental pulse-delay data (see sub-section 3.3.3), an insight is obtained into the contribution of each mode to the overall observed pulse delay. Fig. 3.12 shows the calculated total chromatic dispersion of a few low-order modes for a step-index fibre of the type used in the experiments (sec. 3.4.2). The fibre has a germanosilicate core and a silica cladding, with V = 37.8 at the wavelength, 1356nm, of zero material dispersion. The relative index difference is 1.5%.

It may be seen that the wavelength of zero total dispersion $\hat{\lambda}_{\nu\mu}$ of an individual mode is significantly shifted from the wavelength of zero material dispersion λ_o of the core glass owing to the influence of waveguide dispersion. The latter is dominated by a term involving[9] $-\frac{\Delta n_2}{\lambda c} V \frac{d^2(Vb)}{dV^2}$. The quantity $V\frac{d^2(Vb)}{dV^2}$ is plotted in fig.3.3 for the LP_{01} mode and is negative for large V values, only becoming positive for V < 3. Similarly, for higher-order modes, $V \frac{d^2(Vb)}{dV^2}$ is positive only near cut-off. As a consequence, waveguide dispersion is positive for all but a few modes close to cut-off in a multimode fibre. Since the material dispersion is negative, the wavelength of total chromatic dispersion $\hat{\lambda}_{\nu\mu}$ is moved to progressively <u>shorter</u> wavelengths with increasing mode number, as shown in fig. 3.12. By contrast in single-mode fibres (V < 2.4) the shift occurs to <u>longer</u> wavelength[9,10,16].

The differences between total chromatic dispersion and material dispersion displayed in fig. 3.12 are quite substantial and, if averaged over all modes, would result in a large error in the predicted value for λ_o. The sign of this error would, however, be opposite to that predicted by Jurgensen[9].

3.3.4.2 Pulse delay in multimode step-index fibres

In multimode fibres, all modes influence the observed pulse delay. In order to determine the effect of modal dispersion on the overall optical transit-time it is necessary to sum the individual contributions of each mode. Thus the pulse-delay is given by the first moment of the impulse response:

$$\tau(\lambda) = \frac{\sum_{\nu\mu} p_{\nu\mu}\, \tau_{\nu\mu}}{\sum_{\nu\mu} p_{\nu\mu}} \qquad (3.28)$$

where the weights $p_{\nu\mu}$ are proportional to the power carried by the $LP_{\nu\mu}$ mode and take values in the range 0-1. The chromatic dispersion $d\tau/d\lambda$ is quite different from the dispersion $d\tau_{\nu\mu}/d\lambda$ of individual modes since it includes the variation of the power distribution $p_{\nu\mu}$ with wavelength. Thus if the excitation wavelength increases, the V-value of the fibre is reduced, and the same power is carried by fewer modes. Therefore, in general, the weight $p_{\nu\mu}$ of each mode is a function of wavelength. In the special case of full excitation (i.e. $p_{\nu\mu} = 1$ for all guided modes), the only variations in the power distribution $p_{\nu\mu}$ occur at the mode cut-offs, where the power carried by the mode varies rapidly from 1 to 0 and this leads to singularities in the $\tau(\lambda)$ function as shown in fig. 3.13. This effect is not normally observed, since modes near cut-off usually carry very little power ($p_{\nu\mu} << 1$) after propagating in long fibres.

In order to model pulse-delay experiments accurately it is necessary to choose a suitable distribution $p_{\nu\mu}$. Since the optical power, in the experiments, is launched using a 10cm focal-length lens, the area of the focussed spot is similar to that of the fibre core. Thus the low-order modes are most heavily excited and the distribution $p_{\nu\mu} = 1 - u/V$ may be employed as a realistic model. This function gives weights varying from 1 to 0 with increasing mode number and reflects the lower launching efficiency and greater losses of modes near cut-off.

The variation of pulse transit-time with wavelength has been calculated using equ. 3.28 assuming the distribution $p_{\nu\mu} = 1 - u/V$, and with the same waveguide parameters and refractive-index data as in the previous section. The resultant multimode chromatic-dispersion $d\tau/d\lambda$ is shown in fig. 3.12 as a dotted line which now lies only slightly below the curve of material dispersion $(1/c)dN_1/d\lambda$. The difference between the two curves is of order 0.3ps $nm^{-1}km^{-1}$ and the consequent error, +3nm, produced in the determination of the zero of material dispersion is negligible.

3.3.4.3 Discussion

It is interesting to note that the waveguide contribution to chromatic dispersion in a multimode step-index fibre is opposite in sense to the waveguide dispersion of most individual modes. The reason for this somewhat surprising result lies in the change in the number of guided modes with wavelength and in the re-arranging of their arrival times within the impulse response of the fibre. The chromatic dispersion of a multimode fibre is therefore determined, not solely by changes in the modal group-delays, but also by the accompanying variation in the power carried by each mode and in their relative importance to the average time-of-flight.

In the measurements described in sub-section 3.3.2, the transit-time is measured on the leading edge of the pulse,which is, in principle, coincident with the arrival of the LP_{01} mode in a step-index fibre. The pulse rise-time is degraded by the propagation in the fibre and this indicates that a degree of mode conversion is present. The time-delay which is actually measured is, therefore, greater than the time-of-flight of the lowest-order mode, and less than that of the centre-of-gravity of the pulse. These two extremes respectively under- and over-estimate the wavelength of zero material dispersion of the core glass. The specific location of the experimental result within this interval depends on the level of mode conversion in the fibre. In the case of the fibre modelled in the present analysis,

the use of the leading-edge of the pulse as the time-reference means that the pulse-delay technique places the wavelength of zero material dispersion in an interval ±3nm centered on the correct value. Thus contrary to reference 9 which suggests an error as large as +35nm, the pulse-delay technique accurately determines the material dispersion parameter of the core glass. The accuracy improves with increasing V-value (at constant numerical aperture) and with decreasing numerical aperture (at constant V-value).

3.4 EXPERIMENTAL RESULTS

A range of measurements has been made on silica-based fibres fabricated by chemical vapour deposition [41,42]. One fibre had a graded phosphosilicate core and four others had germanosilicate cores so that the effect on material dispersion of the two main core additives has been examined.

Detailed measurements on silica-cored fibres were also carried out in order to assess the influence of the thermal history of the fibre on its dispersive properties. Silica is the most suitable glass for this comparison since

(a) it is available in very pure form

(b) there are no uncertainties as to the glass composition

and (c) the refractive index of fused silica in an annealed state is very well known[7].

The remaining results included here cover several types of fibre which may well be used in optical communications systems. Some details of the fibres are given in Table 3.1 and the results are summarised in Table 3.2.

3.4.1 Graded Index, Phosphosilicate Fibre

The variation of pulse-delay with wavelength was measured in a $\sim$600 m section of graded-index fibre, VD 150 L, having a phosphosilicate core. The experimental points are indicated by dots in figure 3.14a, while the broken line represents the power series (see equation 3.21) fitted to the data by a least-squares calculation. The coefficients of the power series are given in Table 3.2 and have been used to calculate the material dispersion parameter which is plotted in figure 3.14b (solid line) over the wavelength range of the measurements. For comparison, the material dispersion parameter of pure silica has been deduced from the results of Malitson[7] and is also shown (dotted line).

The material dispersion of phosphosilicate glass is found to

be slightly higher than that of pure silica at the short wavelength end of the range. The difference decreases with increasing wavelength and, in particular, the wavelength of zero material dispersion for the two glasses agree within experimental uncertainties.

The insets in figures 3.14(a) and (b) show the results of the error analysis (see Section 3.3.3) which indicates that the accuracy of the estimate of $M_1(\lambda)$ is better than 1 ps nm^{-1} km^{-1} over the wavelength range 650-1400 nm. The standard deviation of the estimated value of λ_o is 3 nm.

For interest, relative transit-time measurements using the two-pulse technique (cf. 3.3.2.3) are shown in figure 3.15(a) and (b). Although these results agree with those obtained by measuring the absolute pulse transit-time, the accuracy of the two-pulse technique and the wavelength range covered are substantially inferior.

3.4.2 Step-index Fibres with Germanosilicate Cores

A series of three fibres (VD 208, VD 209 and VD 210) were fabricated in order to investigate the dependence of material dispersion on glass composition in germanosilicate fibres.

Using the c.v.d. process, the germanosilicate cores were deposited directly onto the silica substrate tubes. The fibres, therefore, have no deposited cladding or buffer layer. Their numerical aperture can, thus, be used to estimate the refractive index of the core, since that of the cladding material, silica, is well known[7]. In addition, the molar refractivity can be deduced from measurements of the refractive index of bulk samples[22-24]. In this way, the germania content of the fibres can be obtained. Dr. D.N. Payne performed the numerical aperture measurements which led to the following estimates of germania concentration:

VD 208 : 8.1 m%
VD 209 : 11.0 m%
VD 210 : 13.1 m%

A fourth fibre, VD 232 L, was also examined. By comparing electron microprobe measurements of germania content in fibre VD 210 L and in VD 232 L, the dopant concentration of the latter was estimated to be 15.6 m%. It was not possible to determine the core-dopant concentration of VD 232L by numerical aperture measurements because this fibre had a borosilicate cladding layer, the refractive index of which was not accurately known.

A further consequence of the structure of fibres VD 208-210L is that their OH^- ion content is relatively high, particularly in, and near, the cladding. The substrate-tube material is of much lower purity than is the (deposited) core and it is likely that the impurity ions have diffused into the core region during the fabrication of the preform. The resulting impurity profile caused differential mode attenuation in the vicinity of the OH^- ions absorption lines (0.95, 1.24 and 1.39 μm). Near these wavelengths, the pulse-delay measurements were slightly distorted.

The pulse-delay measured in the germanosilicate fibres and the inferred material dispersion parameter are presented in figures 3.16 to 3.19. A salient feature of these results is that, at the emission wavelength of GaAs devices, the magnitude of the material dispersion parameter is greater than that of silica and the difference increases with increasing germania content. For a 13.1 m% concentration, this increase amounts to 25% of the material dispersion of pure silica. In addition, the wavelength, λ_o, of zero material dispersion is progressively shifted to longer wavelengths with increasing germania concentration. This is in contrast with the observations made on a phospho-silicate glass where the value of λ_o was found to be the same as in silica.

The variation of λ_o with glass composition (figure 3.20) is such that λ_o is increased by up to 85 nm over the range of additive concentration used in multimode fibres.

Figure 3.21 shows the variation of pulse delay with wavelength (relative to the delay at 585 nm) for all four germanosilicate fibres already discussed. The results are normalised to a fibre length of 1 km. It is clear from the figure that the total delay difference between 585 nm and λ_o (i.e. the range of the measured transit-times) increases with increasing germania content.

3.4.3 Fibres with Silica Cores

The refractive index of silica has been measured very accurately and over a wide wavelength range by Malitson[7]. The purpose of the measurements on silica fibres presented here is to determine whether the fabrication process has any effect on the refractive index or the dispersion.

It is difficult to make low-loss fibres with pure silica cores. The most obvious approach might be to deposit a borosilicate cladding and a silica core by the c.v.d. process. The deposition of pure silica, however, requires a high burner temperature for the glass to fuse and it usually happens that the support tube collapses before a sufficient amount of core material has been deposited. This problem does not normally arise in the c.v.d. process because the doped silicates which are most commonly used have lower sintering temperatures than silica.

A number of different types of silica fibre were manufactured. The most successful approach was to deposit a borosilicate cladding on the inside of a silica substrate tube, then to insert a rod of high purity silica and to pull the preform thus formed. One such fibre, VD 262L, had a length of 800 m, a numerical aperture of 0.14 and a 77 μm core diameter.

Although the OH^- ion content of fibre VD 262L was relatively high, it was possible to make pulse-delay measurements in the wavelength ranges 0.6-1.2 μm and 1.47-1.64 μm. In view of the high attenuation of this fibre, the single-pass experimental arrangement shown in figure 3.9 was used.

The pulse-delay data are plotted in figure 3.22(a) (dots). The measurement was performed twice, and figure 3.22(a) incorporates both results. Note that there appears to be no delay drift between the two sets of measurements. The length of fibre was accurately determined by winding the fibre on a drum of precisely known diameter. The results shown in figure 3.22(a) have been normalised to a length of 1 km. Also shown (solid line) is the group delay in silica computed from Malitson's silica data[7]. The difference between these and the present measurements corresponds to a change in group index of about 0.2%. The resolution is $\sim$0.02%, and is limited by the measurement of fibre length.

The two most probable causes of the discrepancy are

(a) the difference between the thermal histories of the samples, and
(b) the stresses applied to the core by the rest of the fibre structure.

In an attempt to separate these effects, a plastic-clad silica fibre was measured. A rod of the same grade of silica as that used previously was pulled into a fibre and coated on-line with Sylgard 182 silicone resin. In this way, a fibre with 0.43 numerical aperture and 125 μm core diameter was obtained.

The pulse delay in the silicone-clad fibre was measured at a single wavelength; the result is shown as a cross in figure 3.22(a). The normalised group delay in the two fibres, and predicted by Malitson are (at the wavelength 854 nm):

borosilicate cladding (VD 262L) : 4899.95 ns/km $\pm$ 0.85 ns/km*
silicone cladding (Q & S) : 4897.09 ns/km $\pm$ 0.85 ns/km*
bulk silica : 4888.93 ns/km

---

* The major source of error in the determination of the normalised group delay is the measurement of the fibre length. Thus the fibre is wound on an aluminium drum, the diameter of which is known to 1 part in 10^4; this operation therefore introduces a systematic error of $\pm$ 0.5 ns km^{-1} in the value of group delay. In contrast, the angle of rotation of the drum is known to 1 part in 10^5. The relative values of successive measurements made using the same drum are thus much more accurate than their absolute precision. Hence the difference in group delay between fibre VD 262L and the plastic-clad silica fibre is known to $\pm$ 0.7 ns km^{-1}.

It is clear, therefore, that about one quarter of the discrepancy could be accounted for by the stress applied by the cladding of fibre VD 262L, and the major cause of the increase in group index would be the abrupt chilling experienced by the fibre as it emerges from the furnace.

In order to confirm this observation, an attempt was made to anneal the borosilicate-clad fibre. It was found, however, that the attenuation increased rapidly and irreversibly to several thousand decibels per km after the fibre had been heated to about 1100^{o} C. The origin of this catastrophic increase in attenuation is not known. It did, however, prevent a direct measurement of the change in index during the annealing cycle.

The material dispersion parameter measured in fibre VD 262L is drawn in figure 3.22(b) and it was found to be slightly higher than in bulk samples at most wavelengths. In the vicinity of λ_o, however, the present results are in close agreement with those of Malitson.

3.4.4 Ternary Germanophosphosilicate Fibres

Germanophosphosilicate glasses are now widely used as core materials in graded-index, multimode fibres. The combination of the two additives, germania and phosphorus pentoxide, has proved to be very successful in the fabrication of high-bandwidth, low-loss optical fibres. This ternary glass is easier to deposit and results in better control of the refractive-index profile than is the case for the corresponding binary silicates. Moreover, it has been shown, theoretically[43-45], that fibres with more than one index-modifying additive can be designed to have high bandwidth over an extended wavelength range.

Two graded-index fibres with ternary germanophosphosilicate cores and borosilicate claddings were scanned. Although the nominal concentrations of additives were the same, the refractive index profiles were somewhat different, fibre VD 199 having a larger central dip than fibre VD 202. The effective concentrations of additives were thus different. The launching conditions can also modify the

material dispersion observed in graded-index fibres. The results presented here have, therefore, only qualitative value.

The results for fibres VD 199 and VD 202 are shown in figure 3.23 and 3.24 respectively. There is much less scatter in these data than in the case of the step-index germania fibres (Section 3.4.2) owing to a lower intermodal dispersion and OH^- ion content in the present fibres.

The variation of material dispersion with wavelength has a similar behaviour to that observed in binary germanosilicate glasses. Material dispersion is larger than in silica at wavelengths shorter than 1.27 μm. The wavelength of zero material dispersion is also shifted to longer wavelengths. The shift is smaller than in the germanosilicate fibres, partly because the concentrations of germania used here are lower, and also because the present fibres having graded-index profiles, have effective concentrations of additive lower than the nominal value at the core centre.

3.4.5 Other Fibres

Pulse-delay measurements have also been made on a number of other fibres fabricated with several different processes. In most cases, the fibres have graded refractive-index profiles and, therefore, these measurements give little information on the material properties of the glasses from which the fibres are made. Furthermore, the glass compositions are not usually known. Some of the results have nevertheless been included because fibres of similar design are likely to be used in optical communications systems. The data presented here may therefore be of some use in the design of communication links.

3.4.5.1 Multicomponent glass fibre pulled by the double crucible technique.

The British Post Office has developed[46] a low-loss fibre for the 0.8-0.9 μm region made from multicomponent glasses in the sodium borosilicate system. The fibres are pulled from a double crucible which can, in principle, be refilled continuously and very long lengths of fibre can be obtained from a single drawing operation. The technique

is said to be very reproducible and possibly cheaper than the c.v.d. process. Losses of 4 dB/km at 0.85 μm and bandwidth x distance products of 300 MHz.km have been reported[47]. It is possible that this type of fibre will find applications in medium capacity links over distances of 10 km or less.

A 2.15 km section of fibre (fibre No. 770818/2) was supplied by the British Post Office. The fibre had a minimum loss of 3.9 dB/km at 0.9 μm and a pulse dispersion of 3.6 ns (for the 2.15 km length) at the wavelength 0.85 μm. No data concerning the composition of the fibre was given.

The pulse transit time was measured over the wavelength range 585-1320 nm and the results are shown in figures 3.25 (a) and (b). It was found (fig. 3.25(b)) that, at 0.85 μm, the material dispersion in this fibre is greater, by 25%, than in pure silica. The loss of the fibre increases rapidly beyond 1.3 μm and the wavelength of zero material dispersion could not, therefore, be measured directly. By extrapolating the results, λ_o was estimated, however, to be 1338 nm $\pm$ 7 nm.

3.4.5.2 Fibre made by the 'Phasil' process.

The 'Phasil' (phase separation and leaching) process[48] allows low-loss (< 10 $dB.km^{-1}$), diffusion-graded fibres to be made in large batches at low cost. The process is thus attractive for applications where moderate bandwidths are required over distances of a few kilometres such as in a cable television distribution network.

Pulse-delay measurements were made on a short ($\sim$ 0.485 km) length of 'Phasil' fibre supplied by the British Post Office. The results are shown in figures 3.26(a) and (b). The spectral range covered extends to only 1350 nm, owing to the increasing attenuation of the fibre at longer wavelengths.

3.4.5.3 Germanoborosilicate fibre made by vapour phase oxidation.

Pulse delay measurements were made on a fibre made by Corning Glass Works

using the 'Outside Vapour Phase Oxidation' (o.v.p.o.) process[49]. The o.v.p.o. process allows very good profile control and fibres having very large distance x bandwidth products (~ 2 GHz.km), have been produced[50].

Fibre CGW-P057 was made from germanoborosilicate glass; the exact composition is, however, not known. The measurements were made over a wide wavelength range (600 - 1800 nm) although a spectral region near 1400 nm proved inaccessible owing to the high OH^- ion content of the fibre. The results are shown in figure 3.27. The material dispersion/wavelength curve is similar to that obtained on germanophosphosilicate fibres (see Section 3.4.4).

3.4.6 Pulse-delay Measurements in Single-mode Fibres

In Section 3.2, it was shown that measurements of pulse delay as a function of wavelength in step-index, multimode fibres, by differentiation, the material dispersion of the glass forming the core. In single-mode fibres, however, this is not the case. Thus, the chromatic dispersion of a single-mode fibre depends not only on the dispersive properties of the core material, but also on those of the cladding glass and on the core radius, the numerical aperture and the refractive-index profile. In addition, in single-mode fibres, the various forms of intramodal dispersion, which are often dealt with separately, are in fact interrelated[9,10].

Intramodal, or chromatic dispersion is the only form of pulse-broadening in a single-mode fibre. The lowest-order mode of a circular fibre is degenerate, and is composed of two orthogonally-polarised modes. In non-circular fibres, this degeneracy can be lifted and two modes with orthogonal polarisation and slightly different group velocities are then propagated. This can lead to intermodal pulse-broadening. Most real fibres are therefore not truly single-mode fibres. This type of dispersion was not of sufficient magnitude to be observed in the measurements to be described.

The chromatic dispersion of single-mode fibres is a function of

the properties of the glasses forming the core and the cladding, and of the waveguide parameters. By a suitable choice of these parameters, the wavelength of zero chromatic dispersion can be shifted over a wide range. In particular, it can be made to coincide[51] with the wavelength of minimum loss[52], 1.55 μm, for silica-based fibres. If this were achieved, almost dispersion-free fibres, with losses of the order of 0.2 dB/km would be available.

Measurements of pulse-delay in single-mode fibres allow the wavelength of zero dispersion to be accurately determined. It is therefore possible, with the aid of such data, to modify the fabrication process until fibres are produced with zero chromatic dispersion and a suitable normalised frequency (e.g. V = 2.2) at the wavelength 1.55 μm. This sort of experiment finds further application in the correlation of values of dispersion measured in fibres and those predicted by waveguide theory.

Measurements of pulse-delay were made over a wide range of wavelengths in two fibres made by the British Post Office. These fibres have germanosilicate cores. The refractive indices of the claddings are very close to that of pure silica, but contain fluorine and phosphorus pentoxide dopant. Unfortunately, the exact composition of the glasses is not known. One fibre, fibre No. 9055, was made deliberately with a large numerical aperture, and a small core in an attempt to increase the wavelength of zero dispersion.

The pulse-delay measurements for fibres 9055 and 9052 are shown in figures 3.28(a) and 3.29(a) respectively. Since the pulse-delay/wavelength function is dominated by the behaviour of the glasses forming the fibres, the data is fitted to a series expansion of the Sellmeier equation, as given by equation 3.21. The function $a_{-4}\lambda^{-4} + a_{-2}\lambda^{-2} + a_o + a_2\lambda^2 + a_4\lambda^4$ is a very good representation of the data, and the r.m.s. error in the least squares fit (160 ps for fibre 9052) is limited by the accuracy of the delay measurements. The chromatic dispersion may be calculated from the fitted coefficients as has been described previously and is shown in figure 3.28(b) and 3.29(b). We note that the wavelength of zero chromatic dispersion in fibre 9055 is larger than in fibre 9052,

as a result of the increased waveguide dispersion. The increase in the wavelength of zero dispersion is, however, only 35 nm. Much larger departures from usual values of numerical aperture and core radius would be required for zero dispersion to occur at 1.55 μm. Cohen et al have demonstrated[51] zero total dispersion at 1.55 μm in single-mode fibre having a numerical aperture of 0.25.

3.5 INTERPRETATION OF THE RESULTS

3.5.1 General Comments

The results presented in Section 3.4 provide a direct verification of the existence of a wavelength of zero material dispersion. Thus in all fibres of sufficient transparency to allow pulse delay measurements to be made over a wide wavelength range, a region of negligible material dispersion was found in the vicinity of 1.3 μm. This confirms earlier extrapolations[6] based on measurements of bulk silica[7] and, over a restricted wavelength range, in phosphosilicate fibres[27].

The results obtained on c.v.d. fibres have a similar wavelength dependence to that inferred from refractive index measurements on bulk samples of silica[7]. A variation of up to 25% in material dispersion (at 0.85 μm) was, however, observed over the range of compositions investigated and the wavelengths of zero material dispersion were found to span more than 80 nm. The design of very large capacity systems must therefore take into account the variation with glass composition of the material dispersion parameter.

Multimode fibres with very low loss at 1.3 μm have been reported [53]. The measurements of material dispersion presented in Section 3.4 thus further emphasise the importance of this spectral region. It is therefore likely that high capacity systems using multimode fibres and operating at 1.3 μm will be installed in the near future. Sources (light-emitting diodes[17] and semiconductor lasers[54]) and detectors[55,56] have been recently developed to this end.

3.5.2 The Wavelength of Zero Material Dispersion in Germanosilicate Fibres.

3.5.2.1 Material dispersion in graded-index fibres

Measurements on fibres with binary germanosilicate cores have revealed (see Section 3.4) an increase in material dispersion with increasing germania concentration and a progressive shift of λ_o to longer wavelengths.

In a graded-index fibre with a germano-silicate core, the concentration of additive varies, typically, from a maximum on-axis to zero in the cladding. As a result, the dispersive properties of the transmission medium and, in particular, the wavelength of zero material dispersion, are functions of radial position in the core. A group of modes propagating in a region of low dopant concentration (e.g. helical modes) therefore requires a different operating wavelength for complete elimination of material dispersion than does a group confined near the core centre. Hence in a graded-index fibre, it is not possible to choose a wavelength of operation such that material dispersion is eliminated for all modes and first-order material dispersion is therefore always present to some extent.

Dr. M.J. Adams[57] has analysed the intramodal dispersion in this situation. The effective material dispersion parameter was evaluated for a fully-excited fibre having a graded concentration of germania in the core and a silica cladding. The maximum dopant concentration (at core centre), 13.1 m/o, gives a numerical aperture of ~ 0.25 and is similar to the core-composition of fibre VD 210L (see sub-section 3.4.2). At each wavelength, the fibre was assumed to have the optimum profile parameter α_{opt} obtained from Dr. F.M.E. Sladen's measurements[58]. The results are shown in figure 3.30. The broken lines correspond to the absolute value of the material dispersion parameter in the cladding ($|M_2(\lambda)|$) and at core centre ($|M_1(\lambda)|$). The solid lines are the effective material-dispersion parameter (defined in sub-section 3.2.4) for a source with r.m.s. width 2 σ_s ranging from 1 nm to 100 nm. The lowest curve thus indicates the limitation imposed by first-order

material dispersion. Although it has a minimum $\hat{\lambda}_o$ which falls between the wavelengths of zero material dispersion for core centre $\hat{\lambda}_{01}$ and cladding $\hat{\lambda}_{02}$, first order material dispersion cannot be eliminated. The remaining curves are increasingly dominated by second-order material dispersion but still have a minimum at $\hat{\lambda}_o$.

The total dispersion of the graded-index germanosilicate fibre is shown in figure 3.31, as a function source linewidth. The intermodal dispersion is assumed to be minimised by a correct design of the index profile at each of the wavelengths $\hat{\lambda}_{02}$, $\hat{\lambda}_o$ and $\hat{\lambda}_{01}$. Operation at the optimum wavelength $\hat{\lambda}_o$ results in a bandwidth capability which is only marginally less than that predicted from a consideration of second-order material dispersion (dotted line) alone. On the other hand, at $\hat{\lambda}_{01}$ or $\hat{\lambda}_{02}$, the pulse broadening is dominated by first-order material dispersion and operation at these wavelengths curtails the fibre bandwidth.

Dr. Adams has derived the following approximate expression for intramodal broadening $\sigma_{intramodal}$:

$$\left(\frac{\sigma_{intramodal}}{\sigma_s}\right)^2 = \left(\frac{2M_1 + M_2}{3} - \frac{\Delta n_1 P}{3c\lambda}\right)^2 + \frac{1}{8}\left(\frac{dM_1}{d\lambda}\right)^2 \left(2\sigma_s\right)^2 + O\left(\frac{\Delta^2 M_1}{\lambda c}\right) \qquad (3.29)$$

where P is the profile dispersion parameter, defined by:

$$P = \frac{n_1}{N_1} \frac{\lambda}{\Delta} \frac{d\Delta}{d\lambda} \qquad (3.30)$$

Intramodal broadening is normally dominated by the first term on the r.h.s. of equation 3.29, the zero of which corresponds approximately to the optimum wavelength $\hat{\lambda}_o$. For the small value of P in this spectral region[58], the optimum wavelength is simply given by the weighted mean $\frac{(2M_1 + M_2)}{3}$ i.e. 2/3 of the way between $\hat{\lambda}_{02}$ and $\hat{\lambda}_{01}$. Note, however,

that this wavelength depends on the modal power-distribution within the fibre. Thus, if low-order modes carry most of the power, as might be the case after propagation in a long fibre, the optimum wavelength is closer to $\hat{\lambda}_{01}$.

One consequence of the dependence of effective material dispersion on excitation conditions is particularly relevant to the measurements presented here. Indeed, since the observed dispersion parameter depends on the modal power-distribution, measurements on graded-index fibres cannot be interpreted accurately in terms of the properties of the core or cladding glasses. Measurements on step-index fibres, however, accurately reflect the material dispersion of the core material[33].

3.5.2.2 Composition-dependence of group delay; profile dispersion.

Inspection of figure 3.21 shows that the wavelength-dependence of group-delay is a function of composition in binary germanosilicate glasses. As a result, the variation of transit-time with wavelength is mode-dependent in a graded-index fibre, since high-order modes travel, on average, in a medium of lower dopant concentration than do low-order modes. Thus the modes of a fibre which has an optimal refractive-index profile at one wavelength (i.e. the modes have almost identical transit times) undergo different changes in group delay if the operating wavelength is altered and the fibre is no longer well-equalised. This variation of intermodal dispersion with wavelength is known as profile dispersion. It is clear that profile dispersion and material dispersion are profoundly inter-related. These two forms of dispersion, however, affect the pulse-broadening of a multimode optical fibre, via completely different mechanisms, namely intermodal and intramodal dispersion, respectively.

For power-law profiles of the form:

$$\left.\begin{aligned} n_1^2(r) &= n_1^2(0)\left[1 - 2\Delta\left(\frac{r}{a}\right)^{\alpha}\right] \quad r \leq a \\ n^2(r) &= n_1^2(0)\left[1 - 2\Delta\right] = n_2^2 \quad r \geq a \end{aligned}\right\} \qquad (3.31)$$

Olshansky and Keck[13] have shown that the optimum profile-exponent α_{opt} is given by:

$$\alpha_{opt} = 2 - 2P - \frac{12}{5}\Delta \qquad (3.32)$$

Olshansky and Keck implicitly assume that P is independent of dopant concentration and thus is constant throughout the core of graded-index fibres. If this is not the case, then the optimal profile[59] is not of the power-law type, and the profile dispersion parameter loses much of its significance. Measurements by Fleming[22-23] on bulk samples indicate substantial variations of P with germania concentration. On the other hand, the more recent, and probably more accurate, work of Sladen et al[58] on fibre samples shows, to the contrary, that P is independent of dopant concentration over the range of compositions used in optical fibres.

P can be rewritten in the form:

$$P = 1 - \frac{N_1 - N_2}{N_2 \quad \Delta} \qquad (3.33)$$

where the definitions of N_1, N_2 and Δ (equations 3.7 and 3.12) have been used, and a multiplicative factor of order $(1 - \Delta P)$ has been ignored. From equation 3.33, it is clear that the profile dispersion parameter P represents a correction to the optimum profile exponent, which accounts for the wavelength dependent discrepancy between the relative group index difference $\Delta_g = (N_1 - N_2)/N_2$ and the relative phase index difference $\Delta = (n_1 - n_2)/n_2$.

A corollary stems from the fact that the material dispersion parameter of a phosphosilicate glass is almost identical to that of silica (see Section 3.4). Thus the ratio Δ_g/Δ is also insensitive to wavelength and, as a result, the profile dispersion parameter is almost constant. This has been confirmed by the more direct and more accurate measurements of Dr. Sladen, who found that the optimum profile parameter for fibres with phosphosilicate cores has only a small wavelength dependence[58].

3.5.2.3 Inference of the profile dispersion parameter from pulse-delay measurements.

The profile dispersion parameter P has been deduced[40] from refractive-index measurements on bulk samples of glass[22-24], by interference microscopy on thin slices of fibres[60] and by the direct measurement in fibres of the wavelength-dependence of numerical aperture[58]. Equation 3.33 reveals that a further possibility exists, namely to compare the pulse transit-time in the core and the cladding. To do so, a knowledge of n_1, n_2, N_1 and N_2 is required over a wide wavelength range.

Since it is rather awkward to measure n_1 over a wide spectral range in a fibre, we consider the expression $N_1 = n_1 - \lambda\, dn_1/d\lambda$ which relates the phase and group indices. $N_1(\lambda)$ contains, in principle, enough information to deduce $n_1(\lambda)$ and can be accurately determined from pulse-delay measurements and a knowledge of the fibre length. Now $n_1(\lambda)$ may be written as a power-series (see sub-section 3.3.3) of the form:

$$n_1(\lambda) = b_{-4}\,\lambda^{-4} + b_{-2}\,\lambda^{-2} + b_o + b_2\,\lambda^2 + b_4\,\lambda^4 \qquad (3.34)$$

Thus the group index N_1 can be expressed as

$$N_1(\lambda) = n_1 - \lambda\,\frac{dn_1}{d\lambda} = 5b_{-4}\,\lambda^{-4} + 3b_{-2}\,\lambda^{-2} + b_o - b_2\,\lambda^2 - 3b_4\,\lambda^4 \qquad (3.35)$$

and a one-to-one relationship therefore exists between the coefficients determined from pulse-delay measurements and those representing the phase index.

In order to estimate the accuracy of this procedure, phase and group indices were calculated from published Sellmeier coefficients and two sets of coefficients b_i and a_i were fitted to the results. The phase indices calculated from equation 3.34 and directly from the Sellmeier coefficients agree very well. On the other hand, the values of phase index deduced from the group index are in error by about 1 part in 10^4. Although the origin of this error is not perfectly

understood, it would seem likely that it originates in the truncation of the two power series at orders of λ^2 which may not be equivalent for N_1 and n_1. When the data are fitted to polynomials including terms to order λ^6 and λ^{-6}, the error is found to decrease by an order of magnitude.

The measurements on fibres VD 208L to VD 210L are not sufficiently accurate to be used for a calculation of the phase index from pulse-delay data. On the other hand, fibre VD 232L has a borosilicate cladding which makes the determination of the core index relative to that of silica (for comparison with other measurements of P) very difficult.

With the knowledge of N_1 and n_1, the profile dispersion parameter P can, in principle, be calculated, since the refractive index of silica is well known[7]. The measurements of pulse delay in silica fibres presented in Section 3.4 show, however, a major difference between the properties of bulk and fibre samples, and data obtained on fibres should, strictly, be used in the computation. The use of data obtained on bulk samples could lead to an error of 0.002 in Δ, a relative error of 15% or more.

In a recent publication, Horiguchi, Ohmori and Miya[61] have used the procedure outlined above to calculate P from pulse delay measurements in a graded-index fibre. Starting from group-index data accurate to 1 part in $10^3$and using bulk-sample measurements of the cladding material, remarkable agreement is reached with the results of Ohmori et al[62], where α_{opt} is measured by an independent experiment. This is a very encouraging result and it shows that further work on this subject might be valuable.

3.5.2.4 Interpolation of material dispersion measurements.

Sladen et al[58] have shown that, in binary germanosilicate glasses, the profile dispersion parameter P is independent of the germania content over the range of compositions normally used in optical fibres. Thus the relative group-index difference Δ_g is, from equation 3.33,

proportional to Δ:

$$\Delta_g \equiv \frac{N_1 - N_2}{N_2} = \Delta\,(1 - P) \qquad (3.36)$$

for a fibre having a silica cladding. Hence for another core composition giving a relative index difference Δ_3, the group index N_3 may be found from:

$$\frac{N_1 - N_3}{N_2} = (\Delta - \Delta_3)(1 - P) \qquad (3.37)$$

Equation 3.37 represents a scaling rule for the group index and is a consequence of the independence of P on the index difference Δ. Reordering equation 3.37 and differentiating with respect to wavelength, we obtain a scaling rule for the material dispersion parameter.

$$\frac{M_1 - M_3}{\Delta - \Delta_3} = (1 - P)\,M_2 + N_2\left[\frac{(1 - P)P}{\lambda} - \frac{dP}{d\lambda}\right] \qquad (3.38)$$

Equation 3.38 should prove useful when the dispersive properties of a glass composition are needed, but only its index difference (with respect to silica) is known. One example of its use is the design of single mode fibres with zero dispersion at a specific wavelength: equation 3.38 gives a functional relationship between index difference and material dispersion.

3.5.2.5 Comparison with other published results

The material dispersion parameter can be calculated from a number of measurements made on germanosilicate samples in other laboratories. These include bulk-sample measurements [22-24] and pulse delay measurements on graded-index fibres[28,30].

The wavelength of zero material dispersion as a function of germania concentration obtained from the various experiments, and the values presented here, are shown in figure 3.20. The measurements of Cohen et al

on graded-index fibres lie in general below those presented here for step-index fibres. This is not altogether surprising as it is difficult to interpret measurements taken on graded-index fibres, which represent a weighted mean of the properties of the core and cladding compositions.

There is little agreement between the results obtained on bulk samples in different laboratories, or, indeed, between measurements on step-index fibres, and bulk samples. It is shown in section 3.3.4 that the discrepancy is not attributable to waveguide effects in the measurements on step-index fibres. Another possibility might be the difference in thermal history between the two sets of samples. Clearly, further measurements are called for.

3.5.3 Analysis of Pulse-Delay Measurements on Silica-Core Fibres.

Measurements presented in section 3.4 have shown that the group index observed in fibres having silica cores is larger than would be expected from the refractive-index of silica in bulk form. In addition, a difference in the group delay of silica-core fibres is observed between samples having borosilicate glass, or silicone rubber, claddings. The latter effect is possibly caused by the compressive stress applied by the borosilicate cladding (of fibre VD 262L) to the silica core during the cooling of the fibre as it emerges from the pulling furnace. The stresses would originate in the difference in the expansion coefficients of the core and cladding glasses and would not be present in the fibre clad with silicone, since the latter material supports very little stress. An analysis of the changes in refractive index induced by internal stress is presented in section 3.5.3.1. The discrepancy between measurements on fibres and bulk samples is then discussed in section 3.5.3.2.

3.5.3.1 Effect of internal stress on refractive index.

It is well known[63] that the refractive index of glass is affected by stress, a phenomenon referred to as the 'stress-optical effect'. Most studies of the relationship between stress and refractive index concentrate on the birefringence which develops when glass is subjected

to uniaxial stress. This birefringence results from unequal changes in index along axes parallel and perpendicular to the direction of the applied pressure. If, on the other hand, isotropic pressure is applied (e.g. in the case of a piece of glass placed in a pressure tank), then the change in refractive index is the same in all directions.

The present analysis is concerned with the sensitivity of the refractive index of the fibre core to longitudinal, radial and tangential forces exerted by the rest of the fibre. Following Morey[63] consider a cube of glass, as sketched in figure 3.32. Stresses denoted by T_x, T_y and T_z are applied and lead to strains x_x, y_y and z_z along each axis.

The velocity of a ray of light having an electric field vector along one of the axes $\vec{x}$, $\vec{y}$ or $\vec{z}$ may be written as:

$$\begin{bmatrix} v_x \\ v_y \\ v_z \end{bmatrix} = v + \begin{bmatrix} q & p & p \\ p & q & p \\ p & p & q \end{bmatrix} \begin{bmatrix} x_x \\ y_y \\ z_z \end{bmatrix} \qquad (3.36)$$

where $v = \frac{c}{n}$ is the phase velocity of light in the unstrained material. The strain-optical matrix appearing in equation 3.36 is particularly simple for glasses, since it contains only two different coefficients p and q.

The strains are related to the compressive stresses T by:

$$\begin{bmatrix} x_x \\ y_y \\ z_z \end{bmatrix} = \frac{1}{E} \begin{bmatrix} 1 & -\sigma & -\sigma \\ -\sigma & 1 & -\sigma \\ -\sigma & -\sigma & 1 \end{bmatrix} \begin{bmatrix} T_x \\ T_y \\ T_z \end{bmatrix} \qquad (3.37)$$

where E is Young's modulus and σ is Poisson's ratio.

For small changes in index, one can write:

$$\frac{v_x - v}{v} = \frac{n - n_x}{n} \; ; \; \frac{v_y - v}{v} = \frac{n - n_y}{n} \; ; \; \frac{v_z - v}{v} = \frac{n - n_z}{n} \qquad (3.38)$$

The relationship between strain-induced index variations and applied stress are obtained by combining equations 3.36, 3.37 and 3.38. For weakly-guiding fibres[11], we are only concerned with the refractive index affecting rays propagating in the axial direction $\vec{z}$. Assuming, therefore, that the electric field vector is parallel to $\vec{x}$ (for circularly-symmetric structures there is no loss of generality), the sensitivity of index to stress is thus given by:

$$\frac{n_x - n}{n} = \frac{nq}{cE}\left[T_x - \sigma(T_y + T_z)\right] + \frac{np}{cE}\left[-2\sigma T_x + (1 - \sigma)(T_y + T_z)\right] \qquad (3.39)$$

The strain-optical coefficients p and q cannot be measured directly. Experiments have, however, been performed to determine for silica, the strain-induced birefringence[64] B, and the change in refractive index A caused by isostatic pressure[65]. The quantities may be expressed[63] in terms of the coefficients p and q as:

$$A = \frac{n^2}{cE}(1 - 2\sigma)(2p + q) \qquad (3.40)$$

and

$$B = \frac{n^2}{cE}(1 + \sigma)(q - p) \qquad (3.41)$$

Solving for p and q and substituting into equation 3.39 leads to the following expression for the change in index undergone by light travelling with the electric field vector in the $\vec{x}$ direction:

$$n_x - n = \frac{1}{3}\left[(A + 2B)\,T_x + (A - B)(T_y + T_z)\right] \qquad (3.42)$$

The sign of $n_x - n$ is positive for compressive stress. An advantage of expressing the change in index in the form of equation 3.42 is that the result is not explicitly dependent on Young's modulus or Poisson's ratio, and is given directly in terms of the measured quantities, A and B. From the literature[64,65] the values of the constants are,

for silica:

$$A = 0.925 \times 10^{-11}\ Pa^{-1}$$

and

$$B = 0.341 \times 10^{-11}\ Pa^{-1}$$

In the case of purely axial stress (e.g.: a fibre being pulled in a duct), the stresses in equation 3.42 are given simply by: T_z = applied stress ; $T_x = T_y = 0$, and the index change is given by:

$$n_x - n = \frac{1}{3}(A - B)T_z \qquad (3.43)$$

In the case of the internal stresses caused by expansion coefficient mismatches the axial and transverse stresses are related by[66]:

$$T_z = 2\,T_x = 2\,T_y$$

The resultant index change for rays propagating in the axial direction can then be written as:

$$n_x - n = \frac{1}{3}\left(2A - \frac{B}{2}\right) T_z \qquad (3.44)$$

Assuming that the dispersion is unaffected by the stress, the variation of pulse delay caused by the internal stresses is, therefore:

$$\delta\tau = \frac{1}{3}\frac{L}{c}\left(2A - \frac{B}{2}\right) T_z \qquad (3.45)$$

The level of internal stress which develops during the drawing of a fibre depends on the structure of the waveguide, the glass compositions used and the thickness of the different glass layers. Fibre VD 262L has a silica core and a borosilicate cladding which is surrounded by a silica support tube (the substrate layer). The fibre emerges from the pulling furnace at around 2100°C and cools extremely rapidly. Stress does not develop until the glass is sufficiently viscous to withstand it. (The temperature at which this occurs is referred to as the 'strain temperature' and, by convention, corresponds to a viscosity of $10^{14.6}$ poise.) As soon as the outermost layer

freezes (in this case, the substrate layer), stress begins to build up inside the fibre structure since the borosilicate glass has a much higher expansion coefficient than has silica. As a result, both the silica core and the substrate go into compression and the borosilicate cladding is under tension. A precise evaluation of the stress level is made difficult by the variation of material properties such as expansion coefficient and Young's modulus with glass composition and temperature. The physical properties of doped silica glasses are not well characterised and suitable values must often be interpolated from the scarce data which is available. In addition, two separate temperature ranges must be considered, namely that below the strain point of the cladding (this layer having the lower fusion temperature) and that between the strains points of the two materials.

In the first case, the structure behaves as an elastic solid having internal expansion mismatches and the axial stress is given by [66,67]

$$T_{z_1} = (k_1 - k_2)(T - T_{g_2}) \frac{E}{1-\sigma} \frac{(b^2 - a^2)}{c^2} \qquad (3.46)$$

k_1 and k_2 denote the expansion coefficient of the core and cladding, respectively. T_{g_2} is the strain point of the cladding and T is room temperature. Finally a, b and c represent the outer diameter of the core, cladding and substrate regions, respectively. The sign of T_z is positive if the core is in compression.

In the temperature range bounded by the strain points of the cladding and the substrate materials, the cladding is essentially liquid, but trapped by frozen silica. The expansion coefficient of the liquid borosilicate material is believed to be much larger than when it is solid, whilst its bulk modulus is strongly reduced[67,32]. In addition silicate glasses exhibit hysteresis and, strictly, contraction coefficients, rather than expansion coefficients, should be used[67]. A correction term to equation 3.46 is given in reference 67 and accounts for the stress built up at temperatures higher than the strain point of the cladding. Since data concerning the physical properties of the glasses is scarce, particularly relating to the strain point, the temperature region in which the cladding

is fluid is ignored in the present analysis and the strain point T_{g_2} in equation 3.46 is thus replaced by T_{g_1} (the strain point of silica) so that the entire temperature range over which internal stress can develop is covered. Although this results in an underestimation of the stress level, the error involved (10-20%) is probably not greater than the uncertainties caused by the lack of data concerning material properties.

Furthermore, stresses which build up above the strain points of both materials if the fibre is cooled rapidly have been ignored although they are expected[32] to increase the internal stress level by 10 to 20%.

The mismatch in expansion coefficients is related to the relative index difference (for small additions of boric oxide to silica) by[68]:

$$(k_2 - k_1) = 2.63 \times 10^{-4} \Delta \qquad (3.47)$$

Fibre VD 262L has an index-difference of 0.46% and the expansion coefficient mismatch is thus 1.21×10^{-6} K^{-1}. The remaining parameter values used to calculate the axial stress, from equation 3.46 are as follows:

$$T_{g_1} = 1000^{o}C$$

$$E = 7.18 \times 10^{10} \text{ Pa}$$

$$\sigma = 0.16$$

$$a = 77 \text{ μm} \; ; \; b = 106 \text{ μm} \; ; \; c = 150 \text{ μm}$$

The resultant stress T_{z_1} is 24 MPa, which is in reasonable agreement with the values calculated by Scherer[32], considering the small doping level and cross-sectional area of the cladding in the present fibre. The calculated value of T_{z_1} leads to a change in pulse delay of ~ 0.45 nskm^{-1} - almost one order of magnitude less than the observed

value. Although part of the discrepancy might be accounted for by the oversimplifications of the present analysis (which would underestimate the internal stress) and the accuracy ($\pm$ 0.7 ns km^{-1}) of the measurement, the agreement between theory and experiment is not good. Both results do indicate, however, that the internal stress of the borosilicate-clad fibre is not the dominant cause of the difference between the pulse delay measured in the silica fibre and that deduced from bulk-samples data.

3.5.3.2 Discussion of the pulse-delay measurements on silica-core fibres.

It may be concluded from the previous section that internal stress is not the cause of the discrepancy between the pulse delay in silica fibres and in bulk samples. Other possible causes include:

(a) minor variations in glass composition resulting from different fabrication processes.
(b) waveguide effects in the pulse-delay measurements and
(c) the thermal history of the samples

The cores of both fibres measured in the present experiments were made from silica rods supplied by the firm 'Quartz et Silice'. The silica may contain small amounts of chlorine incorporated during the plasma-activated c.v.d. process used to produce the glass from silicontetrachloride. Chlorine is known[69] to increase slightly the refractive index of fused silica and this effect could therefore cause the observed increase in pulse delay. On the other hand, the measurements of Malitson were also made on samples of synthetic silica[7] and are thus also likely to contain chlorine, although not necessarily in the same concentration. In addition, Malitson[7] made measurements on twelve samples supplied by three different companies. The differences in refractive index between the samples (which presumably were made by slightly different processes) reported by Malitson are orders of magnitude smaller than the increase in index observed in fibres. Furthermore, the measurements of Kobayashi et al[24] on bulk samples of silica made by the v.a.d. process[70] (which would also contain chlorine, but not nessarily the same amount as Malitson's

samples) agree exactly (to seven decimal places) with the results of Malitson. Thus measurements on bulk samples of different origin and made over different wavelength ranges and to different degrees of precision do not show any difference in refractive index whatever. There is, therefore, no direct evidence that the origin of the silica used in the measurements on fibres is causing the observed discrepancy, although this possibility cannot be rejected.

It is well known[11] that, in step-index fibres, the group delay of the various modes ranges from $L N_1/c$ (for low-order modes) to $L(2N_1 - N_2)/c$ (for modes near cut-off). The average group delay in the fibre can thus be different from that in the core material only and this effect could cause an error in the interpretation of the pulse-delay measurements. In the present measurements, however, care was taken to launch low-order modes only. In addition, the drums carrying the fibres were refrigerated in order to release the tension of the fibres and thus reduce mode conversion caused by microbending. Furthermore, the pulse-positions were measured on the leading edge of the pulse which, in step-index fibres, ensures that only low-order modes contribute to the observed delay. In view of these precautions and of the small index-difference (< 0.5%) of the borosilicate-clad fibre, it is felt that waveguide effects have not distorted the pulse-delay measurements significantly.

The remaining possible cause of the discrepancy is the thermal history of the samples. Brückner[31] shows that the refractive index of fused silica increases with fictive temperature until about 1550°C. The maximum difference in refractive index between quenched and annealed samples is about 7×10^{-4}. This leads to a change in pulse delay (assuming that the dispersion is unchanged) of 2.3 ns km^{-1} i.e. one third of the value observed in the present study. Brückner comments, however, that at temperatures of 1600°C and higher, the volume relaxation time is shorter than the quenching time. Fraser[71], who also made measurements on chilled silica found that only the outer portions of his samples were quenched and that the inside had cooled more slowly. It may be, therefore, that fibres, because of their small size, are more highly quenched than larger samples of glass and thus show more extreme effects.

The group index of a dielectric depends, not only on the phase index n, but also on its dispersion $\frac{dn}{d\lambda}$. Thus, if the dispersion is affected by the quenching of the glass it will, in turn, modify the group index. The difference between the group delay measured in fibres and that calculated from bulk samples varies with wavelength. This indicates that the dispersion is affected by the chilling process.

One method of separating the relative contributions of refractive index and dispersion to the observed change in group index using the procedure outlined in section 3.5.2.3. Unfortunately the data obtained on fibre VD 262L do not include any values in the wavelength range 1200 - 1500 nm. As a result, the fitted coefficients are inconsistent with the Sellmeier model, since the fitted function is not constrained to follow the data continuously over a wide wavelength range. In particular, the sign of the coefficients of the fourth powers of wavelength, λ^{-4} and λ^{4} are incorrect. The calculation of phase index from the coefficients of equation 3.21 (a procedure which is not very accurate even with ideal data) is therefore not likely to give any valid results.

It is clear that the measurements presented here need to be confirmed by further experimental work in order to clarify the behaviour of both the refractive index and the dispersion of silica with thermal history.

The present results, if confirmed, could have important consequences. They might, for example, explain the discrepancy[40] between measurements of the profile dispersion parameter and of the material dispersion parameter in bulk samples and in fibres. In addition, estimates of fibre compositions based on refractive-index measurements would have to be revised.

3.6 SUMMARY

A previously known pulse-delay technique for the measurement of material dispersion in optical fibres has been much extended and improved. Thus, the pulse-delay in long optical fibres can be measured very accurately ($\sim$ 150 ps) over a very wide range of wavelengths. A

theoretical study has shown that the chromatic dispersion derived from such measurements provides a faithful representation of the material-dispersion parameter of the glass forming the fibre core. An error analysis indicates that the material dispersion parameter is determined, in most cases, to better than 1ps $nm^{-1}km^{-1}$.

A number of fibres, made by various fabrication processes and incorporating a wide range of glasses have been investigated. Thus it is found that the addition of phosphorus pentoxide to silica does not significantly alter the material dispersion, whereas for germanosilicate glasses, the wavelength of zero material dispersion increases with increasing concentration of additive. As a result, the material dispersion of graded-index germanosilicate fibres cannot be totally eliminated, since the wavelength of zero material dispersion is a function of radial position in the core. An optimum operating wavelength exists, however, and with l.e.d. sources and fibres having well-designed refractive-index profiles, the bandwidth is limited by second-order material dispersion.

The material dispersion of silica-core fibres is shown to be much the same as calculated from refractive index measurements on bulk samples. The group index in this type of fibre is, however, substantially higher than in bulk samples, an effect which is attributed primarily to the quenching of the fibres during the drawing process.

Results concerning other commonly-used fibre designs have also been presented. In addition, the pulse-delay technique is shown to be very suitable for the determination of the chromatic dispersion of single-mode fibres.

3.7 REFERENCES TO CHAPTER 3

1 R.C.A., Optical Communications Products catalogue.

2 Laser Diode Laboratories Inc. C.W. lasers are available with spectral widths in the range 1-4nm and operating in the 820-850nm region.

3 M. Nakamura, K. Aiki, J. Umeda, A. Yariv, H.W. Yen and T. Morikawa: 'Ga As - Ga_{1-x} $A\ell_x$ As double-heterostructure distributed-feedback diode lasers: *Appl. Phys. Lett.* 1974, *25* pp.487-488.

4 J.V. Wright and B.P. Nelson. 'Pulse compression in optical fibres'. *Electron. Letts.* 1977, *13*, pp.361-363.

5 C. Baack, G. Elze, G. Walf, G. Gliemeroth, D. Krause, N. Neuroth. 'Optical transmission experiment at 1.12Gbits/s using a graded-index fibre with a length of 1.652km'. *Electron. Letts.* 1977, *13*, pp.452-453.

6 D.N. Payne and W.A. Gambling. 'Zero material dispersion in optical fibres'. *Electron. Letts.* 1975, *11*, pp.176-8.

7 I.H. Malitson 'Interspecimen comparison of the refractive-index of fused silica'. *J. Opt. Soc. Am.* 1965, *55*, pp.1205-1209.

8 J.E. Midwinter: 'A study of intersymbol interference and transmission medium instability for an optical fibre system'. *Opt. & Quant. Electron.* 1977, *9*, pp.299-304.

9 K. Jurgensen: 'Dispersion minimum of monomode fibres'. *Appl. Opt.* 1979, *18*, (8), pp.1259-1261.

10 W.A. Gambling, H. Matsumura and C.M. Ragdale: 'Mode dispersion, material dispersion and profile dispersion in graded-index single-mode fibres' *IEE J. of Microwaves, Optics and Antennas* , 1979, *3*(6), pp. 239-246. (This work was also presented in an invited paper at the fourth European Conference on optical communication, Genoa, 1978.)

11 D. Gloge: 'Weakly-guiding fibres'. *Appl. Opt.* 1971, *10*, pp.2052-2058.

12 D. Gloge: 'Dispersion in weakly-guiding fibres'. *Appl. Opt.* 1971, *10*, pp.2442-2445.

13 R. Olshansky and D.B. Keck: 'Pulse broadening in graded-index optical fibers'. *Appl. Opt.* 1976, *15*, pp.483-491.

14 R.W. Christy: 'Classical Theory of Dispersion'. *Am. J. Phys.* 1972, *40*, pp.1403-1419.

15 L.E. Sutton and O.N. Stavroudis: 'Fitting refractive index data by least squares'. *J.Opt. Soc. Am.* 1961, *51*, pp.901-905.

16 K.P. Kapron, 'Maximum information capacity of fibre-optic waveguides'. *Electron. Lett.* 1977, *13*, pp.64-66.

17 A.G. Dentai, T.P. Lee, C.A. Burrus and E. Buehler: 'Small-area high-radiance In GaAs P c.w. ℓ.e.d.s emitting at 1.30μm'. *Electron. Lett.* 1977 *13*, pp.484-485.

18 W.M. Muska, T. Li, T.P. Lee and A.G. Dentai: 'Material-dispersion-limited operation of high-bit-rate optical-fibre data links using l.e.d.s.' *Electron. Lett.* 1977, *13*, pp.605-607.

19 R. Olshansky: 'Mode coupling effects in graded-index optical fibres'. *Appl. Opt.* 1975, *14*, (4) pp.935-945.

20 M. Eve: 'Multipath time dispersion theory of an optical network'. *Opt. & Quant. Electron.* 1978, *10*, pp.41-51.

21 W.J. Stewart: 'Wavelength filtering effects in multimode fibres'. Proc. Optical Communication Conference, Amsterdam, September, 1979. Paper 12.3.

22 J.W. Fleming: 'Material and mode dispersion in GeO_2 - B_2O_3 - SiO_2 glasses'. *J. Am. Ceram. Soc.*, 1976, *59*, pp.503-507.

23 J.W. Fleming: 'Material dispersion in lightguide glasses. *Electron. Letts.* 1978, *14*, pp.326-328.

24 S. Kobayashi, S. Shibata, N. Shibata and T. Izawa: 'Refractive-index dispersion of doped fused silica'. Int. Conf. on Integrated Optics and Optical Fibre Communication, Tokyo, 1977. pp.309-312.

See also (by the same authors): 'Characteristics of optical fibers in infrared wavelength region'. *Rev. Electrical Commun. Lab.* 1978, *26*, pp.453-467.

25 T. Tanifuji and M. Ikeda: 'Simple method for measuring material dispersion in optical fibres". *Electron. Letts.* 1978, *14*, pp.367-369.

26 D. Gloge, E.L. Chinnock and T.P. Lee: 'GaAs twin-laser set-up to measure mode and material dispersion in optical fibres'. *Appl. Opt.* 1974, *13*, pp.264-265.

27 B. Luther-Davies, D.N. Payne and W. A. Gambling: 'Evaluation of material dispersion in low-loss phosphosilicate-core optical fibres'. *Opt. Commun.* 1975, *13*, pp.84-88.

28 L.G. Cohen and Chinlon Lin: 'Pulse delay measurements in the zero material dispersion wavelength region for optical fibers'. *Appl. Opt.* 1977, *16*, (12), pp.3166-3169.

29 D.N. Payne and A.H. Hartog: 'Determination of the wavelength of zero material dispersion in optical fibres by pulse-delay measurements'. *Electron. Letts.* 1977, *13*, pp.627-629.

30 L.G. Cohen, C. Lin, W.G. French and V.A. Foertmeyer: 'Pulse-delay measurements in the zero-material-dispersion region for germanium-and phosphorus-doped silica fibres'. *Electron. Lett.* 1978, *14*, (6) pp.170-172.

31 R. Bruckner: 'Properties and structure of vitreous silica . Part I'. *J. Non-Cryst. Solids,* 1970,*5*, pp. 123-175.

32 G.W. Scherer: 'Optical profile distortion caused by thermal stresses'. Proc. Fifth European Conference on Optical Communication, Amsterdam, September, 1979, paper 10.5.

See also: G.W. Scherer: 'Stress-induced index profile distortion in optical waveguides' - to appear in Applied Optics.

33 A.H. Hartog: 'Influence of waveguide effects on pulse-delay measurements of material dispersion in optical fibres'. *Electron. Lett.* 1979,*15*, pp.632-634.

34 A.H. Hartog, A.J. Conduit and D.N. Payne: 'Variation of pulse delay with stress and temperature in jacketed and unjacketed optical fibres'. *Opt. & Quant. Electron.* 1979, *11*, pp.265-273.

[35] K. Daikoku and A. Sugimura: 'Direct measurement of wavelength dispersion in optical fibres - difference method'. *Electron. Lett.* 1978, *14*, pp.149-151.

[36] A. Sugimura and K. Daikoku: 'Wavelength dispersion of optical fibers - directly measured by 'difference method'' in the 0.7 - 1.6 μm range'. *Rev. Sci. Instrum.* 1979, *50* (3), pp. 343-346.

[37] C. Lin, L.G. Cohen, W.G. French and H.M. Presby: 'Measuring dispersion in single-mode fibers in the 1.1-1.3μm spectral region - a pulse synchronisation technique'. Proc. Optical Communication Conference, Amsterdam, September, 1979, Paper 14.3.

[38] Chinlon Lin: Private communication.

[39] P.G. Guest: 'Numerical methods of curve fitting'. Cambridge University Press, 1961.

[40] M.J. Adams, D.N. Payne, F.M.E. Sladen and A.H. Hartog: 'Wavelength-dispersive properties of glasses for optical fibres: the germania enigma'. *Electron. Lett.* 1978, *14*, pp.703-705.

[41] D.N. Payne and W.A. Gambling: 'New silica-based low-loss optical fibre'. *Electron. Letts.* 1974,*10*, p.289.

[42] J.B. MacChesney, P.B. O'Connor and H.M. Presby: 'A new technique for the preparation of low-loss and graded-index optical fibres'. *Proc. IEEE* 1974,*62* p.1280.

[43] I.P. Kaminow and H.M. Presby: 'Profile synthesis in multi-component glass optical fibers'. *Appl. Opt.*1977, *16*, pp.108-112.

[44] E.A.J. Marcatili: 'Modal dispersion in optical fibers with arbitrary numerical apertures and profile dispersion'. *Bell Syst. Tech. J.* 1977,*56*, pp.49-63.

[45] R. Olshansky: 'Optical waveguides with low pulse dispersion over an extended spectral range'. *Electron. Letts.*1978, *14*, (11), pp. 330-331.

[46] K.J. Beales, C.R. Day, W.J. Duncan and G.R. Newns: 'Low-loss optical fibres prepared by the double crucible technique'. Proc. 3rd European Conference on Optical Communication, Munich September, 1977, pp.18-20.

[47] K.J. Beales, C.R. Day, W.J. Duncan, A.G. Dunn, P.L. Dunn, G.R. Newns and J.V. Wright: 'Low-loss graded index fibre by the double crucible technique'. Proc. 5th European Conference on Optical Communication, Amsterdam, September, 1979, paper 3.2.

[48] P.B. Macedo, J.H. Simmons, J. Olson, R.K. Mohr, M. Samanta, P.K. Gupta, T.V. Litovitz: 'Molecular stuffing of phasil glasses for graded-index optical fibres'. Proc. 2nd European Conference on Optical Communcation, Paris, September, 1976.

[49] R.D. Maurer: 'Doped-deposited-silica fibres for communications *Proc. IEE.* 1976, *123*, pp.581-585.

[50] D.B. Keck and R. Bouillie: 'Measurements on high-bandwidth optical waveguides'. *Opt. Commun.* 1978, *25*, pp.43-48.

[51] L.G. Cohen, Chinlon Lin and W.G. French: 'Tailoring zero chromatic dispersion into the 1.5-1.6μm low-loss spectral region of single mode fibres'. *Electron. Lett.* 1979,*15*, pp.334-335.

[52] T. Miya, Y. Terunuma, T. Hosaka and T. Miyashita: 'Ultimate low-loss single-mode fibre at 1.55μm'. *Electron. Lett.* 1979, *15*, pp.106-108.

[53] M. Nakahara, K. Chida, F. Hanawa, S. Sudo and M. Horiguchi: 'Fabrication of low-loss and wide-bandwidth v.a.d. optical fibres at 1.3μm wavelength. *Electron. Lett.* 1980, *16*, (3), pp.102-103.

[54] C.C. Shen, J.J. Hsieh and T.A. Lind: '1000-hour continuous CW operation of double-heterostructure GaIn AsP/InP lasers'. Topical Meeting on Optical Fiber Transmission Williamsburg, February, 1977, paper WB4.

[55] H.D. Law, L.R. Tomasetta, K. Nakano and J.S. Harris: '1.0-1.4μm high-speed avalanche photodiodes'. *Appl. Phys. Lett.* 1978, *33*(5) pp.416-417.

[56] C.A. Burrus, A.G. Dentai and T.P. Lee: 'In Ga AsP p-i-n photodiodes with low dark current and small capacitance. *Electron. Lett.* 1979, *15* (20) pp.655-657.

[57] M.J. Adams, D.N. Payne, F.M.E. Sladen and A.H. Hartog: 'Optimum operating wavelength for chromatic equalisation in multimode optical fibres'. *Electron. Lett*, 1978, *14*, pp.64-66.

[58] F.M.E. Sladen, D.N. Payne and M.J. Adams: 'Definitive profile-dispersion data for germania-doped silica fibres over an extended wavelength range'. *Electron. Lett.* 1979, *15* (15) pp.469-470.

[59] J.A. Arnaud: 'Optimum profiles for dispersive multimode fibres'. *Opt. and Quant. Electron.* 1977, *9*, pp.111-119.

[60] H.M. Presby and I.P. Kaminow: 'Binary silica optical fibers: Refractive index and profile dispersion measurements.' *Appl. Opt.* 1976, *15*, pp.3029-3036.

[61] M. Horiguchi, Y. Ohmori and T. Miya: 'Evaluation of material dispersion using a nanosecond optical pulse radiator'. *Appl. Opt.* 1979, *18*, (13), pp.2223-2228.

[62] Y. Ohmori, K. Chida, M. Horiguchi and I. Hatakeyama: 'Optimum profile parameter on graded-index optical fibre at 1.27 wavelength'. *Electron. Lett.* 1978, *14*, pp.764-765.

[63] G.W. Morey: '*Properties of glass*' Rheinhold Publishing Corporation, New York, 1938.

[64] W. Primak and D. Post: 'Photoelastic constants of vitreous silica and its elastic coefficient of refractive index'. *J. Appl. Phys.* 1959, *30*, (5), pp.779-788.

[65] K. Vedam, E.D.D. Schmidt and R. Roy: 'Non-linear variation of refractive index of vitreous silica with pressure to 7 k bars'. *J. Am. Ceram. Soc.* 1966, *49*, (10), pp.531-535.

[66] R.B. Calgaro, private communication. Mr. Calgaro has extended the stress analysis for a two-layer structure (reference [67]) to a three-layer structure.

67 D.A. Krohn: 'Determination of axial stress in clad glass fibers'. *J. Am. Ceram. Soc.* 1970, *53*, (9), pp.505-507.

68 D.N. Payne, private communication. Relation 3.47 is arrived at by compiling data (published and unpublished) from various sources.

69 D. Kuppers and J. Koenings: 'Preform fabrication by deposition of thousands of layers with the aid of plasma-activated CVD'. Proc. Second European Conference on Optical Communications, Paris, September, 1976, paper II.2, pp.49-54.

70 T. Izawa, S. Kobayaski, S. Sudo and F. Hanawa: 'Continuous fabrication of high silica fiber preform'. 1977 International Conference on integrated optics and optical fiber communication. Paper C1.1, pp.375-378.

71 D.B. Fraser: 'Factors influencing the acoustic properties of vitreous silica'. *J. Appl. Phys.* 1968, *39*, (13), pp.5868-5878.

Fibre	Length(km)	Type	Core composition	Cladding Composition
VD 150L	0.6127	graded	P_2O_5(15m%), SiO_2	SiO_2
VD 208L	0.8480	step	GeO_2(8.1m%) , SiO_2	SiO_2
VD 209L	0.6862	step	GeO_2(11.0m%) , SiO_2	SiO_2
VD 210L	1.2447	step	GeO_2(13.1m%) , SiO_2	SiO_2
VD 232L	1.0677	step	GeO_2(15.6m%) , SiO_2	SiO_2
VD 262L	0.7870	step	SiO_2	B_2O_3/SiO_2
VD 199L	∿1.078	graded	$GeO_2P_2O_5/SiO_2$	B_2O_3/SiO_2
VD 202L	1.2828	graded	$GeO_2/P_2O_5/SiO_2$	B_2O_3/SiO_2
BPO 770818	∿2.15	graded	$Na_2O/B_2O_3/SiO_2$	$Na_2O/B_2O_3/SiO_2$
Phasil	∿0.465	graded	$Na_2O/B_2O_3/SiO_2$	$Na_2O/B_2O_3/SiO_2$
CGW-P057	∿0.99	graded	$GeO_2/B_2O_3/SiO_2$	B_2O_3/SiO_2
9055	∿2.45	single mode	GeO_2/SiO_2	$P_2O_5/F/SiO_2$
9052	∿6.1	single mode	GeO_2/SiO_2	$P_2O_5/F/SiO_2$

Table 3.1 : Characteristics of the fibres used for pulse-delay measurements

Fitted Coefficients

Fibre	Figure number	a_{-4} x 10^{12}	a_{-2} x 10^{6}	a_{2} x 10^{-6}	a_{4} x 10^{-12}	Mean Residual (ps)	Wavelength of zero chromatic dispersion (nm)
VD 150 L	14	-0.586118	35.5008	13.7900	-0.154598	155	1272 ± 3.1
VD 208 L	16	3.97318	15.4461	-9.72806	4.61941	370	1324.7 ± 3.0
VD 209 L	17	0.586153	35.6022	11.0889	0.131064	300	1331.0 ± 3.4
VD 210 L	18	1.30788	31.7003	3.95604	1.58870	635	1356.0 ± 4.6
VD 232 L	19	-0.064246	40.1979	11.6017	0.047453	260	1358.6 ± 1.4
VD 262 L	22	-0.0192169	34.3184	14.8163	-0.556377	160	1274.2 ± 1.5
VD 199 L	23	-0.304769	37.1561	16.5905	-0.998200	280	1290.5 ± 2.8
VD 202 L	24	0.530387	31.2420	8.97107	0.593267	185	1304.9 ± 1.2
BPO 770818	25	0.522837	38.4661	13.2738	-0.304544	240	1338.0 ± 7.2
Phasil	26	0.661591	33.4507	7.63600	1.58044	135	1278.9 ± 6.6
CGW-P057	27	0.694403	31.5114	8.75013	0.671473	250	1307.9 ± 1.8
9055	28	5.13098	18.3657	1.90037	1.12166	130	1394.1 ± 1.1
9052	29	2.80752	24.2446	5.50216	0.671774	160	1359.6 ± 0.4

Table 3.2: Results of pulse delay measurements

The material dispersion parameter (ps nm^{-1} km^{-1}) may be found, for any wavelength λ (nm), from the expression

$$M(\lambda) = 1000\ (-4\ a_{-4}\ \lambda^{-5} - 2\ a_{-2}\ \lambda^{-3} + 2\ a_{2}\ \lambda + 4\ a_{4}\ \lambda^{3})$$

For the singlemode fibres, 9055 and 9052, the value thus obtained is the total chromatic dispersion.

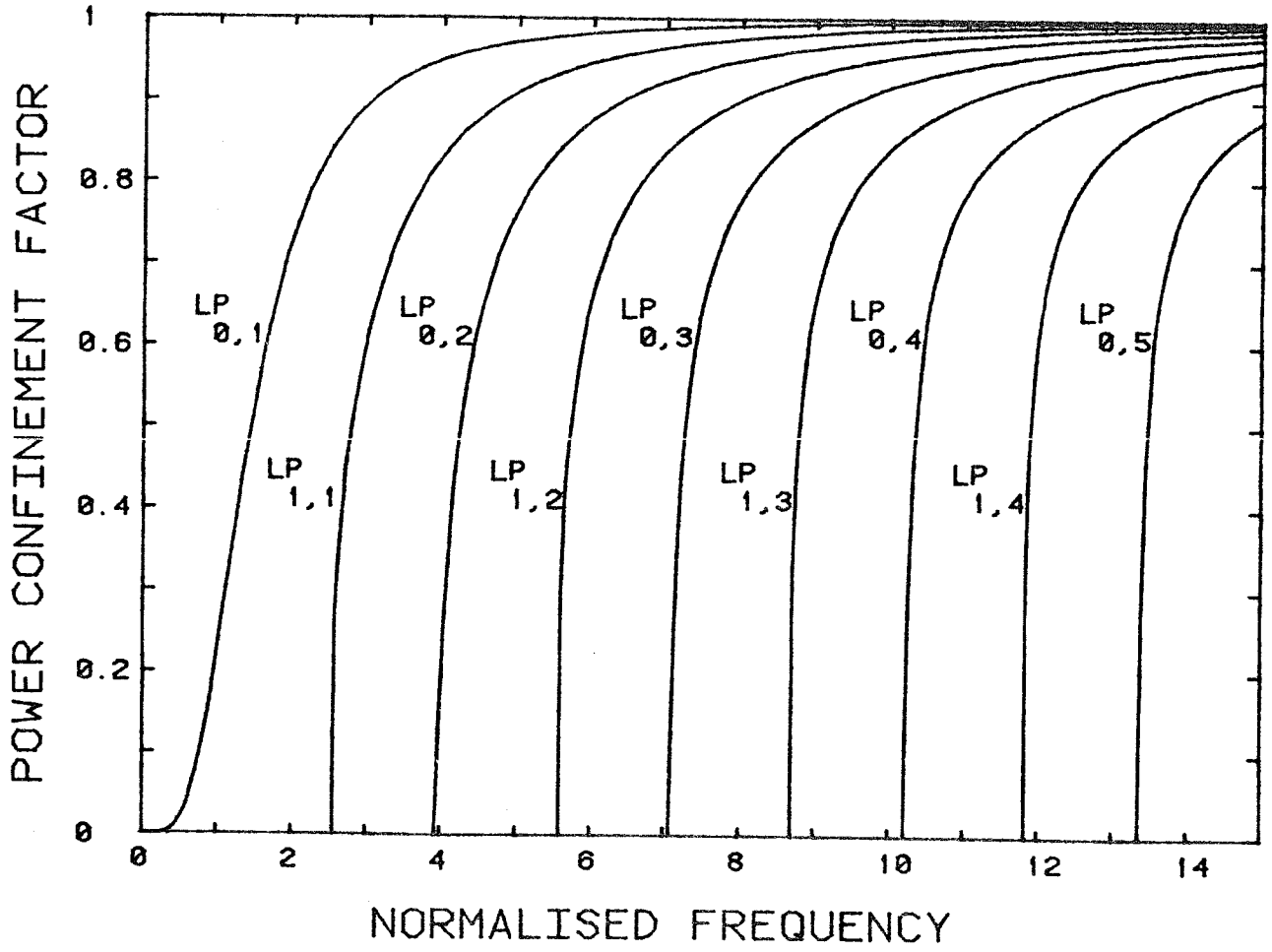

Figure 3.1: Variation of the power confinement factor Γ with normalised frequency (V-value) for a few low-order modes of a step-index fibre.

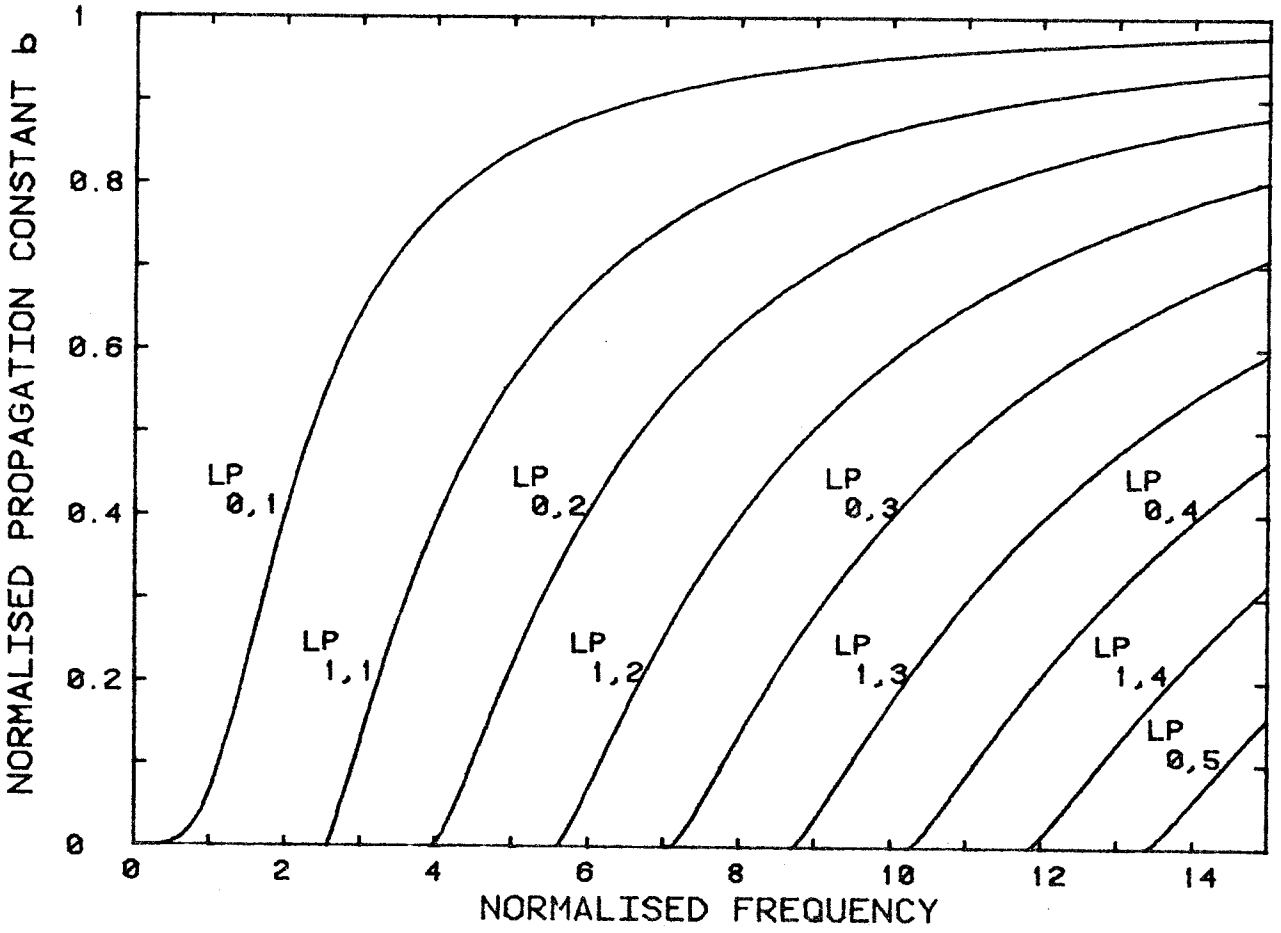

Figure 3.2: Variation of the normalised propagation constant b with normalised frequency (V-value) for a few low-order modes of a step-index fibre.

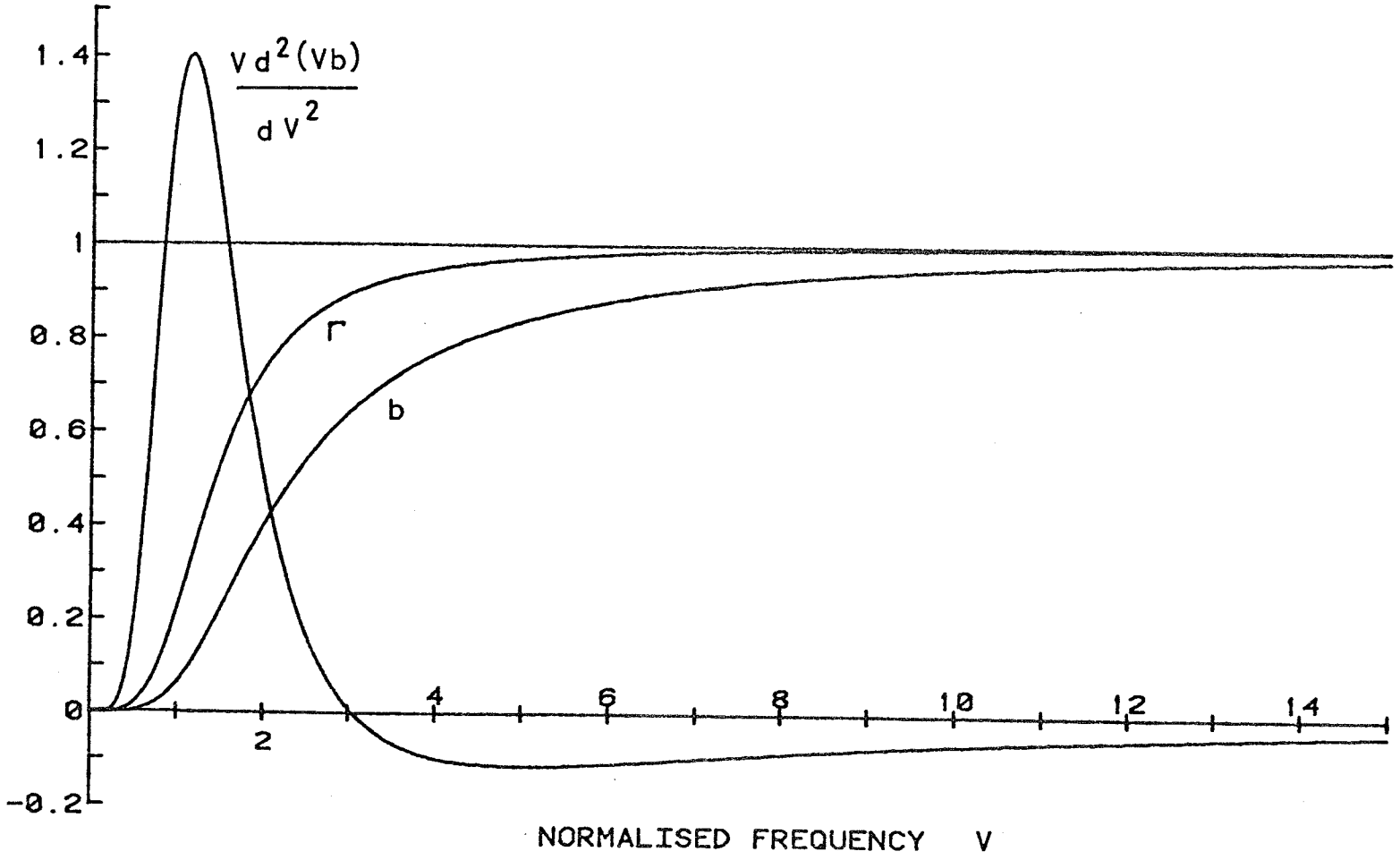

Figure 3.3: Comparison of the normalised propagation constant b, the power confinement factor Γ and the waveguide dispersion parameter $V\, d^2(Vb)/dV^2$ for the lowest-order (LP_{01}) mode of a step-index fibre.

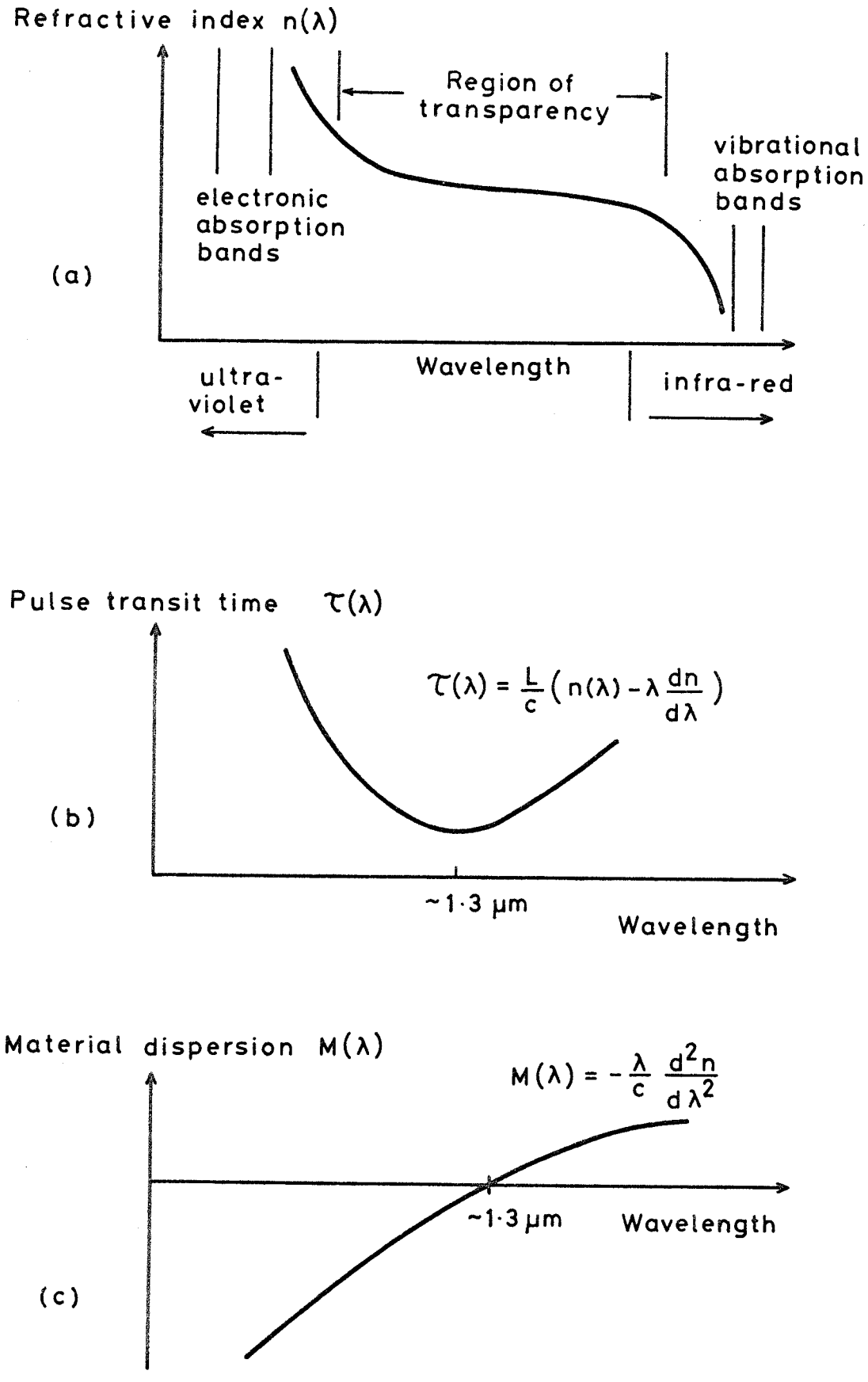

Figure 3.4:

Schematic representation of the wavelength-dependence of refractive index, pulse transit-time and material dispersion parameter in silica-based glasses.

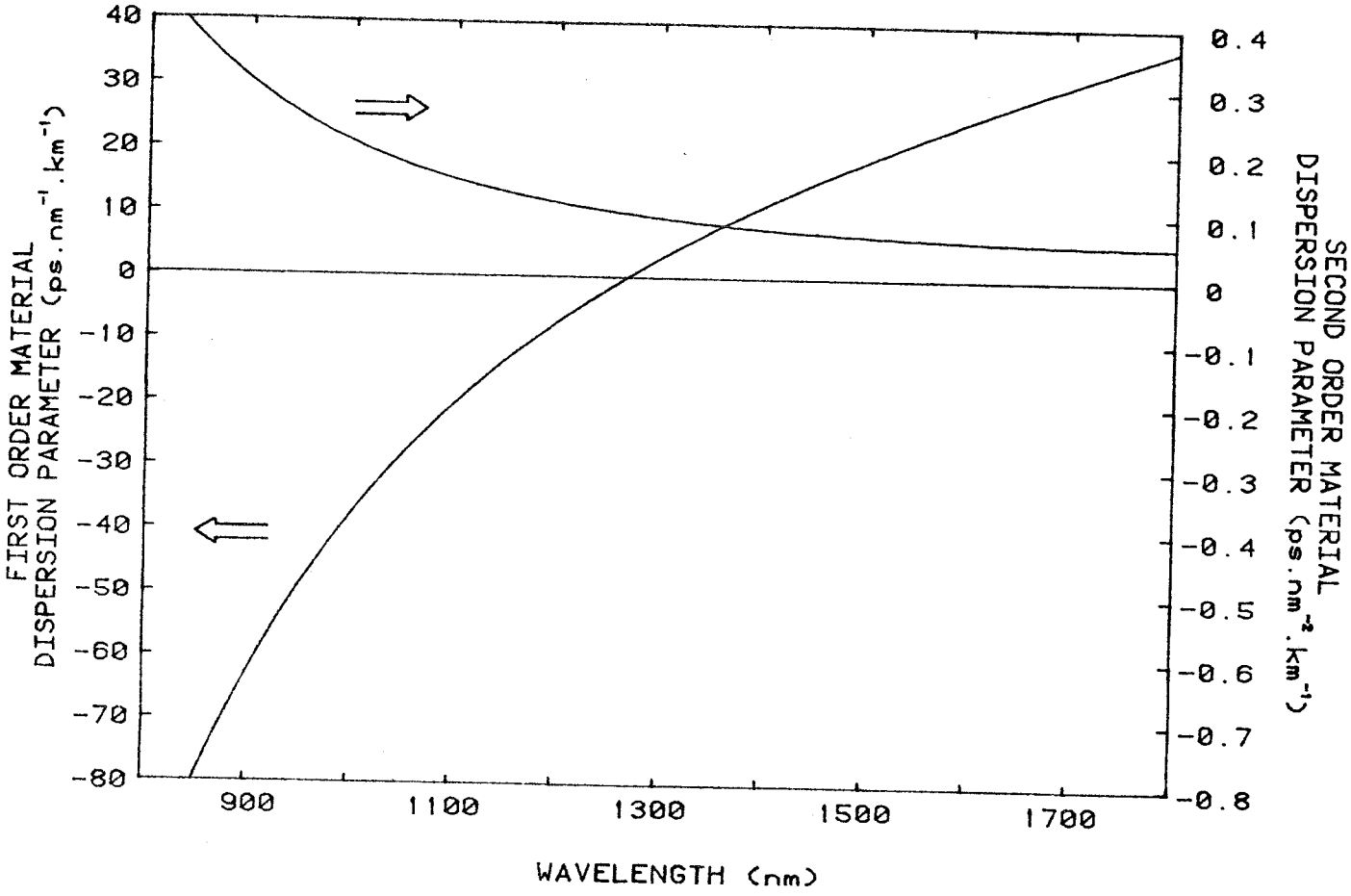

Figure 3.5: Wavelength-dependence of the first- and second-order material dispersion parameters of fused silica.

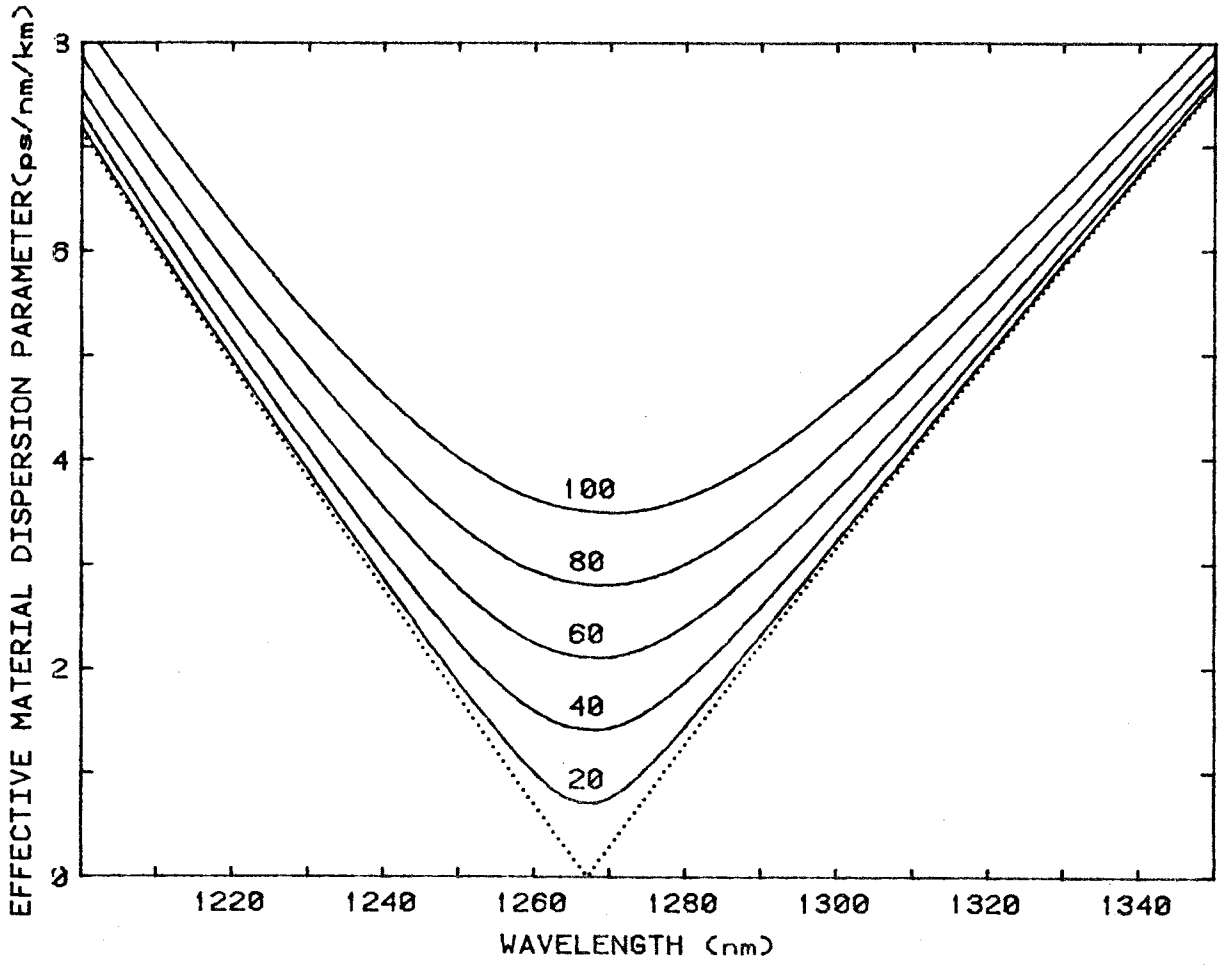

Figure 3.6: Wavelength-dependence of the effective material dispersion parameter of silica for the source linewidths indicated. The dotted curve shows the modulus of the first-order material-dispersion parameter, which applies to very narrow linewidths.

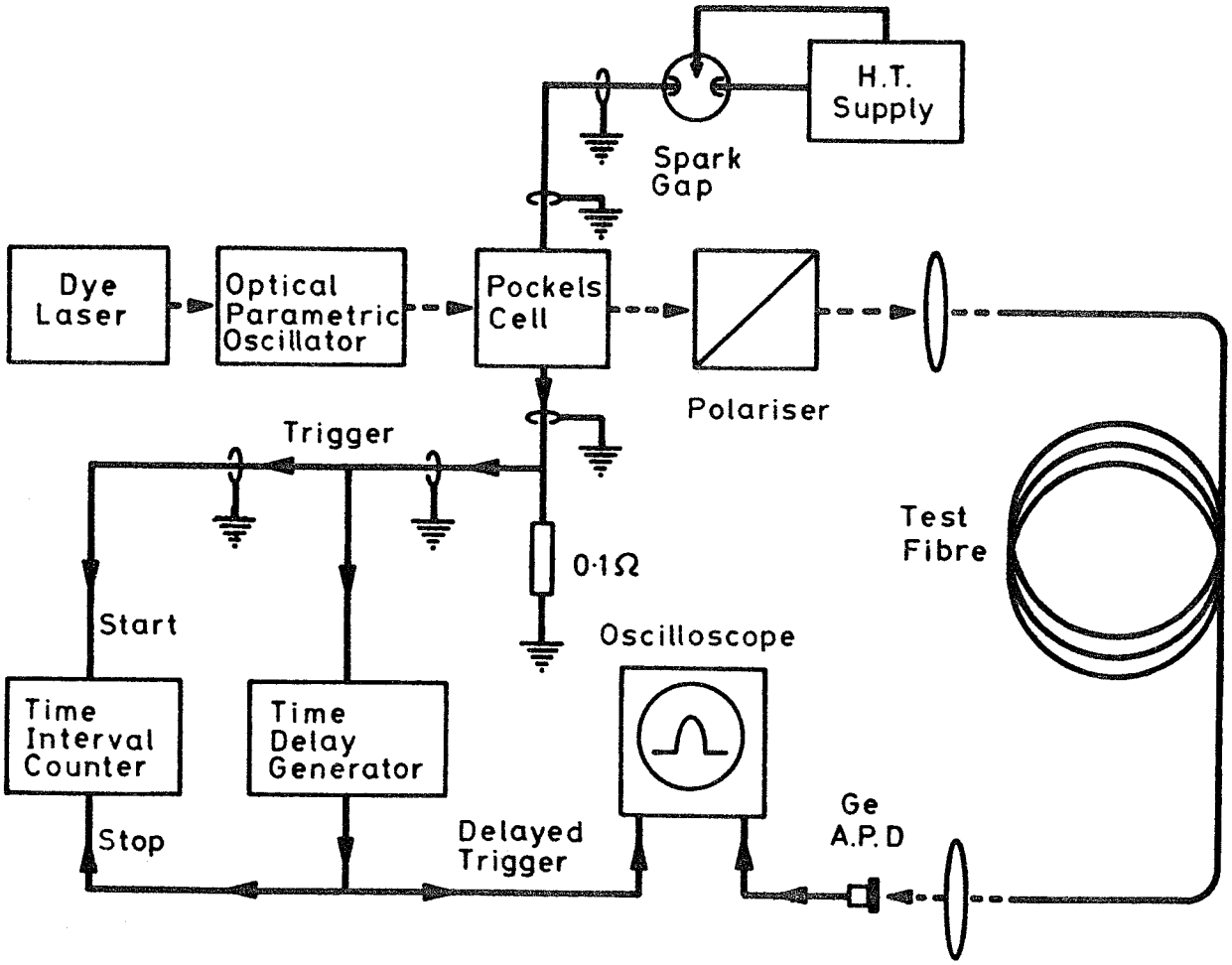

Figure 3.7: Basic arrangement of the dye-laser system for pulse-delay measurements in optical fibres.

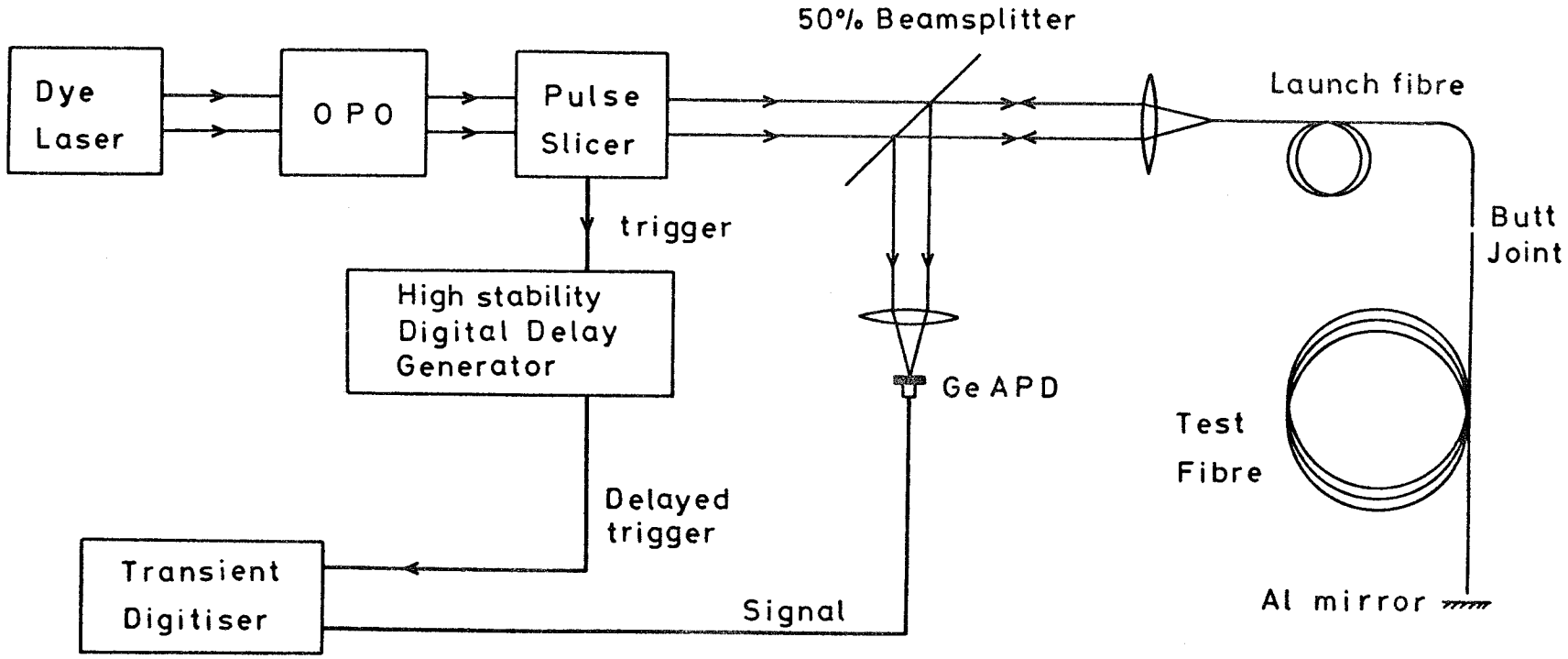

Figure 3.8: Improved experimental arrangement for pulse-delay measurements using a double passage through the fibre. A time-reference is obtained from the front-face reflection of the test fibre.

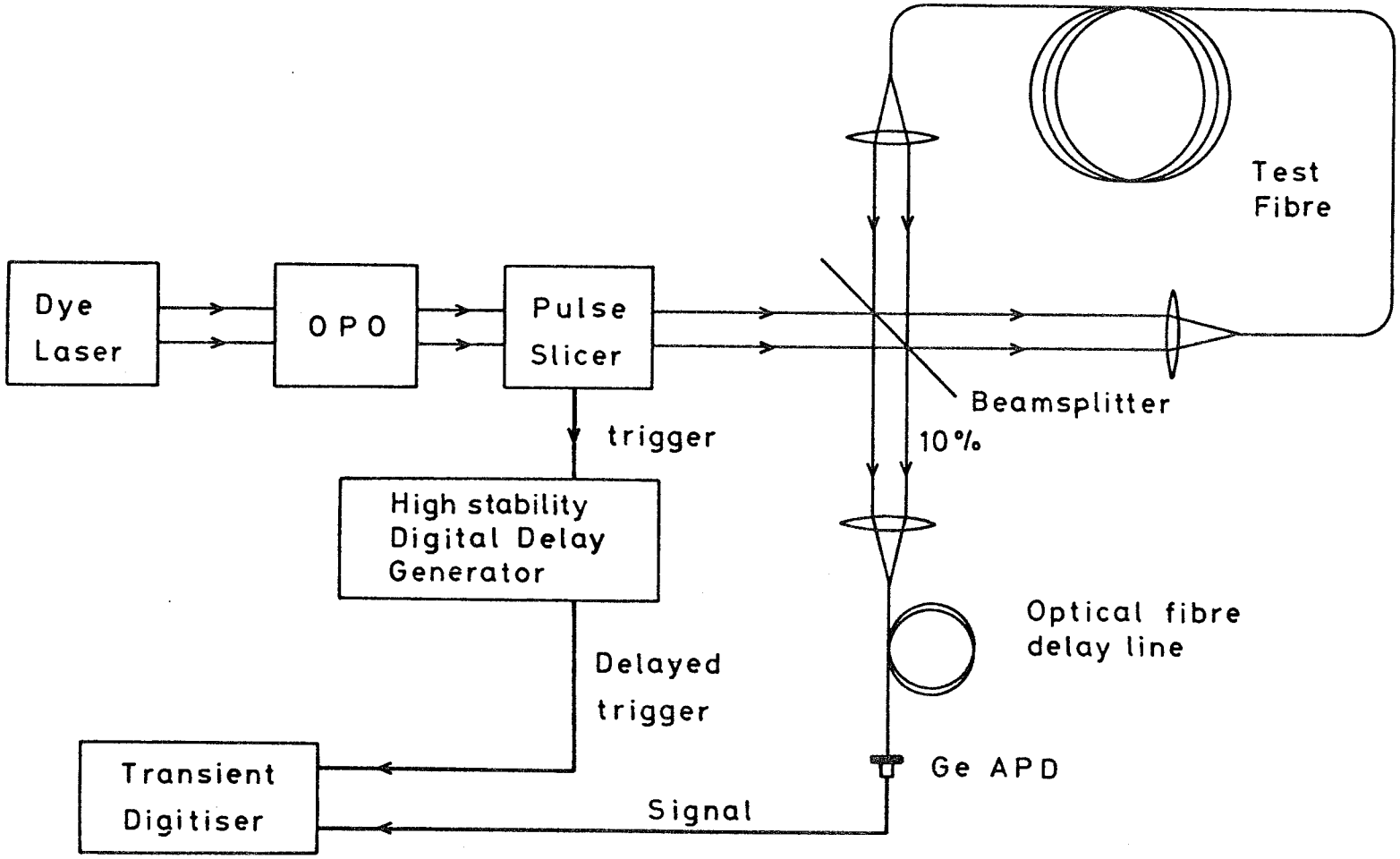

Figure 3.9: Single-pass variant of the arrangement shown in figure 3.8. The time-reference is now obtained from the 10% beamsplitter.

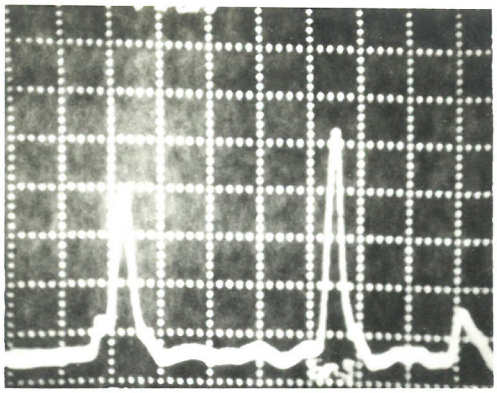

λ = 894 nm

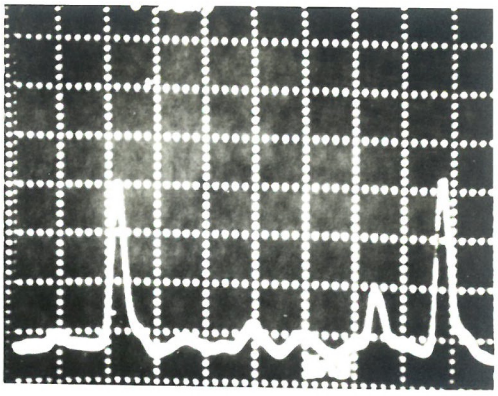

λ = 1260 nm

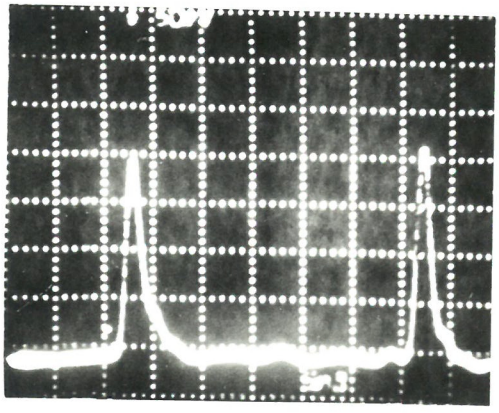

λ = 970 nm

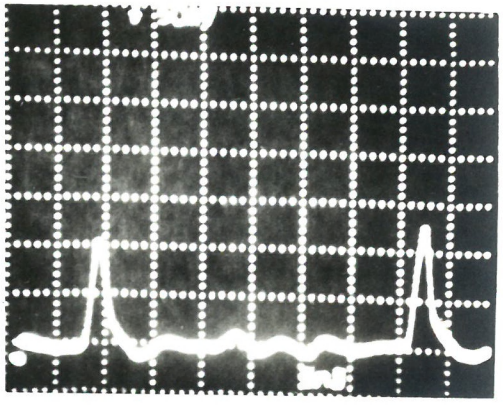

λ = 1306 nm

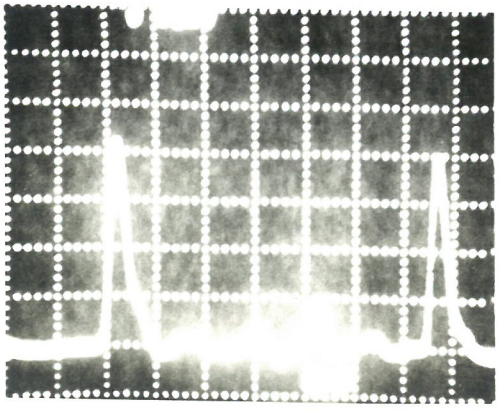

λ = 1153 nm

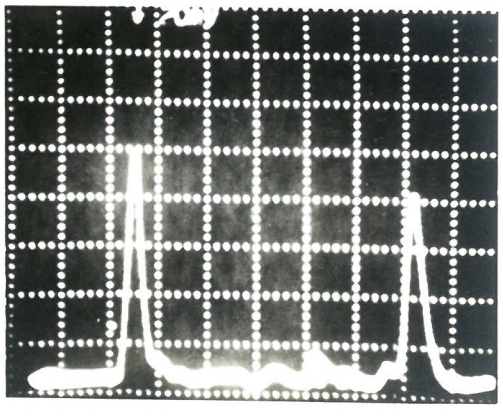

λ = 1667 nm

Figure 3.10: Oscilloscope traces recorded during a measurement of material dispersion on fibre VD 150 (see table 3.1) by the two pulse-technique. The wavelength of the infrared pulse (generated by the O.P.O.) is indicated under each photograph. The wavelength of the visible pulse (produced by the dye-laser and appearing to the right of the infrared pulse) is 606 nm in all cases. The horizontal scale is 5 ns/div.

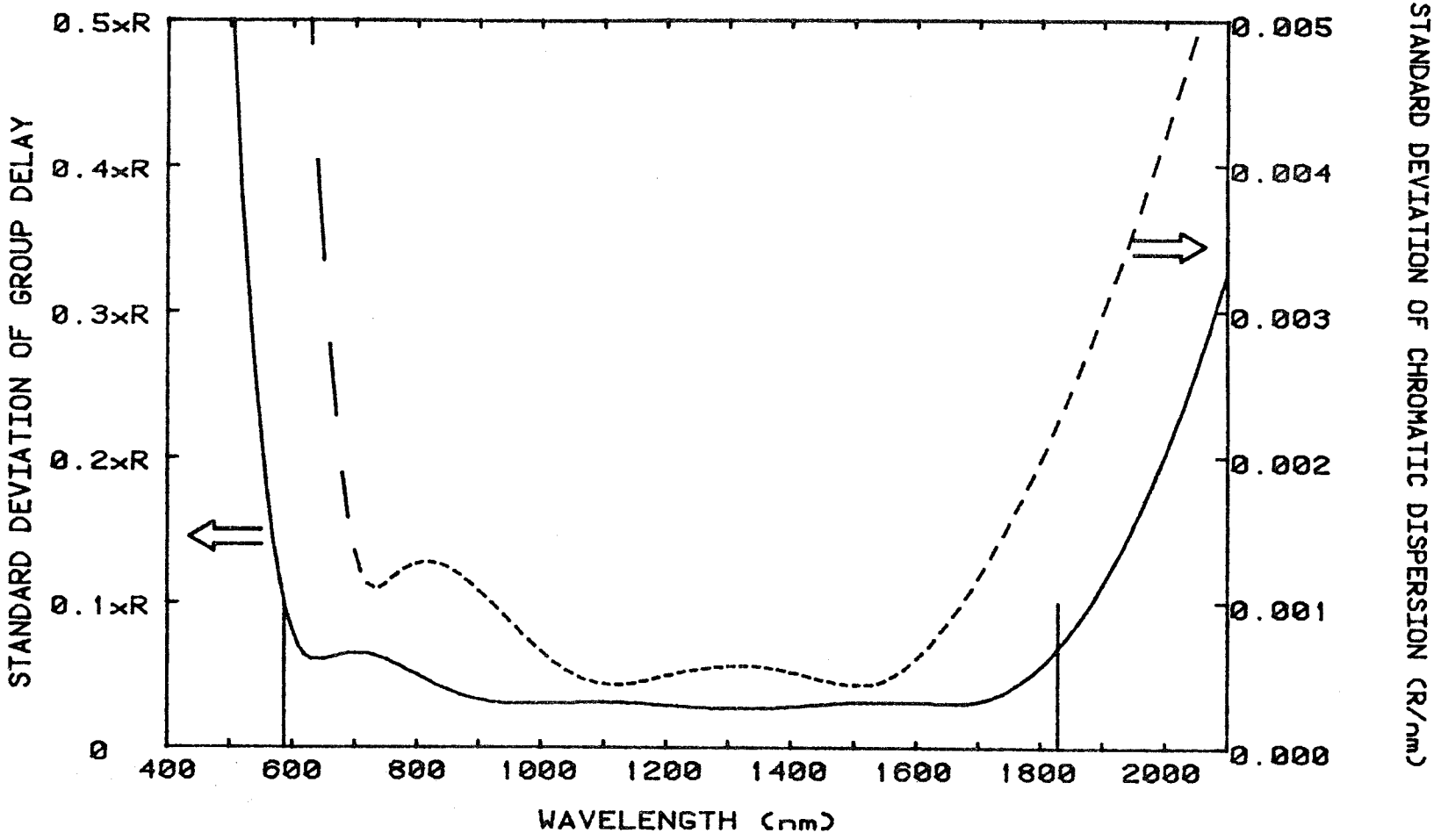

Figure 3.11: Error analysis of typical pulse-delay data. Measurements were made at 5 nm intervals in the wavelength ranges 590-630 nm and 800-1820 nm (extremes are indicated by vertical bars). The solid line shows the variation with wavelength of the standard deviation of the pulse delay, expressed as a fraction of the mean residual R. The broken line shows the standard deviation of the material dispersion parameter, also scaled to the mean residual.

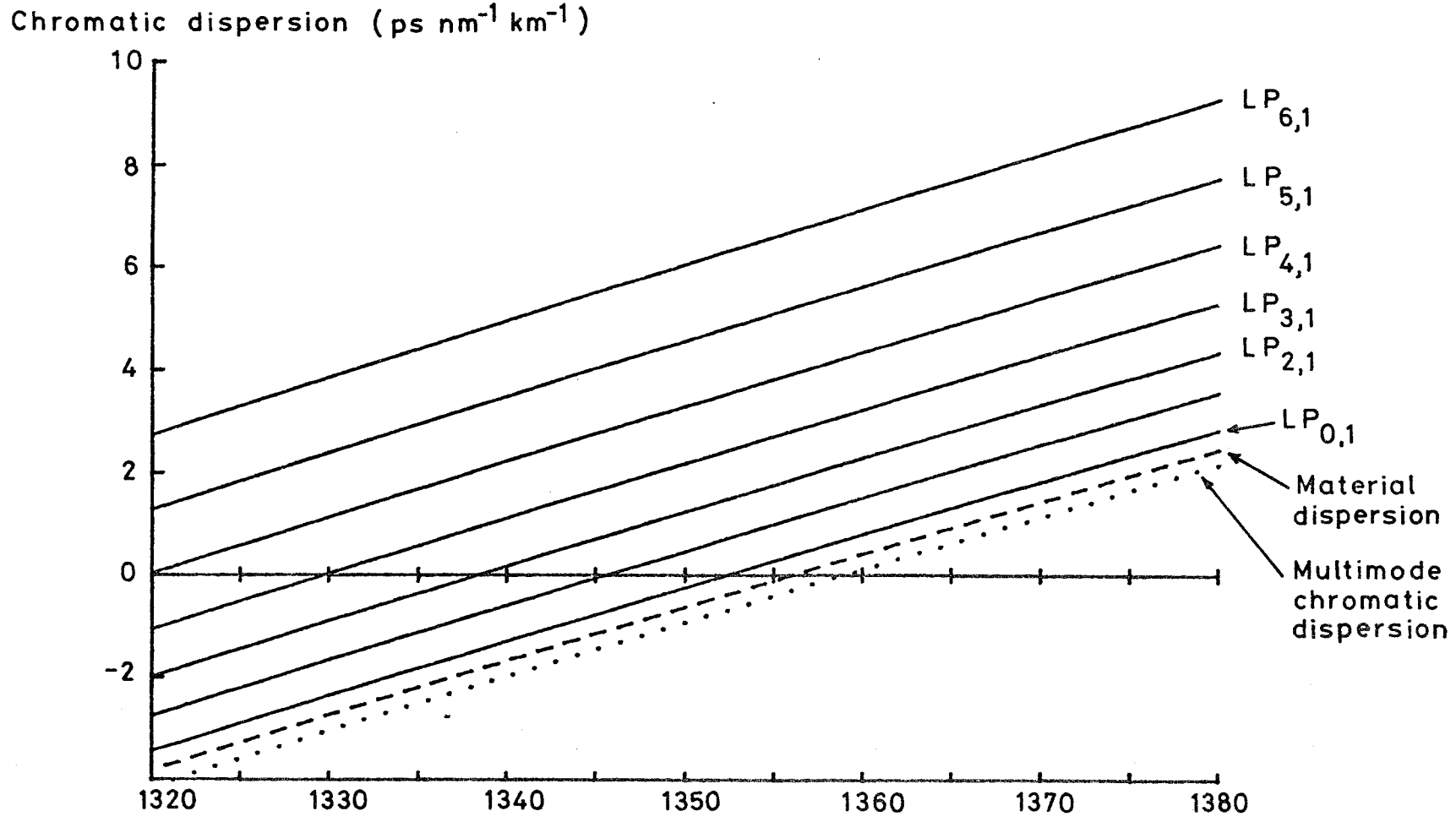

Figure 3.12: Chromatic dispersion calculated for a step-index multimode fibre.

Solid lines: total dispersion of individual low-order LP modes,

Broken line: material dispersion of the core glass,

Dotted line: multimode chromatic dispersion; the modal power distribution is assumed to be: $p_{\nu\mu} = 1 - u/V$.

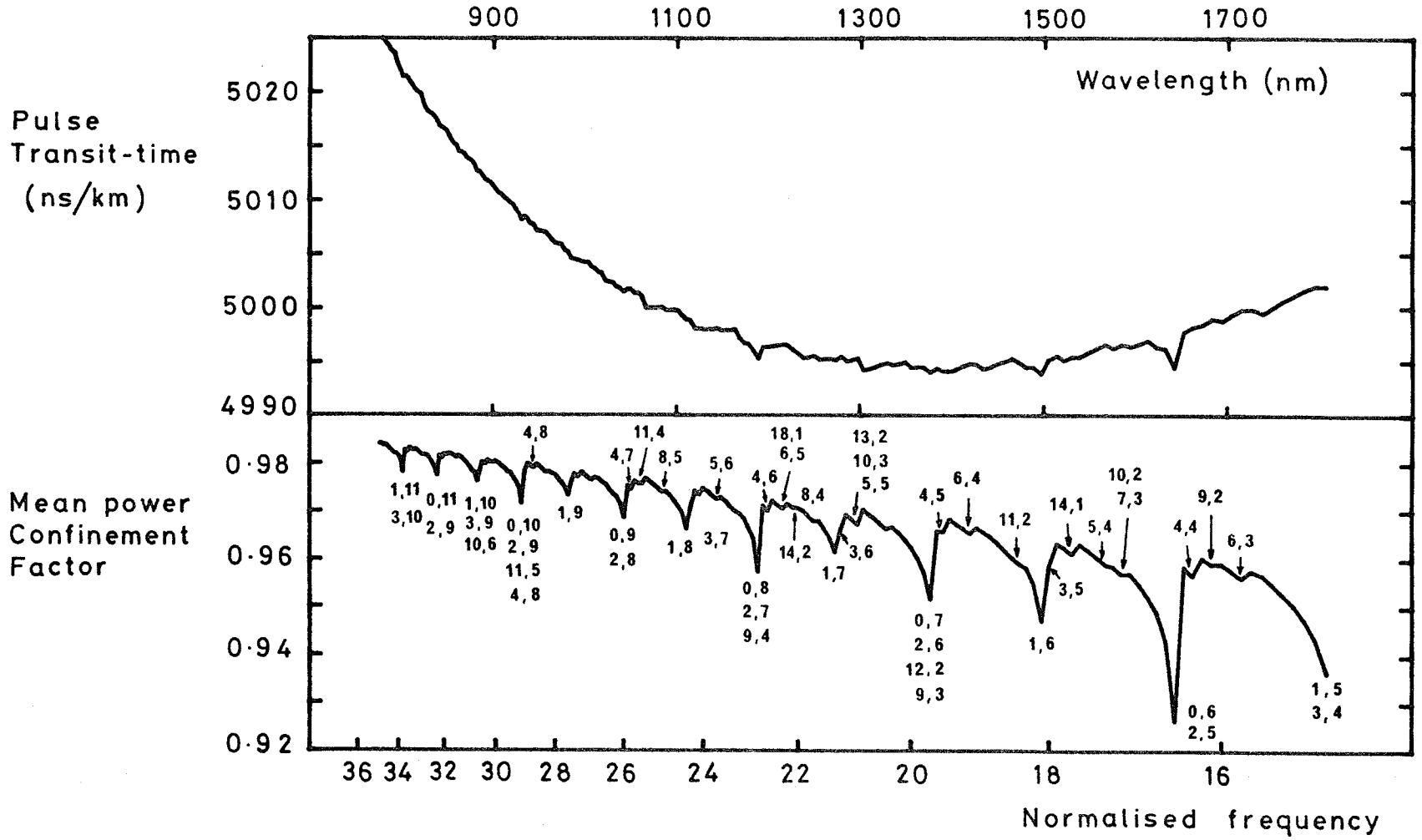

Figure 3.13: Calculated pulse transit-time (top) and mean power confinement factor (bottom) for a fully-excited multimode step-index fibre. The fibre is assumed to have the composition of VD 210L (see Table 3.1) and a V-value of 20 at λ = 1356 nm. The cut-off wavelength of several modes has been indicated (using the LP mode designation) near the corresponding feature of the power confinement/wavelength function.

Figure 3.14

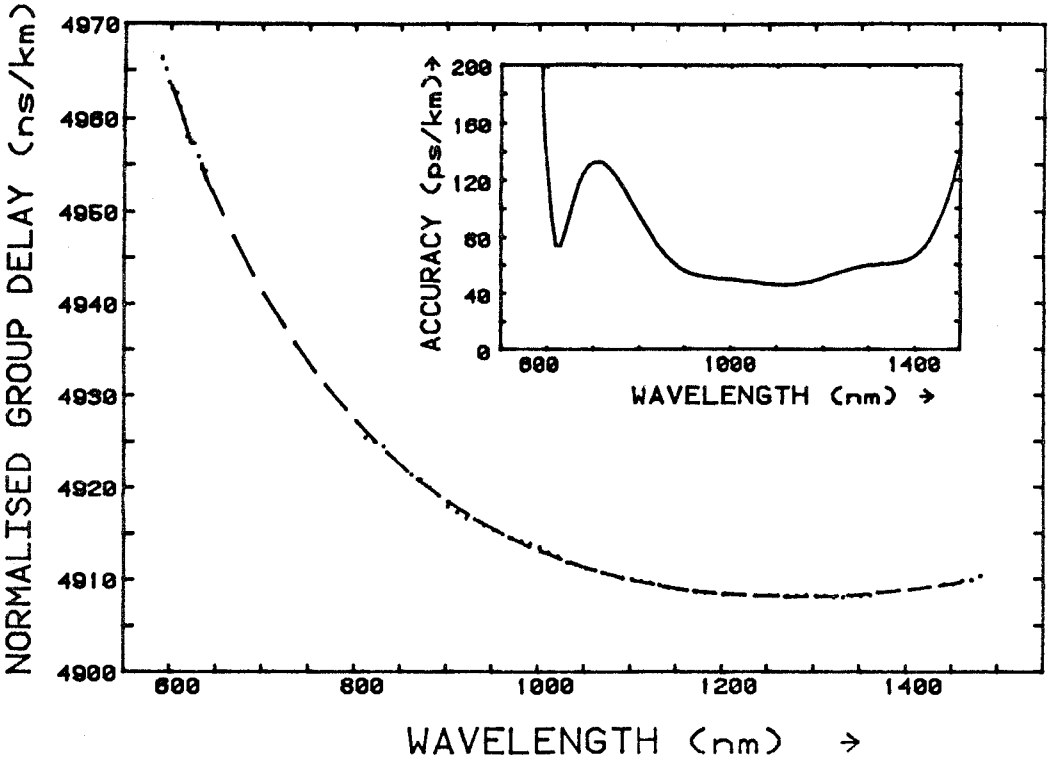

(a) Variation of normalised pulse-delay with wavelength measured in a graded-index phosphosilicate fibre, VD 150L (dots). The broken line shows the power series (eqn. 3.21) fitted to the data.

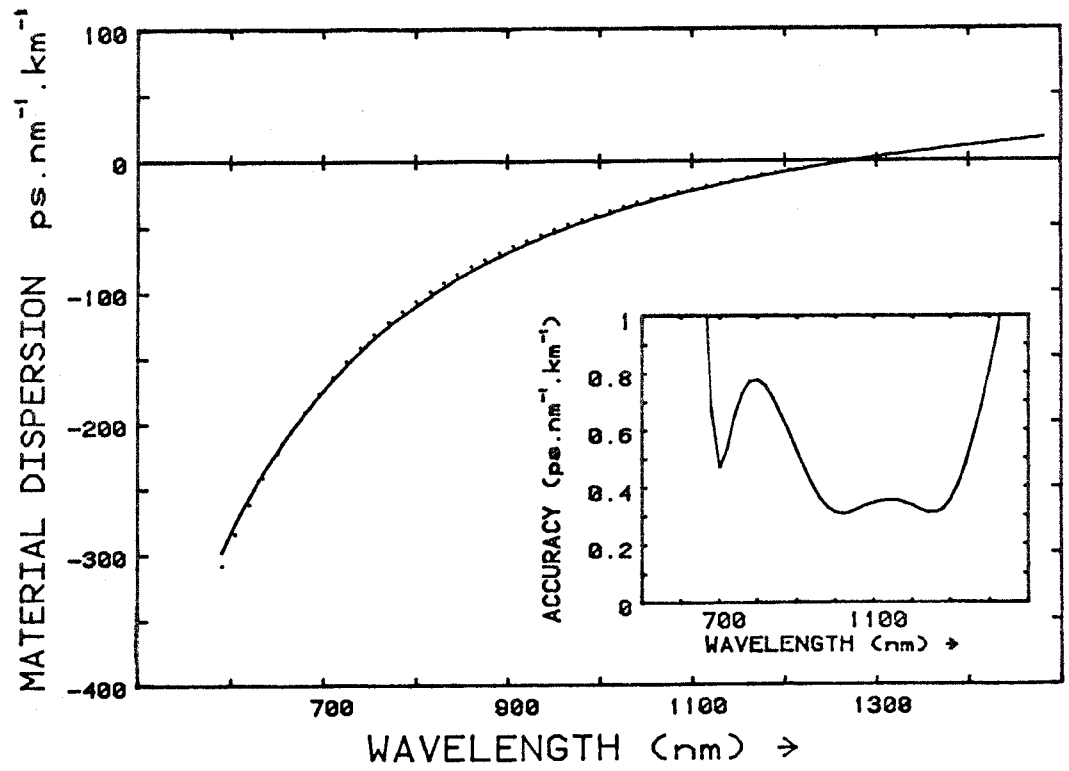

(b) Material dispersion parameter inferred by differentiation of the fitted function (solid line). For comparison, the dotted line shows the material dispersion parameter of silica in bulk form. In both parts of the figure, an inset indicates the standard deviation of the fitted values.

Figure 3.15

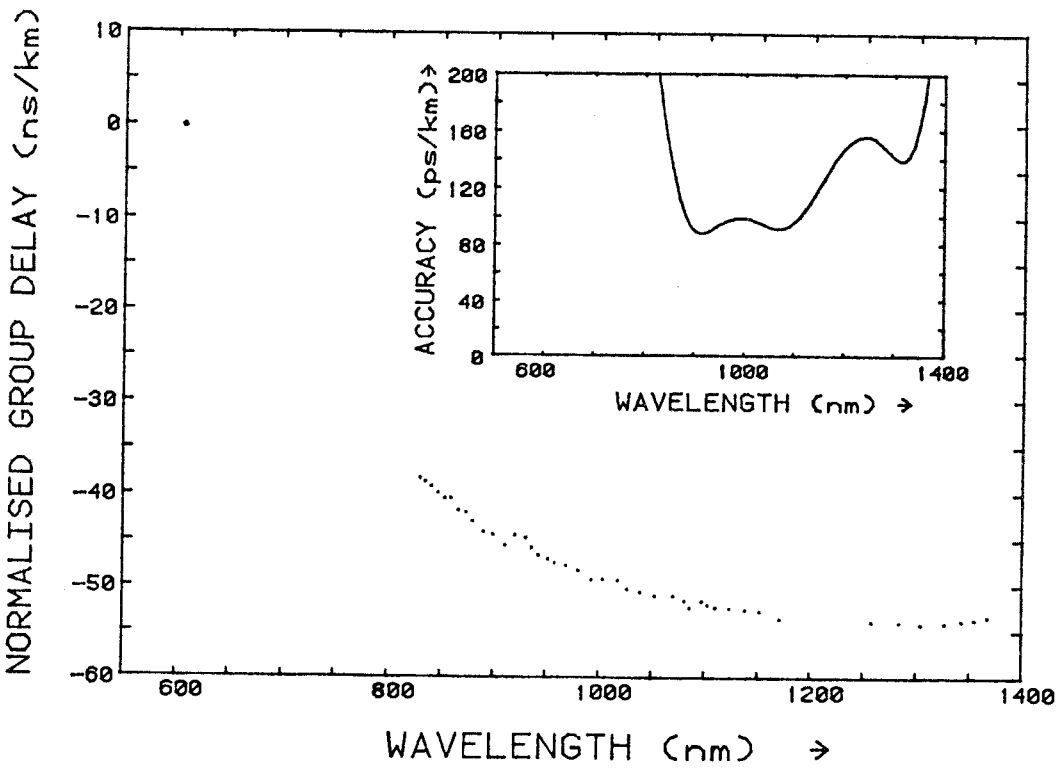

(a) Normalised variation of pulse transit-time with wavelength measured in fibre VD 150L using the two-pulse technique. The delays shown are measured relatively to that at 606 nm. For clarity, the fitted function has been omitted for this and subsequent figures.

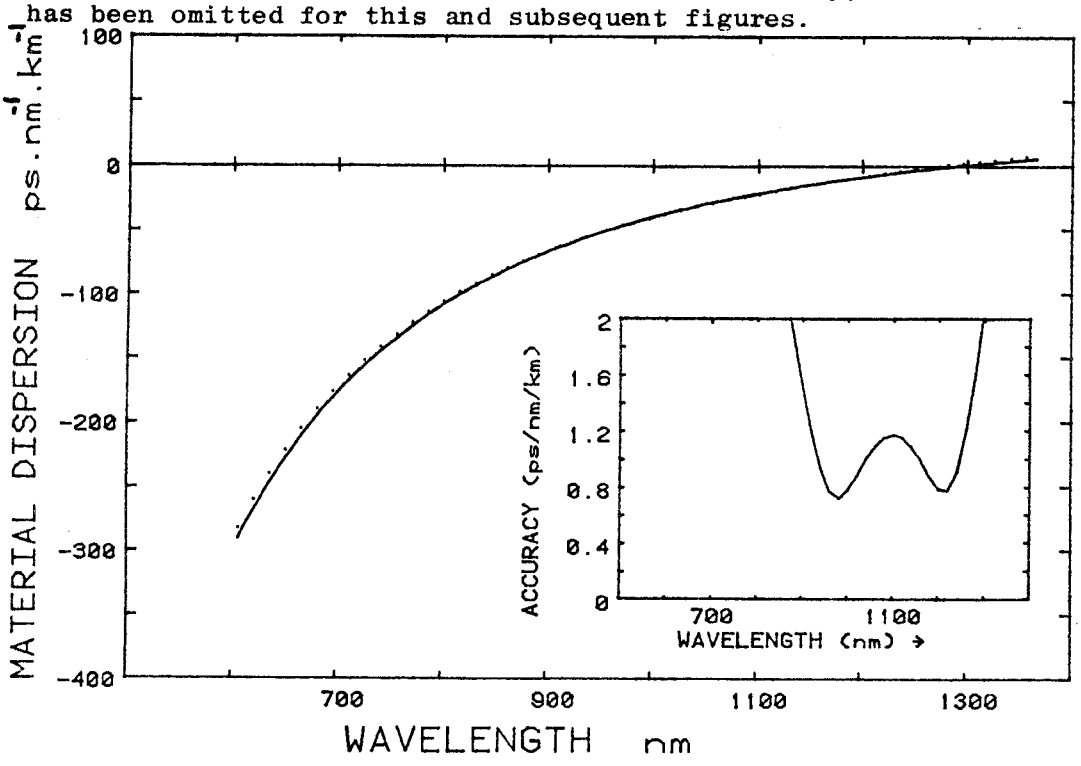

(b) Material dispersion parameter inferred from (a) (solid line). The dotted line shows the material dispersion of silica in bulk form.

The insets show the standard deviation of the fitted values.

Figure 3.16

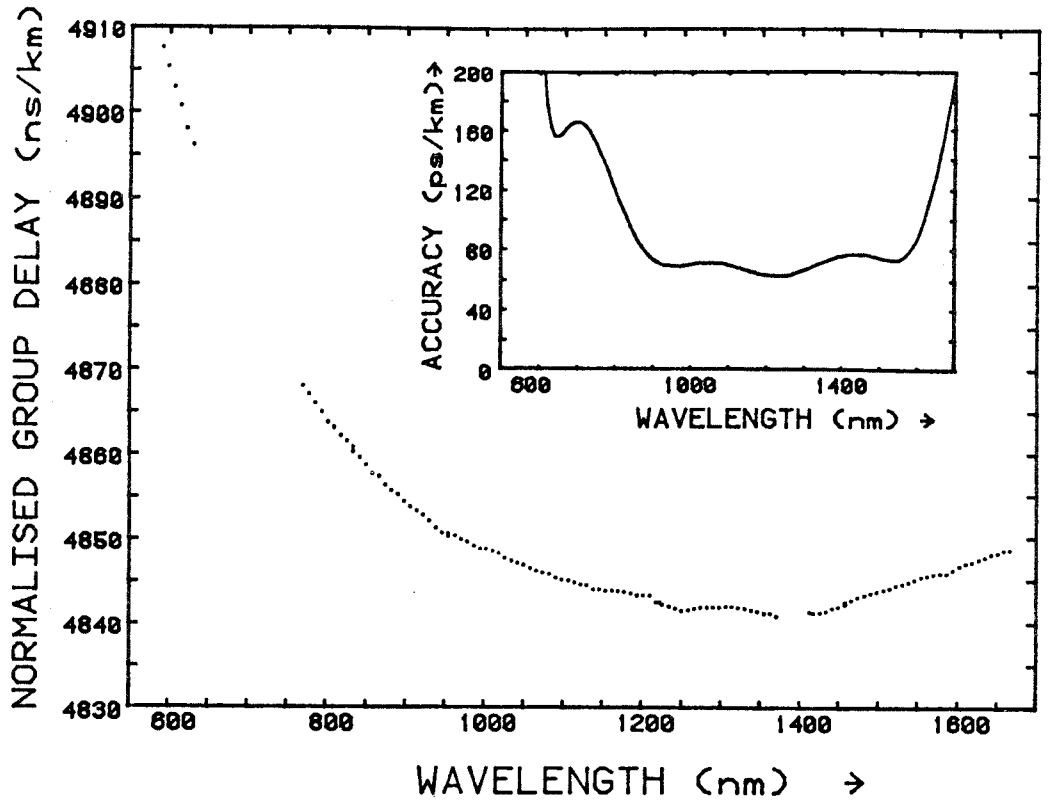

(a) Variation of normalised pulse transit-time with wavelength, measured in a step-index germanosilicate-core fibre, VD 208L.

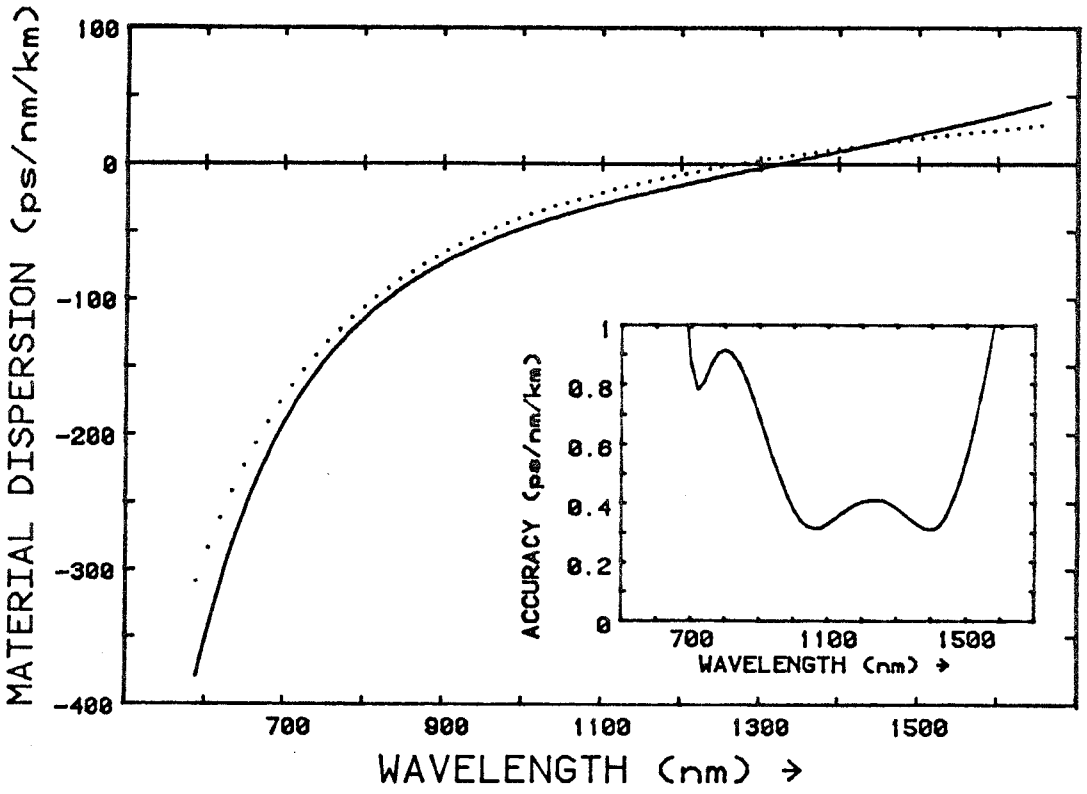

(b) Wavelength-dependence of the material dispersion parameter ($ps.nm^{-1}.km^{-1}$) inferred from (a) (solid line). The dotted curve shows, for comparison, the material dispersion parameter of silica in bulk form.

The standard deviation of the fitted values is indicated in the insets of (a) and (b).

Figure 3.17

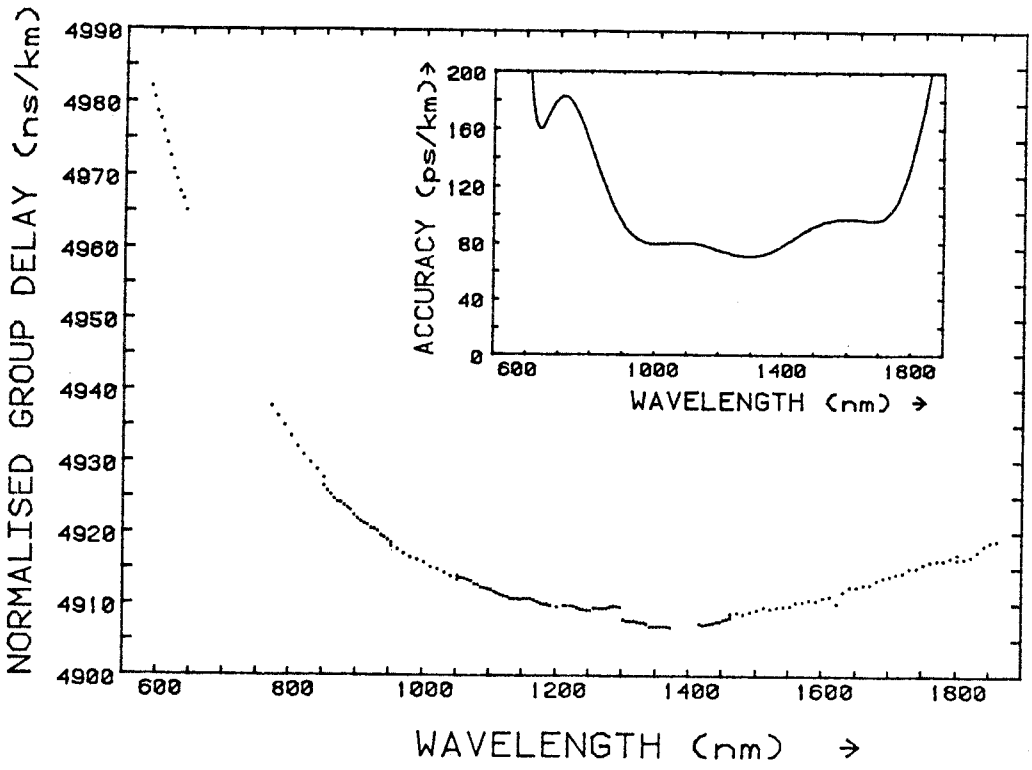

(a) Variation of normalised pulse transit-time with wavelength, measured in a step-index germanosilicate-core fibre, VD 209L.

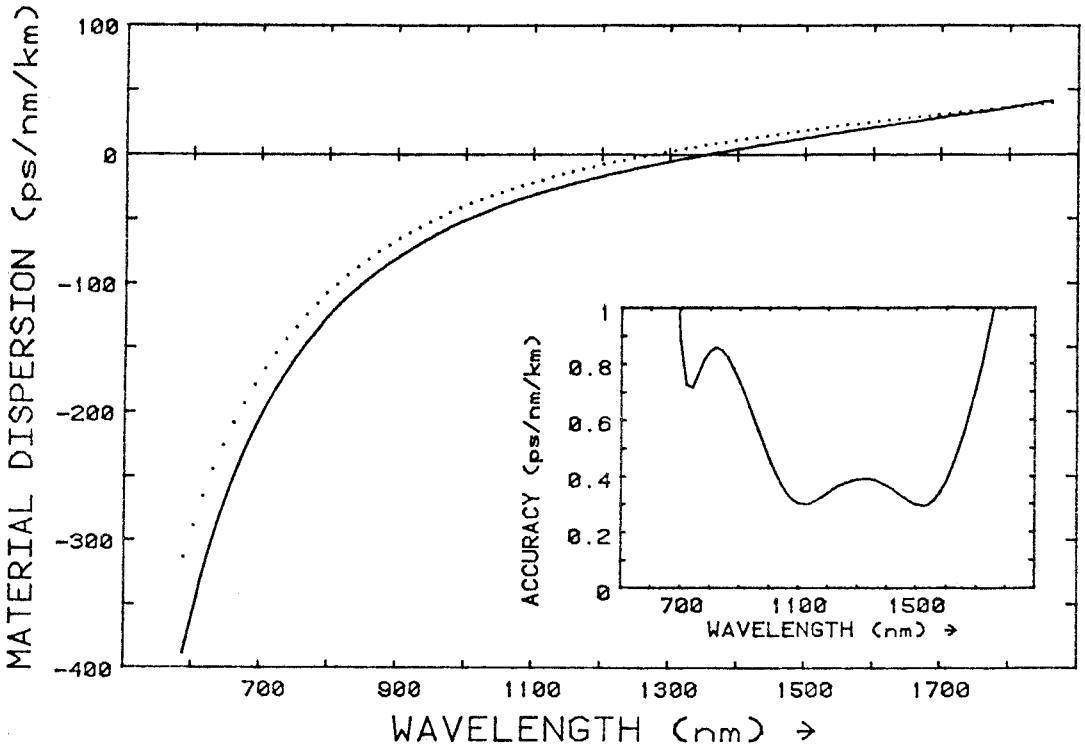

(b) Wavelength-dependence of the material dispersion parameter ($ps.nm^{-1}.km^{-1}$) inferred from (a) (solid line). The dotted curve shows, for comparison, the material dispersion parameter of silica in bulk form.

The standard deviation of the fitted values is indicated in the insets of (a) and (b).

Figure 3.18

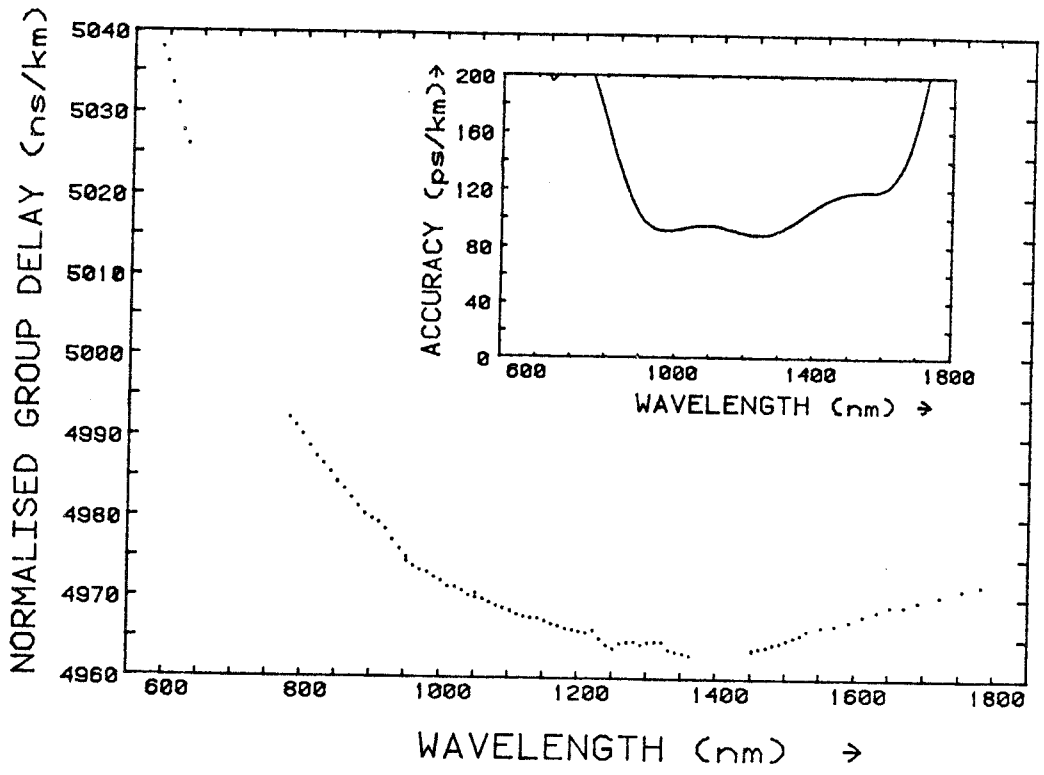

(a) Variation of normalised pulse transit-time with wavelength, measured in a step-index germanosilicate-core fibre, VD 210L.

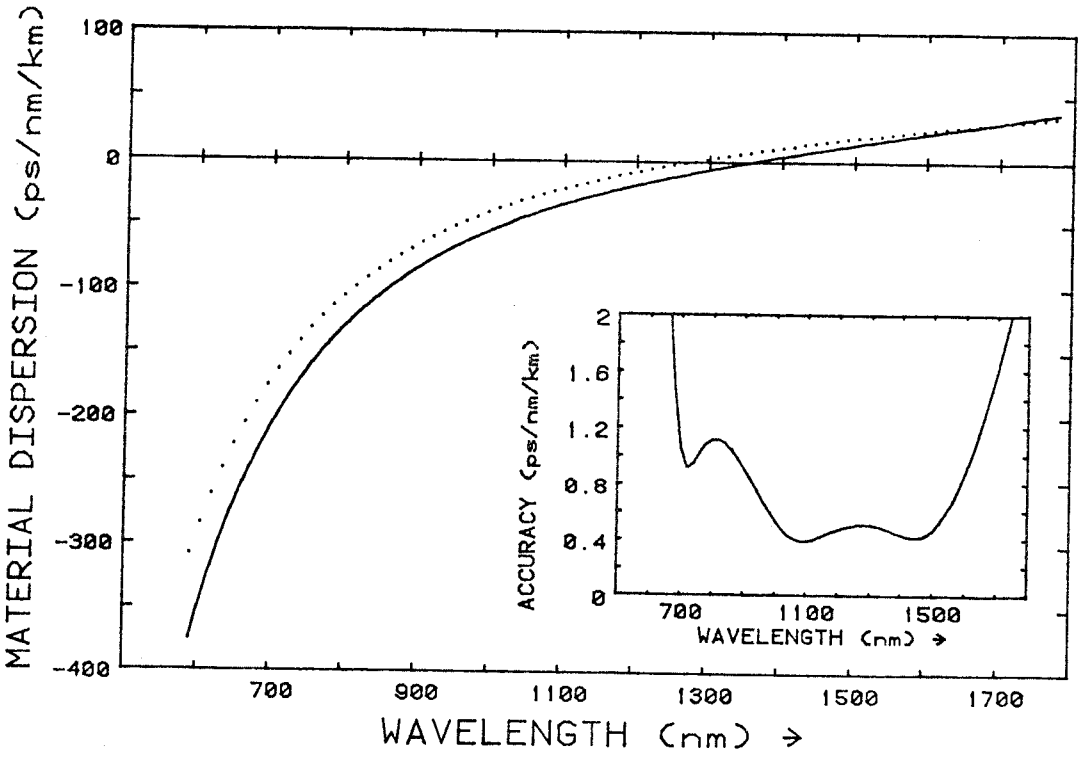

(b) Wavelength-dependence of the material dispersion parameter ($ps.nm^{-1}.km^{-1}$) inferred from (a) (solid line). The dotted curve shows, for comparison, the material dispersion parameter of silica in bulk form.

The standard deviation of the fitted values is indicated in the insets of (a) and (b).

Figure 3.19

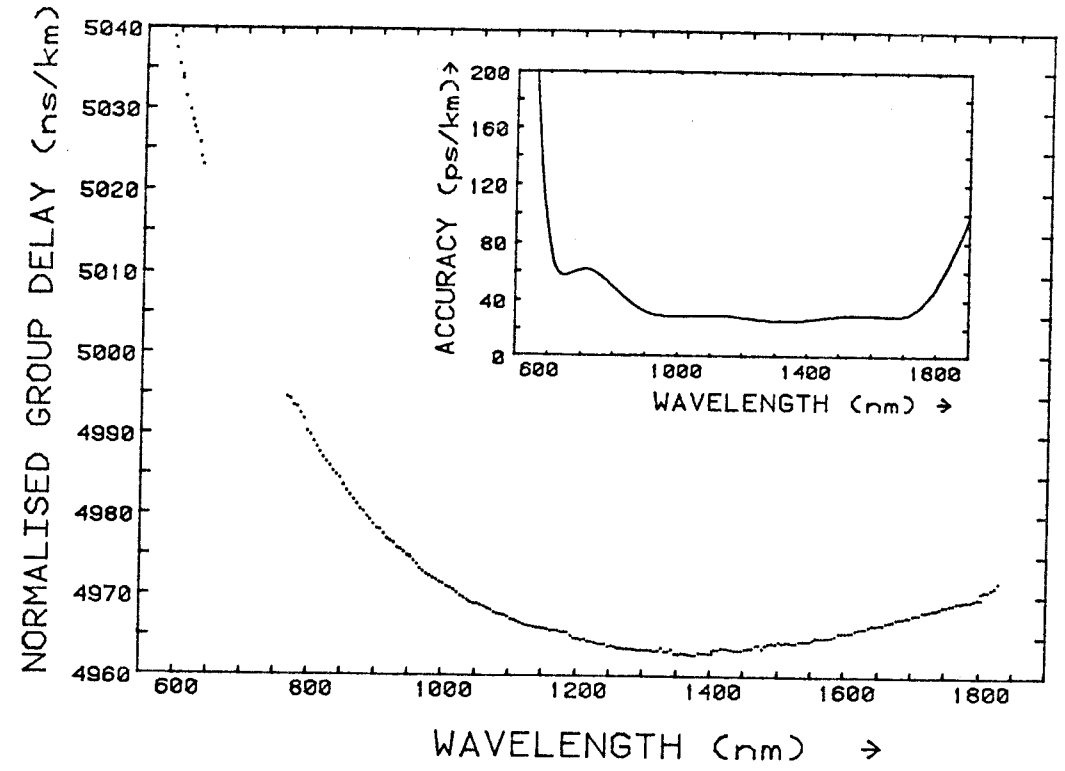

(a) Variation of normalised pulse transit-time with wavelength, measured in a step-index germanosilicate-core fibre, VD 232L.

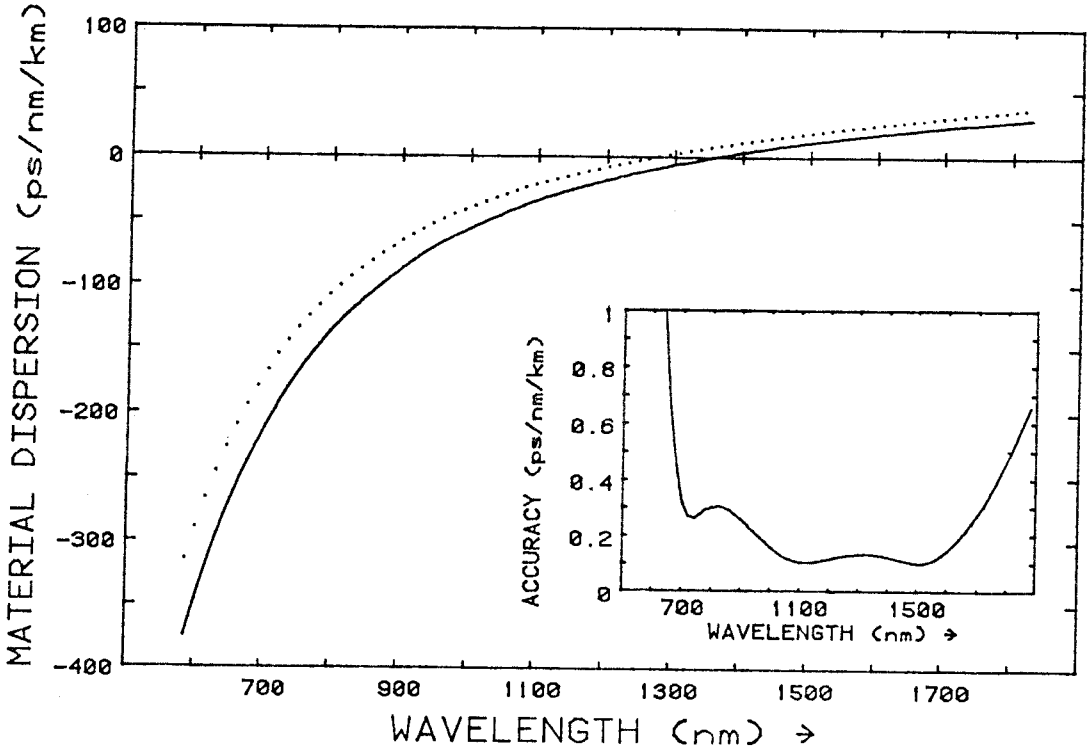

(b) Wavelength-dependence of the material dispersion parameter ($ps.nm^{-1}.km^{-1}$) inferred from (a) (solid line). The dotted curve shows, for comparison, the material dispersion parameter of silica in bulk form.

The standard deviation of the fitted values is indicated in the insets of (a) and (b).

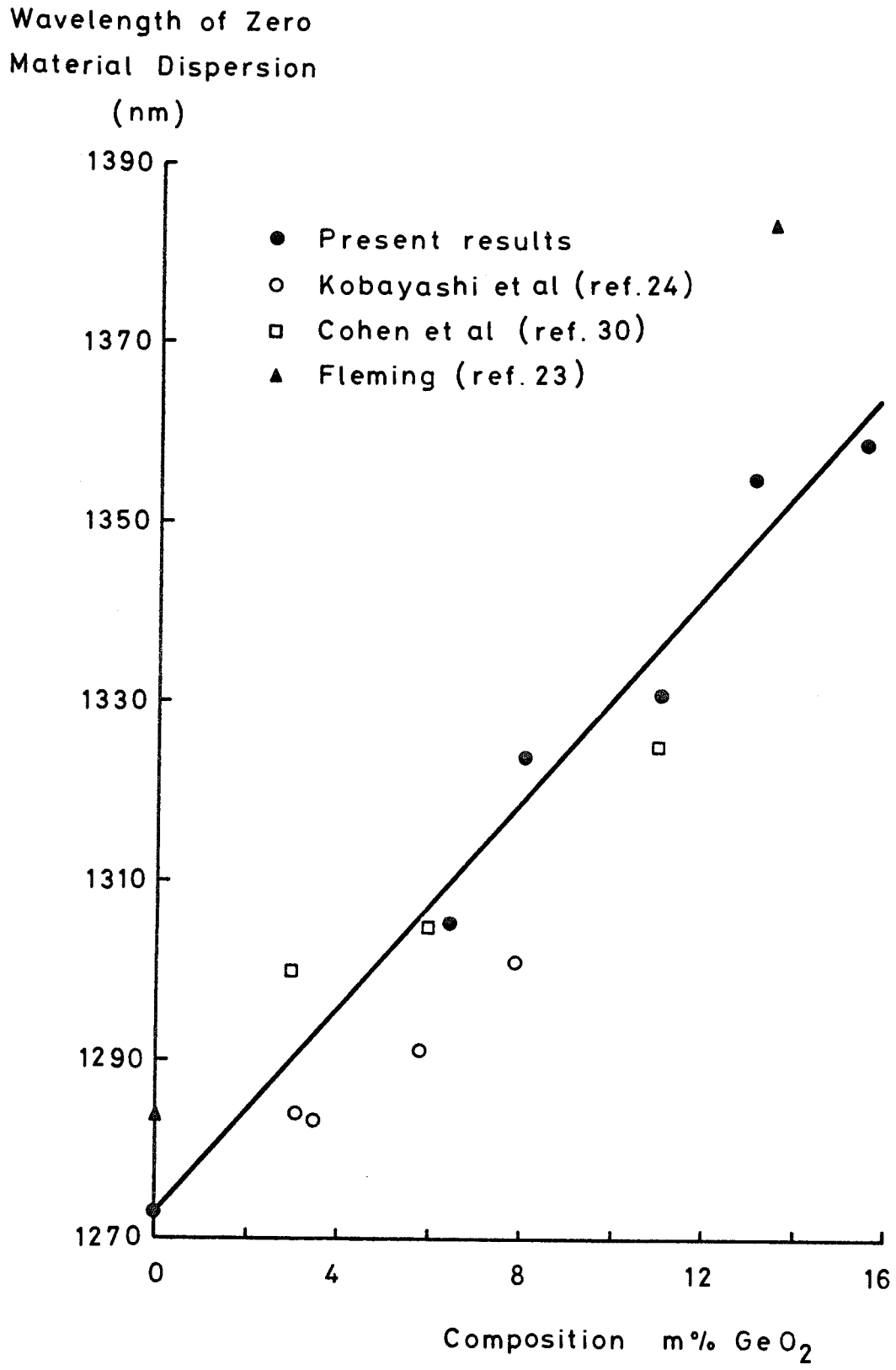

Figure 3.20: Variation of the wavelength of zero material dispersion of germanosilicate glasses with the concentration of germania. The values obtained in the present study are compared with those reported by other authors.

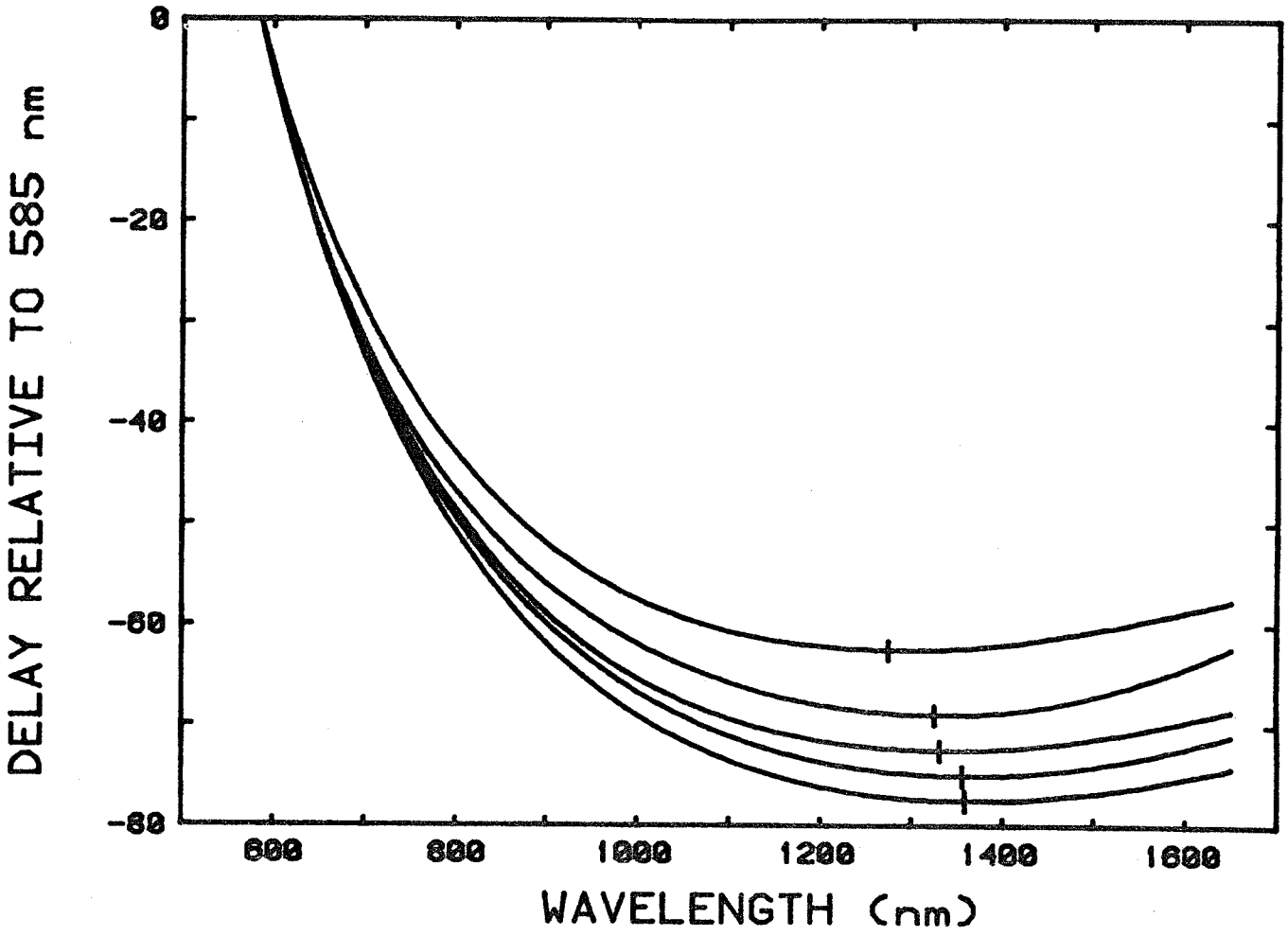

Figure 3.21: Departure, with increasing wavelength, of the normalised pulse-delay from the value measured at λ = 585 nm. The curves were measured in the following fibres (from top to bottom): VD 262L (pure silica core), VD 208L (8.1 m/o GeO_2), VD 209L (11.0 m/o GeO_2), VD 210L (13.1 m/o GeO_2) and VD 232L (15.6 m/o GeO_2).

Figure 3.22

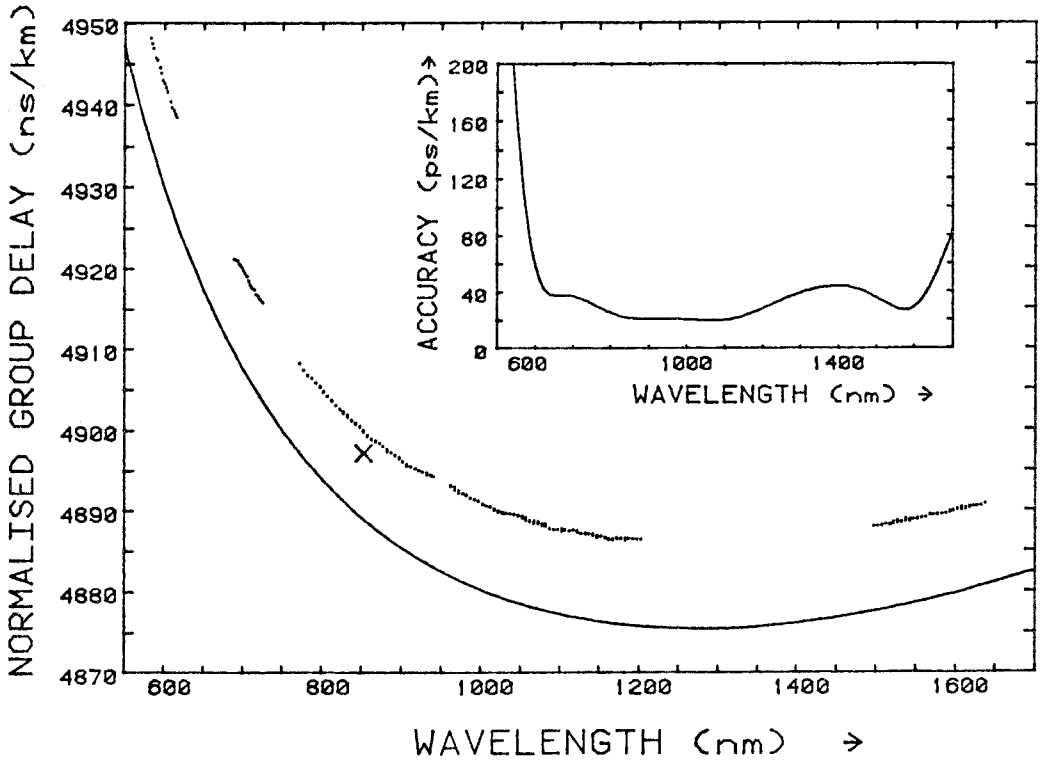

(a) Wavelength-dependence of normalised pulse delay measured in a silica-core fibre having a borosilicate cladding, fibre VD 262L (dotted curves). The cross shows the delay measured in a silicone-clad, silica-core fibre. The solid line is calculated from the refractive index of silica in bulk form.

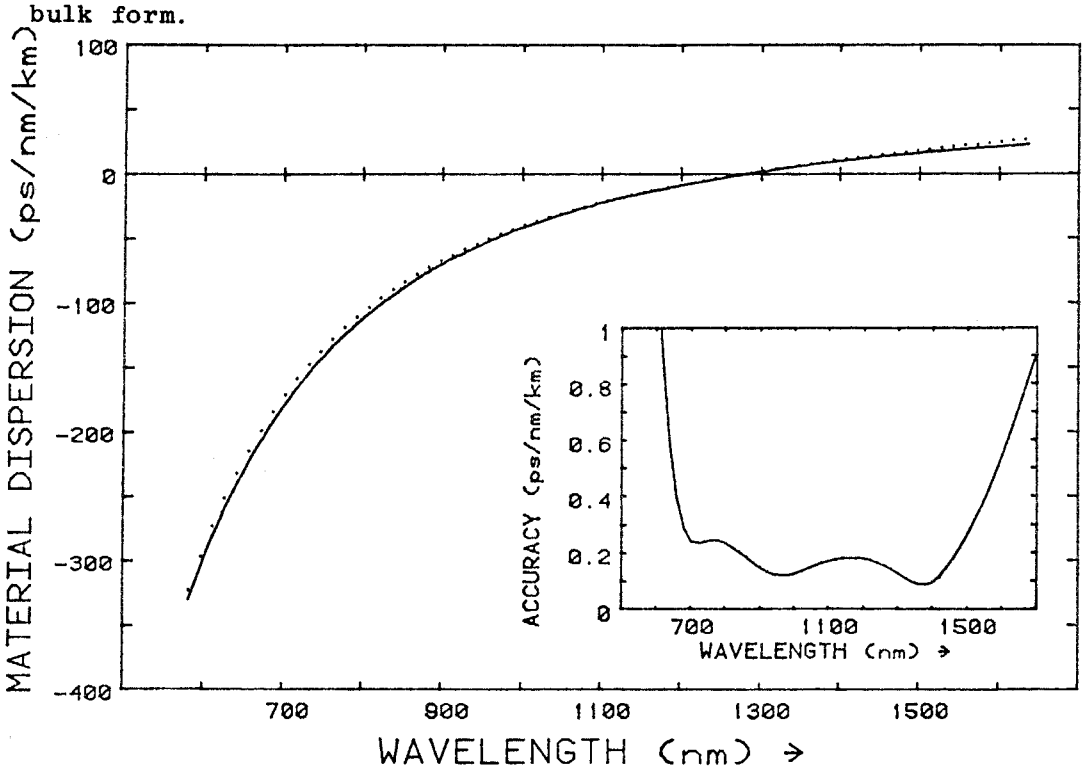

(b) Material dispersion parameter inferred from the measured transit times (solid curve). The dotted line shows the material dispersion of silica in bulk form.

The insets show the standard deviation of the fitted values.

Figure 3.23

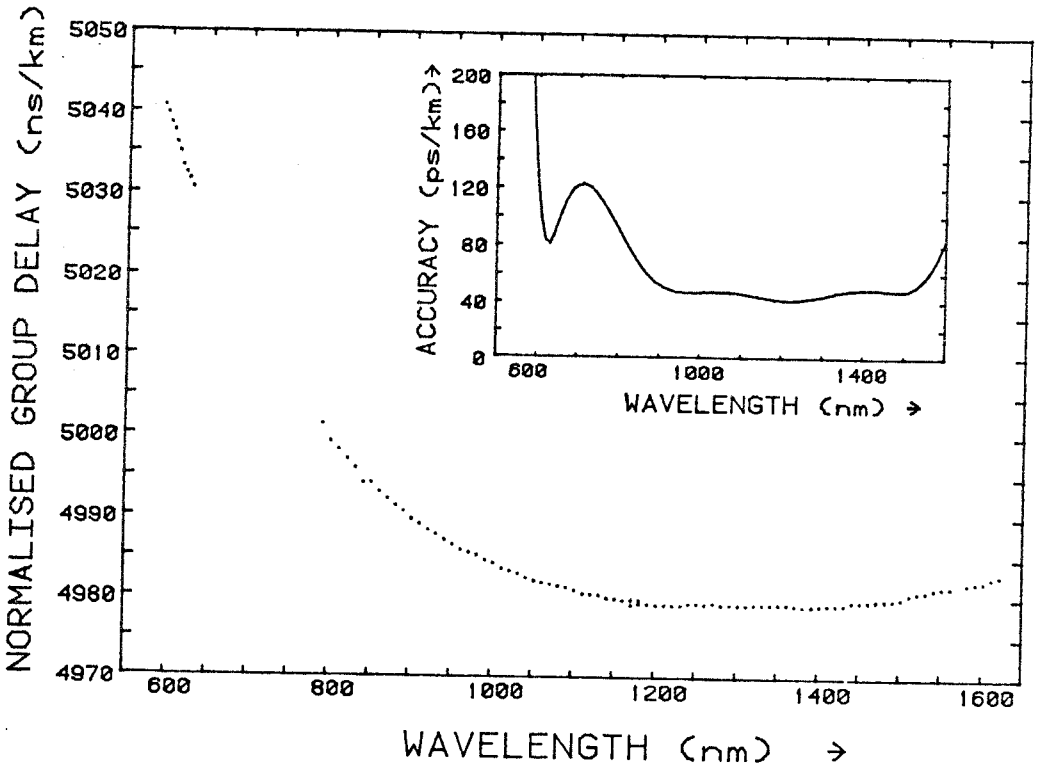

(a) Variation of normalised pulse transit-time with wavelength, measured in a graded-index germanophosphosilicate fibre, VD 199L.

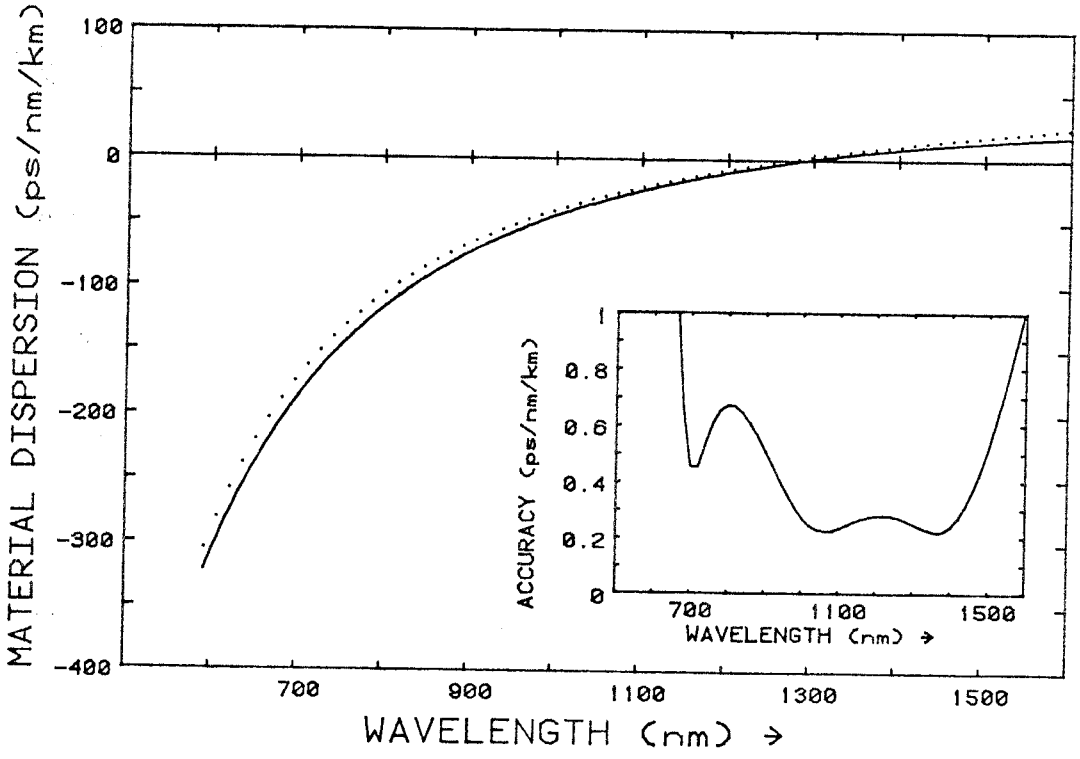

(b) Wavelength-dependence of the material dispersion parameter ($ps.nm^{-1}.km^{-1}$) inferred from (a) (solid line). The dotted curve shows, for comparison, the material dispersion parameter of silica in bulk form.

The standard deviation of the fitted values is indicated in the insets of (a) and (b).

Figure 3.24

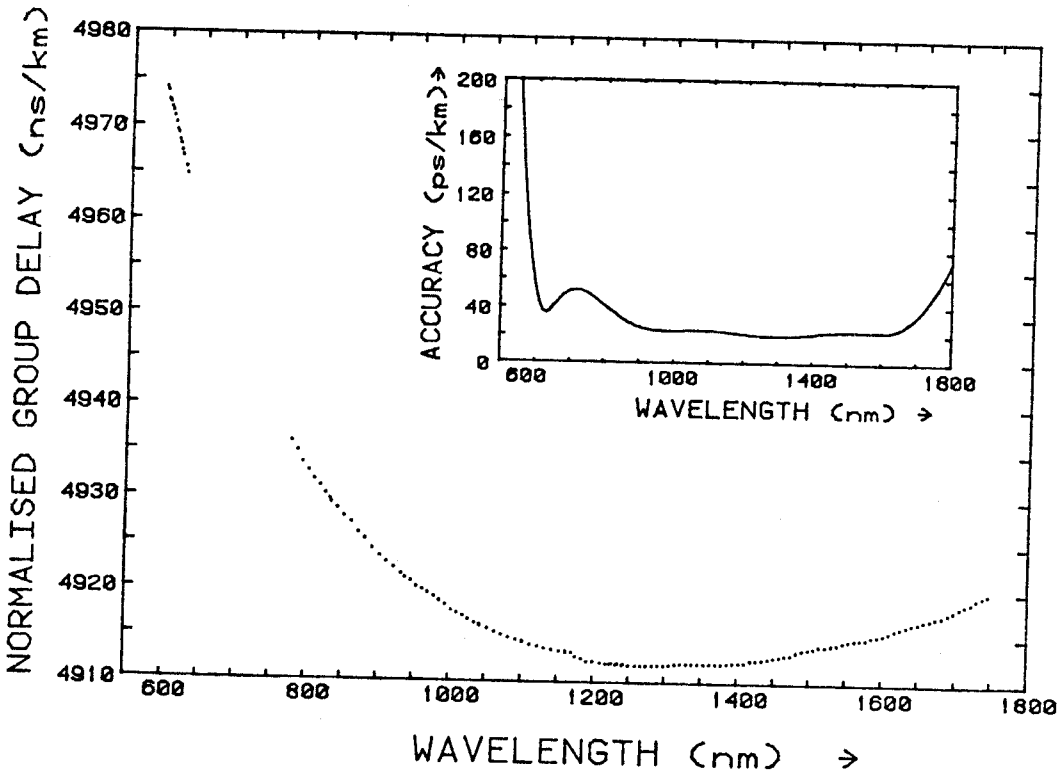

(a) Variation of normalised pulse transit-time with wavelength, measured in a graded-index germanophosphosilicate fibre, VD 202L.

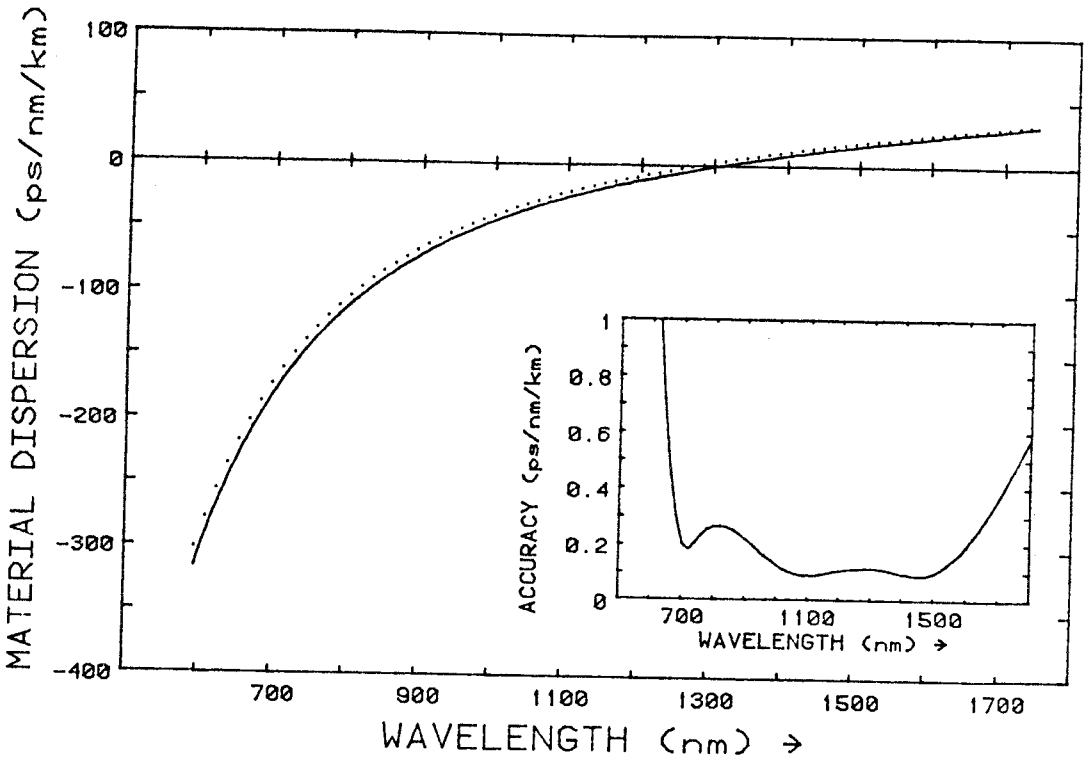

(b) Wavelength-dependence of the material dispersion parameter ($ps.nm^{-1}.km^{-1}$) inferred from (a) (solid line). The dotted curve shows, for comparison, the material dispersion parameter of silica in bulk form.

The standard deviation of the fitted values is indicated in the insets of (a) and (b).

Figure 3.25

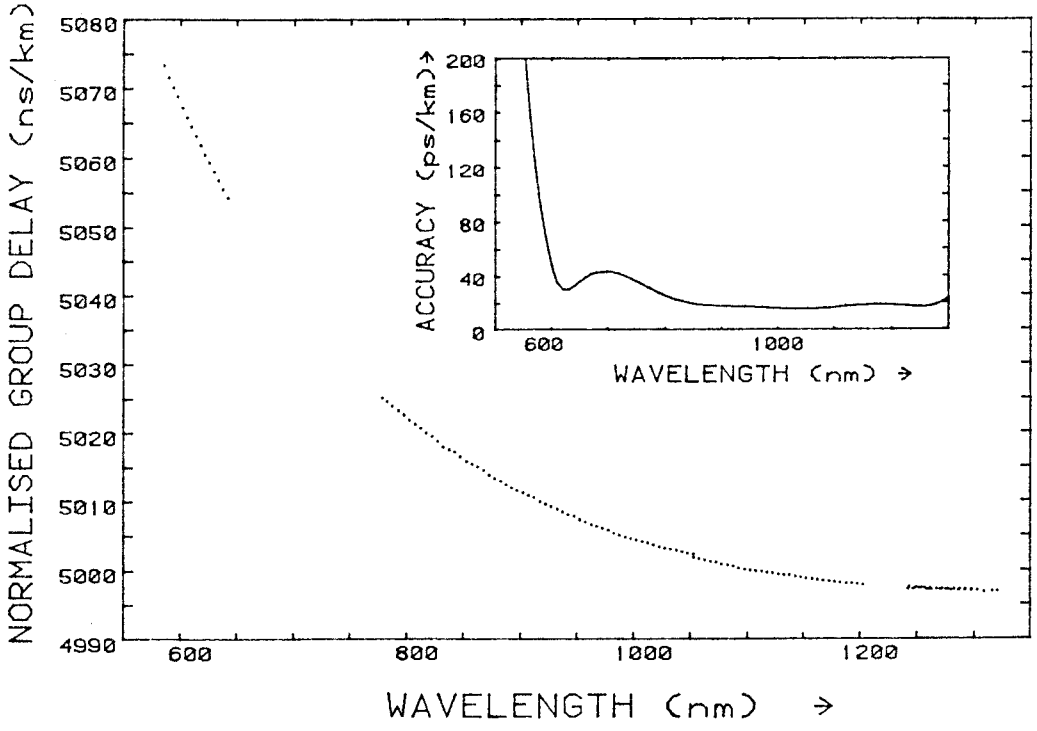

(a) Variation of normalised pulse transit-time with wavelength, measured in a sodiumborosilicate fibre made by the double crucible process, fibre no. 770818/2.

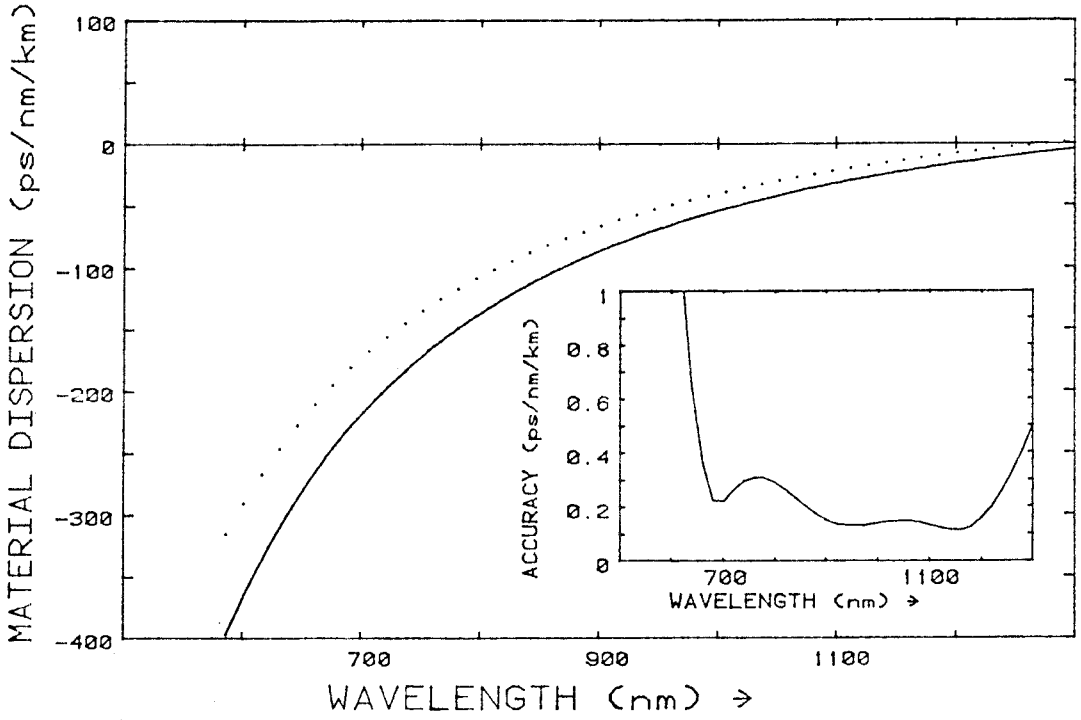

(b) Wavelength-dependence of the material dispersion parameter ($ps.nm^{-1}.km^{-1}$) inferred from (a) (solid line). The dotted curve shows, for comparison, the material dispersion parameter of silica in bulk form.

The standard deviation of the fitted values is indicated in the insets of (a) and (b).

Figure 3.26

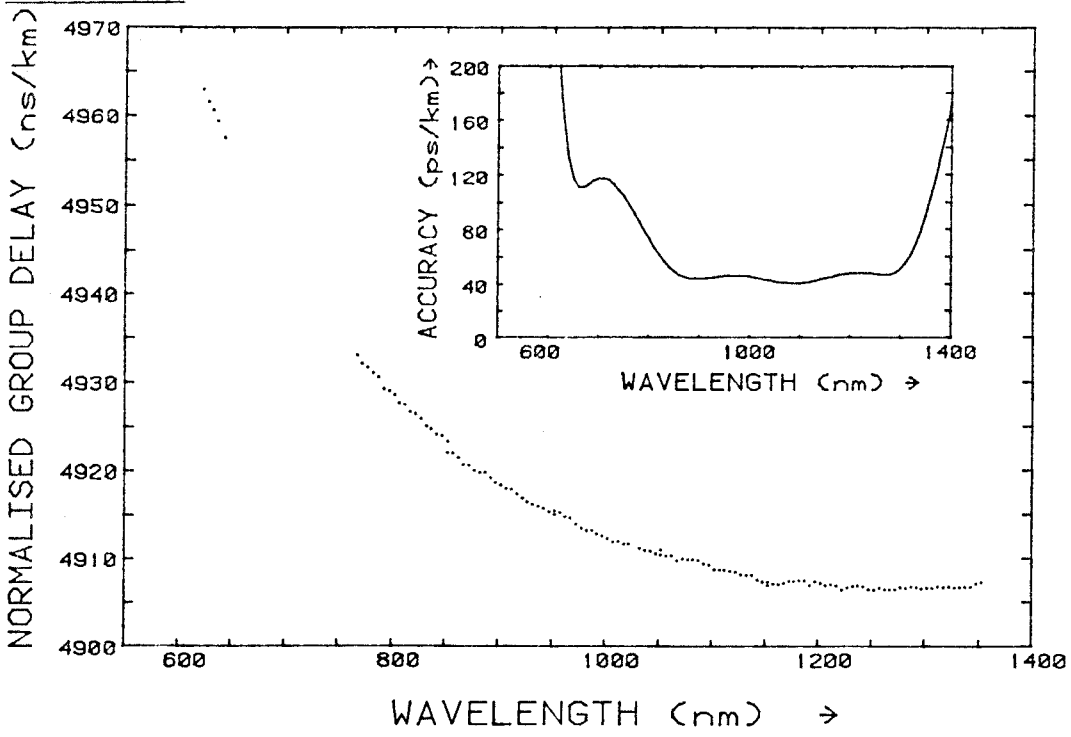

(a) Variation of normalised pulse transit-time with wavelength, measured in a Phasil fibre.

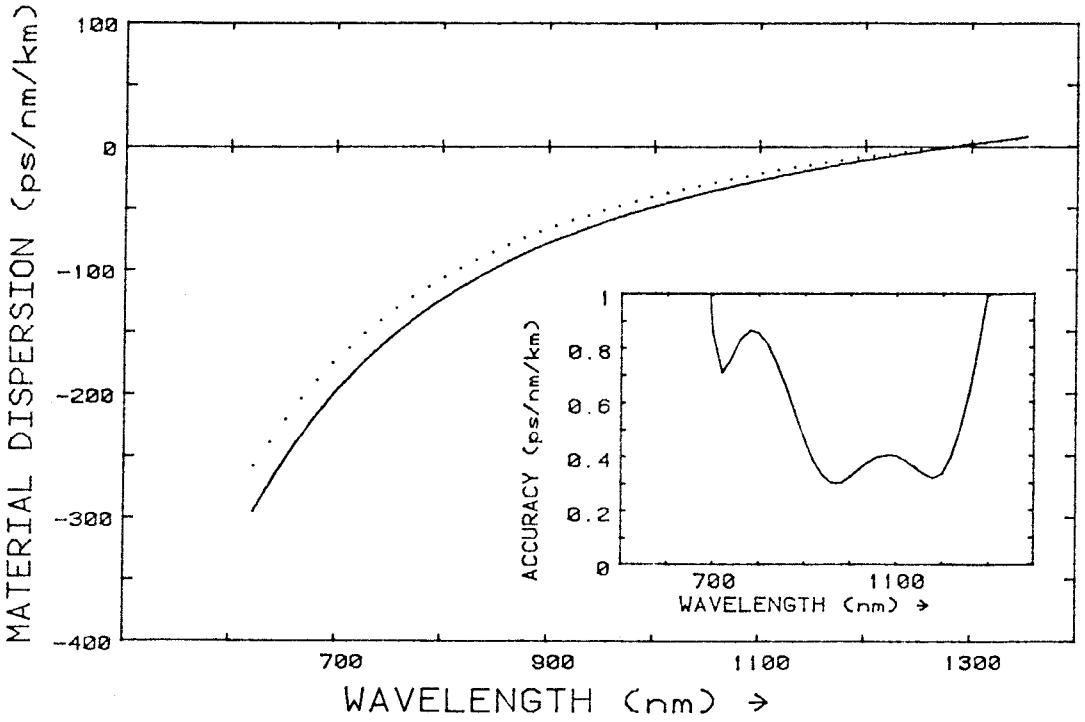

(b) Wavelength-dependence of the material dispersion parameter ($ps.nm^{-1}.km^{-1}$) inferred from (a) (solid line). The dotted curve shows, for comparison, the material dispersion parameter of silica in bulk form.

The standard deviation of the fitted values is indicated in the insets of (a) and (b).

Figure 3.27

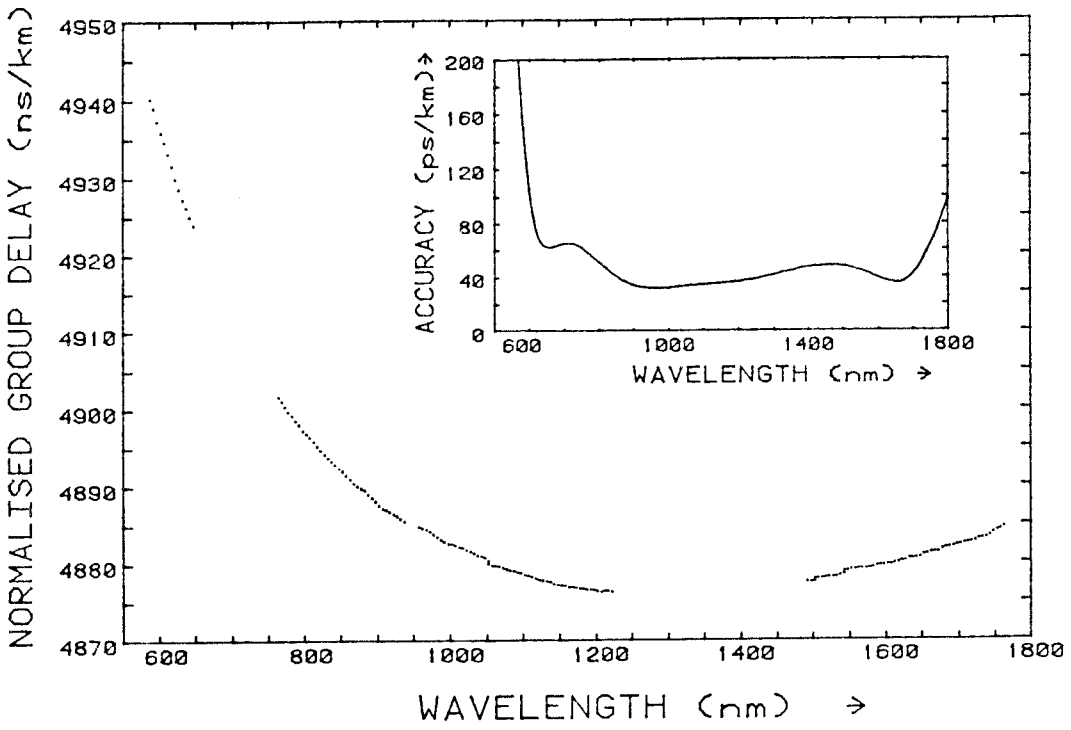

(a) Variation of normalised pulse transit-time with wavelength, measured in a graded-index germanoborosilicate fibre, fibre GW-P057.

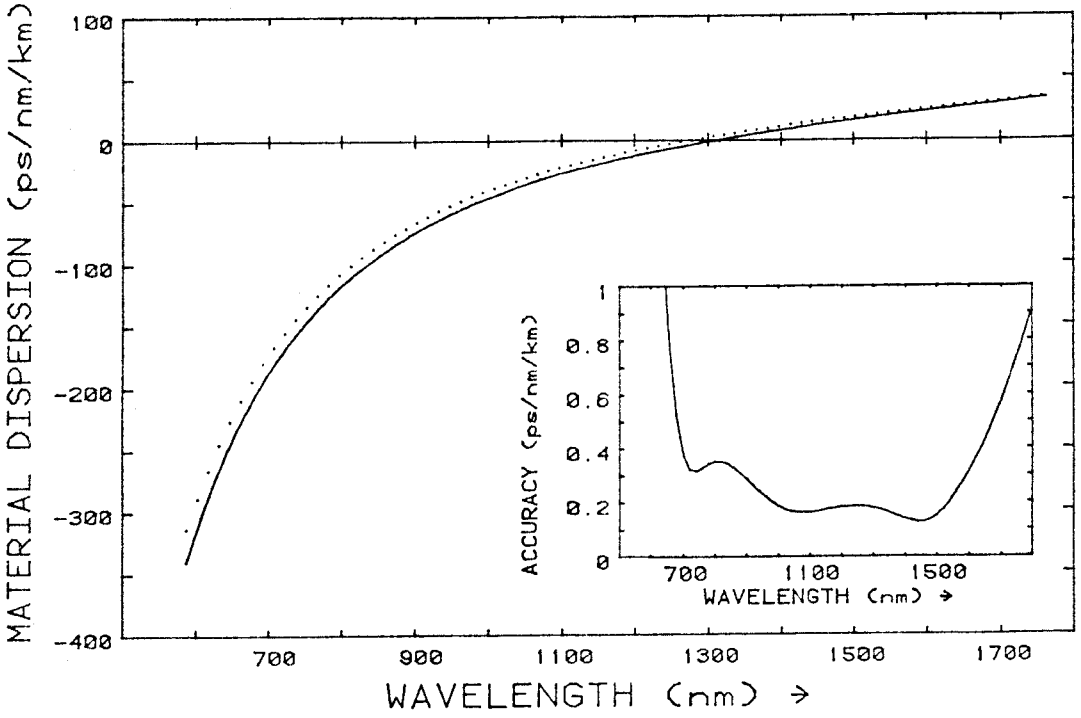

(b) Wavelength-dependence of the material dispersion parameter ($ps.nm^{-1}.km^{-1}$) inferred from (a) (solid line). The dotted curve shows, for comparison, the material dispersion parameter of silica in bulk form.

The standard deviation of the fitted values is indicated in the insets of (a) and (b).

Figure 3.28

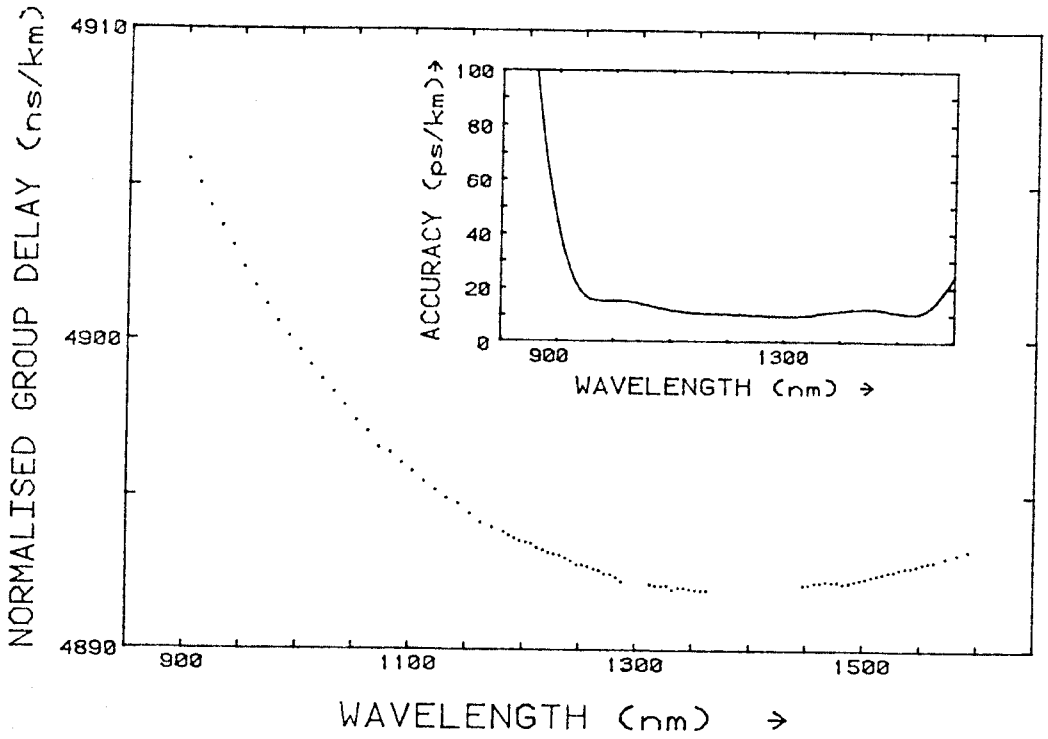

(a) Normalised pulse-delay measured in a single mode fibre, no. 9055.

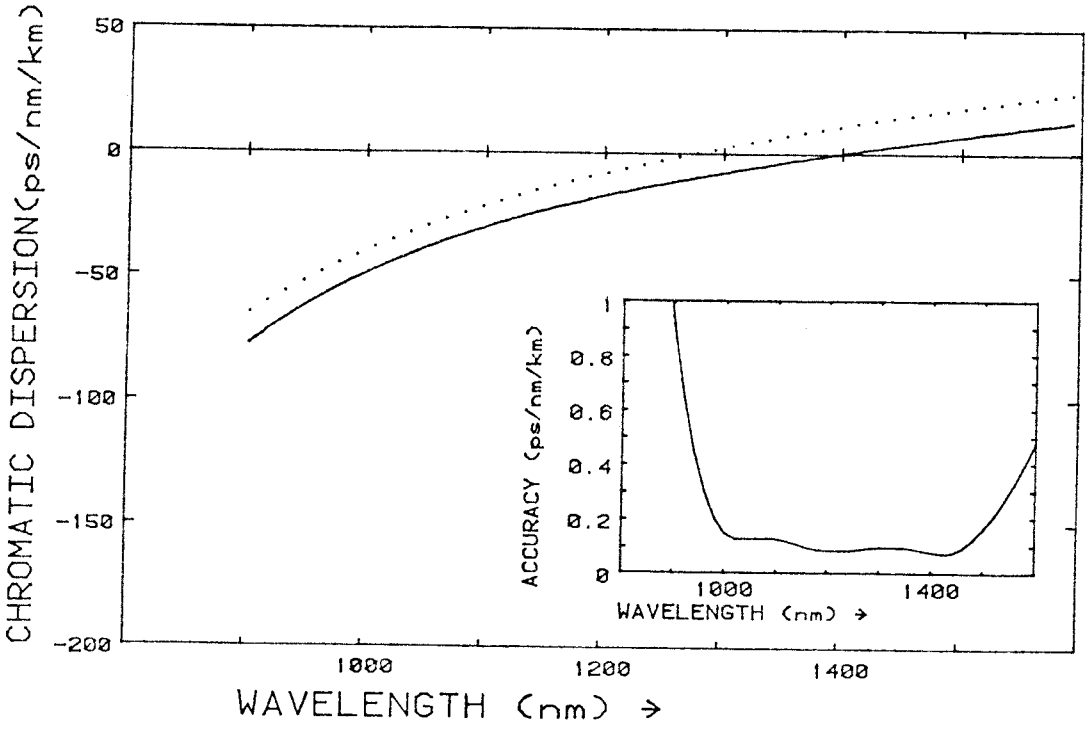

(b) Wavelength-dependence of total chromatic dispersion, inferred from (a), (solid line). The dotted line gives the material dispersion of pure silica, for comparison.

The insets in (a) and (b) give the standard deviation of the fitted values.

Figure 3.29

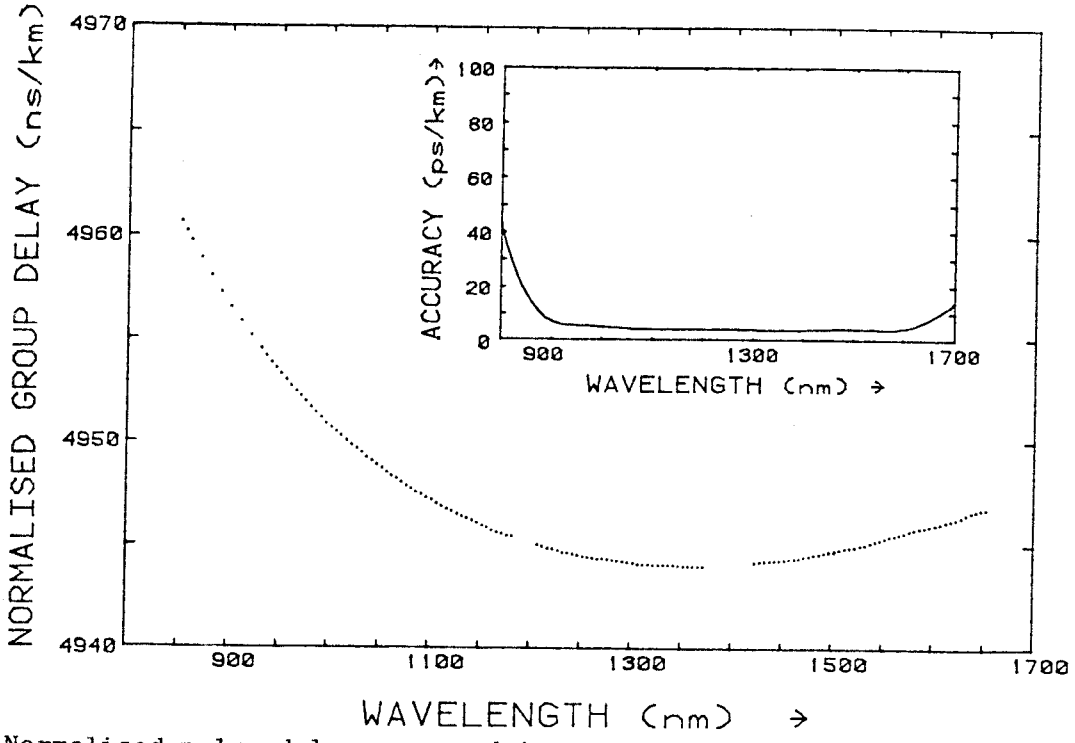

(a) Normalised pulse-delay measured in a single mode fibre, No. 9052.

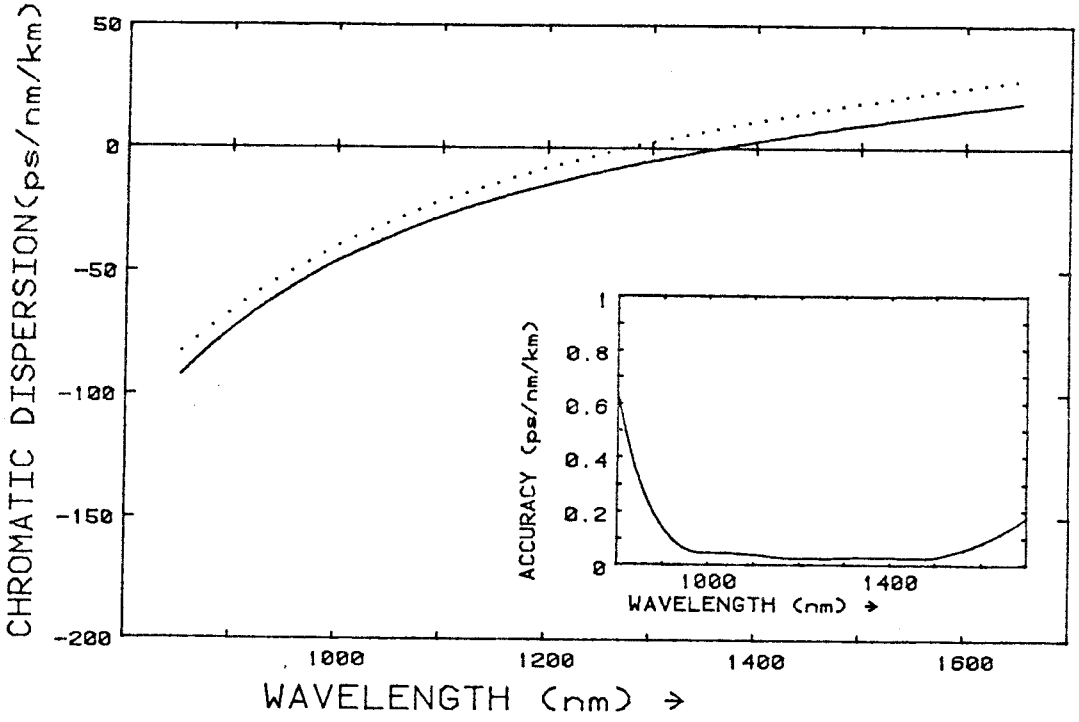

(b) Wavelength-dependence of total chromatic dispersion, inferred from (a), (solid line). The dotted line gives the material dispersion of pure silica, for comparison.

The insets in (a) and (b) give the standard deviation of the fitted values.

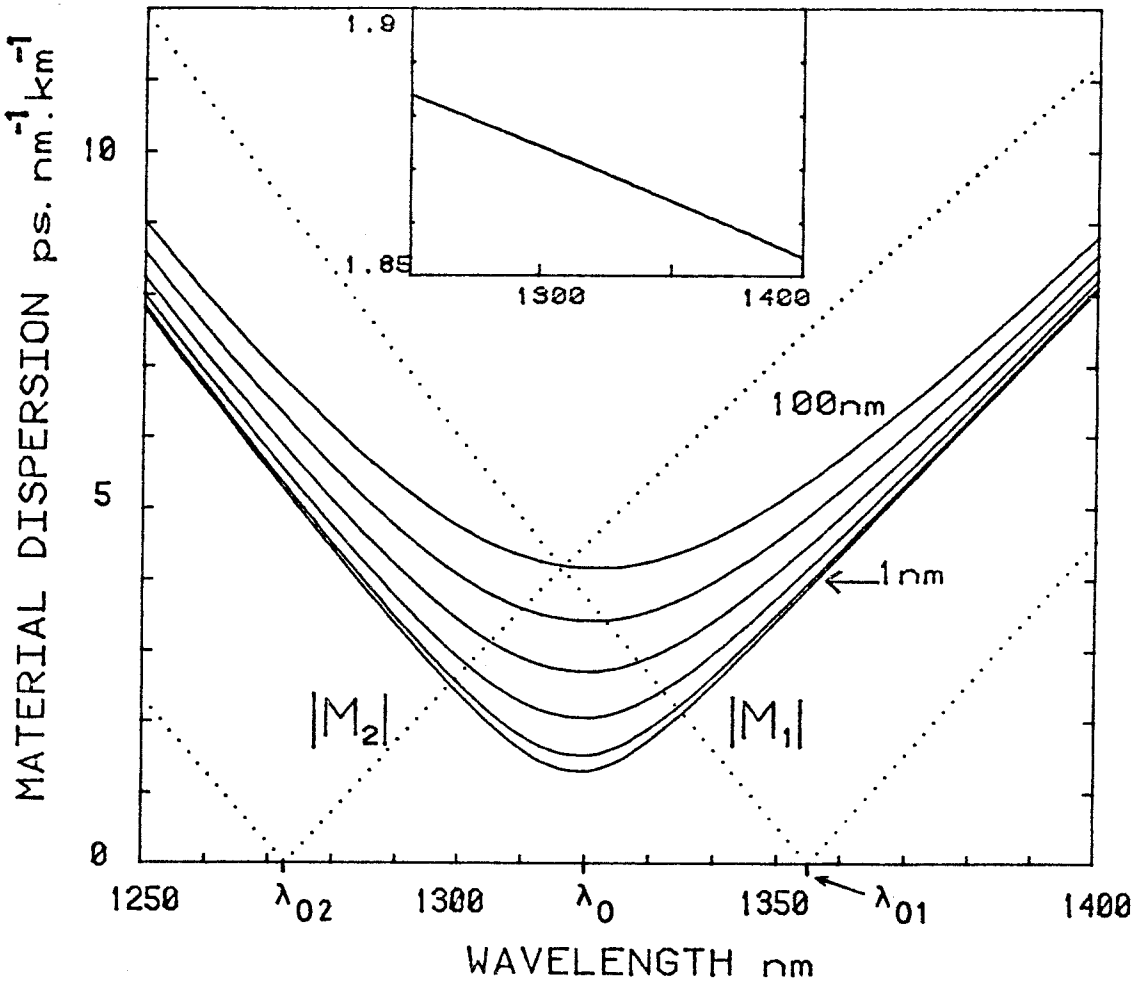

Figure 3.30: Effective material dispersion in multimode, graded-index fibres.

Dotted lines: Material-dispersion parameter $|M_1|$ measured for a 13 m/o GeO_2/SiO_2 composition (VD 210L) and $|M_2|$ calculated for silica.

Solid lines: Effective material-dispersion parameter calculated for a graded-index fibre having 13 m/o GeO_2/SiO_2 at core centre and silica cladding. Curves shown are for source spectral widths $2\sigma_s$ of 1,20,40,60 and 100 nm.

Inset: Measured wavelength-dependence of optimum profile parameter $\alpha = 2 - 2P$ for germania-doped fibres.

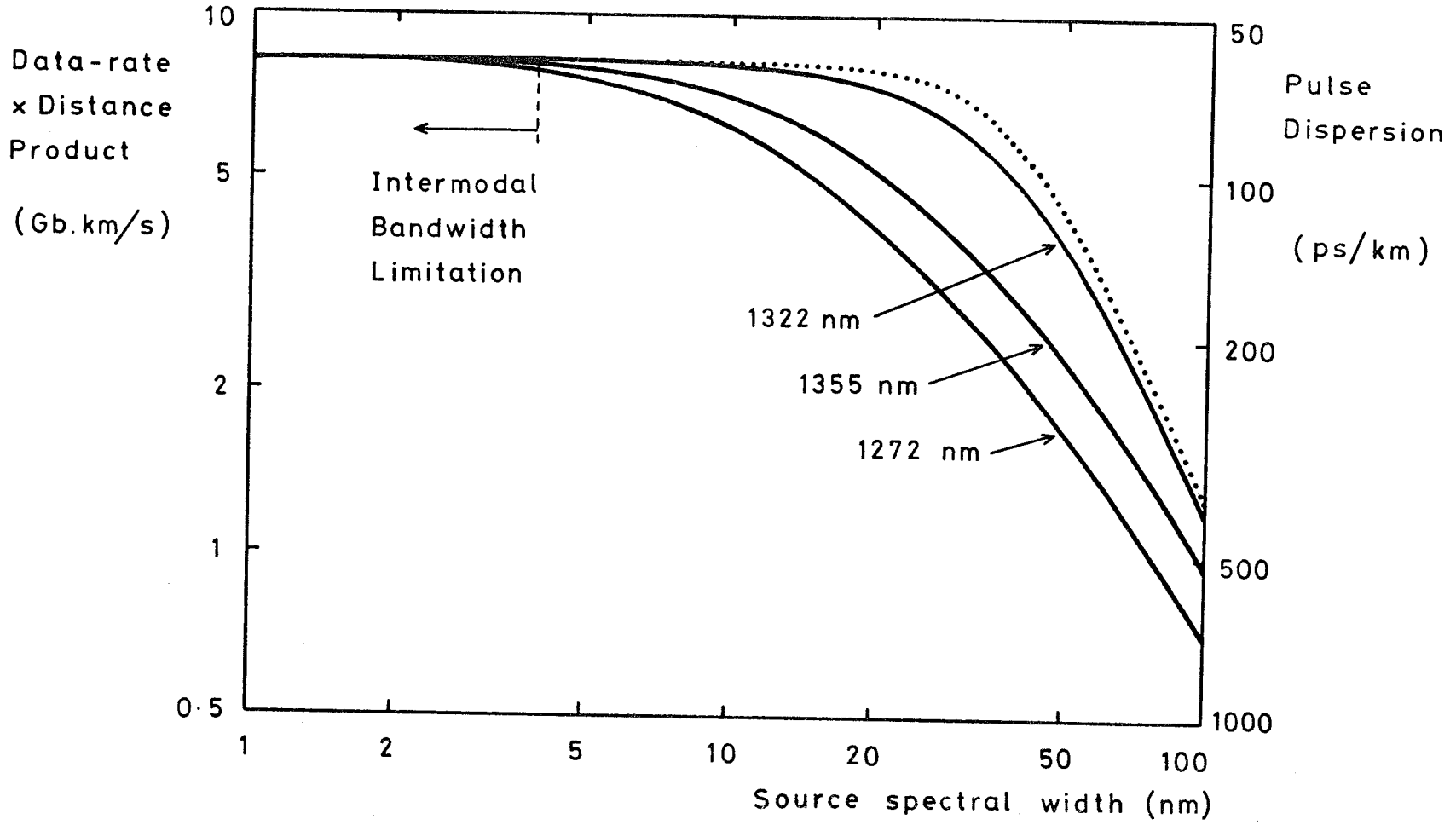

Figure 3.31: Dependence of r.m.s. pulse dispersion 2 σ and data-rate X distance product on r.m.s. source spectral width 2 σ_s for the fibre of Figure 3.30.

Curves indicate the effect of operating at wavelengths λ_{01}, λ_{02} and λ_0 (see Figure 3.30). Dotted curve shows the result for $M_1 = M_2$ (see Figure 3.6).

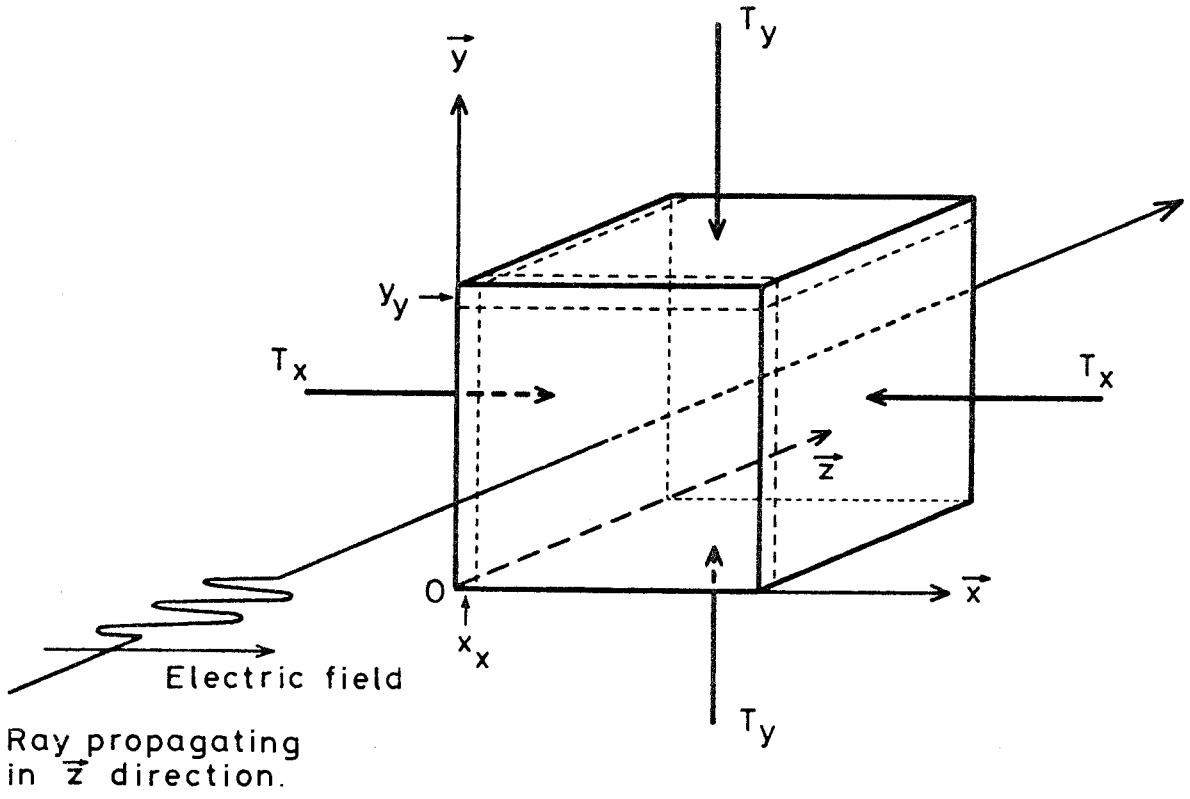

Figure 3.32: Schematic diagram showing the coordinates, the stresses, the strains and a possible ray path, to illustrate the discussion of the stress-optical effect.

CHAPTER 4 - WAVELENGTH-DEPENDENT MEASUREMENTS OF INTERMODAL DISPERSION

4.1 INTRODUCTION

Until recently, only multimode fibres were considered suitable as a transmission medium for optical-fibre communication systems. Single-mode fibres had been temporarily rejected by system designers since a number of problems, such as jointing, microbending losses and fabrication tolerances had not then been solved. In addition, it is necessary to use laser sources with monomode fibres, since the output of light-emitting diodes cannot be launched efficiently into waveguides having small cores and low numerical apertures. Lasers are more expensive and less reliable than light-emitting diodes and, therefore, multimode fibres are still of great interest for long-distance, medium capacity fibre links.

Material dispersion can seriously degrade the bandwidth of optical fibres particularly when the optical source has a large linewidth, as in a light-emitting diode. The contribution of this effect can, however, be substantially reduced by a judicious choice of the operating wavelength. At the optimum wavelength for chromatic equalisation [1], the bandwidth of most presently-available multimode fibres is limited by intermodal dispersion. Most manufacturers wish to maximise the bandwidth of their fibres and therefore wish to reduce all forms of dispersion.

Intermodal dispersion originates in transit-time differences between the many modes of a multimode optical fibre. The most critical factor governing this form of dispersion is the radial variation of refractive-index, i.e. the refractive-index profile. The well-known power-law profile, or α-profile[(2)], has been the subject of many theoretical calculations. In particular, Olshansky and Keck[(3)] have shown that the exponent α_{opt} of the optimum power-law profile is a function of the materials from which the fibre is made and of the wavelength of operation, an effect known as 'profile dispersion'. As a consequence, a fibre designed to exhibit low pulse distortion at one wavelength is likely not to perform so well at another.

The residual intermodal dispersion of fibres having optimal

power-law profiles has been predicted[3] to be as low as 25 ps km^{-1} for a numerical aperture of 0.2. When the present study was undertaken, this value had not been even approached* in real fibres[4,5]. Although the cause of this shortfall in bandwidth is not perfectly understood, it would appear that minute perturbations of the index profile can have a major detrimental influence in fibres with near-optimum profiles[6-13].

Much effort has been devoted to the measurement and analysis of pulse broadening in multimode optical fibres[4-13]. There is comparatively little published work, however, concerning the measurement of the wavelength dependence of intramodal broadening in very-high-bandwidth fibres[5]. In particular, the correlation between the values of bandwidth measured at various wavelengths and those which might be predicted from the refractive-index profile has not been investigated in detail.

In this chapter, detailed measurements are presented of the wavelength-dependence of intermodal dispersion in multimode, graded-index fibres. Although a number of fibres have been measured, the discussion to follow is restricted to three fibres supplied by the British Post Office. The fibres were made by Corning Glass Works using the OVPO fabrication process. Some details of the fibres are given in Table 4.1; all three had graded-index cores doped with germania and boric oxide.

Table 4.1 Fibres used for the intermodal dispersion measurements

Fibre	Core diameter (μm)	Numerical aperture
PO 181	63	0.184
PO 182	60	0.196
PO 180	62	0.177

* During the drafting of this thesis, a fibre made by the v.a.d. process and having a bandwidth within a factor of 2 of that predicted by the theory of power-law profiles was reported in: K. Yoshida et al.: 'Ultra-wide bandwidth optical fibres fabricated by VAD method', proc. Sixth European Conference on Optical Communication, York, Sept. 1980, p. 6.

Extensive and detailed refractive-index measurements have been made on these fibres by my colleague, Dr. F.M.E. Sladen[14]. Detailed data are thus available concerning the refractive-index profile of the fibres and the profile dispersion parameter which determines the optimum refractive-index profile for a given glass system. The experimental techniques used to obtain the refractive-index data have been published[15-18], and are described briefly in section 4.2. With this data and using mathematical techniques developed by Dr. M.J. Adams and Dr. A. Ankiewicz, it is possible to make predictions of the bandwidth of these fibres as a function of wavelength. The corresponding measurements are described in section 4.3 and, in section 4.4, the experimental and predicted values of bandwidth are compared and discussed.

The same fibres have also been used to investigate the wavelength-dependence of bandwidth in jointed pairs of fibres. Fibres with different index-profiles have maximum bandwidth at different wavelengths owing to the effect of profile dispersion. The intermode dispersion varies rapidly, in good-quality fibres, in the vicinity of the optimum wavelength. Eve[19] has shown theoretically that bandwidth-compensation occurs in jointed fibres with index-profile parameters on opposite sides of the optimum value. The effect has been demonstrated in an experimental link[20]. An extension of Eve's theory[21] to include the wavelength-dependence shows that, in principle, the bandwidth is less sensitive to wavelength in pairs of jointed, but dissimilar, fibres than in single fibres. An experimental investigation of this effect is presented in section 4.5.

4.2 CALCULATION OF FIBRE BANDWIDTH FROM REFRACTIVE-INDEX DATA

4.2.1 Power-law Profiles

Gloge and Marcatili[2] investigated theoretically the pulse broadening of fibres having refractive-index distributions n(r) of the form:

$$n^2(r) = \begin{cases} n_1^2\left(1 - 2\Delta\left(\frac{r}{a}\right)^{\alpha}\right) & r \leq a \\ n_1^2\left(1 - 2\Delta\right) & r \geq a \end{cases} \qquad 4.1$$

where r is the radial coordinate, a is the core radius, n_1 the refractive index at core centre and $\Delta = \frac{n_1 - n_2}{n_2}$ is the relative maximum index-difference. Using the WKB approximation, Gloge and Marcatili evaluated the dispersion as a function of the profile parameter α and showed that an optimum value, which minimises the pulse broadening exists.

The effect of the wavelength-dispersion of the core and cladding materials was subsequently taken into account by Olshansky and Keck[3] who showed that the value of α which minimises the r.m.s. impulse response is approximately:

$$\alpha_{opt} = 2 - 2P(\lambda) - \frac{12}{5}\Delta \qquad 4.2$$

where the profile dispersion parameter $P(\lambda)$ represents the contribution of material effects and is given by:

$$P(\lambda) = \frac{n_1(\lambda)}{N_1(\lambda)} \frac{\lambda}{\Delta(\lambda)} \frac{d\Delta(\lambda)}{d\lambda} \qquad 4.3$$

Since P is a function of wavelength, it follows that the value of the optimum profile exponent α_{opt} also varies with operating wavelength. Hence a fibre exhibiting very low intermodal dispersion at one wavelength is unlikely to perform as well at another. The bandwidth of an α-law fibre is thus a sensitive function of wavelength and usually has a sharp peak in the region of the maximum.

The r.m.s. width σ of the impulse response P(t) of the fibre is defined[3] as:

$$\sigma = \left[\frac{\int_0^\infty P(t)\ t^2\ dt}{\int_0^\infty P(t)\ dt} - \tau_1^2 \right]^{\frac{1}{2}} \qquad 4.4$$

where the mean delay τ_1 is given by:

$$\tau_1 = \frac{\int_0^\infty P(t)\ t\ dt}{\int_0^\infty P(t)\ dt} \qquad 4.5$$

The r.m.s. pulse broadening of a fibre having the optimum profile exponent is:

$$\sigma_{opt} \simeq \frac{L}{c} N_1 \frac{\Delta^2}{20\sqrt{3}} \qquad 4.6$$

where L is the fibre length and c the speed of light in free space.

The relationship between profile dispersion and material dispersion is discussed in Chapter 3, where it is shown that profile dispersion results from the variation of material dispersion with glass composition.

It is implied in the theory of Olshansky and Keck that P is purely a property of the additive used to modify the base glass and thus to produce a waveguide structure. Hence it is assumed that P is independent of the relative index-difference Δ and does not vary across the core of a graded-index fibre. It may be shown (from equ. 4.3) that this assumption (often referred to as 'the "linear" or "homogeneous" profile dispersion assumption') is verified if, for example, the dispersion $\frac{dn}{d\lambda}$ is proportional to the refractive index, in a given glass system. It would not seem unlikely that this condition should be satisfied for the small dopant concentrations found in many types of fibres.

Early measurements of P on thin samples[22], by an interferometric technique, and on bulk samples[23-25] by the minimum deviation method (see Chapter 3) have indicated, however, substantial departures of P from linearity. According to these data, the Olshansky-Keck theory is not valid and more complex forms of theoretical analysis are required. On the basis of a selection of these measurements, Arnaud[26] and Geckeler[27] have predicted optimum profiles, which are not of the power-law type.

On the other hand, the more recent and probably more reliable measurements of Sladen[18] show clearly that, for germania-doped silica fibres having numerical apertures as large as 0.25, the profile-

dispersion parameter is independent of the glass composition. Thus, it seems that, for germania-doped fibres at least, the theory of Olshansky and Keck is valid.

The profile dispersion data used in this study was obtained by Dr. F.M.E. Sladen on a sample of fibre P0181. The results should apply equally to the remaining fibres since the compositions are very similar. The profile dispersion parameter $P(\lambda)$ is deduced from wavelength-dependent measurements of numerical-aperture. Details of the experimental technique may be found in references 14, 17 and 18. The variation of $\alpha_{opt} = 2 - 2P(\lambda)$ with wavelength is shown in fig. 4.1. It was not possible to obtain reliable data at wavelengths longer than about 1200 nm owing to the presence of a narrow layer of differing refractive index at the core-cladding interface. This layer caused differential mode attenuation effects which precluded accurate determination of the numerical aperture at longer wavelengths. The data is reliable, however, over the spectral region in which the pulse broadening measurements were made.

4.2.2 Fibres with arbitrary (circularly symmetric) profiles.

It will be assumed that the refractive-index distribution $n(r,\lambda)$ takes the form:

$$n^2(r,\lambda) = n_1^2(\lambda)\left[1 - 2\Delta(\lambda) \cdot f(r)\right] \qquad 4.7$$

where $f(r)$ is a profile grading function given by

$$f(r) = \begin{cases} 0 & r = 0 \\ 1 & r \geq a \end{cases}$$

and $f(r)$ is otherwise arbitrary. Note that the form of $n(r,\lambda)$ implies (a) that the fibre is circularly-symmetric and (b) that $f(r)$ is independent of wavelength and therefore that the condition for linear profile dispersion is fulfilled.

Although the theory of fibres with α-profiles is well developed and used extensively, this type of refractive-index distribution is rarely

found in practice. The profile of low-loss fibres made by the c.v.d. process is formed by a number of glass layers and approximates a power-law distribution with a staircase function. The layers do not always diffuse into one another in later stages of fibre fabrication and a considerable amount of structure is usually discernible in index profiles, particularly near the core centre. A further type of profile imperfection often encountered is a central dip caused by evaporation of dopant from the inner layers during the collapse stage of preform fabrication. Finally, structure is usually found near the core-cladding interface, particularly when B_2O_3 dopant (which depresses the index of silica) is used to form a barrier layer against impurity diffusion, or to enhance the numerical aperture.

It is known theoretically[6-10] that profile imperfections can cause a severe degradation in bandwidth. In the present chapter, calculations of fibre bandwidth based on the profiles of real fibres are presented and they are compared directly with values measured in the same fibres. The comparison covers a wide wavelength range which includes regions of low dispersion where the profiles are near to optimum.

No analytic solutions are available for the impulse response of fibres with arbitrary profiles. Two approaches have been used in the past to circumvent this difficulty and have been tried in the present study.

(a) 'Equivalent' α-profiles.

In the first approach, a power-law is fitted to the measured index distribution and the function thus found is used in the calculations. This method can give fibre manufacturers useful information about the general shape of the profiles produced and can indicate where corrections are necessary to eliminate profile errors. The fine structure of the profile is ignored, however, and, as a result, predictions of bandwidth do not reflect the measured values. On the other hand, it is still interesting to compare the measured wavelength of maximum bandwidth with that calculated from the fitted profile.

Here the α values were assigned to the measured index distributions using a new technique developed by Dr. M.J. Adams, some details of which have been described in reference 14. The impulse response can then be calculated from the 'equivalent' power-law profile using closed-form expressions[2,3].

(b) Numerical evaluation of the impulse response.

The WKB method[2,3], the variational method[11] (supplemented in ref. 11 by finite element techniques), perturbation theory[6], ray-tracing techniques[28] and other numerical procedures have been used to calculate the impulse response of optical fibres with arbitrary profiles. The present study is based on a ray-tracing algorithm developed by Dr. A. Ankiewicz[28]

In essence, the transit times of a number of individual rays are calculated by integrating the ray equations from the inner to the outer caustics or turning points. The singularities which occur at the caustics in the ray- or WKB-formulations are circumvented by making use of a technique based on Chebyshev polynomials[28]. The integral expression for the ray transit-time can then be evaluated rapidly, conveniently and accurately.

The parameters of the rays, or ray invariants, are chosen so as to simulate excitation by a Lambertian source; i.e. in the mode picture, all modes carry equal power. Other forms of fibre excitation may be modelled by weighting each ray with an appropriate factor. The distribution used here is equivalent, in the mode picture, to weighting each mode in proportion to its normalised propagation constant b (defined in Chapter 3). This provides a reasonable representation of the equilibrium excitation conditions in long fibres[29]. Thus low-order modes have a coefficient of nearly 1 whilst modes near to cut off have weights near 0 and have much less influence on the result. In addition, the weighting of the rays is modified to account for the difference in the degeneracy[30] of those LP modes having zero azimuthal order number (two-fold degeneracy) and those having non-zero azimuthal order number (four-fold degeneracy). It was found, however, that the exact form of the weighting function

does not significantly affect the predicted impulse response.

The impulse response is calculated from the transit-time of approximately 5000 rays. A histogram is formed by collecting the rays into 32 time slots according to their propagation delay and then summing the weights of all rays in each time interval. The Fourier transform of the resulting impulse response is the modulation transfer function, from which the fibre bandwidth is deduced. An example of an impulse response obtained in this way is shown in figure 4.2(a), together with the corresponding transfer function (b).

4.2.3 Refractive-index-profile Data

The refractive-index profiles of the three fibres studied here were measured by Dr. F.M.E. Sladen using the near-field scanning (NFS) technique[14,16]. The latter involves the excitation of a short length ($\sim$ 30 cm) of fibre and observing the intensity distribution across the fibre core. The refractive-index profile is deduced from the near-field intensity by application of a correction factor which accounts for the presence of leaky modes. The apparatus developed by Dr. Sladen allows measurements to be made over the wavelength range 0.45 - 1.05 μm with, typically, a spatial resolution better than 0.5% of the fibre diameter[14,31].

Theoretical studies of non-circular fibres[32,33] have indicated that leaky modes are very strongly attenuated in fibres having nearly parabolic ($\alpha \approx 2$) profiles in the presence of even small degrees of ellipticity. As a result, there has been reluctance to correct for leaky modes or indeed to use the NFS technique altogether[34]. Extensive experimental studies of the technique[14] have indicated little evidence, however, of increased leakly-mode attenuation and the accuracy of the correction factors has been verified[14] by comparison with profiles obtained by interference microscopy and microprobe analysis, and by comparison of corrected near-field distributions measured at different wavelengths. In addition, the profiles of the fibres used in the present work were measured by Dr. K.I. White, of the British Post Office, with the refracted near-field scanning technique[34] which does not require correction

for leaky modes. Comparison of the results indicates that, in the present fibres at least, there is no increased leaky mode attenuation caused by non-circularity and that the full correction must be applied.

Although the reasons for the disagreement with theoretical calculations are not clear, there seems to be sufficient evidence to support the use of leaky-mode correction factors, particularly for the present work. A possible explanation is that the non-circularity in the present fibres affects mainly a small region near the core centre; the core geometry is much more circular near the core-cladding interface and most of the leaky-mode power is carried in this region. In addition, unpublished work by Dr. A. Ankiewicz indicates that the ripples which exist in the profiles of c.v.d. fibres reduce the leaky mode attenuation of non-circular fibres. Finally, recent work by Ramskov Hansen et al[35,36] shows that small departures of the profile exponent from $\alpha = 2$ can result in leaky-mode correction factors for moderately elliptical fibres being almost as large as those of circular fibres.

Measurements of refractive-index profile were made at 50 nm intervals over the wavelength ranges 0.5 to 0.9 μm (for fibre PO 181) and 0.5 to 1.0 μm (for fibres PO 182 and PO 180) with, for each fibre, an additional result at 0.675 μm. In fibres PO 181 and PO 182, the measurements were repeated, but scanning across diameters orthogonal to those previously measured. In addition, a sample taken from the other end, end 2, of the 1 km length of fibre PO 181 was measured over the 0.5 - 0.9 μm wavelength range but only for one orientation of the fibre cross-section.

A few examples of results for fibre PO 181 are shown in figures 4.3, 4.4 and 4.6. Figs. 4.3 and 4.4 illustrate scans made along two orthogonal diameters of the fibre at a wavelength of 0.6 μm and show the lack of mirror symmetry in a single scan, while a comparison of the two shows the lack of circular symmetry. Stereoscan studies[14] have revealed that this absence of symmetry is a result of irregularities in the first few layers, possibly due difficulties encountered in the early stages of the deposition or in

the consolidation of the soot deposit into a glass preform.

The lack of symmetry naturally presents the problem of determining a unique function f(r) from the available data, since equation 4.7 implies that the fibre is circularly symmetric, a hypothesis upon which the ray-tracing algorithm (sec. 4.2.2) is based. In all rigour, the profile ought to be measured as a function of two variables over the entire fibre cross-section. This is obviously impractical and therefore, for each scan, the left- and right-hand sides were averaged. In the case of fibres PO 181 and PO 182, for which two profile measurements along orthogonal diameters are available at each wavelength, the estimates of f(r) obtained from each scan were used to calculate the impulse response. In addition, the data were combined to give f(r) as the arithmetic mean of 4 measured distributions and the resulting profile forms the basis of further bandwidth calculations. The profile obtained in this way from the scans of figs. 4.3 and 4.4 is shown in fig. 4.5. Note that the major features of the profile are retained, with the central dip and the layer structure still clearly defined. Since the fibre is non-circular, the detailed shape of the profile is altered by the averaging, which enhances the features which are symmetric at the expense of those which are not. However, this appears to affect only a few layers near the core centre and the area involved is small in comparison with the cross-section of the core. The effect of the averaging procedure on the predictions of bandwidth may be estimated by comparison of the results obtained from one or two scans (see Section 4.4). Figure 4.6 shows a profile measurement made on fibre PO 181 at the wavelength of 0.9 μm. Comparison with figures 4.3 and 4.4 shows that the resolution of the near-field scanning technique decreases with increasing wavelength[14,31] and the layer structure is therefore less apparent in the scans made at longer wavelengths. The localised variations of glass composition and internal stress which affect the refractive index are obviously the same at each wavelength. The apparent change of the profile occurs because the features of the profile are comparable in size with one wavelength* of light and the ability of any optical technique to

---

* The resolution of the NFS technique depends on the number of modes propagated by the fibre[31]. The size of the smallest profile feature which can be resolved is inversely proportional to the V-value of the fibre and thus increases with increasing wavelength.

resolve them therefore varies rapidly with the wavelength of the source.

Note that the impulse response is similarly affected by the change in fine structure of the profile. This adds an extra wavelength dependence of bandwidth - quite separately from that due to profile dispersion.

The variation of f(r) with wavelength is probably not sufficient to invalidate the assumption of linear profile dispersion which is implicit in equation 4.7. This is confirmed by calculations of equivalent profile-exponent[14] from the measured index distributions which show no significant change with wavelength. Thus, although the fine structure of the index-profiles does vary substantially, the general shape of the profile is largely independent of wavelength.

Two different approaches were adopted to deal with the problem of determining a profile function of relevance to the bandwidth measurements from the available data. In the first, the measured (suitably averaged) result for f(r) at each wavelength is used in the ray-tracing programme. In the second approach the available data for f(r), taken from a complete set of measurements, is averaged over wavelength and the resulting profile is used in the calculation of impulse response. Figure 4.7a shows the complete set of profile measurements on end 1 of fibre PO 181 and the corresponding average is given in 4.7b. Under the assumption of linear profile dispersion, this averaging procedure probably gives the best estimate of the general shape of the profile at the expense, however, of some loss of resolution of the fine structure. In addition, the sensitivity of the ray-tracing method to small features of the profile is independent of wavelength. The influence, on the computed impulse response, of the wavelength-dependence of the measured profile is thus lost as a consequence of the averaging procedure.

4.3 MEASUREMENT OF THE BANDWIDTH AS A FUNCTION OF WAVELENGTH

The information-carrying capacity of an optical fibre can be described either by its frequency response or, equivalently, by its impulse response. Both functions have been measured directly in optical fibres[4-5, 11-13, 37-39] but time-domain measurements are much better suited to the CMX-4 system which was used to provide tunability, narrow linewidth and high output power in short pulses.

The impulse response of an optical fibre is the variation of output power with time, when the fibre is excited by a pulse of unit energy and vanishingly-short duration. In practice of course, the optical pulses launched into a fibre have a finite width and, in addition, some distortion is introduced by the limited frequency response of the detector and oscilloscope used to record the output of the fibre. There is therefore a minimum pulse width, which is observed even in the absence of any distortion introduced by propagation in the fibre. This could be referred to as the impulse response of the measurement system. The pulse which appears at the output of the fibre is the convolution of the impulse response of the fibre and that of the system.

If the impulse response of the measurement system is much narrower than that of the fibre, then its effect can usually be neglected. In most practical cases, however, a deconvolution must be performed in order to obtain an accurate estimate of the impulse response of the fibre. It is therefore necessary to record precisely the input waveform, as well as the output waveform.

The experimental arrangement, described in section 4.3.1,was designed to allow an accurate deconvolution of the response of the measurement system. The launching conditions which were used are discussed in section 4.3.2. Finally, section 4.3.3 shows how the results are processed to obtain the fibre bandwidths.

4.3.1 Experimental Arrangement

The CMX-4 system which was used in these experiments has relatively large fluctuations of amplitude and pulse-duration (although variations of the latter have been much reduced by the use of the pulse-sharpening spark-gap). One is therefore faced with the choice of averaging many pulses, in order to smooth the fluctuations, or to perform the entire measurement with a single pulse.

A sampling oscilloscope used in conjunction with some form of signal averaging would give a very wide bandwidth and adequately-low noise, and could be used to smooth out the inter-pulse fluctuations. A possible arrangement, which was investigated, is to feed the output of the oscilloscope's vertical amplifier to a boxcar integrator and drive the time-base of the oscilloscope with a slowly rising voltage ramp. The pulse-repetition rate of the laser is so low, however, that the acquisition of a single trace requires approximately one hour, when the time constant of the boxcar integrator is sufficient for adequate noise-rejection. This large scanning time creates serious drift problems. Since signal averaging and the use of a sampling oscilloscope are precluded, the measurement must be performed on a single laser pulse, using a real-time oscilloscope.

The experimental arrangement is shown in figure 4.8. A very short pulse is extracted by the electro-optic modulator from the output of the dye-laser or the O.P.O. The optical pulse is sampled by a pellicle beamsplitter before it is launched into the fibre. The reflected pulse is a reference signal, which is detected by a germanium avalanche photodiode and displayed on the oscilloscope. A record of the system impulse response is thus obtained. The same photodiode is used to detect the pulse emerging from the fibre which is being measured. At each shot of the laser, therefore, the internally-triggered oscilloscope sweeps twice in rapid succession, displaying two pulses. Figure 4.9 shows a typical oscilloscope trace. The narrower pulse (left-hand side peak) is the reference, sampled at the fibre input.

The second pulse is measured after propagation through fibre PO 181 at the wavelength of 835 nm. We note that the reference pulse has a width of 0.8 ns at half height. The oscillations which follow the pulse originate primarily in the vertical amplifier of the oscilloscope and are superimposed upon a 'tail' in the pulse response of the photodiode. The oscilloscope used is a Tektronix R7912 transient digitiser which has a bandwidth of 500 MHz and which can record a single event on a storage monitor at sweep speeds of up to 500 ps/div. The graticule on the R7912 is electronically generated, and its production greatly increases the re-arming time of the instrument. The graticule is therefore switched off in order to record the input and output pulses, and is written onto the monitor screen after the two traces have been stored.

An advantage of the experimental arrangement presented here, is that the effect of changes in the rise-time of the pulse slicer is eliminated since the traces which are recorded correspond to the same shot of the spark-gap. A more usual way of performing this experiment is to use two detectors and a dual-channel oscilloscope. This can lead to errors, since the impulse response of the detectors or oscilloscope amplifiers may not be identical. The present arrangement has therefore the further advantage that rigorously identical signal paths are provided for the input and output waveforms. The only difference between the pulses originates from the propagation through the fibre.

It is important, in measurements of intermodal dispersion, to ensure that material dispersion has a negligible contribution to the pulse-broadening. Measurement of the material dispersion parameter in a fibre of similar composition to those tested here (see Chapter 3) revealed that intramodal dispersion which results from the source spectral spread is less than 38 ps km^{-1} at all wavelengths covered in the present study, and less than 20 ps km^{-1} in the infra-red. The material dispersion contribution to the overall pulse dispersion is therefore negligible and the observed pulse waveforms thus provide an accurate measure of the intermodal delay differences.

4.3.2 Launching Conditions

The values quoted for the bandwidth or the pulse dispersion of a multimode fibre are usually understood to refer to full excitation, i.e. the same power is launched into each mode. This excitation condition is established when an incoherent source, such as a tungsten lamp or more importantly an l.e.d., covers the entire area of the core[40]. Full excitation would thus be a logical choice for characterising a system driven by a light-emitting diode. It must be pointed out, however, that in most practical cases, mode-coupling and differential mode attenuation ensure that, at the output end, the fibre is far from fully excited. The modal power-distribution almost inevitably changes with distance and may reach a state of equilibrium[29] which depends on the level of mode coupling and differential mode attenuation.

In a long communications link, consisting of several $\sim$ 1 km sections of fibre, all fibres, except the first, are excited with the equilibrium conditions of their predecessor. In addition, the joints can influence the modal power distribution, although this could be a minor effect with low-loss jointing techniques such as fusion-splicing.

It would appear, therefore, that the equilibrium distribution is at least as valid a condition for fibre characterisation as full excitation. The measurements described below were performed partly in order to compare the dispersion of individual fibres with that of jointed pairs. It is clear that, in this case, the equilibrium distribution is the most appropriate launching condition.

The result of a pulse dispersion measurement can depend strongly on the launching conditions[13]. This is particularly the case where the refractive-index profile present fine structure, or when a laser source, which can excite only a few modes, is used. Thus minor changes in the position, or the angle of incidence of the laser spot on the fibre face can lead to substantial variations in the measured impulse response[13].

The sensitivity of the measured impulse response to launching conditions is demonstrated in figure 4.10. Both photographs refer to the same fibre measured at a wavelength of 900 nm. In the first picture, (a), the fibre was excited with a near-equilibrium distribution. The impulse response has a main peak which is followed by a slowly-decaying tail. In the case of picture (b), however, the same fibre was excited with a high proportion of power concentrated in a small (5-10μm) spot at the centre of the input face. These launching conditions have caused a second peak to appear in the impulse response.

Predictions of information-carrying capacity based on these measurements would probably differ by a factor of 2 or more. Values quoted for bandwidth or pulse dispersion can therefore be very misleading, if they are not accompanied by sufficient information on launching conditions.

In order to obtain reproducible results it is important to make the power-distribution in the fibre as independent as possible of the position, size, and angle of incidence of the laser spot. In addition all the output power should be collected by the detector.

In the present measurements a mode-scrambler ensured that a near-equilibrium power distribution existed at the input end and was independent of the launching conditions. A focussed laser beam impinging coaxially on the centre of a fibre face and having a relatively large (20-30 μm) spot diameter launches power mainly into low-order modes. The function of the mode scrambler is to convert this power to a much wider mode spectrum which is insensitive to the position and size of the spot.

Several types of mode-scrambler were tried and a number of measurements were performed to test their effectiveness. The impulse response of a fibre does not give a reliable, or sensitive, indication of the launching conditions, since a reduction in the portion of the mode spectrum which is excited does not necessarily narrow the output pulse[41].

It was therefore decided to use the near-field pattern to compare the excitation conditions produced by different mode scramblers. The near-field pattern is measured (with a scanned photodiode-array) at the output of a 1 km section of fibre and compared with that observed after a 1 m section. If the near-field patterns are identical, then the launching conditions approach equilibrium. This criterion provides a useful indication of how fully a fibre is excited.

The most effective mode scrambler of those which have been tried is a $\sim$ 25 m section of graded-index fibre tightly coiled on a drum. A series of sharp kinks are imposed on this fibre near the launching end and, as a result, power is converted from the low-order modes predominantly excited by the laser to a wider mode spectrum. A further redistribution of power occurs in the remaining section of launch fibre before the pulse reaches the butt-joint and is launched into the test fibre.

It is important to choose a fibre with a core size similar to that of the test fibre and with a smooth refractive-index profile. In particular, a central 'pip' occurs in the profile of C.v.d. fibres when the dopant evaporation during the collapse stage of preform production is overcompensated. This type of structure in the profile can trap light and lead to a bright central spot in the near-field. The launching conditions are then very different from a state of equilibrium and, moreover, they are very sensitive to the position of the laser spot on the input face of the launch fibre.

Figure 4.11 shows the near field patterns recorded after 1 m and 1 km sections of fibre PO 181. Although there is considerably more structure after a short length, the overall shape of the two near-field patterns are very close. By contrast, figures 4.12 a-d show a range of near-field patterns observed after a 1 km section of the same fibre under different excitation conditions. These pictures show that, since marked differences in modal power distribution remain even after a 1 km section, there is little mode coupling in this fibre. This intrinsic absence of mode conversion was preserved by the use of a

split drum, which allowed the tension in the fibre to be relieved during the measurement.

4.3.3 Deconvolution of the system response

The impulse response of the fibre may be defined as the variation of output power with time when the fibre is excited with a vanishingly-narrow pulse of unit energy. Assuming that the fibre has a linear power reponse[42], the transfer function is the Fourier transform of the impulse response. The bandwidth of the fibre is defined as the frequency at which the transfer function falls to one half of its value at zero frequency. This definition corresponds to the 3 dB(optical) and 6dB(electrical) bandwidths commonly used in the literature.

The modulation transfer function of the fibre is obtained by dividing the normalised frequency spectrum measured at the fibre output by that measured at the input. In this way, as described earlier, the influence of the measurement system on the frequency spectrum at the output of the fibre is, in principle, removed. In the case of time-domain measurements, the input and output frequency spectra are obtained by taking the Fourier transform of the reference and output pulse, respectively. The input pulse, containing power over a wide frequency spectrum is launched into the fibre. The fibre acts as a low-pass filter and attenuates some frequency components more strongly than others; the filter characteristic, or transfer function, is derived by comparison of the input and output spectra.

The input and output waveforms (in the form of a photograph - e.g. figure 4.9) are measured at 128 equally-spaced points on the time axis. To do this accurately and as rapidly as possible, the photograph is fixed to the platen of a Tektronix 4662 plotter which is interfaced to a Tektronix 4051 mini-computer. The plotter carries a cross-hair which is made(with a joystick)to follow the oscilloscope traces recorded on the photograph. The x and y coordinates of each point are thus entered into the computer as they are measured.

The zero level of each pulse is adjusted to remove the slight offset which occurs when the signal amplitude is very small; the offset is caused by scattered light received by the detector during the 1 μs dye-laser pulses. Each pulse is then 'windowed' to avoid spurious effects caused by truncation of the waveforms at each end (i.e. at time t = 0 and T). The data is thus multiplied by the function:

$$w(t) = \begin{cases} \frac{1}{2}\left[(1-\cos\left(\frac{10\,\pi\,t}{T}\right)\right] & , \quad o \leq t \leq \frac{T}{10} \\ 1 & \frac{T}{10} \leq t \leq \frac{9}{10}\,T \\ \frac{1}{2}\left[(1-\cos\left(\frac{10\,\pi\,(t-T)}{T}\right)\right] & , \frac{9}{10}\,T \leq t \leq T \end{cases} \qquad (4.8)$$

which ensures that the 'windowed' data and its derivatives match at either end of the time interval. The data set is then extended by the addition of zero-valued data, the effect of which is to leave the sampling interval unchanged, but to increase the effective time-span of the measurement by a factor of 4. When the Fourier transform is calculated, therefore, the frequency range (which depends on the sampling interval) is not altered. The spectral components are now more closely spaced, however, and the frequency resolution is thus improved.

The frequency spectra corresponding to the pulses of figure 4.9 are shown in figure 4.13. For a fibre of this high bandwidth (approximately 1 GHz), the input (curve A) and output (curve B) are very similar and are dominated by the frequency response of the apparatus. It is therefore found that the transfer function (represented by solid line C) has fallen by only a few decibels at frequencies where the input spectrum contains very little power. The transfer function is thus dominated by noise at frequencies greater than about twice the bandwidth of the measurement system. This effect ultimately sets the limit on the bandwidth extension which can be obtained by deconvolution techniques. In order to estimate the bandwidth of very-low-dispersion fibres, the high-frequency data are truncated and replaced by a Gaussian amplitude

response fitted to the measurements, the fitting procedure using only that portion of the data which is clearly not completely corrupted by noise. The frequency at which the extrapolation begins is about 1 GHz and, at this frequency, the input frequency spectrum has fallen by about 10dB with respect to its value at zero frequency. The extrapolated section of the transfer function is shown as a dashed line in figure 4.13. Similarly, the phase of the transfer function is assumed to be linear at frequencies higher than that at which the truncation is performed (see inset on figure 4.13).

The tranfer function obtained by the above technique was used to calculate the impulse response, shown in figure 4.14, with an inverse Fourier transform. The impulse response shows an undershoot which, for an optical pulse, is not physically valid. The transfer functions of optical fibres have been predicted theoretically[43] and measured[39], and are known to possess a series of low amplitude side-lobes at high frequencies. These side-lobes are, of course, not present in the extrapolated transfer function and their absence may be the cause of the undershoot of the deconvolved impulse response. The calculated impulse response was also found to be very sensitive to seemingly minor variations in the transfer function. Since the deconvolved impulse responses were evidently not reliable, comparisons between measurements on fibres and theoretical predictions were made in the frequency domain. Thus the bandwidth determined as described above was compared with the value calculated by taking the Fourier transform of the predicted impulse response.

Naturally the use of longer fibres would improve the precision of the measurement of bandwidth x distance products. In longer fibres, however, it is more likely that mode conversion would affect the pulse broadening and thus make comparisons with theoretically predicted dispersion more difficult. In addition, the present study shows that the index profile can vary substantially over a 1 km distance. This effect is likely to be even more severe in longer fibres. Measurements of very long fibres are thus not of much scientific value unless they are complemented by measurements of the same fibres cut into shorter sections.

4.4 RESULTS AND DISCUSSION

The experimental and mathematical techniques described in sections 4.2 and 4.3 have allowed: a) the measurement of bandwidth over a wide wavelength range and b) the calculation of bandwidth from measurements of the refractive index profile and of the profile dispersion parameter. The latter data have been processed in several different ways to predict the bandwidth. The results for each of fibres PO 181, PO 182 and PO 180 are given below and are compared with measured values. All fibres had a length of 1 km and the values of bandwidth given below are thus(numerically), equivalent to bandwidth x distance products expressed in units of MHz. km.

4.4.1 Results For Fibre PO 181

The bandwidth measured as a function of wavelength in fibre PO 181 is shown in figure 4.15, each cross representing an experimentally-determined value. The results show a considerable variation of bandwidth with wavelength, in qualitative agreement with the theory of Olshansky and Keck. The fibre is optimal at a wavelength near 800 nm where the measured bandwidth rises to about 1.2 GHz. It decreases rapidly with departure from the optimum wavelength, falling to 450 MHz at 480 nm and 1175 nm, corresponding to a drop by nearly a factor of 3 in less than 400 nm. Hence a link using these or similar fibres and operating at 0.85 μm could probably not be upgraded to give wide bandwidth operation at 1.3 μm, an option which many system designers wish to retain for the time when suitable sources and detectors become available.

The scatter of the results indicates that the higher values of bandwidth measured approach the limitations of the apparatus. Nevertheless, the pulse-broadening is still clearly apparent near the optimum wavelength (e.g. figure 4.9), and the values shown in figure 4.15 are thus representative of the bandwidth of the fibre and not of the resolution of the equipment.

Also shown in figure 4.15 is the wavelength-dependence of bandwidth calculated for a fibre having a power-law profile with exponent 1.95. This curve was obtained using the ray-tracing programme, in order to include the source weighting function discussed in section 4.2.2; the result differs little, however, from that of the standard W K B approximation[3] for Lambertion excitation. The value, 1.95, of the profile exponent is the equivalent - α for end 1 (the end at which most of the data was taken) of fibre PO 181. It is worth noting that, although measurements of profile along different radii do not have identical equivalent - α values, the average α values for measurements at each wavelength are all near 1.95.[14]

The bandwidths predicted for the fibre with $f(\frac{r}{a}) = (\frac{r}{a})^{1.95}$ are greater, at all wavelengths, than the experimentally-determined values. The difference is most noticeable near the optimum wavelength, where the fibre with an α-profile has a bandwidth of about 12 GHz - an order of magnitude greater than was measured. The shortfall in bandwidth is almost certainly attributable to the deviations from the ideal power-law which were observed in the profile of the real fibre. Nevertheless, the wavelength of minimum dispersion are in good agreement.

The bandwidth of fibre PO 181 was calculated with the aid of the ray-tracing programme using the profile measurements made at each end of the 1 km section, and averaged over the entire wavelength range. The results are shown in figure 4.16 as a solid curve (predictions for end 1) and a broken line (based on profile data for end 2); the experimentally-determined values have been reproduced (crosses) for comparison. For both curves, the greatest predicted value of bandwidth is in good agreement with the experimental results. It is interesting to note that the predictions of the wavelength-dependence of bandwidth for each end are quite different and thus indicate a substantial change in profile along the length of the fibre. It has been shown[44] that, for fibres with length-dependent α-profiles, the bandwidth is dictated largely by the average exponent and that quite large deviations of the α-value about the mean have little effect on

the wavelength-dependence of bandwidth. There is also evidence[44] that other forms of profile-distortion (such as ripples) can also be compensated by complementary distortion in other parts of the fibre. It is therefore not surprising to find the experimentally determined bandwidth/wavelength curve lying between those predicted from profiles measured at each end. That its position should be so symmetric is, however, somewhat fortuitous since the variation of the profile along the fibre is only known from two samples which may or may not be representative of the average index distribution. The agreement, which was noted earlier, between the measured optimum wavelength and that predicted from the profile exponent, is thus also at least partly coincidental.

The dotted curve in figure 4.16 shows the bandwidth predicted from the profile measured at end 1 (and averaged over wavelength) when no correction is made for leaky modes. This curve, which might peak somewhere in the ultra-violet, is clearly in poor agreement with the experimentally-determined values. Comparison of all curves in figure 4.16 clearly indicates the necessity to correct the profiles obtained by the NFS technique.

The individual profile measurements (averaged from side to side) were also used to evaluate the bandwidth. The results are shown in figure 4.17, with two different symbols indicating profile measurements along orthogonal diameters. The bandwidths obtained from individual profile measurements are much lower than the experimental results (crosses) and those calculated from profiles averaged over all wavelengths. Moreover there is no marked wavelength dependence. This is rather surprising since, in addition to the effect of profile dispersion, one would expect a much greater increase in bandwidth, at longer wavelengths, caused by the apparent change in the fine detail of the index profile. It is likely that the deviations of the individual profiles from the ideal power-law are sufficient, not only to lower the fibre bandwidth, but also to alter substantially its wavelength-dependence.

Bandwidths predicted (using the ray-tracing programme) from profile

measurements averaged, at each wavelength, over orthogonal directions of scan are shown in figure 4.18. Larger values of bandwidth and a stronger wavelength-dependence are found than with results based on individual profile scans. The values now predicted from measurements at each wavelength closely follow the curve (solid line) obtained by averaging the complete profile data set, although the measurements do not extend to sufficiently long wavelengths to enable a comparison of the position of the peaks. Examinations of figures 4.3, 4.4 and 4.5 shows that the averaging of profiles over different orientations induces very little apparent loss of the ripples near the core centre. A possible explanation for the substantial improvement brought about by averaging is that the slight departure of the profile from circular symmetry causes the individual scans to be non-optimal, while their average is nearer to an α-profile.

The variation of bandwidth shown in figure 4.18 arises partly from profile dispersion and partly from the apparent wavelength-dependence of the fine structure in the profile. In order to separate the two effects, profile data measured at a single wavelength are used to calculate the fibre bandwidth over a wide spectral range. Any wavelength-dependence of bandwidth may then be attributed purely to profile dispersion. Figure 4.19 shows the spectral bandwidths predicted from profiles measured at 550 nm, 850 nm and 900 nm (averaged over two directions of scan). All three curves in this figure show some variation of bandwidth with wavelength, as a result of profile dispersion, with peaks in the region 950 nm-1150 nm. It is clear, however, that the profiles measured at the longer wavelengths exhibit larger maximum values of bandwidth due to the apparent change in profile with wavelength.

4.4.2 Results for fibre PO 182

The results of bandwidth measurements on fibre PO 182 are shown in figure 4.20. As with fibre PO 181, there is a strong variation with wavelength, showing a clear optimum, in this case at about 1050 nm. The 'equivalent-α' value for profiles measured on fibre PO 182 is 1.96 and the bandwidth corresponding to this α-profile is shown in 4.20 as

a solid line. The theoretical maximum is at a shorter wavelength than that measured. In fact, on the basis of the equivalent α-values, the optimum is predicted to shift to shorter wavelengths by ~30 nm in comparison with fibre PO 181. This is in contrast with the ~270 nm shift to longer wavelengths which is actually observed. The most likely explanation for the discrepancy is, as with fibre PO 181, a variation of the profile along the length of the fibre. Unfortunately measurements made at the other end of the fibre are not available to support or disprove this suggestion.

The results of the ray-tracing programme are shown in figure 4.21. Bandwidths predicted from profile measurements at individual wavelengths (and averaged over two directions of scan) show no significant wavelength-dependence, and are usually lower than the measured values. The bandwidth calculated from the index-profiles averaged over the wavelength range 500-1000 nm and over two orthogonal diameters are indicated by a solid line in figure 4.21. The optimum wavelength predicted by ray-tracing is much shorter than the measured optimum. This behaviour is similar to that predicted from the the 'equivalent-α profile'. In addition, the maximum calculated bandwidth is lower than that observed experimentally. For fibre PO 182, therefore, the agreement is rather poor between the measured bandwidth and that calculated from the refractive index profile at one end of the fibre.

This discrepancy was investigated further. The impulse responses calculated by ray-tracing are found to contain a small pre-pulse, which is particularly apparent at wavelengths where the (predicted) bandwidth is large. As an example, the impulse response calculated at the wavelength 400 nm is shown in figure 4.22(a). A small amplitude pulse preceeds the main pulse by about 1.2 ns and degrades the bandwidth.

In order to relate this feature of the impulse response to profile imperfections, the transit-times of individual rays have been compared to the position of their caustics. In figure 4.23, a sample of the rays in fibre PO182 at λ = 400 nm is mapped in a plane whose co-ordinates are the inner and outer caustics. Each ray can be specified

by the radial position of its caustics, and thus has a unique location in the diagram. The rays have been classified according to their arrival times and the darkest areas in figure 4.23 indicate the fastest rays. A salient feature of the diagram is that rays with outer caustics at the normalised radius $\frac{r}{a} = 0.86$ arrive well before the other rays. This suggests that, at this radial position, there exists an imperfection in the refractive-index profile which causes pulse distortion at all wavelengths. The deviation of the measured profile from the fitted power-law is an estimate of the radial distribution of profile distortion. The 'profile error', $\left[f(r)-(\frac{r}{a})^{1.96}\right]$, is plotted in figure 4.24. As expected, a deviation from the power law is found at the normalised radius of 0.86. Note that, although this distortion may appear large in comparison with the deviations found at most other radii, it represents a change of only 3×10^{-4} in refractive index. It has been shown[45], that in fibres with parabolic index profiles, r = 0.86 x a is precisely the radius at which the greatest proportion power is carried. The profile error at $\frac{r}{a} = 0.86$ could therefore have a more serious effect on the bandwidth than the larger deviations found near the core centre. The influence of the imperfection was estimated by repeating the ray-tracing calculation but eliminating all rays with outer caustics beyond 0.8 x a. The resulting bandwidth/wavelength curve, drawn as a broken line in figure 4.21, shows an improvement by up to 200 MHz km in bandwidth and some shift of the whole curve to longer wavelengths. Hence this confirms that the profile distortion at $\frac{r}{a} = 0.86$ is, at least partially, responsible for the low values predicted for the maximum bandwidth of this fibre. Moreover, figure 4.22 (b) shows that, when those rays with caustics beyond the normalised radius of 0.8 are removed, the pre-pulse disappears from the predicted impulse response.

Naturally, one would expect that the experimentally-determined values would be similarly affected by the profile imperfection which has been discussed and it is then somewhat surprising to find measured bandwidths as large as 1150 MHz km. A tentative explanation might be that the profile changes with length and the defect which has been discussed is compensated in another section of the fibre. Alternatively,

the excitation conditions simulated in the calculation may not reflect sufficiently accurately those established in the fibre during the bandwidth measurements.

4.4.3 Results for fibre PO 180

The bandwidths measured in fibre PO 180 are shown in figure 4.25. The fibre is optimal near 900 nm, with a maximum bandwidth similar to that observed in fibres PO 181 and PO 182. The bandwidth calculated for a fibre having an α-profile 'equivalent' to that measured in fibre PO 180 is shown as a solid line in figure 4.25. As was the case for fibres PO 181 and PO 182, the curves lies higher, at all wavelengths than the measured bandwidths. On the other hand, the values calculated directly from the measured profile (and shown as a broken line in figure 4.25) are much lower than the measured values, and appear to have little wavelength-dependence. The index data used here were taken along a single diameter and are the average of measurements made over a wide wavelength range at one end of the fibre.

The 'profile error' of fibre PO 180, $\left[f(r) - (\frac{r}{a})^{1.96}\right]$ is shown in figure 4.26 and reveals that the index profile departs at almost all radii from the average $\alpha = 1.96$ power-law. These profile distortions are the most likely explanation for the consistently low values of bandwidth predicted. Other mechanisms, such as azimuthal asymmetry or length-dependence of the profile, may compensate the errors observed in the index profile and lead to the high values of bandwidth which are measured. Thus in spite of the considerable amount of data available concerning the profile of fibre PO 180, not enough is known to enable an accurate prediction of its bandwidth/wavelength characteristic to be made. This emphasises the fact that extremely detailed profile information is needed in order that predicted bandwidths should agree with measured values.

4.5 MEASUREMENTS IN JOINTED PAIRS OF FIBRES

4.5.1 Background

It has been shown[3,2] that the bandwidth of multimode fibres with power-law profiles may be optimised by a suitable choice of the profile parameter α. If the value of α is too small, the fibre is said to be over compensated and, as a result, the higher-order modes travel faster than low-order modes. Conversely, in undercompensated fibres, the low-order modes arrive first. If two fibres with profile parameters on either side of the optimum are jointed together, the differential mode delays of the first fibre can be compensated in the second[19].

In practice, of course, mode coupling in joints and in the fibres, and departures from the ideal power-law profiles, limit the extent to which intermode-delay compensation occurs. There is nevertheless substantial experimental evidence[20] of intermodal delay compensation in long optical links. In addition, Marcuse has shown[44] that when there is a longitudinal variation of the profile parameter, the overall bandwidth is determined mainly by the average value of α.

The r.m.s. pulse-broadening s in a pair of fibres is given by[19]

$$s^2 = s_1^2 + s_2^2 + 2s_1 s_2 r_{12} \qquad (4.9)$$

where s_1 and s_2 represent the broadening of the individual fibres and r_{12} is a correlation coefficient which varies between -1 and +1. r_{12} describes the amount of compensation which occurs in the jointed link. Low values of $|r_{12}|$ indicate the presence of mode coupling, in which case equation (4.9) is approximated by the well-known result for a Gaussian network.

$$s^2 = s_1^2 + s_2^2 \qquad (4.10)$$

Note that this leads to a square-root dependence of bandwidth on length in long links.

Values of r_{12} approaching +1 occur when the fibres are either both undercompensated or both overcompensated and when there is little mode conversion. The pulse broadening of such a set of fibres has a linear length dependence.

If the fibres in a jointed pair have profile parameters on opposite sides of the optimum (i.e. one is overcompensated and the other is undercompensated), then optical equalisation can take place. In this case the sign of r_{12} is negative. It has been shown[20] that the intermodal broadening of a long optical link can be made almost as high as that of individual (and much shorter) fibres by jointing the fibres in such a way that equalisation takes place at each joint.

Now consider the wavelength-dependence of bandwidth in a jointed pair of fibres with power-law profiles. In the region bounded by the optimum wavelength of each fibre, the correlation coefficient is negative and optical equalisation should occur. Outside of this wavelength region, both fibres are either over-or under-compensated and the correlation coefficient is positive. The bandwidth of such a jointed pair is expected[19] to be similar to that of a single fibre having a profile exponent equal to that of the average of the profile parameter of each fibre. Thus the wavelength of optimum bandwidth for the jointed pair is the average of the optimum wavelength for each fibre.

4.5.2 Experimental Results.

The fibres analysed in section 4.4 were jointed in pairs and the bandwidths of the resulting 2 km-sections were measured as a function of wavelength. The experimental techniques are identical to those discussed above. The deconvolution of the system response, however, was performed at the British Post Office by M. Eve and R. Kashyap. The reciprocals of the bandwidths x distance products measured in the three fibre pairs, PO 181 + 180, PO 181 + 182 and PO 182 + 180 are shown in figures 4.27 - 4.29 together with the results for the individual fibres, for comparison. In a linear network, the values for the spliced pairs would be the sum of the reciprocal bandwidth of

each fibre, thus the normalised reciprocal bandwidth would be the average of that observed in each section. Examination of figures 4.27 to 4.29 shows that in the wavelength region between the optimum of each fibre, the dispersion remains low, which indicates that optical compensation is occurring. A particularly striking example is the pair PO 181 + PO 180 where the reciprocal bandwidth of the fibre - pair in the wavelength region 800 - 900 nm is far less than the average of the reciprocal bandwidth of individual fibres. The jointed pair thus shows, at some wavelengths at least, much greater bandwidth than would be predicted from the linear network model. The bandwidths achieved are not always greater than would be predicted from the Gaussian model i.e. a $(\text{distance})^{-\frac{1}{2}}$ length dependence of bandwidth. It might therefore be argued that the experimental results can be explained in terms of mode conversion, rather than optical compensation. Although some mode conversion is inevitable, it does not account for the observations on the following grounds:

(a) small amounts of mode conversion are likely to degrade, rather than enhance[46], the bandwidth in the wavelength region where optical compensation is thought to occur,

(b) the length-dependence of bandwidth outside the region where the fibres are compensating is approximately linear,

(c) the mode conversion in these fibres, in common with others made by the OVPO process,[5] was found to be quite low during the experiments designed to determine suitable launching conditions (see section 4.3.2). Similarly the butt-joints used to splice the fibres in pairs were carefully aligned and are felt to have caused little mode conversion. Note, however, that an abrupt change of the index profile will necessarily cause some transfer of power between modes.

Further experiments would be necessary to separate clearly and quantitatively the effects of mode conversion and optical compensation. A particularly powerful technique in this respect would be the differential mode delay experiment[47] in combination with some means of determining the level of mode conversion.

In addition to an improvement in bandwidth of fibre links, optical

compensation reduces its wavelength-dependence. Thus inspection of figure 4.27 - 4.29 shows that the bandwidth varies little in the region of optical compensation. Thus if the fibres in the optical link are placed in such a way that they are successively over-and-undercompensated there exists a wavelength region where the bandwidth is almost constant. This might allow tolerances on the profiles of individual fibres to be relaxed . Alternatively, the high-bandwidth 'window' could be exploited to increase the link capacity using wavelength-division multiplexing.

Unfortunately, a system which relies on optical compensation to achieve a high bandwidth is very inflexible since the fibre cables (which might comprise many fibres) are no longer equivalent and must be jointed in a particular sequence for optimum performance. An alternative approach is to use silicate glasses incorporating more than one index-modifying additive. The design flexibility thus provided allows fibres with low dispersion over a wide spectral range[48-50] to be fabricated. Ternary glasses such as germanophosphosilicates or germanoborosilicates are, in any case, very attactive from the point of view of preform production.

4.6 SUMMARY

Bandwidths have been measured over a very wide wavelength range in good-quality graded-index fibres. A new arrangement of the tunable dye-laser/optical parametric oscillator system avoids errors caused by variations in pulse shape between successive pulses. The bandwidth is deduced by taking the Fourier transform of the pulses launched into, and received from, the fibre. Values up to 1GHz can normally be obtained directly from the transfer function and an extrapolation routine has been developed to estimate the magnitude of still greater bandwidths.

All three fibres investigated exhibit bandwidths greater than 1GHz (in 1 km sections) somewhere in the wavelength region 700-1100 nm. Very detailed refractive index profile and profile dispersion data are available for these fibres and, with the aid of a ray-tracing algorithm, a comparative study was made of bandwidths predicted from the refractive-index data and measured in pulse-broadening experiments. Several characteristics of the index profiles were shown to have a profound effect on pulse propagation. Thus most profiles manifest deviations from a power law such as a central dip or a layer structure near the centre. These imperfections probably dominate the pulse broadening at those wavelengths where the fibre is otherwise well compensated. They also influence the wavelength-dependence of bandwidth in a more subtle way since their effect becomes less pronounced with increasing wavelength.

Variations of the profile along the length of the fibres affect predictions of bandwidth since the profile measured at one end is then not usually representative of the average profile. Because of this effect, it was possible to obtain good agreement with theory in the case of only one fibre for which profiles had been measured at both ends (and then only if one assumes that the two samples are representative of the profile averaged along the fibre length).

Finally, the absence of circular symmetry also makes more difficult the correlation between refractive-index profiles and measured bandwidth.

Thus, in spite of the good circularity of the fibres cores their profiles depart from mirror symmetry (along single diameters) and from circular symmetry. Good agreement between predicted and measured values of the highest bandwidth was achieved only when the average of the profiles measured along orthogonal diameters was used in the ray-tracing algorithm. It might be that, in fibres with still higher bandwidth and more perfect profiles, departures from circular symmetry would have a direct detrimental effect on the fibre bandwidth.

In order to obtain consistently good agreement between the theory of intermodal dispersion and pulse-broadening measurements in fibres having profile imperfections of the type described, it is essential to make profile measurement at several points along the length of the fibre, across several diameters and possibly at each wavelength of interest.

4.7 REFERENCES TO CHAPTER 4

[1]M.J. ADAMS, D.N. PAYNE, F.M.E. SLADEN and A.H. HARTOG: 'Optimum operating wavelength for chromatic equalisation in multimode optical fibres.' Electron. Lett. 1978, 14, pp. 64-66.

[2]D. GLOGE and E.A.J. MARCATILI: 'Multimode theory of graded-core fibers.' Bell Syst. Tech. J. 1973, 52, 1562-1578.

[3]R. OLSHANSKY and D.B. KECK: 'Pulse broadening in graded-index optical fibers.' Appl. Opt. 1976, 15, pp. 483-491.

[4]J.P. HAZAN, J.J. BERNARD and D. KUPPERS: 'Medium numerical aperture, low-pulse-dispersion fibre.' Electron. Lett. 1977, 13, pp. 540-542.

[5]D.B. KECK and R. BOUILLIE: 'Measurements on high-bandwidth optical waveguides.' Opt. Commun. 1978, 25, pp. 43-48.

[6]R. OLSHANSKY: 'Pulse broadening caused by deviations from the optimal index profile.' Appl. Opt. 1976, 15 (3), pp. 782-788.

[7]D. MARCUSE: 'Calculation of bandwidth from index profiles of optical fibers 1: Theory.' Appl. Opt. 1979, 18, pp. 2073-2080. Correction: Applied Optics 1980, 19, pp. 188-189.

[8]K. BEHM: 'Dispersion in CVD-fabricated fibres with a refractive index dip on the fibre axis.' Arch. Electron. & Ubertragungstech. 1977, 31, pp. 45-48.

[9]K. BEHM: 'Group delay in CVD-fabricated fibres with diffused stair-like index profiles.' Arch. Electron & Ubertragungstech. 1976, 30, pp. 329-331.

[10]D. MARCUSE and H.M. PRESBY: 'Effects of profile deformations on fiber bandwidth.' Appl. Opt. 1979, 18, pp. 3758-3763.

[11]K. OKAMOTO: 'Comparison of calculated and measured impulse responses of optical fibres.' Appl. Opt. 1979, 18, pp. 2199-2206.

[12]H.M. PRESBY, D. MARCUSE and L.G. COHEN: 'Calculation of bandwidth from index profiles of optical fibers, 2: Experiment.' Appl. Opt. 1979, 18, pp. 3249-3255.

[13]J.J. RAMSKOV HANSEN and E. NICOLAISEN: 'Propagation in graded-index fibres: comparison between experiment and three theories.' Appl. Opt. 1978, 17, pp. 2831-2835.

[14]F.M.E. SLADEN: 'Fibres for optical communications.' Ph.D. Thesis, Southampton University, 1979.

[15]F.M.E. SLADEN, D.N. PAYNE and M.J. ADAMS: 'Determination of optical fiber refractive index profiles by a near-field scanning technique.' Appl. Phys. Lett. 1976, 28, pp. 255-258.

[16]M.J. ADAMS, D.N. PAYNE and F.M.E. SLADEN: 'Correction factors for the determination of optical-fibre refractive index profiles by the near-field scanning technique.' Electron. Lett. 1976, 12, p. 281-283. (Erratum ibid 1976, 12, p. 348.)

[17]F.M.E. SLADEN, D.N. PAYNE and M.J. ADAMS: 'Measurement of profile dispersion in optical fibres: A direct technique.' Electron. Lett. 1977, 13, pp. 212-213.

[18]F.M.E. SLADEN, D.N. PAYNE and M.J. ADAMS: 'Definitive profile-dispersion data for germania-doped silica fibres over an extended wavelength range.' Electron. Lett. 1979, 15, (15), pp. 469-470.

[19]M. EVE: 'Multipath time dispersion theory of an optical network.' Opt. & Quant. Electron. 1978, 10, pp. 41-51.

[20]M. EVE, P.C. HENSEL, D.J. MALYON, B.P. NELSON, J.R. STERN, J.V. WRIGHT and J.E. MIDWINTER: 'Transmission studies on three graded-index fibre cable links installed in operational ducts.' Opt. & Quant. Electron. 1978, 10, pp. 253-265.

[21]M. EVE, A.H. HARTOG, R. KASHYAP and D.N. PAYNE: 'Wavelength dependence of light propagation in long fibre links.' Proc. Fourth European Conference on Optical Communication, Genoa, September 1978. pp. 58-63.

[22]H.M. PRESBY and I.P. KAMINOW: 'Binary silica optical fibers: refractive index and profile dispersion measurements.' Appl. Opt. 1976, 15, pp. 3029-3036.

[23]J.W. FLEMING: 'Material and mode dispersion in GeO_2. B_2O_3. SiO_2 glasses.' J. Am. Ceram. Soc. 1976, 59, pp. 503-507.

[24]J.W. FLEMING: 'Material dispersion in lightguide glasses.' Electron. Lett. 1978, 14, pp. 326-328.

[25]S. KOBAYASHI, N. SHIBATA, S. SHIBATA and T. IZAWA: 'Characteristics of optical fibers in infrared wavelength region.' Rev. of the E.C.L. NTT, Jap. 1978, 26, pp. 453-467.

[26]J.A. ARNAUD: 'Optimum profiles for dispersive multimode fibres.' Opt. & Quant.Electron. 1977, 9, pp. 111-119.

[27]S. GECKELER: 'Nonlinear profile dispersion aids optimisation of graded-index fibre.' Electron. Lett. 1976, 13, pp. 440-442.

[28]A. ANKIEWICZ: Ph.D. Thesis. Australian National University, Canberra, 1978.

[29]L. JEUNHOMME, M. FRAISE and J.P. POCHOLLE: 'Propagation model for long step-index optical fibers.' Appl. Opt. 1976, 15, pp. 3040-3046.

[30]D. GLOGE: 'Weakly-guiding fibres.' Appl. Opt. 1971, 10, pp. 2252-2258.

[31]M.J. ADAMS, D.N. PAYNE, F.M.E. SLADEN and A.H. HARTOG: 'Resolution limit of the near-field scanning technique.' 3rd European Conference on Optical Communication, Munich, September 1977 Conference Proceedings pp. 25-27.

[32]K. PETERMANN: 'Uncertainties of the leaky mode correction for near square law optical fibres.' Electron. Lett. 1977, 13, pp. 513-514.

[33]A. ANKIEWICZ: 'Core fields in graded fibres with non-circular index contours.' Opt. & Quant. Electron. 1979, 11, pp. 525-539.

[34]K.I. WHITE: 'Practical application of the refracted near-field technique for the measurement of optical fibre refractive index profiles.' Opt. & Quant. Electron. 1979, 11, pp. 185-196.

[35]J.J. RAMSKOV-HANSEN, A. ANKIEWICZ and M.J. ADAMS: 'Attenuation of leaky modes in graded non circular multimode fibres.' Electron. Lett. 1980, 16 (3), pp. 94-96.

[36]J.J. RAMSKOV-HANSEN, M.J. ADAMS, A. ANKIEWICZ and F.M.E. SLADEN: 'Near-field correction factors for elliptical fibres.' Electron. Lett. 1980, 16, pp. 580-581.

[37]D. GLOGE, E.L. CHINNOCK and R.H. RING: 'Direct measurement of the (baseband) frequency response of multimode fibers.' Appl. Opt. 1972, 11, pp. 1534-1538.

[38]L.G. COHEN, I.P. KAMINOW, H.W. ASTLE and L.W. STULZ: 'Profile dispersion effects on transmission bandwidths in graded-index optical fibers.' IEEE J. Quant. Electron. 1978, QE-14, pp. 37-41.

[39]C.Y. BOISROBERT, A. COZANNET and C. VASSALO: 'Sweep-frequency transfer function measurement applied to optical fibre.' Proc. Conference on precision electrical measurements. Boulder, Colorado 1976, pp. 91-93.

[40]D. MARCUSE: 'Excitation of parabolic-index fibers with incoherent sources.' Bell Syst. Tech. J. 1975, 54, pp. 1507-1530.

[41]R.A. SAMMUT: 'Pulse dispersion in partially-excited graded-index fibres.' Opt. & Quant. Electron. 1977, 9, pp. 61-74.

[42]C. VASSALLO: 'Linear power responses of an optical fiber.' IEEE Transactions on microwave theory and techniques 1977, MTT-25, pp. 572-576.

[43]E.J. BOCHOVE and A. COZANNET: 'Low-pass filter characteristics of multimode graded index fibres.' Opt. & Quant. Electron. 1977, 9, pp. 135-141.

[44]D. MARCUSE: 'Multimode fiber with z-dependent α-value.' Appl. Opt. 1979, 18, pp. 2229-2231.

[45]A. ANKIEWICZ and C. PASK: 'Geometric optics approach to light acceptance and propagation in graded-index fibres.' Opt. & Quant. Electron. 1977, 9, pp. 87-109.

[46]S.D. PERSONICK: 'Time dispersion in dielectric waveguides.' Bell Syst. Tech. J. 1970, 50, pp. 843-859.

[47]R. OLSHANSKY and S.M. OAKS: 'Differential mode delay measurement.' Proc. Fourth European Conference on Optical Communication, Genoa 1978, Paper III.1.

[48]E.A.J. MARCATILI: 'Modal dispersion in optical fibres with arbitrary numerical aperture and profile dispersion.' Bell Syst. Tech. J. 1977, 56, pp. 49-63.

[49]I.P. KAMINOW and H.M. PRESBY: 'Profile synthesis in multicomponent glass optical fibers.' Appl. Opt. 1977, 16, pp. 108-112.

[50]R. OLSHANSKY: 'Optical waveguides with low pulse dispersion over an extended spectral range.' Electron. Lett. 1978, 14, pp. 330-331.

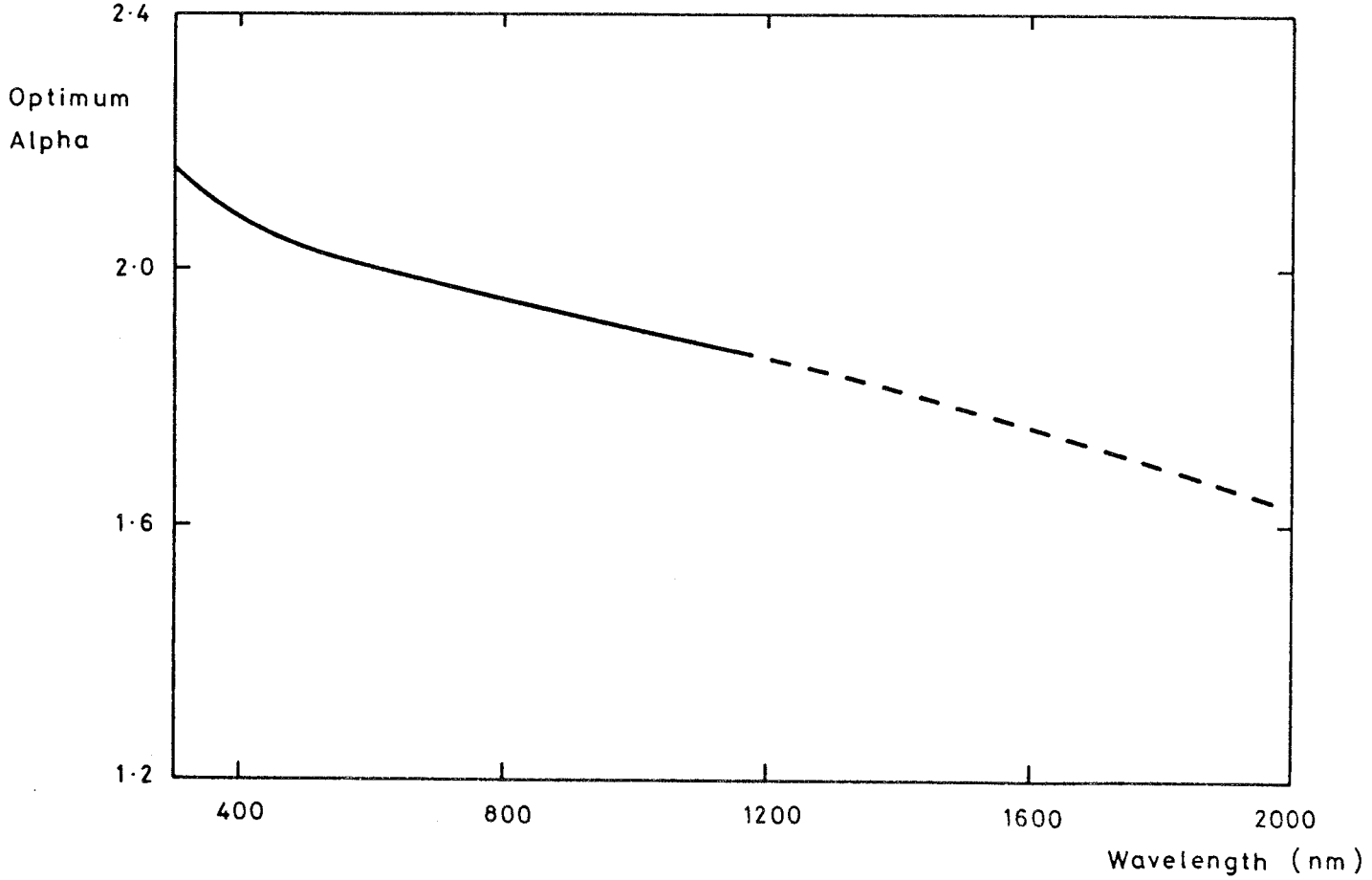

Figure 4.1: Optimum profile parameter measured in fibre PO 181 as a function of wavelength. The solid line indicates the range of measurement.

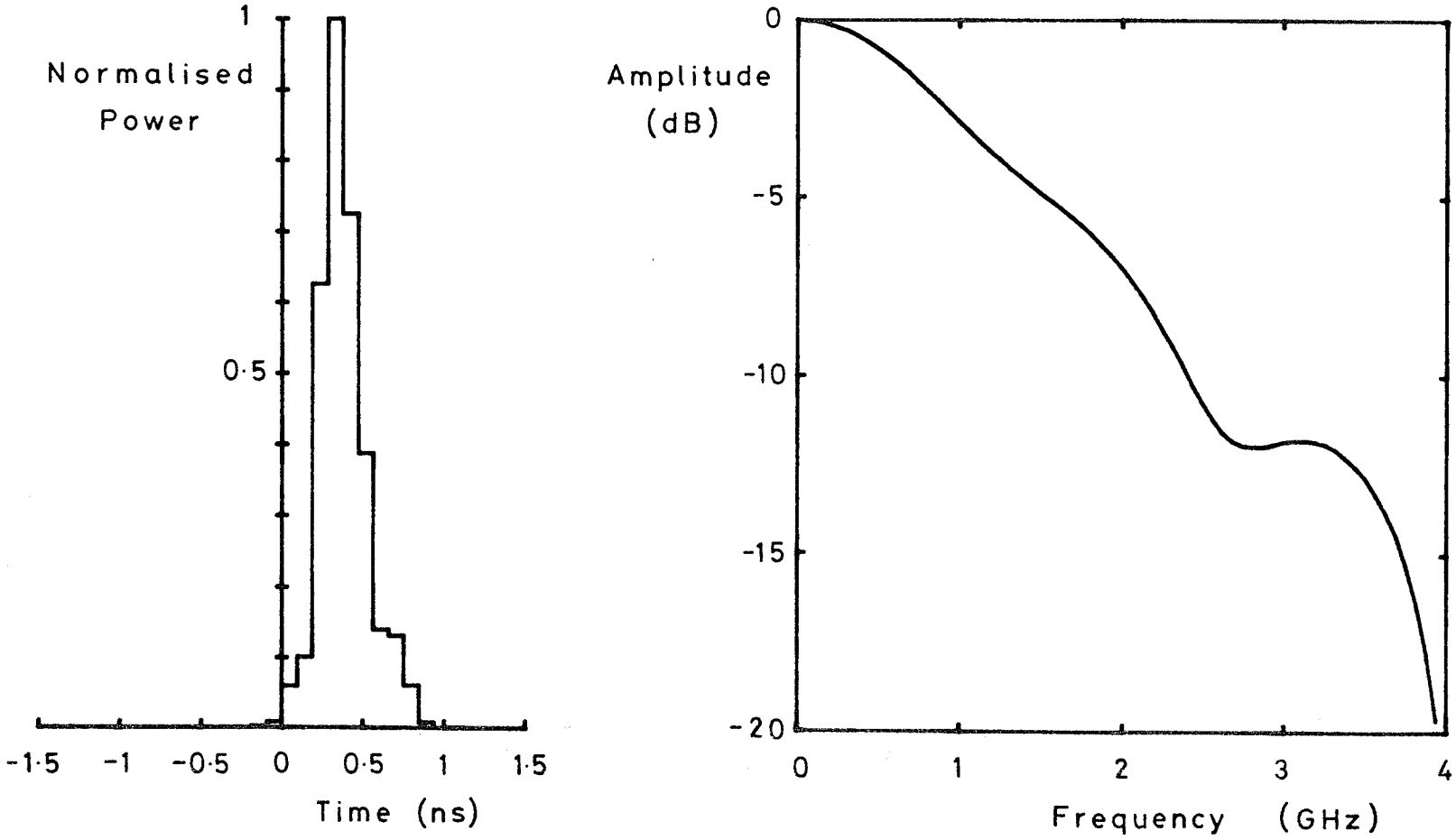

Figure 4.2

(a) Typical impulse response calculated using the ray-tracing algorithm, and (b) the corresponding amplitude transfer function.

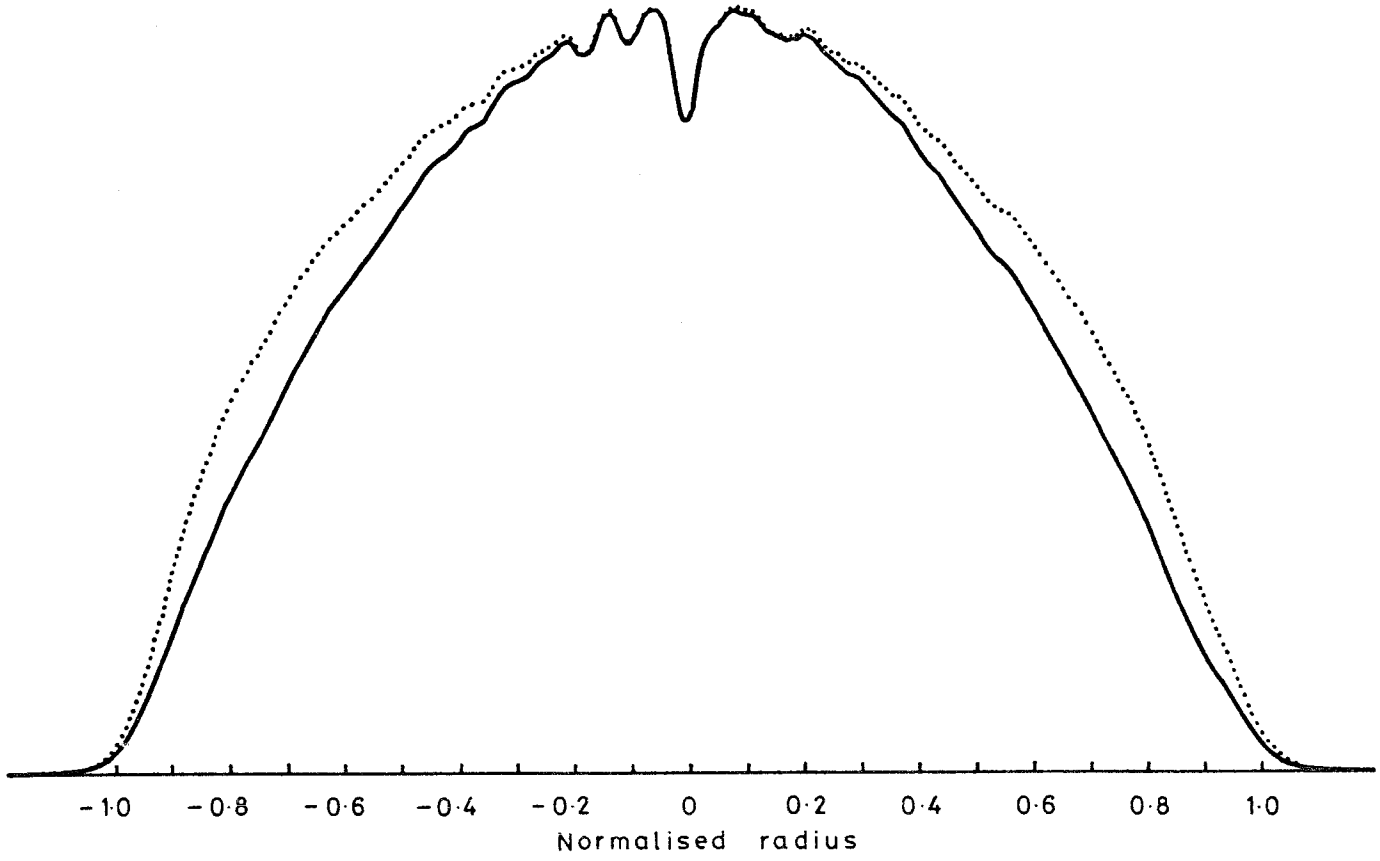

Figure 4.3: Refractive index profile of fibre PO 181 at a wavelength of 600 nm. The dotted line shows the measured near-field intensity; the solid line is the refractive-index profile after correction for leaky modes.

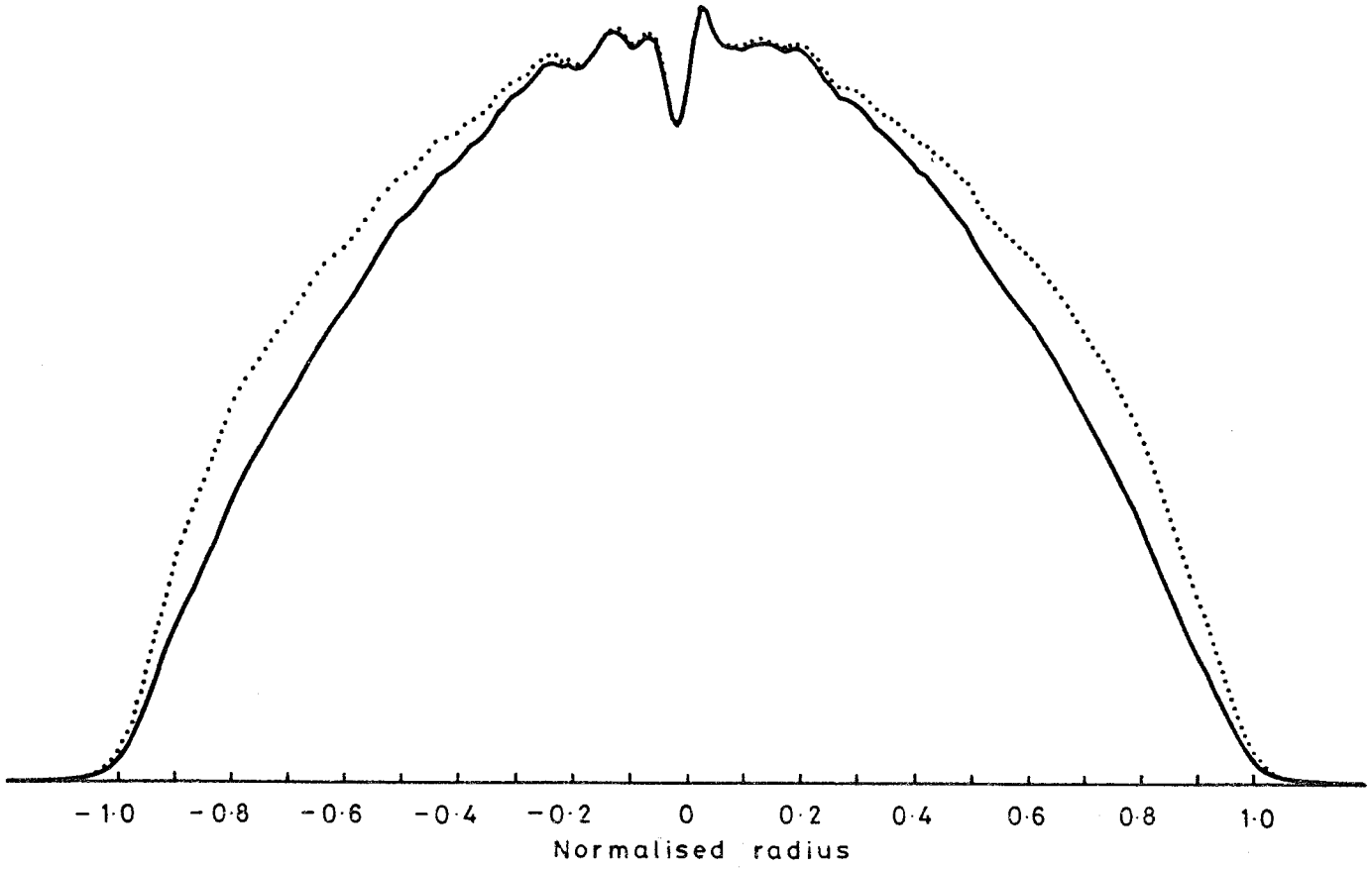

Figure 4.4: Refractive index profile of fibre PO 181 at a wavelength of 600 nm, measured along a diameter orthogonal to that of Fig. 4.3. The dotted line shows the measured near-field intensity and the solid line represents the refractive index after correction for leaky modes.

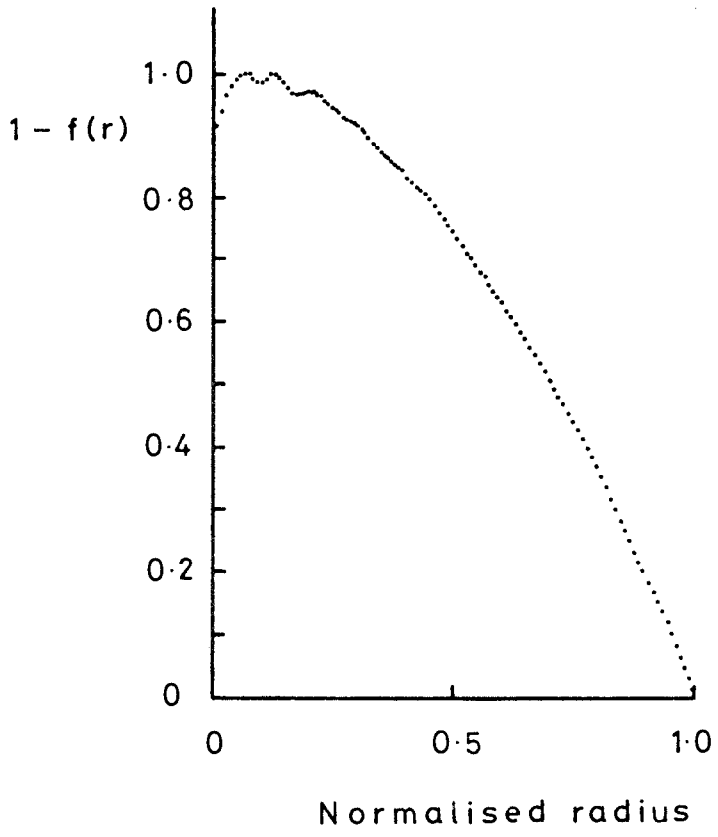

Figure 4.5: Refractive-index profile of fibre PO 181 obtained by averaging the data of Figs. 4.3 and 4.4.

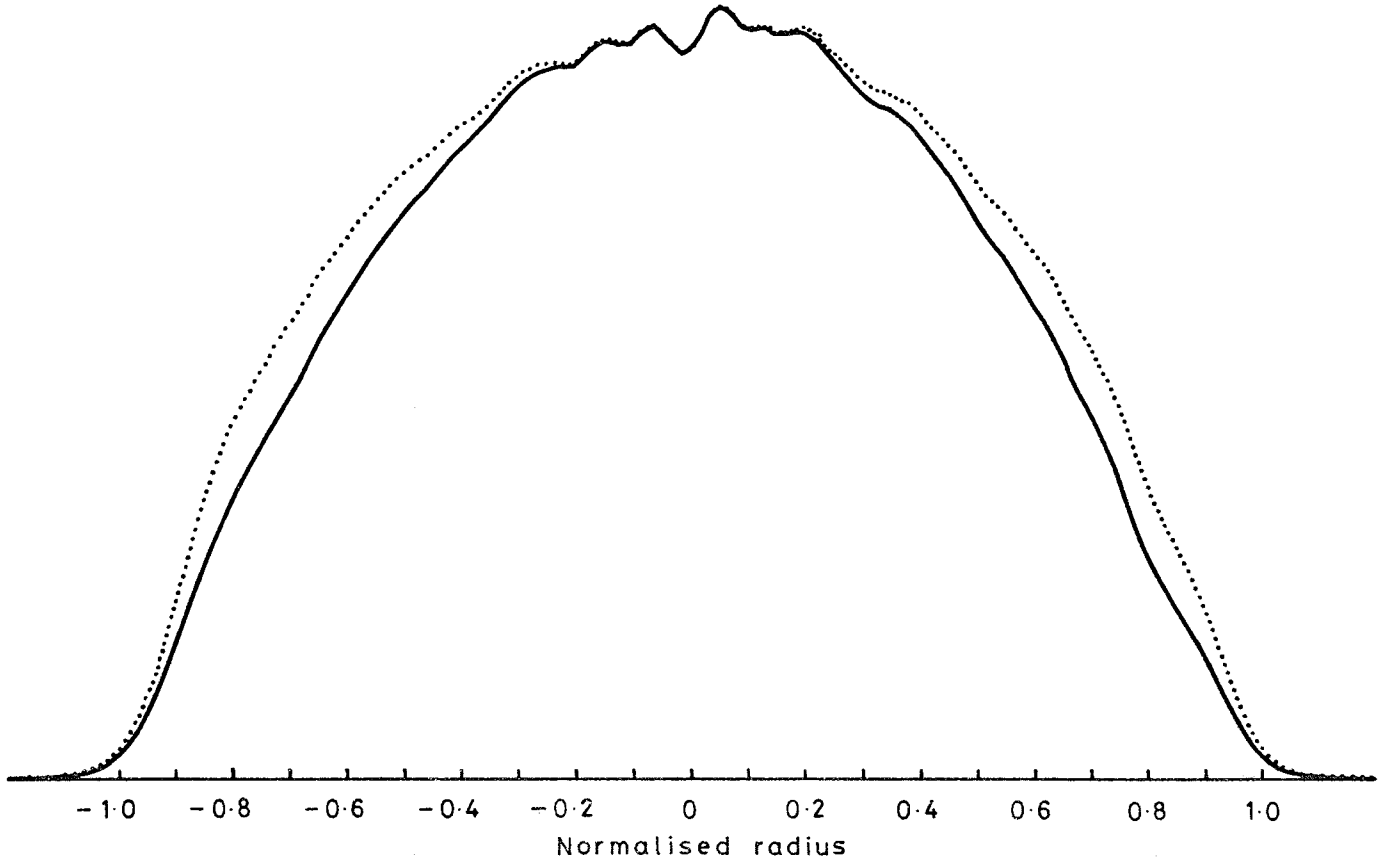

Figure 4.6: Refractive-index profile measured in fibre PO 181 at a wavelength of 900 nm. The dotted line shows the measured near-field intensity; the solid line represents the refractive index profile after correction for leaky modes.

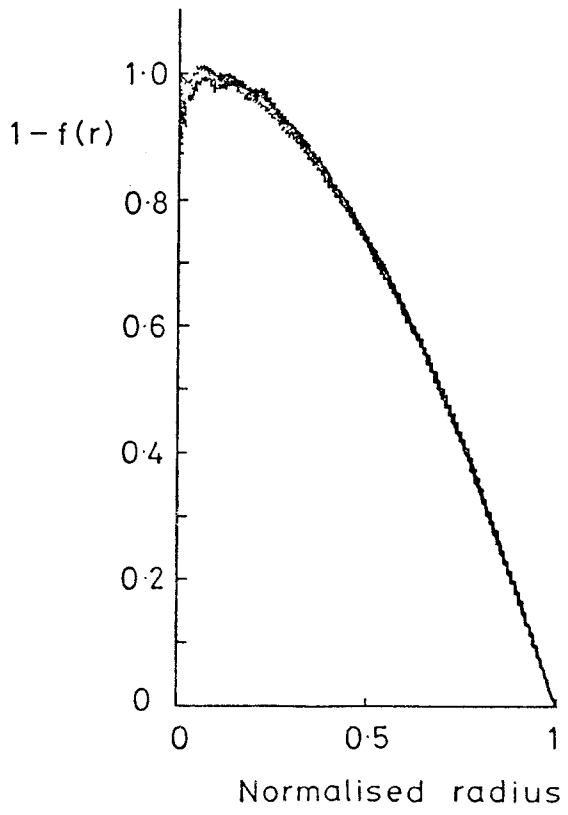

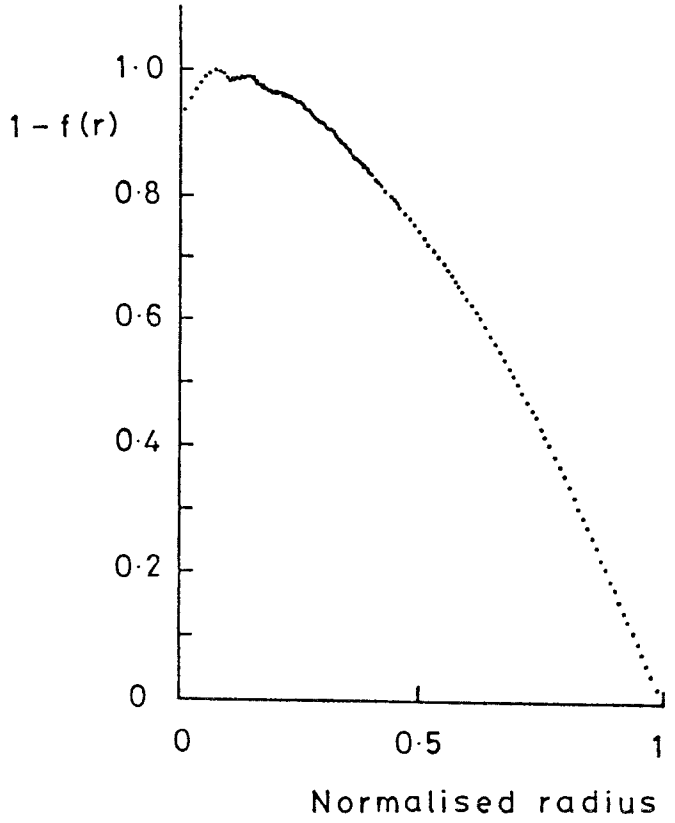

Figure 4.7

(a) Superposition of all available profile measurements for one end of fibre PO 181. The data covers the wavelength range 500-900 nm and two orthogonal directions of scan.

(b) average profile for fibre PO 181 obtained from the data in (a).

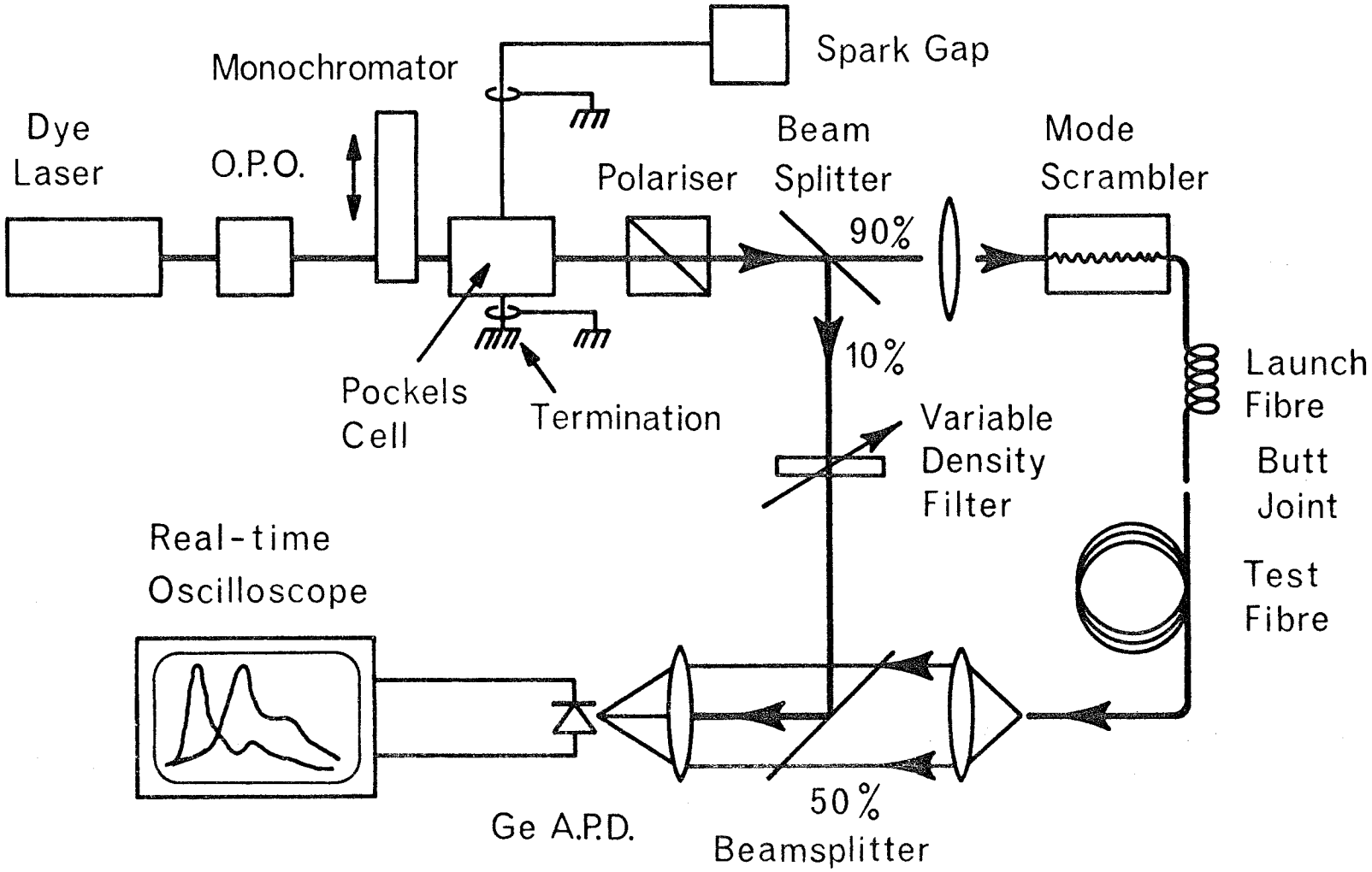

Figure 4.8: Experimental arrangement for the measurement of pulse broadening.

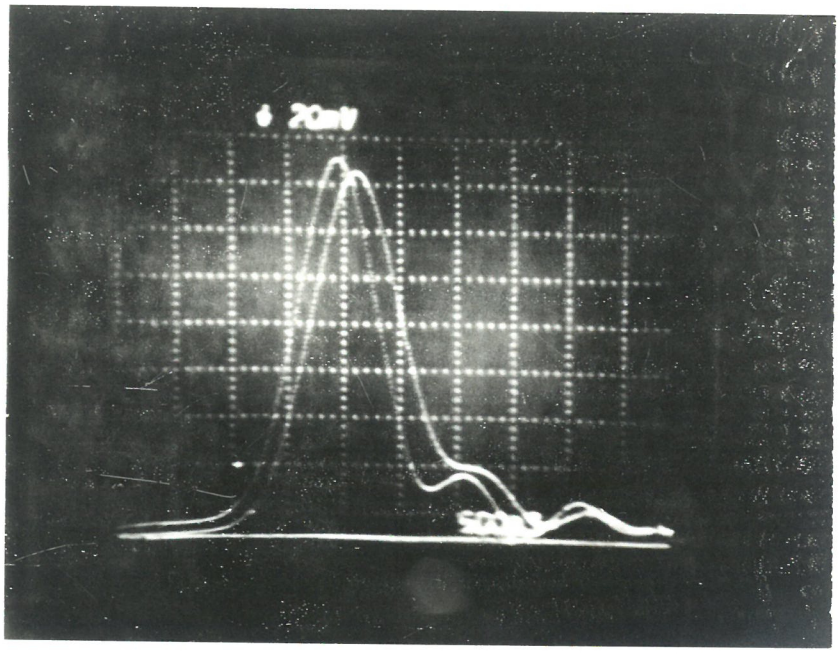

Figure 4.9: Pulse broadening measurement in fibre PO 181 at a wavelength of 835 nm. The narrower pulse is measured at the fibre input, the broader pulse at the output. The horizontal scale is 500 ps/div.

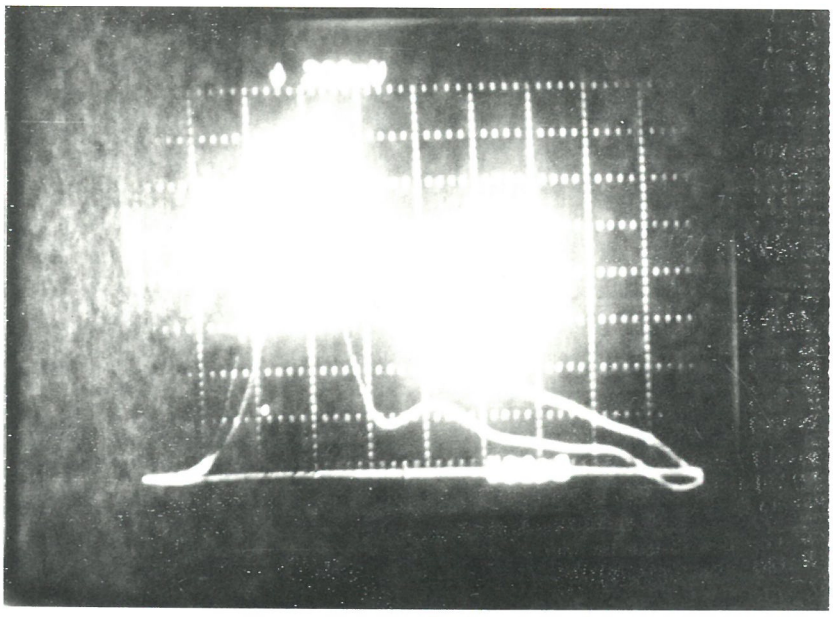

(a) under equilibrium launching conditions

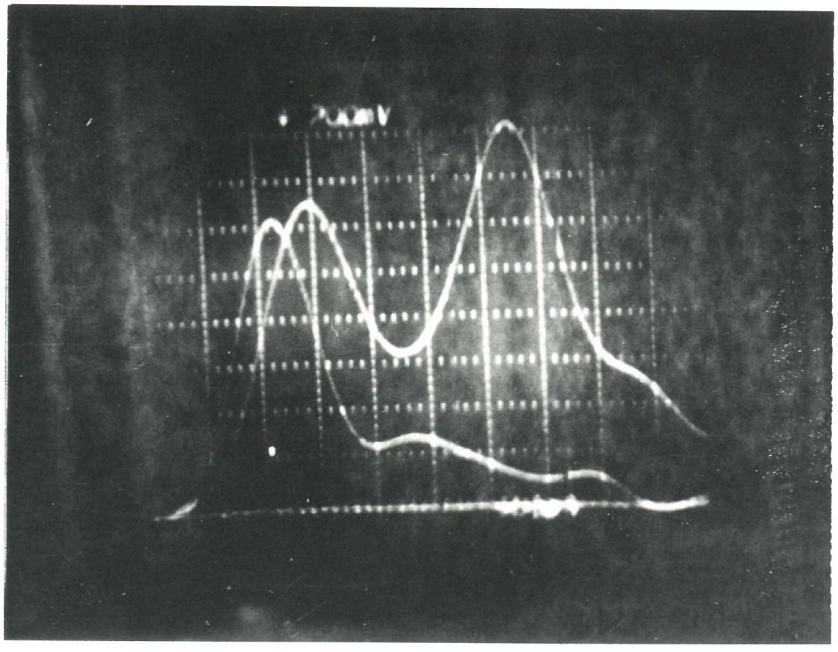

(b) launching from a small spot at the centre of the input face.

Figure 4.10: Two measurements of pulse broadening in the same 1 km length of multimode fibre at a wavelength of 900 nm under different launching conditions

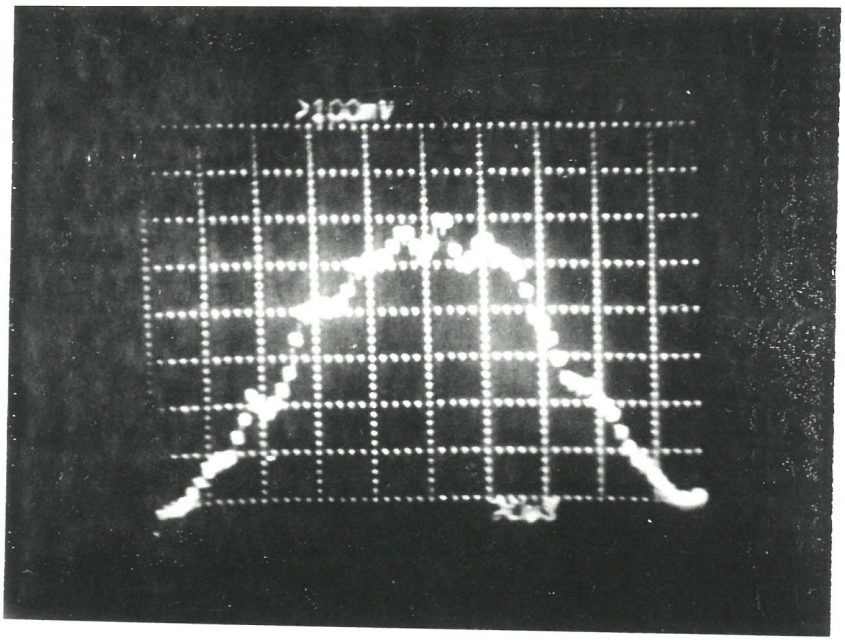

(a) after a 1 m section of fibre PO 181

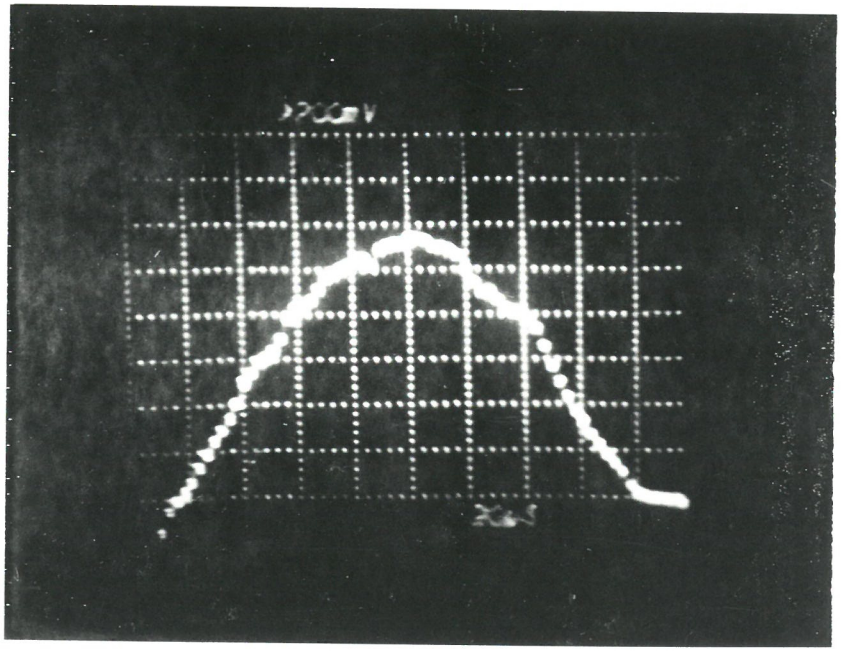

(b) after a 1 km section of fibre PO 181

Figure 4.11: Near fields measured at the output of two sections of fibre each excited with the mode scrambler.

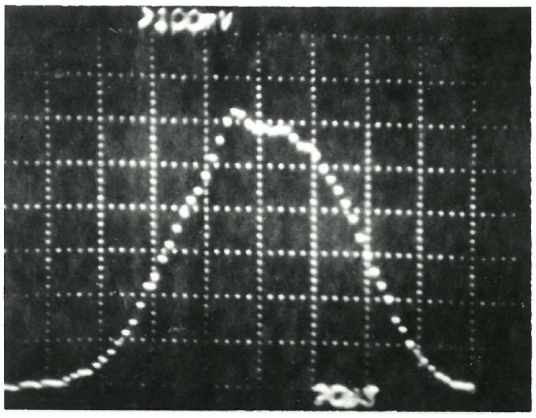

(a)

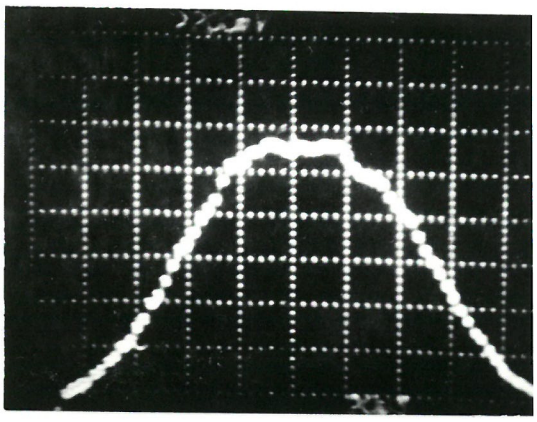

(b)

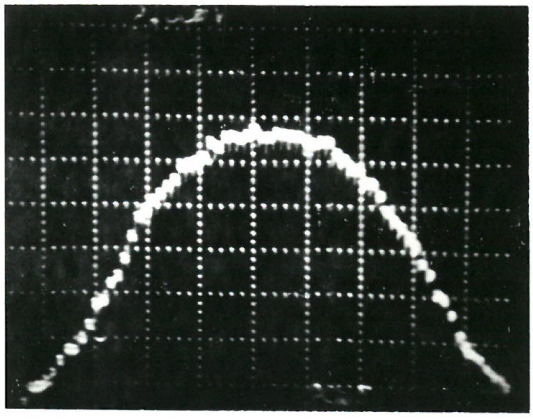

(c)

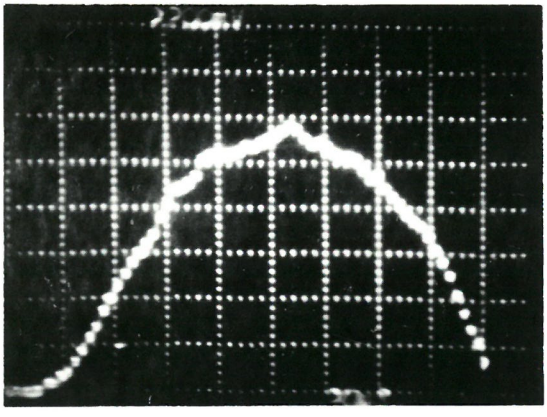

(d)

Figure 4.12: Near fields measured at the output of fibre PO 181 under a range of launching conditions.

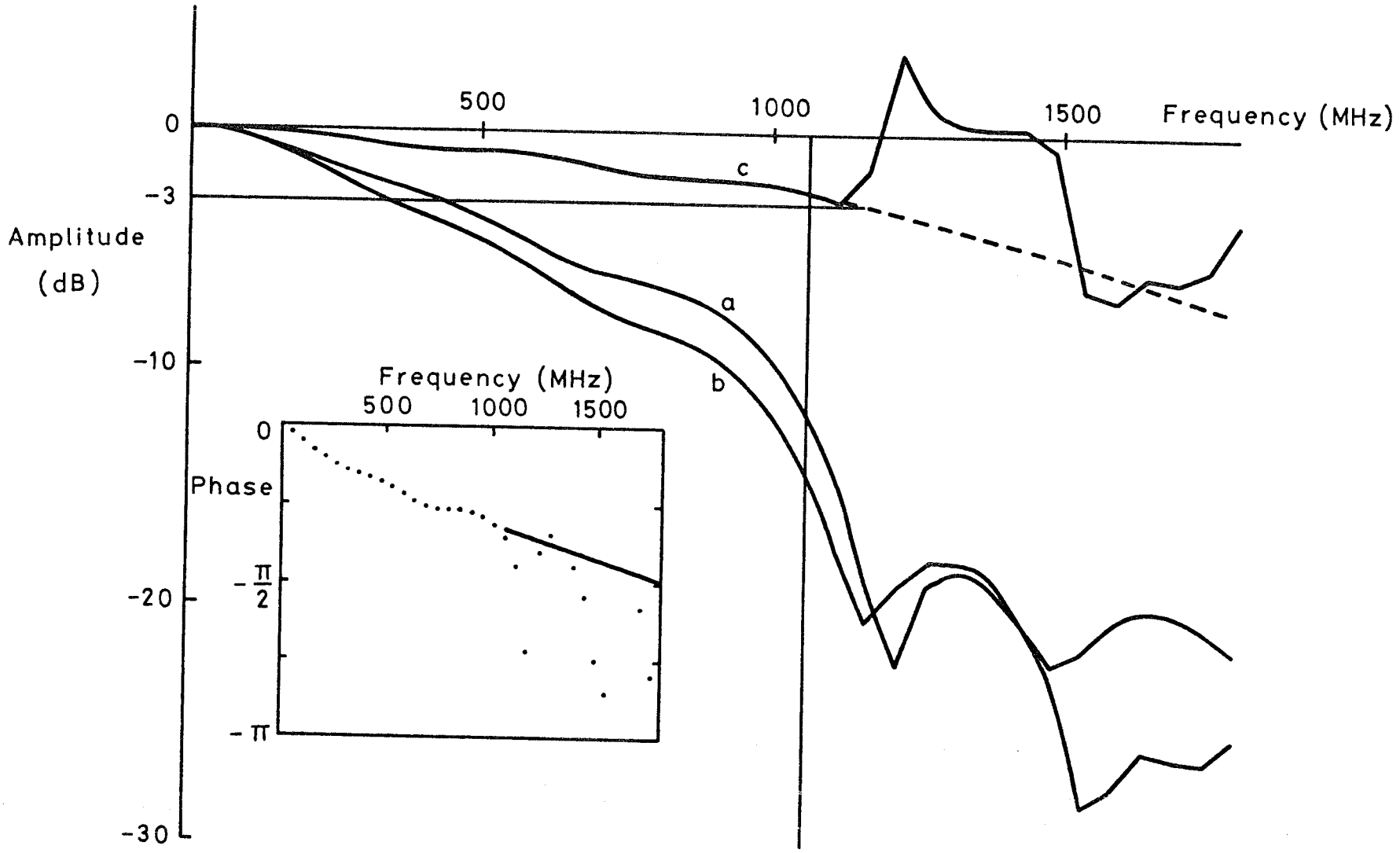

Figure 4.13: Characteristics of fibre PO 181 at 835 nm in the frequency domain. Curves (a) and (b) represent the amplitude frequency spectra of the input and output pulses, respectively, shown in Figure 4.9. Curve (c) is the amplitude of the transfer function. The phase of the transfer function is shown in the inset.

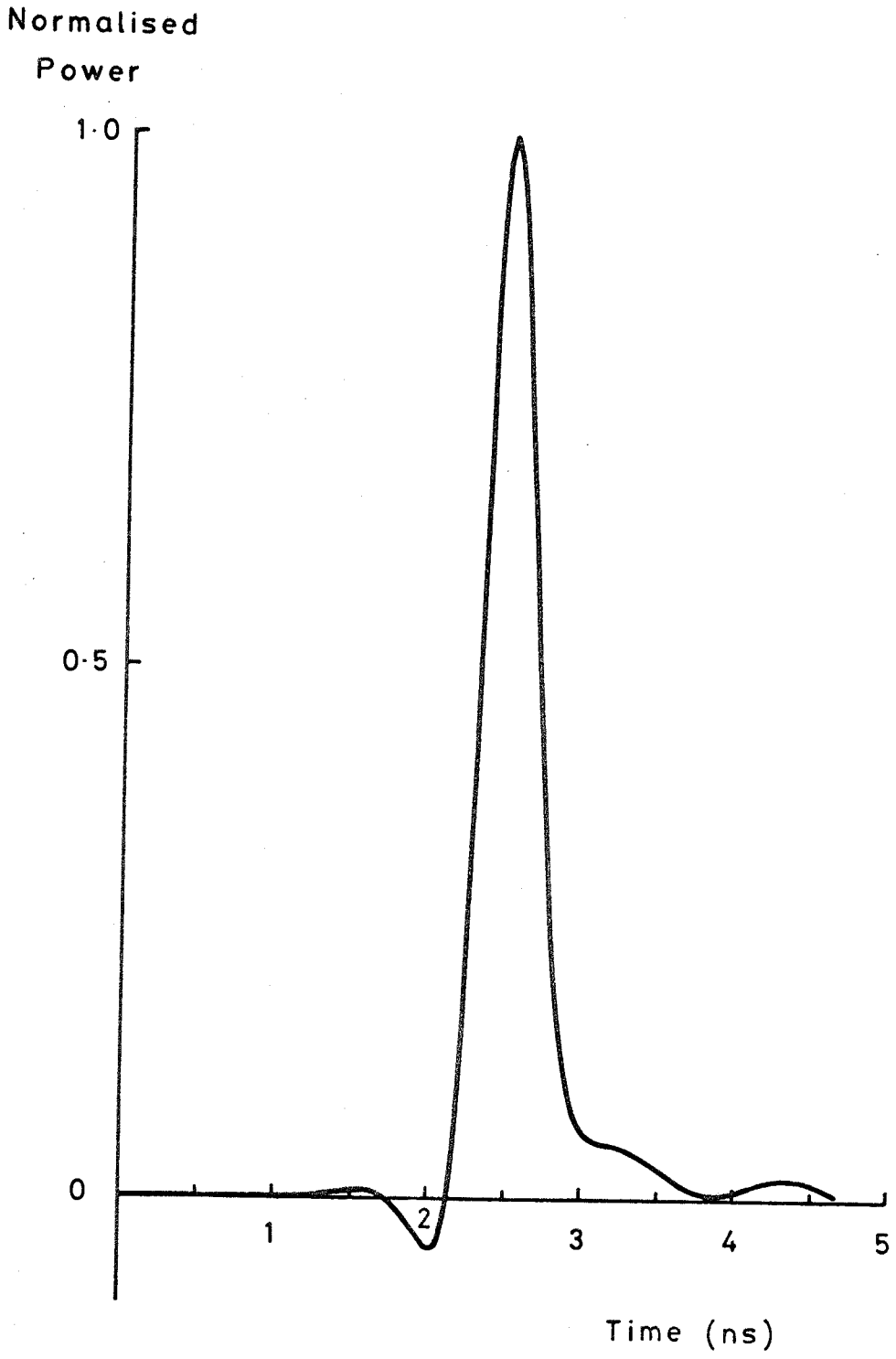

Figure 4.14: Deconvolved impulse response of fibre PO 181 at 835 nm.

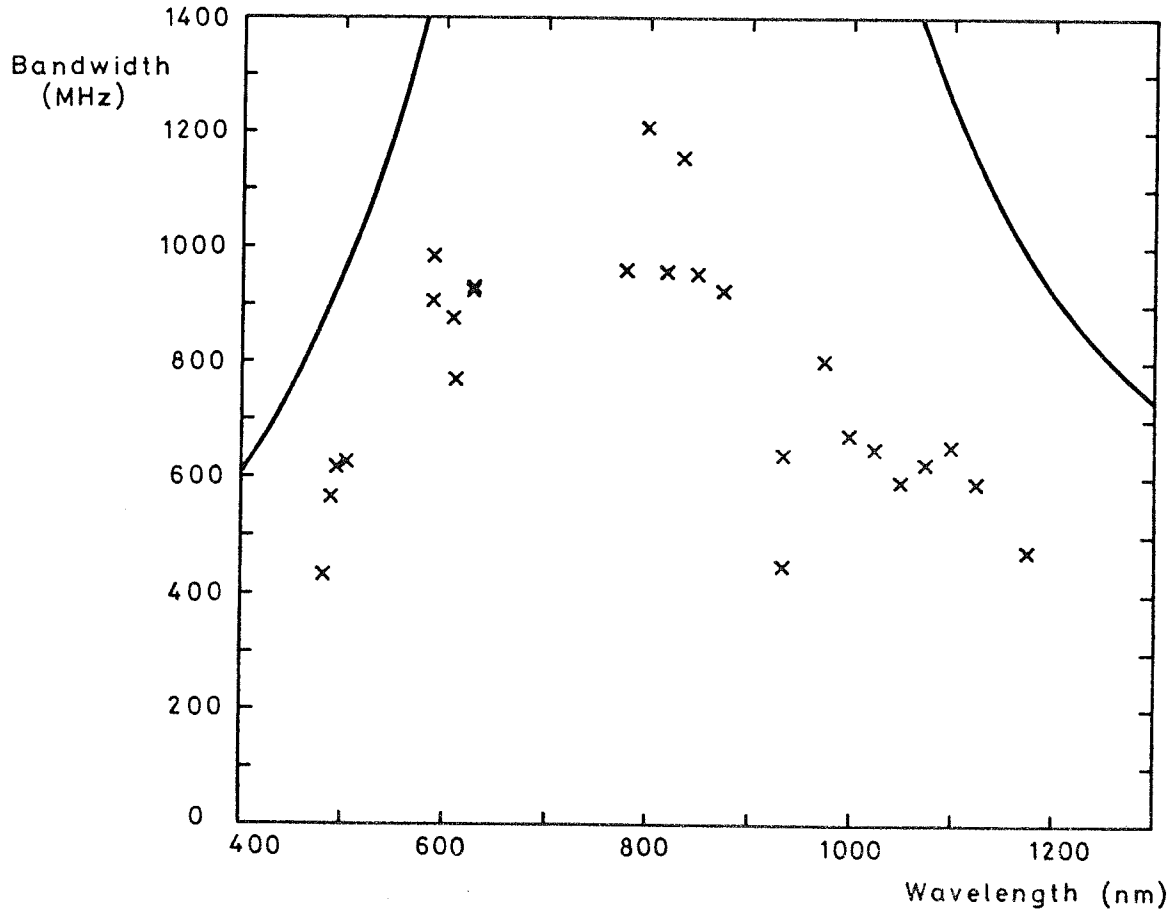

Figure 4.15: Wavelength-dependence of bandwidth of fibre PO 181. Crosses represent experimentally-determined values; the solid line shows the bandwidth calculated for a power-law profile having $\alpha = 1.95$.

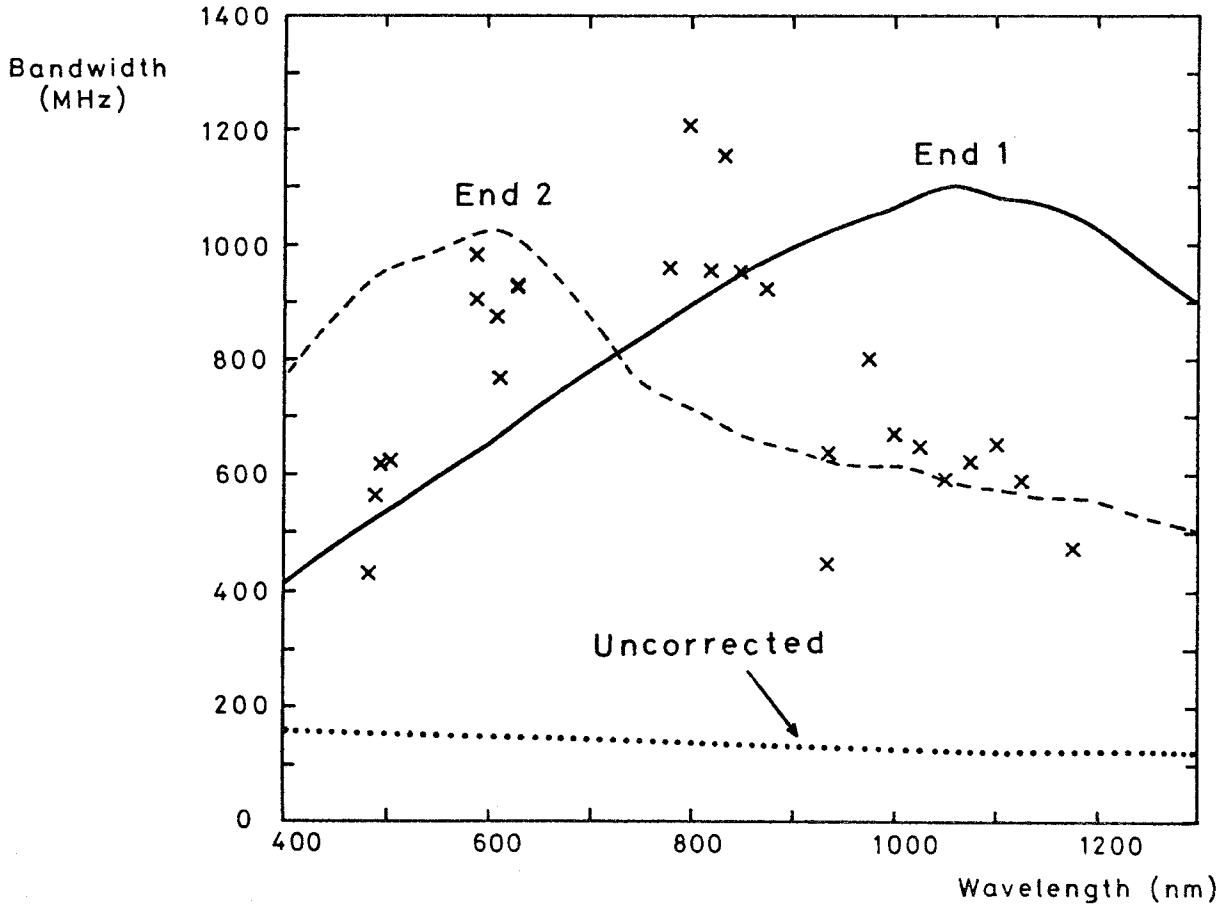

Figure 4.16: Comparison of the measured wavelength-dependence of bandwidth of fibre PO 181 (crosses) with that predicted from the average of all available profile data for end 1 (solid curve) and end 2 (broken line). The dotted line shows the bandwidth predicted from the data for end 1 if the measured near-fields are not corrected for leaky modes.

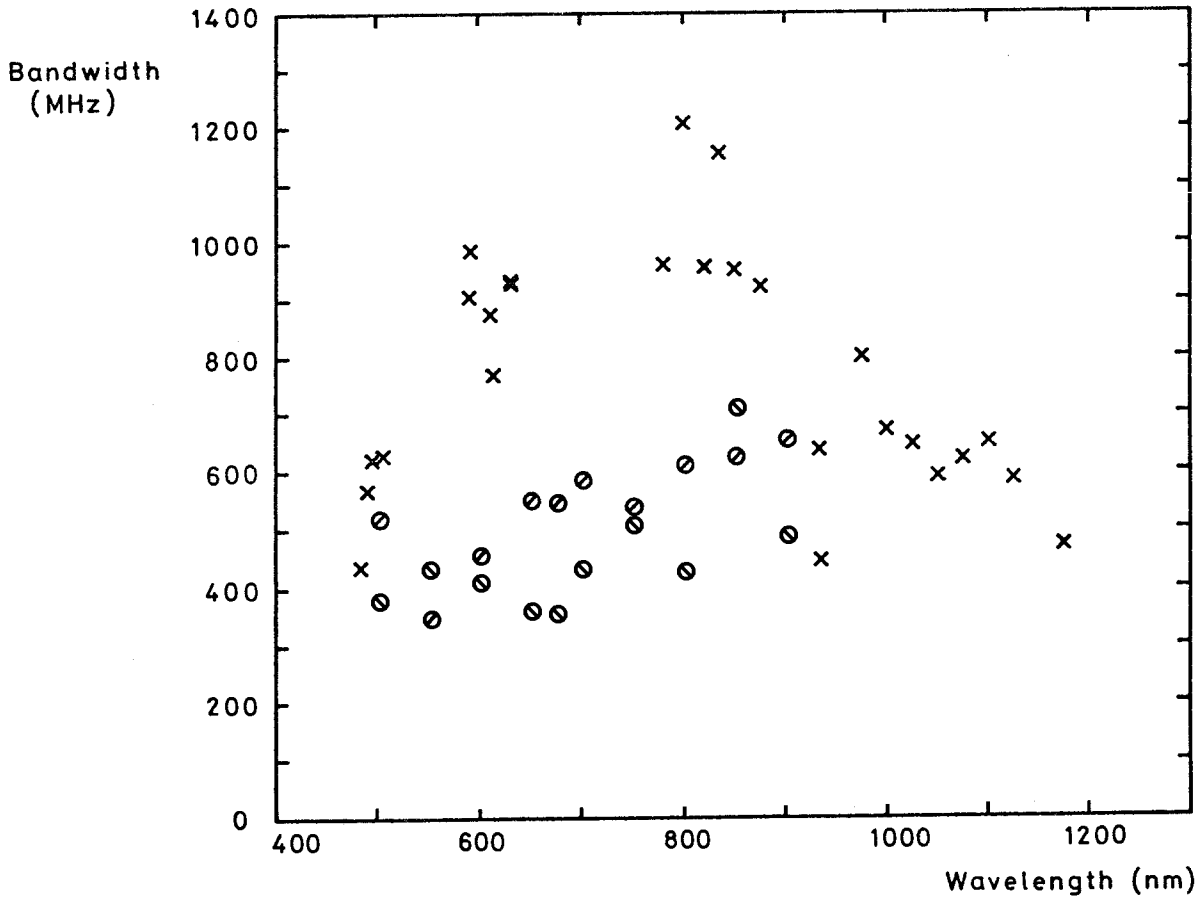

Figure 4.17: Comparison of the measured (X) wavelength-dependence of bandwidth of fibre PO 181 with the predicted from near-field scans recorded along orthogonal diameters (Ø and Ø) at various wavelengths.

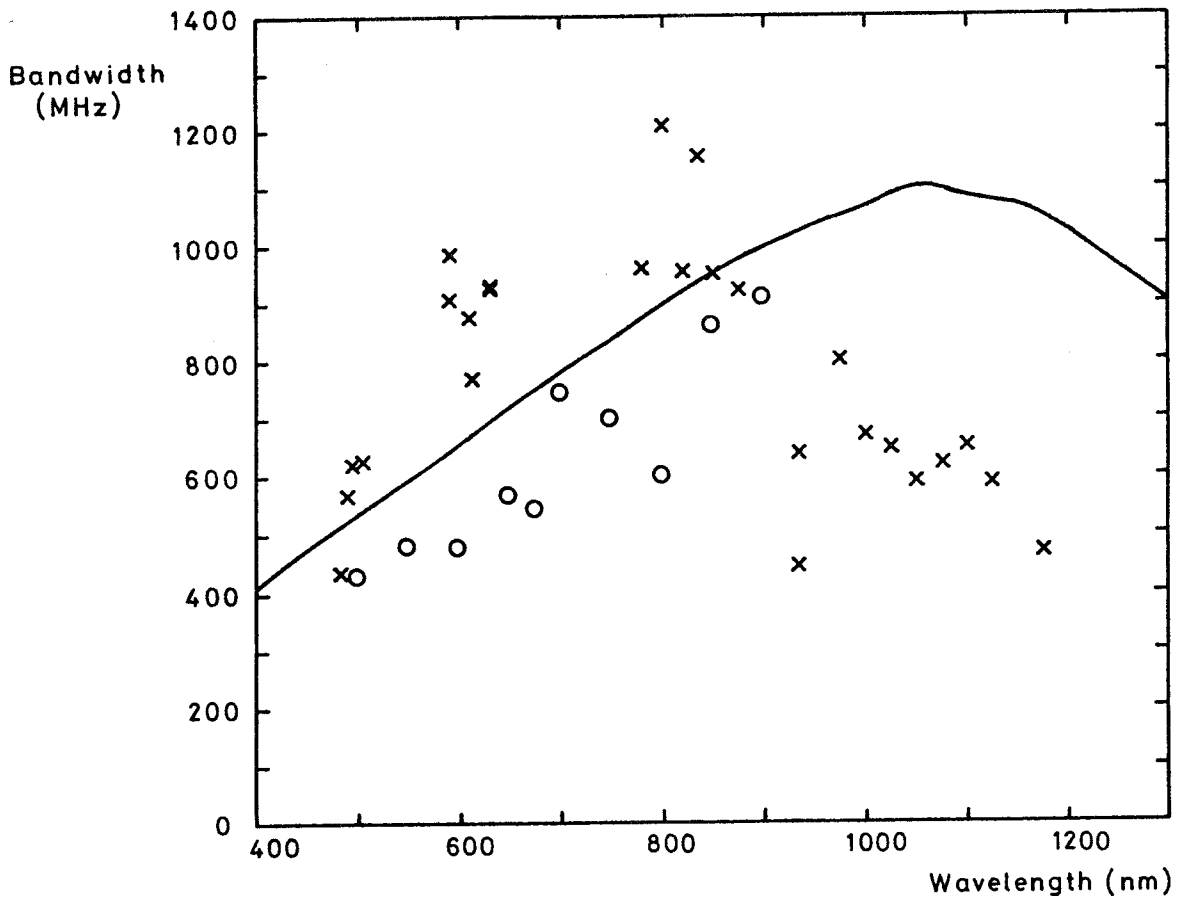

Figure 4.18: Comparison of the measured (X) wavelength-dependence of bandwidth of fibre PO 181 with that predicted from measured refractive index profiles averaged over two orthogonal directions of scan (O) at each wavelength.

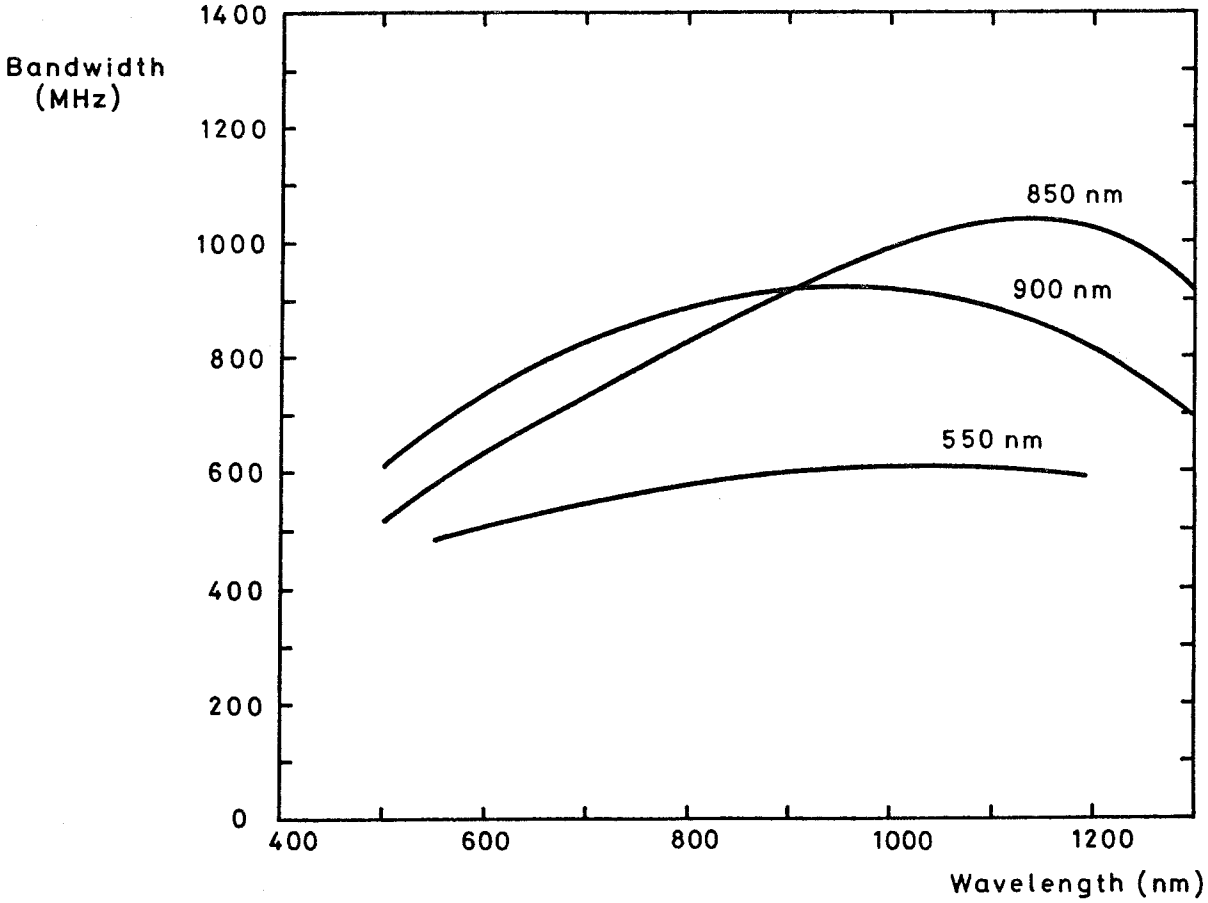

Figure 4.19: Wavelength-dependence of bandwidth predicted from refractive-index profiles measured in fibre PO 181 at three wavelengths and averaged over two directions of scan.

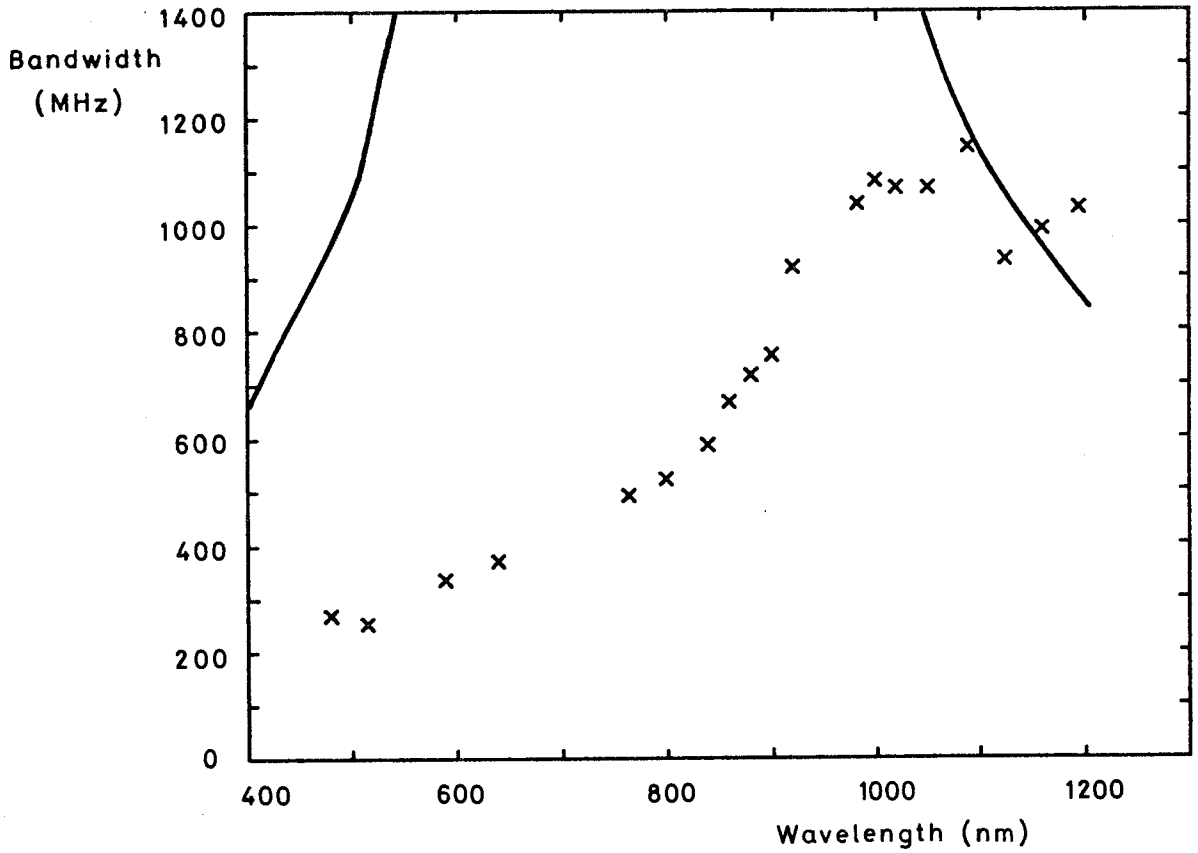

Figure 4.20: Wavelength-dependence of bandwidth in fibre PO 182. Crosses indicate experimentally-determined values. The solid line is for a power-law profile with $\alpha = 1.96$.

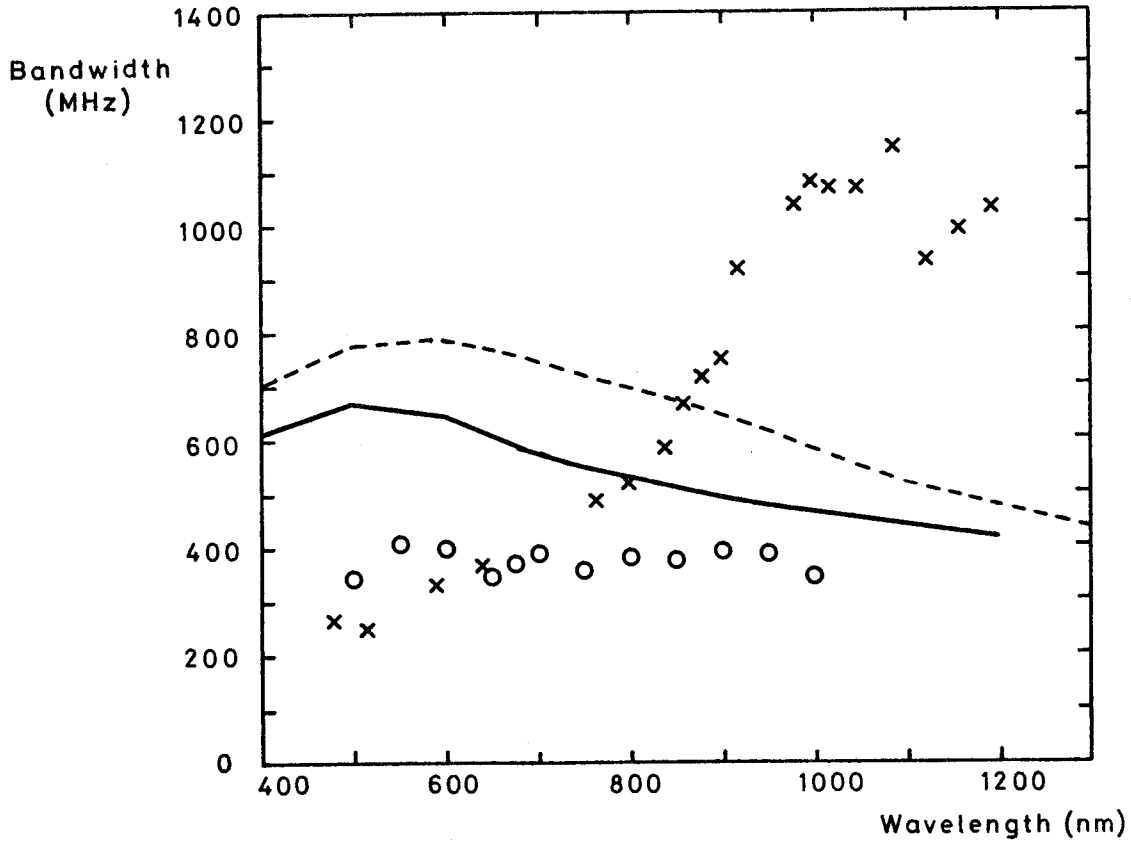

Figure 4.21: Wavelength-dependence of bandwidth in fibre PO 182. Crosses represent experimentally-determined values, whereas circles (O) show values predicted from the index profile (averaged over orthogonal directions of scan) obtained at various wavelengths. The solid curve is predicted using all available profile data; the broken curve is calculated using all available profile data and excluding rays having outer turning points beyond r/a = 0.8.

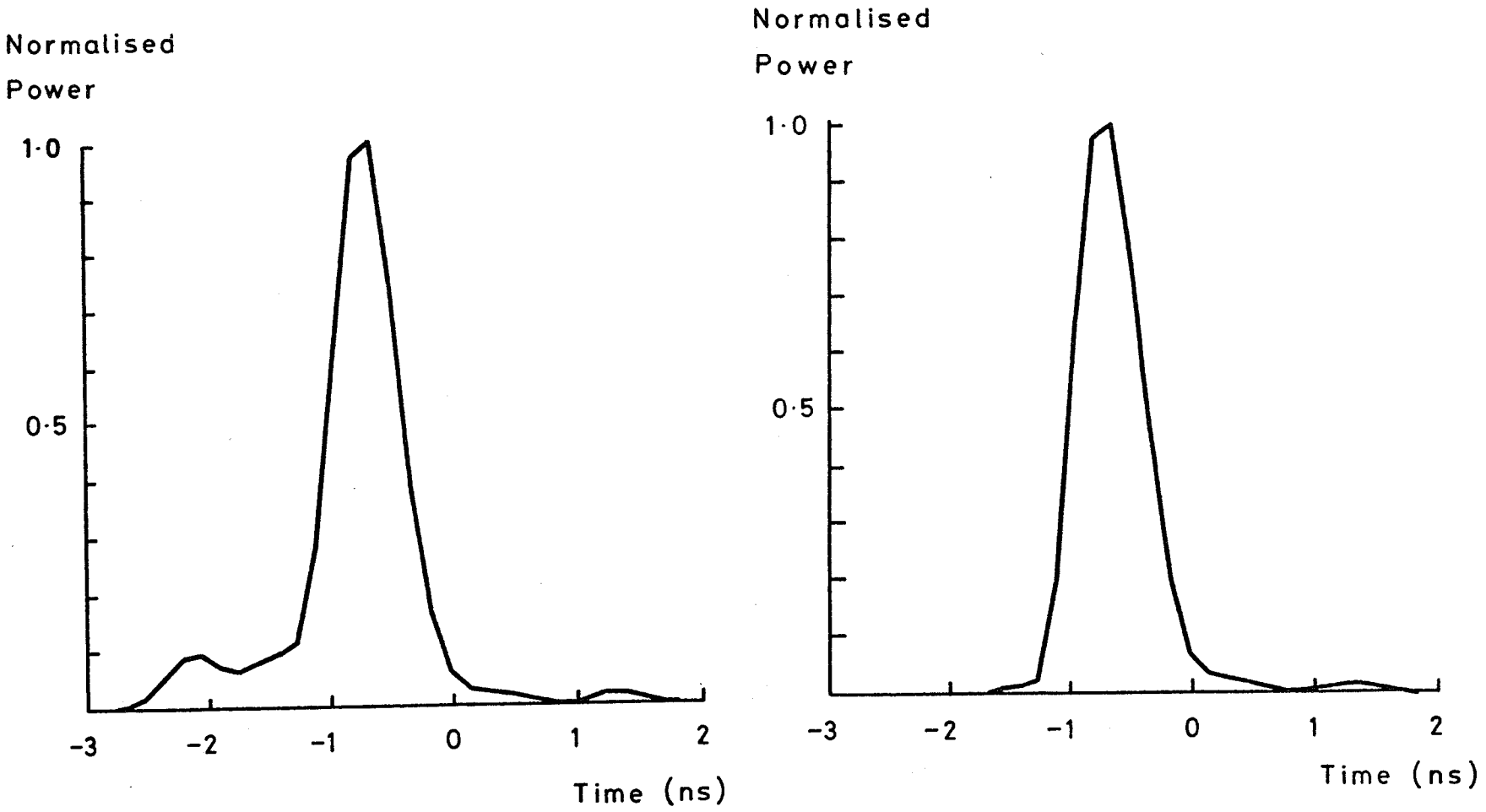

Figure 4.22: Impulse response predicted by ray-tracing for fibre PO 182 at a wavelength of 400 nm

(a) using all rays

(b) excluding rays having outer turning points beyond r/a = 0.8. The time origin is the arrival of the axial ray.

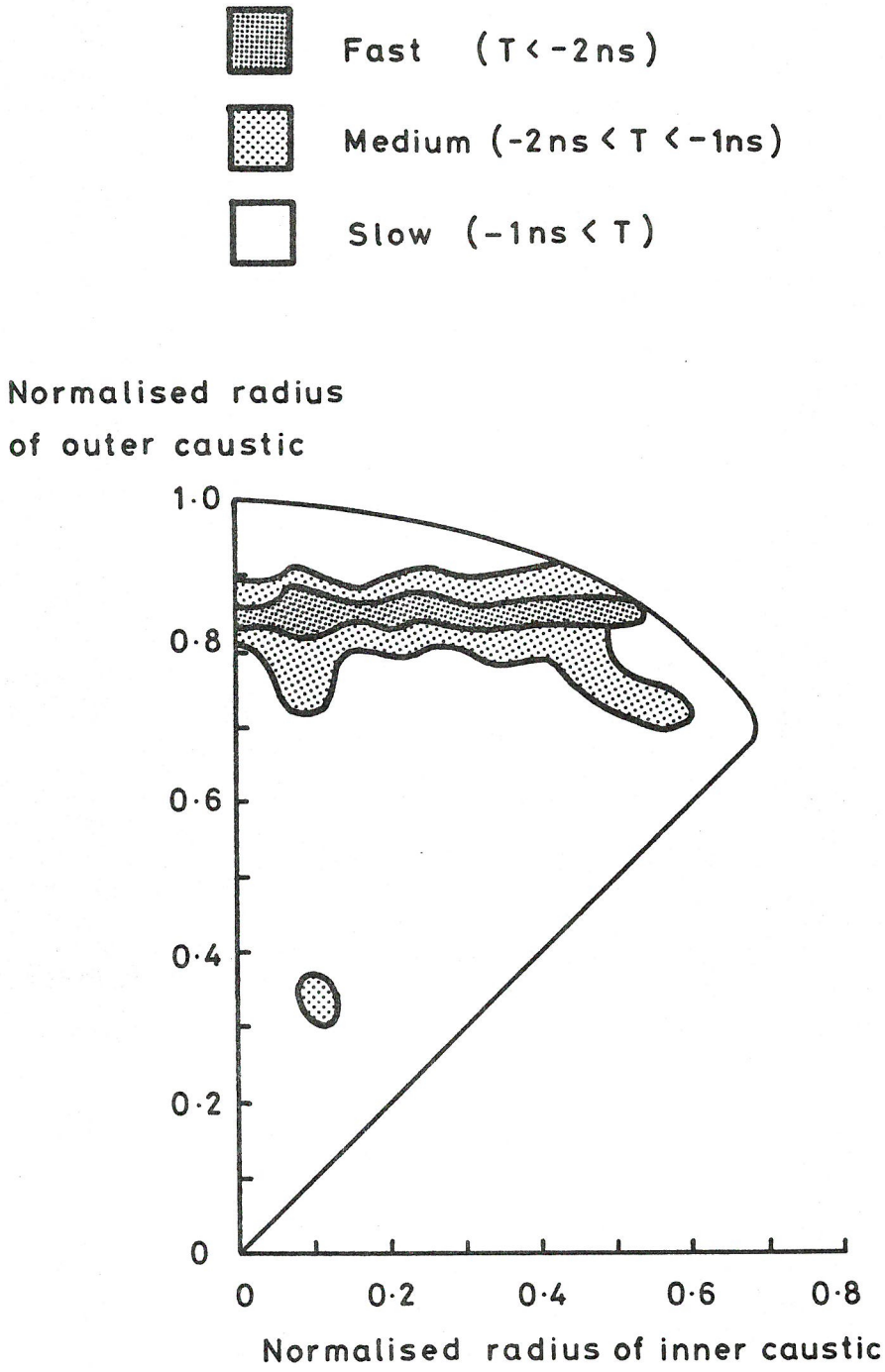

Figure 4.23: Distribution of the relative transit times of the rays in fibre PO 182 at 400 nm according to the position of their caustics.

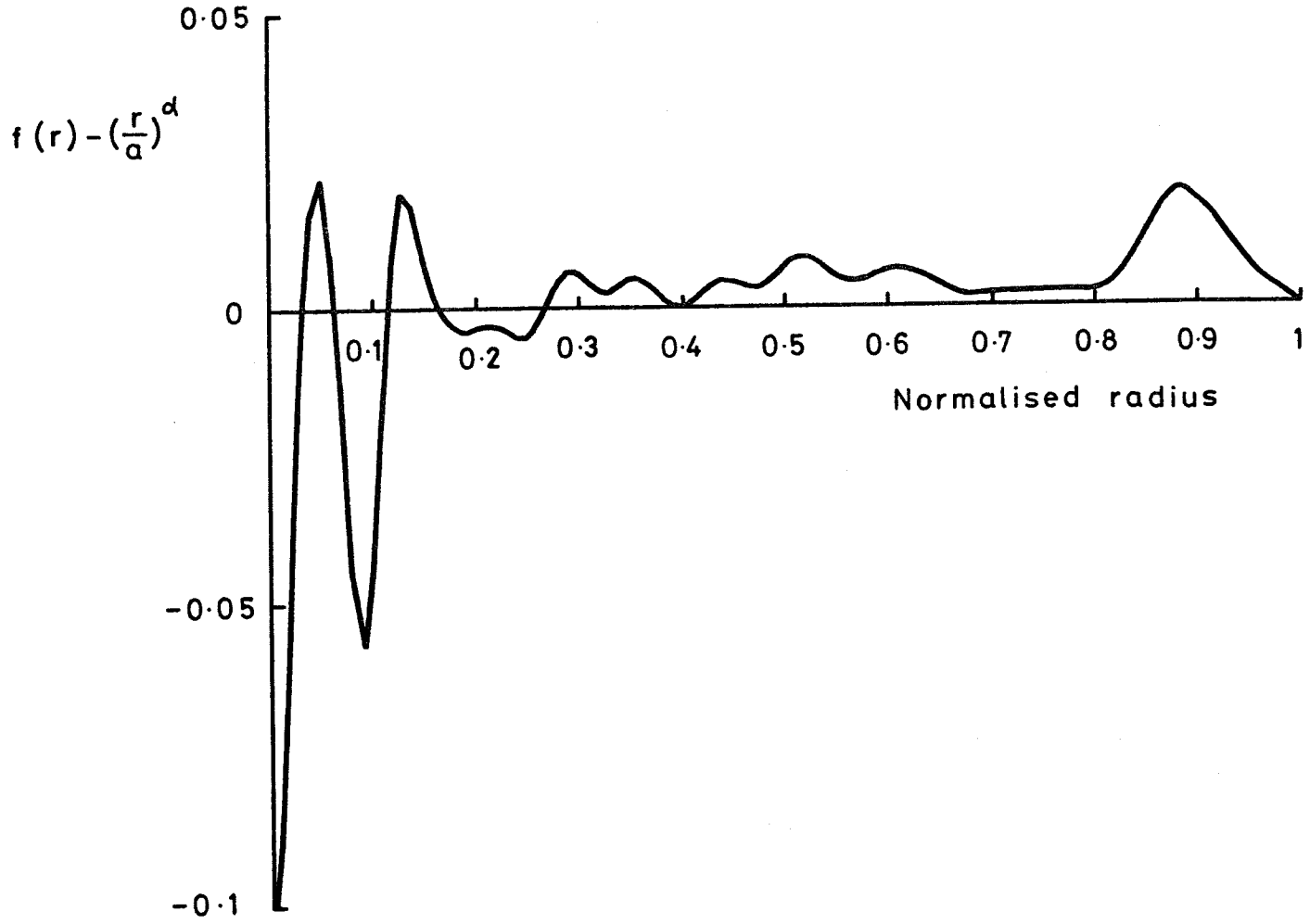

Figure 4.24: Deviation of the average profile of fibre PO 182 from the power-law having $\alpha = 1.96$.

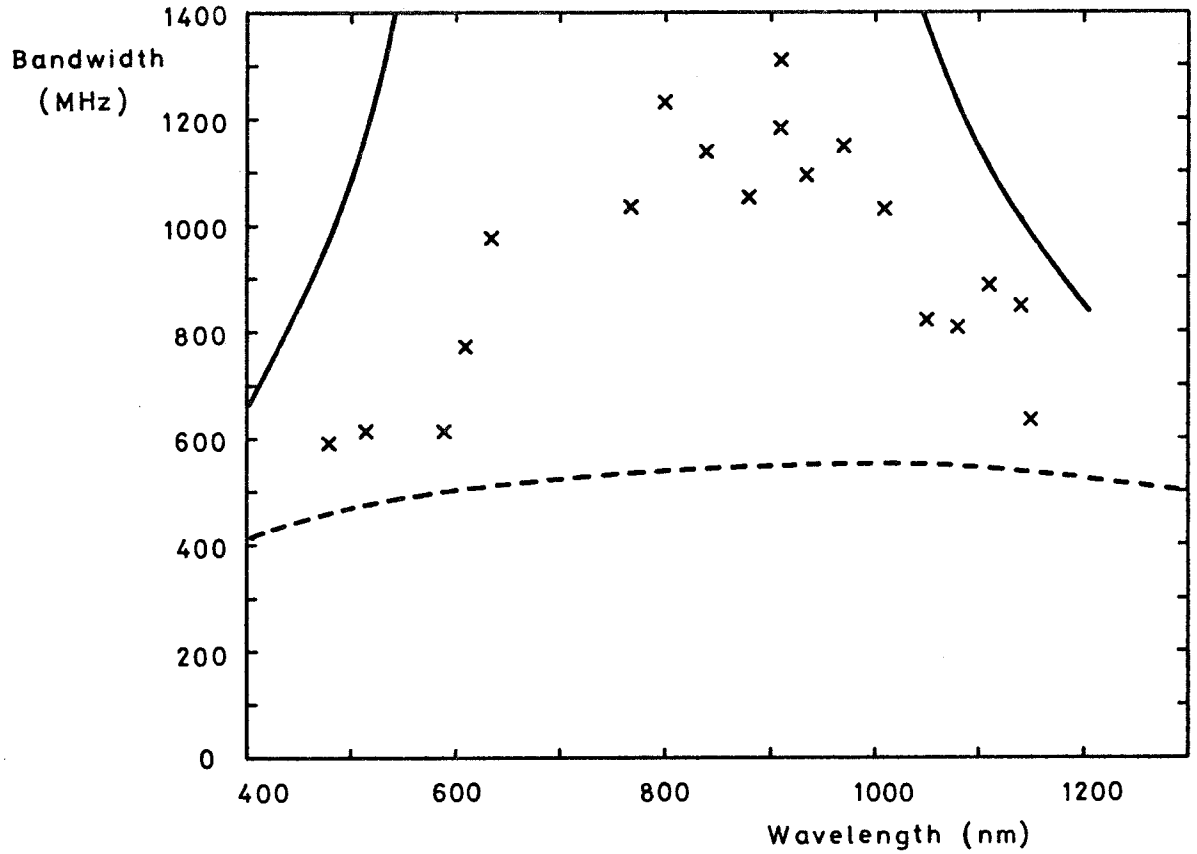

Figure 4.25: Comparison of measured and predicted bandwidth for fibre PO 180.

Crosses: experimentally-determined values.

Solid lines: prediction for the power-law profile having $\alpha = 1.96$.

Broken line: prediction based on the profile data measured at one end and averaged over the wavelength-range 500-1000 nm.

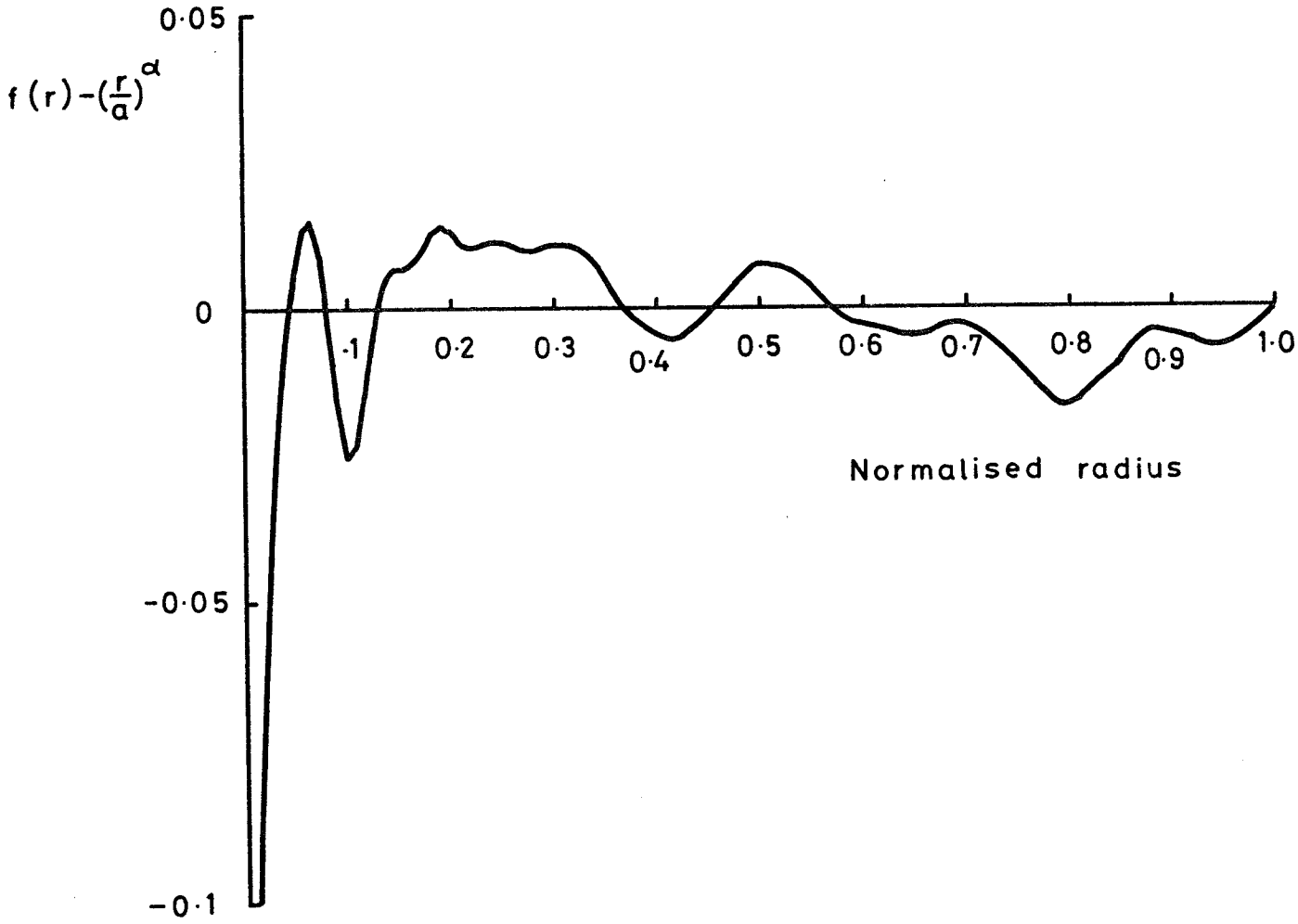

Figure 4.26: Deviation of the average profile of fibre PO 180 from the power-law having $\alpha = 1.96$.

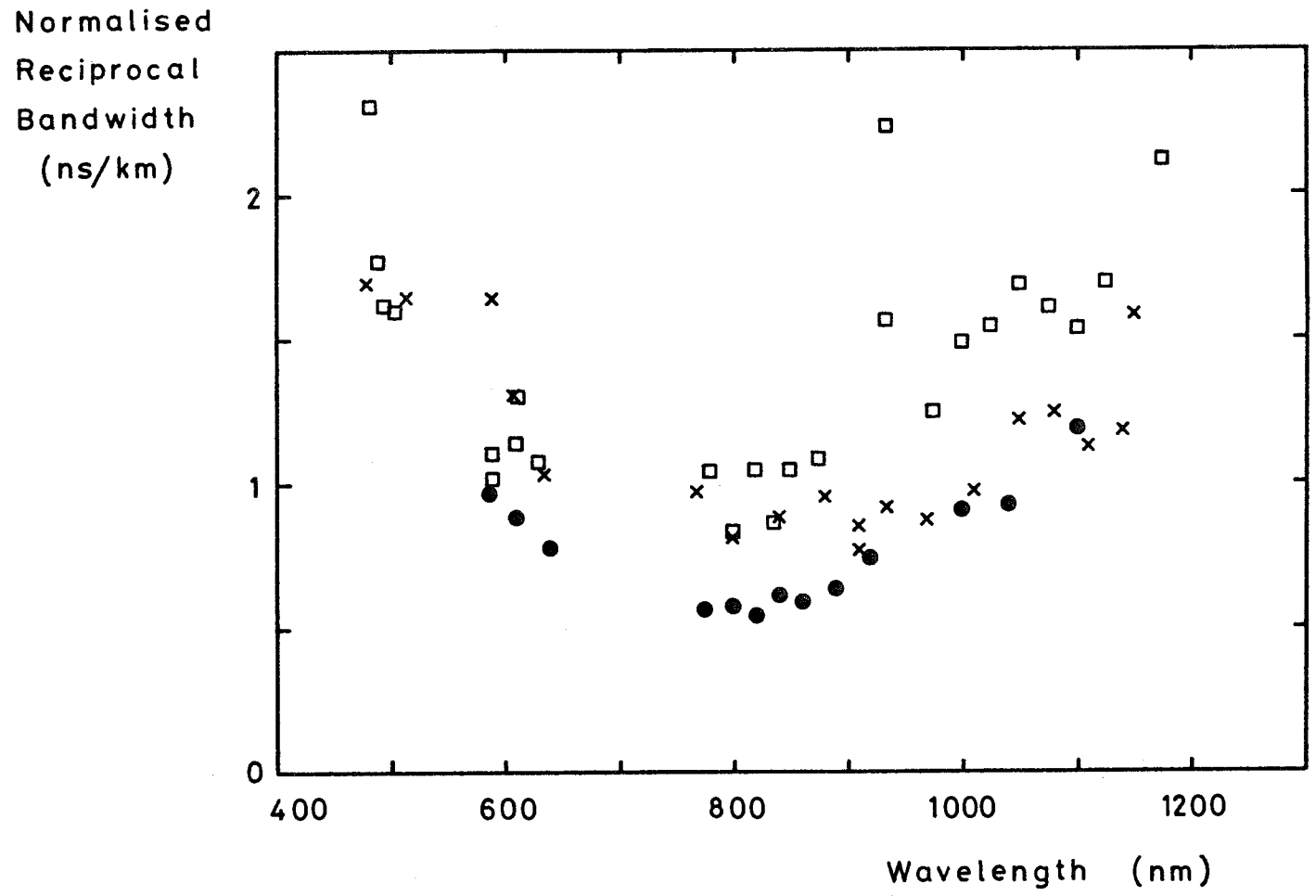

Figure 4.27: Reciprocal of the bandwidth X distance product measured in fibres PO 180 (×) and PO 181 (□), and in the two fibres jointed together (●).

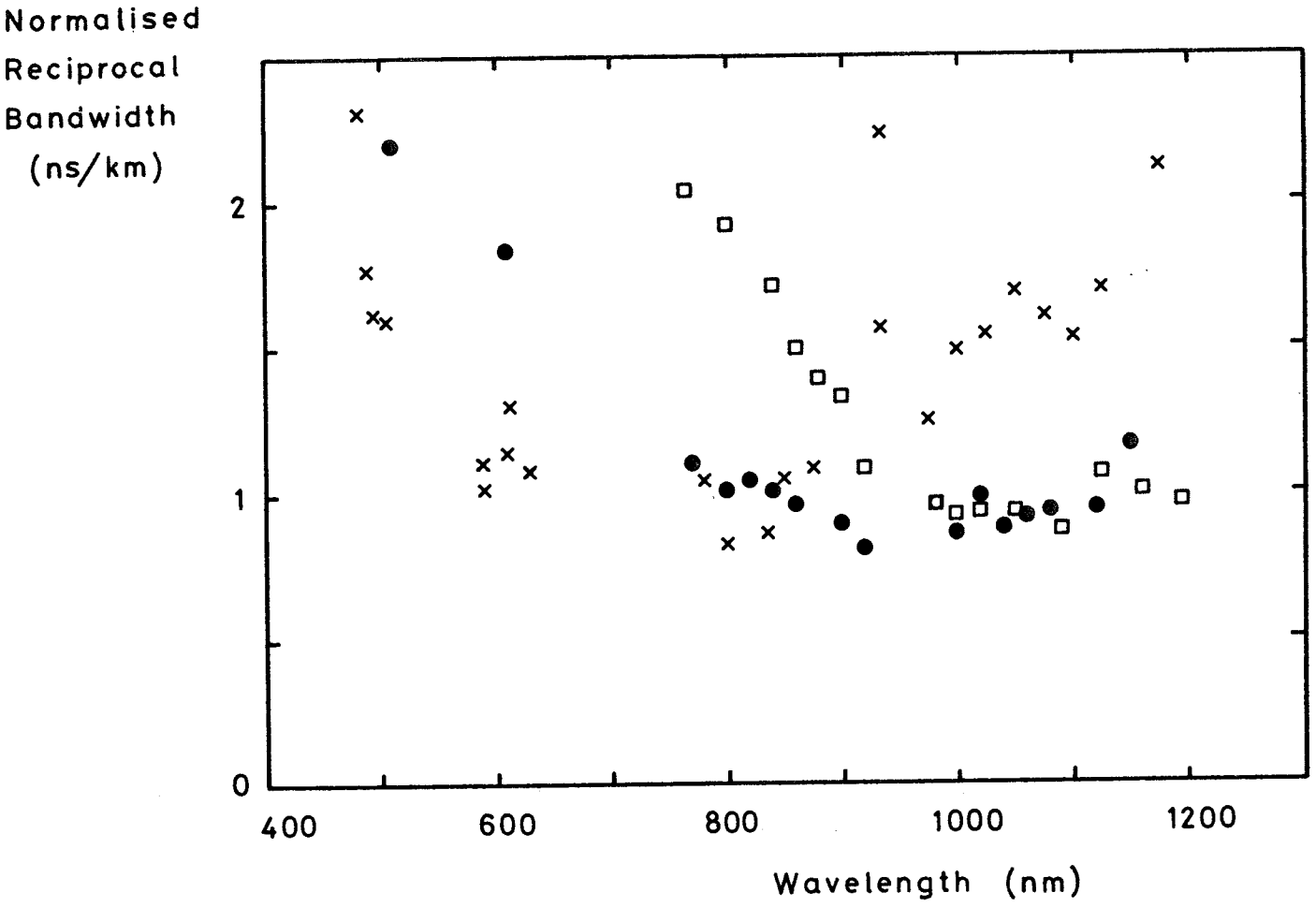

Figure 4.28: Reciprocal of the bandwidth X distance product measured in fibres PO 181 (×) and PO 182 (□), and in the two fibres jointed together (●).

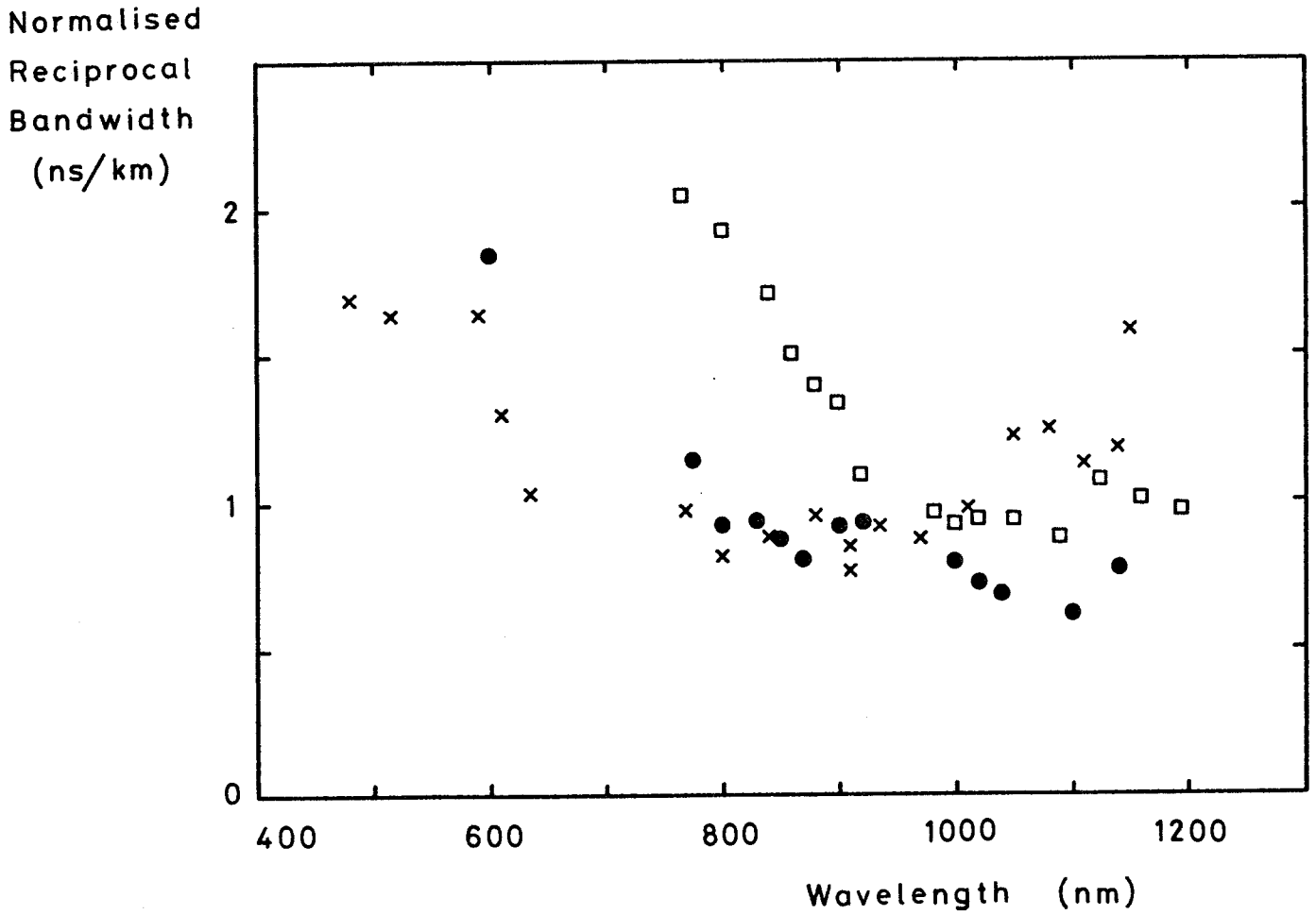

Figure 4.29: Reciprocal of the bandwidth X distance product measured in fibres PO 180 (×) and PO 182 (□), and in the two fibres jointed together (●).

CHAPTER 5 - THE INFLUENCE OF STRESS AND TEMPERATURE ON THE PULSE TRANSIT-TIME IN OPTICAL FIBRES

5.1 INTRODUCTION

In the course of the measurements of pulse delay as a function of wavelength (see Chapter 3), substantial long-term variations in the results were observed. The variations still occurred after the major sources of drift in the instrumentation had been eliminated. The next logical step was, therefore, to investigate the drift in delay which originates in the fibre itself. This study, which was carried out with Mr. A.J. Conduit, is described in the present chapter.

The long-term stability of the pulse transit-time is not normally important in optical fibre communications. When remote events must be precisely synchronised, however, or when the clock for several digital channels is carried over a separate fibre[1], it is necessary to consider carefully the delay stability of the waveguides. In addition, optical fibres are increasingly used as delay-lines for signal processing applications[2] such as transversal filtering. Fibres are very attractive for this type of application since large delay x bandwidth products (as large as 5000 for presently available multimode fibres and at least 5×10^5 for monomode fibres) and very low losses are attainable. It is desirable in these applications, that the delay should be extremely stable. A similar requirement exists when fibres are used in sensors[3], such as strain gauges.

In the present study, the stability of the pulse transit time is assessed for variations of temperature and axially-applied stress. The results should provide useful data for the design of optical delay lines. Both unjacketed and plastic-clad fibres have been tested and it is shown that the application of a secondary nylon coating considerably degrades the delay stability. In addition the dependence of pulse delay on tension suggests the use of this type of measurement as a diagnostic test for residual stress levels

in optical cables[4]. The latter measurement is of some importance to cable designers since, ideally, the fibre should be neutrally stressed in order to avoid static fatigue and microbending effects. As an example of the proposed technique, a determination of the residual compressive stress level in the fibre from pulse-delay measurements following the application of a Nylon 6 overjacket, is described in the present chapter. In addition the effect of various environments (air, water, salt solutions and so on) is examined.

5.2 THEORY

As discussed in Chapter 3, the pulse transit time τ in a multimode fibre of length L may be found approximately from

$$\tau = \frac{L}{c} N_1$$

where c is the speed of light in vaccuo and N_1 is the group index of the core material. Changes in longitudinally-applied stress σ and temperature T alter both the fibre length and the refractive index, each of which affect the transit time. The variation of pulse delay with temperature is given by

$$\frac{d\tau}{dT} = \frac{1}{c}\left(N_1 \frac{dL}{dT} + L \frac{dN_1}{dT}\right) \qquad (5.1)$$

and the variation with stress by:

$$\frac{d\tau}{d\sigma} = \frac{1}{c}\left(N_1 \frac{dL}{d\sigma} + L \frac{dN_1}{d\sigma}\right) \qquad (5.2)$$

Values for the thermal expansion coefficient $\frac{dL}{dT}$ and the temperature coefficient of refractive index $\frac{dn_1}{dT}$ $\left(\simeq \frac{dN_1}{dT}\right)$ are given in Reference 5 for bulk fused silica. The calculated respective contributions of the two terms to the total variation of pulse delay are shown in Table 5.1. It may be seen that the two changes occur in the same sense and that the refractive index variation dominates. Summing the two delays leads to a combined change with temperature of 40ps km^{-1} K^{-1}.

The change in refractive index with applied stress is a result of the stress-optical effect and is discussed in Chapter 3 (section 3.5.3). In addition, fibre tension produces an elongation which may be found from Young's modulus $E = L\, d\sigma/dL$. Table 5.1 gives estimates of the time-delay components resulting from known values of $dn_1/d\sigma$ and $dL/d\sigma$ for silica[6,7] and reveals that the two terms contribute in opposite senses to the overall variation of time delay with applied stress. In contrast with the dependence on temperature, it is now the change in fibre length which primarily controls the change in index, giving an overall effect of 62.2 ps km^{-1} for a stress of 1 MPa.

Departures from the above calculated values are expected in practice due to the presence of graded concentrations of P_2O_5 and GeO_2 in the fibre cores[8] and the chilled state of the fibres. The latter is a result of the rapid cooling experienced during the fibre drawing process.

The application of a close-fitting polymer over-jacket to the fibre modifies the temperature dependence of pulse delay, owing to the large expansion coefficient of plastic materials. Using a simplified elastic model of fibre and coating, which neglects any radial stress component, the following expression for the effect of temperature on a jacketed fibre is arrived at:

$$\left(\frac{d\tau}{dT}\right)_{\text{jacketed}} = \frac{A_P}{A_F} E_P k_P \left(\frac{d\tau}{d\sigma}\right)_F + \left(\frac{d\tau}{dT}\right)_F \qquad (5.3)$$

where A is the cross-sectional area, E the Young's modulus and k the expansion coefficient. The subscripts P and F refer respectively to the plastic over-jacket and the fibre. For a typical fibre of 125 μm diameter having a primary silicone coating of 250 μm diameter and a 500 μm diameter nylon over-jacket, for which $E_p = 3.1 \times 10^9$ Pa, $k_p = 8.3 \times 10^{-5}\ K^{-1}$, the variation of pulse delay with temperature is estimated to be 185 ps $km^{-1}K^{-1}$ (neglecting the contribution of the soft silicone buffer layer and any shearing force which may occur in it). The delay stability is thus expected to be nearly an order of

of magnitude worse than for an unjacketed fibre.

5.3 EXPERIMENTAL PROCEDURE

Optical pulses of 0.35 ns duration from a GaAs injection laser operating at 0.9 μm are launched into the fibre and the pulse transit time measured using a time-delay generator and sampling oscilloscope. In order to improve the timing stability and eliminate errors which may result from long-term variations in the laser turn-on time, a technique has been evolved which uses a marker pulse reflected from the input to the test fibre to provide a time reference. As shown in Fig.5.1, the laser output is focused into a 25 m 'pigtail' of graded-index fibre, to which the test fibre is butt-coupled. The 8% Fresnel reflection which occurs at the joint returns a pulse to the fibre input, from where it is directed to a silicon avalanche photodetector by means of a 50% beam splitter. An aluminium mirror butted against the far end of the test fibre similarly returns a pulse to the APD. The time difference between the two pulses is found by positioning each to the same point on a sampling oscilloscope display using a variable pulse-delay generator. The electrical delay introduced in each case is then accurately determined with a time interval counter. The difference between the readings obtained for the reference pulse and the pulse returned from the remote end of the test fibre gives double the fibre transit time.

The advantage of the above technique is that long-term trigger-delay drifts in the timing circuitry can be eliminated, since they are common to both measurements. Furthermore, the back-reflection technique improves the sensitivity of the experiment, since it doubles the effective length of the fibre. Two further considerable advantages for field measurements are that access to only one end of the fibre is required and that test fibres may be easily interchanged without the necessity for re-alignment of the optics.

The experimental arrangement is similar to that described in

Chapter 3 and shown in Fig.3.8. An advantage which results from the substitution of a GaAs laser for the dye-laser/OPO system is that the equipment then becomes sufficiently small for the experiment to be transported without difficulty. A second major advantage is that the 20 kHz pulse repetition rate of the semiconductor laser allows a sampling oscilloscope to be used (instead of the transient digitiser) and, in this way the time resolution is improved by a factor of $\sim$ 3.

Pulse-delay measurements have been performed on fibres having only a primary coating of silicone rubber and on fibres jacketed with a secondary coating of Nylon 6. The former were made to assess the intrinsic effects of tension and temperature on silica-based fibres (the silicone rubber contributes little to the observed delays) and to compare the results with those calculated previously. The measurements on nylon-jacketed fibres can then be interpreted in the light of the known behaviour of the fibre under stress.

The variation of pulse delay with applied tension in unjacketed fibres was evaluated by suspending the fibre horizontally between two sheaves of eight low-friction pulleys spaced up to 90m apart. Intermediate supports were provided for the fibre strands at intervals of approximately 20 m so as to reduce sag. A calibrated tension could be evenly distributed amongst the fibre sections by applying a known force to one of the pulley blocks and the resulting elongation determined by noting the block displacement. Measurements were made on three graded-index fibres having similar $GeO_2/P_2O_5/SiO_2$ core compositions in effective lengths (2 x actual length) ranging from 0.67 - 1.6 km.

The temperature-dependence of delay was assessed in both unjacketed and jacketed fibres by removing them from the drum and freely suspending the coils in a chamber whose temperature could be controlled over the range $-30^{o}C$ to $+ 100^{o}C$ to within $\pm 0.5^{o}C$. The chamber consisted of a commercial freezer modified by the addition of heating elements, fans and a set of thermocouples. Care was

taken to ensure that no additional stresses were applied to the fibre. The effect of water and salt water on the jacketed fibres over the temperature range 0-50°C was determined by immersing the loose coils of fibres in a temperature-controlled liquid bath. The jacketed fibres were conditioned to their environments (air or liquid) by performing a stabilising soak at ∿ 60°C for period of up to a few days.

5.4 EXPERIMENTAL RESULTS

5.4.1 Effect of Applied Tension on Unjacketed Fibres

Transit-time measurements were made on an unjacketed, silicone-coated fibre, Fibre A, with characteristics given in Table 5.2. The experimental results for the variation of both pulse delay and fibre elongation with applied tension are shown in Fig.5.2. For the diameter, 122.5 μm, of Fibre A, a tension of 1 g-wt corresponds to a stress of about 0.83 MPa and a strain of ∿ 1.16×10^{-5}.

The extension curve exhibits a zero offset which is attributed to the uptake of the sag in the fibre at low values of tension. In contrast, the time-delay curve does not, within experimental uncertainties, show such an effect. The measured tension thus accurately reflects that applied to the fibre.

A straight-line least-squares fit to the data of Fig.5.2 leads to a value of 53.7 ps km^{-1} MPa^{-1} for the variation of time delay with applied tensile stress. This is substantially less than the figure of 62.2 ps km^{-1} MPa^{-1} calculated for fused silica (Table 5.1), even taking into account the 3% uncertainty in the experimental value. The uncertainty results mainly from the determination of the fibre diameter. On the other hand, the least-squares fit to the extension data indicates that the change in length contributes 70.6 ps km^{-1} MPa^{-1} to the variation of pulse delay in good agreement with the value of 68.7 ps km^{-1} MPa^{-1} calculated from the published results for pure silica[7]. Note, however, that the present measurement of elongation is

not as accurate as that of pulse delay, owing to the difficulty of measuring precisely the displacement of the block of pulleys. The major departure from the fused silica values lies in the effect of stress on the refractive index of the glass, where a much larger sensitivity than expected is found (Table 5.1). The stress-optical contribution to pulse delay given in the Table is obtained by substracting two measured values of similar magnitude, both of which are subject to error. A somewhat more precise approach is to compare the slope of the time delay/extension curve, 37.6 ps/cm, to the accurately measured group delay, 49.35 ps/cm. The difference between these values may then be attributed to the slight reduction in index which affects the whole fibre as a result of tensile stress. It is possible, in this way, to evaluate the stress-optical coefficient of pulse delay, which comes to -10.6 ps/km^{-1} MPa^{-1}. The substantial difference between the latter value and that given in Table 5.1 demonstrates that the present experiment is not sufficiently accurate to provide a precise determination of the longitudinal stress-optical effect. Nevertheless, it is clear that the fibre exhibits a much larger stress-optical effect that is predicted from silica data. This is perhaps not surprising in view of the presence of GeO_2 and P_2O_5 in the fibre core and the large differences found in practice between the stress-optical coefficients of glasses having different compositions. Measurements on two other fibres produced similar results, indicating that the discrepancy can be attributed to a material property.

5.4.2 Effect of Temperature on Unjacketed Fibres

Pulse delays were measured as a function of temperature in a 600 m length of silicone-coated fibre, Fibre B, (Table 5.2) produced from the same preform as Fibre A. The results over the temperature range -30 to +100°C are shown in Fig.5.3, normalized to a fibre length of 1 km. The fibre length was determined by measuring the time delay at 20°C and comparing this with the delay measured in an accurately known short length of fibre. The latter gave a value for the group index of 1.4798 ± 0.04%.

The least-squares fit to the data of Fig.5.3 gives a delay variation of 35.7 ps km^{-1} K^{-1}, a value which is somewhat smaller than the calculated figure of 40 ps km^{-1} K^{-1} for pure silica. The experiment repeated in the reverse temperature direction produced a similar result and showed no hysteresis in the measurement.

5.4.3 Residual Fibre Stress Introduced by Jacketing with Nylon

During the cabling process, stresses are unavoidably applied to the optical fibre and some of these may remain in the finished product. For example, the high-temperature extrusion of the secondary coating is expected to result in longitudinal compression of the fibre on cooling, owing to the difference in expansion coefficients between glass and plastic. Although compressive stresses applied to the fibre may possibly result in improved strength characteristics, they may also have detrimental effects such as increased microbending losses.

An experiment was conducted on 600 m of fibre, Fibre C, (Table 5.2) from the same production batch as those used previously, in order to determine the residual stresses within the fibre and thus demonstrate the use of pulse-delay measurements for cable diagnostics. Initially, the silicone-coated fibre was freely suspended in a stress-free state and the pulse transit time determined. A secondary layer of Nylon 6 was then applied by extrusion to give an outer diameter of 0.5 mm. Care was taken to ensure that all fibre pieces broken off during the extrusion process and for the purposes of end preparation were taken into account.

It was found that the transit time after jacketing had decreased by 2.44 ns km^{-1} which from the stress/pulse delay calibration previously performed (Section 5.4.1) indicates a residual compressive stress of 45 MPa (a compressive force of 58g-wt). Such a figure is an order of magnitude less than that estimated from the known[9] expansion coefficient and Young's modulus of nylon, although it should be noted that an exact analysis is complicated by the fact that the

remaining stress is dependent on the extrudate cooling conditions and the time allowed for stress relief by plastic creep. The relatively low level of residual compression found in the fibre indicates that considerable stress relief had taken place in the period immediately following extrusion.

Note that radial stress applied by the coating to the fibre would result in an underestimate of the longitudinal stress. This effect could be important in some cable structures. In the present case, however, it is unlikely to affect the result significantly since the nylon jacket does not grip the primary coating very tightly (as witnessed by the presence of air between the two layers) and since the primary coating buffers the fibre. In addition, the jacketing material is likely to be oriented preferentially parallel to the fibre axis (although the degree of polymer orientation would depend strongly upon the extrusion conditions). In those cases where it is thought that radial, as well as longitudinal, stress is present, it is possible to separate the two effects by measuring the change in fibre length resulting from the application of a coating, as well as the variation of pulse transit time.

5.4.4 Delay Stability in Jacketed Fibres

The temperature stability of pulse delay was investigated in Fibre C, after jacketing with Nylon 6 as described above. After an initial annealing period during which the transit time decreased slightly, the fibre was freely suspended in air and the time delay monitored as the temperature was cycled over the range -30 to + 50°C. Several interesting effects were observed which could be attributed to the known creep behaviour of plastic materials. The thermal history of the fibre/plastic composite and the duration of the experiment were found to influence the time delay measured at any point in the temperature range. For example, static measurements at -30°C following a prolonged period spent at 50°C would result in an upward drift in pulse delay of as much as 4 ns km^{-1}. Conversely, measurements at 50°C after stabilization at - 30°C produced a downward

drift of similar magnitude. Furthermore, the delay was observed to exhibit hysteresis.

This behaviour is illustrated in Fig.5.4. The curves show the results of an experiment in which the temperature was continuously cycled at a rate of approximately 10^{o} C/hour. One and three-quarter cycles were performed under these conditions (solid lines, curves 1-4) and are seen to produce almost coincident time-delay hysteresis loops. Curve 5 (dashed), on the other hand, shows a measurement taken in the direction of increasing temperature after the above temperature cycles had been interrupted at - 30^{o} C for 12 hours. The static period has resulted in an upward drift in pulse delay of 1 ns which, on resumption of temperature cycling, leads to a curve lying above those previously determined, although tending towards them at higher temperatures. Similarly, curve 6 (dashed) shows the effect of a 12 hour pause at 50^{o} C, which produced a 0.5 ns drop in delay. The difference is gradually eliminated as the temperature is cycled.

The departure of the delay curves in Fig.5.4 from the simple straight-line characteristic exhibited by the unjacketed fibre (Fig. 5.3) is the result of the mechanical properties of the secondary coating and the forces it exerts on the fibre. Plastics by their very nature do not exhibit simple elastic and thermal behaviour[10-12]; unlike silica, they are non-Hookean and such quantities as Young's modulus and thermal expansion coefficient are dependent on the magnitude of the applied load, the time scale and the temperature of the experiment. Furthermore, the thermal history, water content and degree of crystallinity of the plastic affect their properties.

Clearly, the hysteresis and time-dependent behaviour of the pulse delay shown in Fig.5.4 are a result of stress relief in the fibre caused by plastic creep of the nylon over-jacket. The reason, however, for the marked change in slope at approximately 30^{o} C is not at present understood, although we note that both the expansion coefficient and tensile modulus of nylon vary non-linearly with

temperature. As a consequence of the effect, the temperature coefficient of time delay is no longer uniquely defined, being both time dependent and temperature dependent. Nevertheless, averaging the slopes of curves 1 and 2 below 10^{o} C leads to a working figure of 170 ps km^{-1} K^{-1}. This is in good agreement with the value of 185 ps km^{-1} K^{-1} calculated previously.

The temperature stability of time delay in the jacketed fibre, Fibre C, should be compared with that of the primary-coated fibre, Fibre B, for which a value of 35.7 ps km^{-1} K^{-1} was found. The application of the protective jacket degrades the stability by nearly a factor of five. Furthermore, it should be recognised that the incorporation of the jacketed fibre into a larger cable structure having the same high expansion coefficient will produce a still greater variation.

5.4.5 Effect of Water Ingress on Jacketed Fibres

The influence of moisture ingress on the performance of jacketed fibres was assessed by immersing Fibre C, loosely coiled, in a water bath. Experiments were also conducted whilst the fibre was immersed in a 20 wt% aqueous NaCl solution. Sufficient time was allowed for the fibre to reach equilibrium (72 hours and 36 hours at 50^{o}C for water and NaCl solutions, respectively [9]). The pulse-delay performance for temperature cycles over the range 0-50^{o} C is given in Fig. 5.5. Also shown are the results previously presented (Fig.5.4) for the same fibre, Fibre C, suspended in air and, to aid comparison, for the unjacketed fibre, Fibre B (Fig.5.3). The results are all normalized to a length of 1 km. This was achieved as outlined in Section 5.4.2 by precisely determining the time delay in the unjacketed fibres and comparison with the delay in a known short length of the same fibre. The length of Fibre C was known from the results obtained prior to extrusion of the plastic jacket. However, confimation of the measurement was obtained by removal of the jacket in concentrated nitric acid on completion of the temperature experiments. This also served to verify the effect found in Section 5.4.3,namely that the time delay decreased after jacketing. It was ascertained that removal of the jacket now produced an increase in pulse delay and that the final value was in close agreement with that found prior

to extrusion of the nylon.

The curves of Fig.5.5 show that both water and salt solutions produce a marked increase in time delay, suggesting that a release residual compressive fibre stress has occurred. Hysteresis behaviour is observed and curve gradients are closer to that of the unjacketed fibre, indicating that the liquids have caused a softening of the jacketing plastic, i.e. reduced its modulus. In addition, the curve for water immersion lies above that of the unjacketed fibre indicating that the fibre is in fact in tension. This may be seen more clearly by noting that at any temperature the time-delay difference between the jacketed fibre and the unjacketed one is an indication of the stress that the sheath is applying to the fibre. With the aid of the calibration figure for the dependence of time delay with stress for these fibres, we may map Fig.5.5 into the residual stress versus temperature curves shown in Fig. 5.6, where the negative sign indicates fibre compression.

Fig.5.6 reveals that at room temperature the residual compressive longitudinal force exerted on the fibre by dry nylon (after conditioning) is in the region of 100 g-wt. The ingress of water into the plastic has relieved the initial compression which existed after extrusion and in fact has caused the fibre to become tensioned. This effect is consistent with the known[9] volume expansion and reduction of Young's modulus which accompanies water saturation (9.5 wt%) of Nylon 6.

The subsequent immersion in a salt solution caused the fibre to return to compression, although not to the level observed in air. This was accompanied by a significant increase in attenuation (6 dB km^{-1}) with little change in pulse dispersion, an effect which was not observed in water. Furthermore, on removal from the salt solution and drying, the attenuation became so high as render further measurements impossible. This was found even if the fibre was rinsed in de-ionized water for two days prior to drying; however, re-immersion in water restored the transmission. Similar behaviour was found in

aqueous $CaCl_2$ solutions. Clearly the effect is attributable to an increase in microbending loss in the fibre caused by a change in the nylon characteristics. The mechanism whereby such kinking can occur as a result of increased radial pressure exerted by the plastic, but with little change in stress in the axial direction is not at present clear.

Although the levels of salt concentration used in these experiments are high, the effects observed are indicative of the performance of Nylon 6 as a jacketing material in hostile environments. A more appropriate choice in these cases would be polypropylene, which exhibits a low level of hygroscopy and high resistance to chemical attack.

Experiments performed on nylon-jacketed fibres immersed in organic solvents such as fomaldehyde and glycol-methanol (1:1) similarly produced changes in the fibre stress levels, although their effect on pulse dispersion and attenuation have not been measured.

5.5 SUMMARY

Measurements of the stability of the optical pulse delay in both unjacketed and jacketed fibres have been presented. In the case of unsheathed fibres, an evaluation of the dependence of delay on fibre tensile stress and temperature reveals that the effects are linear, having values of 53.7 ps km^{-1} MPa^{-1} and 35.7 ps km^{-1} K^{-1}, respectively. Calculation of the expected values for bulk fused silica indicates that the variation with stress is dominated by the physical change in fibre length and that with temperature by the change in refractive index. Comparison of the silica values with those determined experimentally demonstrates significant departures for P_2O_5/GeO_2 -doped fibres, particularly for the stress-induced index change.

For fibres jacketed with nylon, it was observed that the

presence of the sheath produced much larger and non-linear excursions of time delay with temperature. The departure of the performance of the jacketed fibre from that of the unclad fibre has been used to evaluate the effect of the sheath on residual fibre stress levels. The physical properties of the plastic jacketing material have been shown to induce time-delay drift and hysteresis following temperature variations. In addition, the ingress of water modifies the plastic properties and causes significant delay variations. Furthermore, immersion in salt and $CaCl_2$ solutions irreversibly impairs optical transmission, indicating that nylon is unsuitable for use as a cladding material in hostile environments.

We thus see that the temperature stability of the transit time can be severely degraded by encapsulation of the fibre in plastic materials having a high expansion coefficient. This is a consequence of the sensitivity of the delay to applied longitudinal stress. Thus plastic-jacketed fibres or epoxy-potted coils should not be used in applications which require high time stability, for example in fibre delay lines and strain gauges.

On the other hand the stress dependence of delay can be used to provide a powerful diagnostic tool for cable stress analysis. This was demonstrated by an experiment to determine the fibre compression induced by application of a nylon jacket, where a residual compressive force of 58 g-wt was found. Application of the method to determine residual stresses after each stage of cable manufacture is possible; for example, after stranding, sheathing and armouring. In addition, it is envisaged that periodic tests on installed cables could be used to provide information on long-term cable creep effects.

5.6 REFERENCES

1 E.F. ANDERSEN: 'Temperature effects on dispersion and propagation delay in multifibre cables'. Proceedings of the Sixth European Conference on Optical Communication, York, 1980, pp.169-172.

2 C.T. CHANG, J.A. CASSABOOM and H.F. TAYLOR: 'Fibre-optic delay line devices for R.F. signal processing'. *Electron. Lett.*, 1978, *14* (5), pp.130-132.

3 M. JOHNSON and R. ULRICH: 'Fibre-optical strain gauge'. *Electron. Lett.* 1978, *14* (14), pp. 432-433.

4 A.J. CONDUIT, A.H. HARTOG and D.N. PAYNE: 'Residual stress diagnosis in jacketed optical fibres by a pulse delay technique'. Proceeding of the Fifth European Conference on Optical Communication, Amstersdam 1979, pp.8.2.1 - 8.2.4.

5 'American Institute of Physics Handbook'. (McGraw-Hill, New York, 1972), p. 4-138.

6 W. PRIMAK and D. POST: 'Photoelastic constants of vitreous silica and its elastic coefficient of refractive index'. *J. Appl. Phys.* 1959, *30* (5), pp.779-788.

7 R. BRUCKNER: 'Properties and structure of vitreous silica. Part I'. *J. Non Crystalline Solids* 1970, *5*, pp.123-175.

8 G.W. MOREY: 'Properties of glass'. Rheinhold Publishing Corporation, New York, 1938.

9 S. GROSS (Editor): 'Modern Plastics Encyclopedia', McGraw-Hill, New York, 1969.

10 L.E. NIELSEN: 'Mechanical properties of polymers'. Reinhold Publishing Co., New York, 1962.

11 R.M. OGORKIEWICZ: 'Engineering properties of thermoplastics' J. Wiley and Sons Ltd., New York, 1970.

12 N.G. MCCRUM, B.E. READ and G. WILLIAMS: 'Anelastic and dielectric effects in polymeric solids'. J. Wiley and Sons Ltd., New York, 1967.

Component	With temperature (ps km^{-1} K^{-1}	With longitudinal stress (ps km^{-1} MPa^{-1})
effect on delay due to variation of index N_1	38	-6.5(-16.9)
effect on delay due to variation of length L	2	68.7(70.6)
Combined calculated effect on delay	40(35.7)	62.2(53.7)

Table 5.1 Calculated components of the temperature and stress dependence of time delay in bulk fused silica. The bracketed figures refer to the experimentally-determined values for unjacketed silica fibres doped with P_2O_5/GeO_2.

	Fibre A	Fibre B	Fibre C
Approx. length, m	800	600	600
Numerical aperture	0.21	0.21	0.21
Core diameter, μm	65	65	65
Fibre diameter, μm	122.5	122.5	125
Silicone coating diameter, μm	250	250	250
Nylon 6 diameter, μm	un-jacketed	un-jacketed	500

Table 5.2 Properties of fibres used in pulse-delay measurements. All fibres have $P_2O_5/GeO_2/SiO_2$ cores and a B_2O_3/SiO_2 buffer layer.

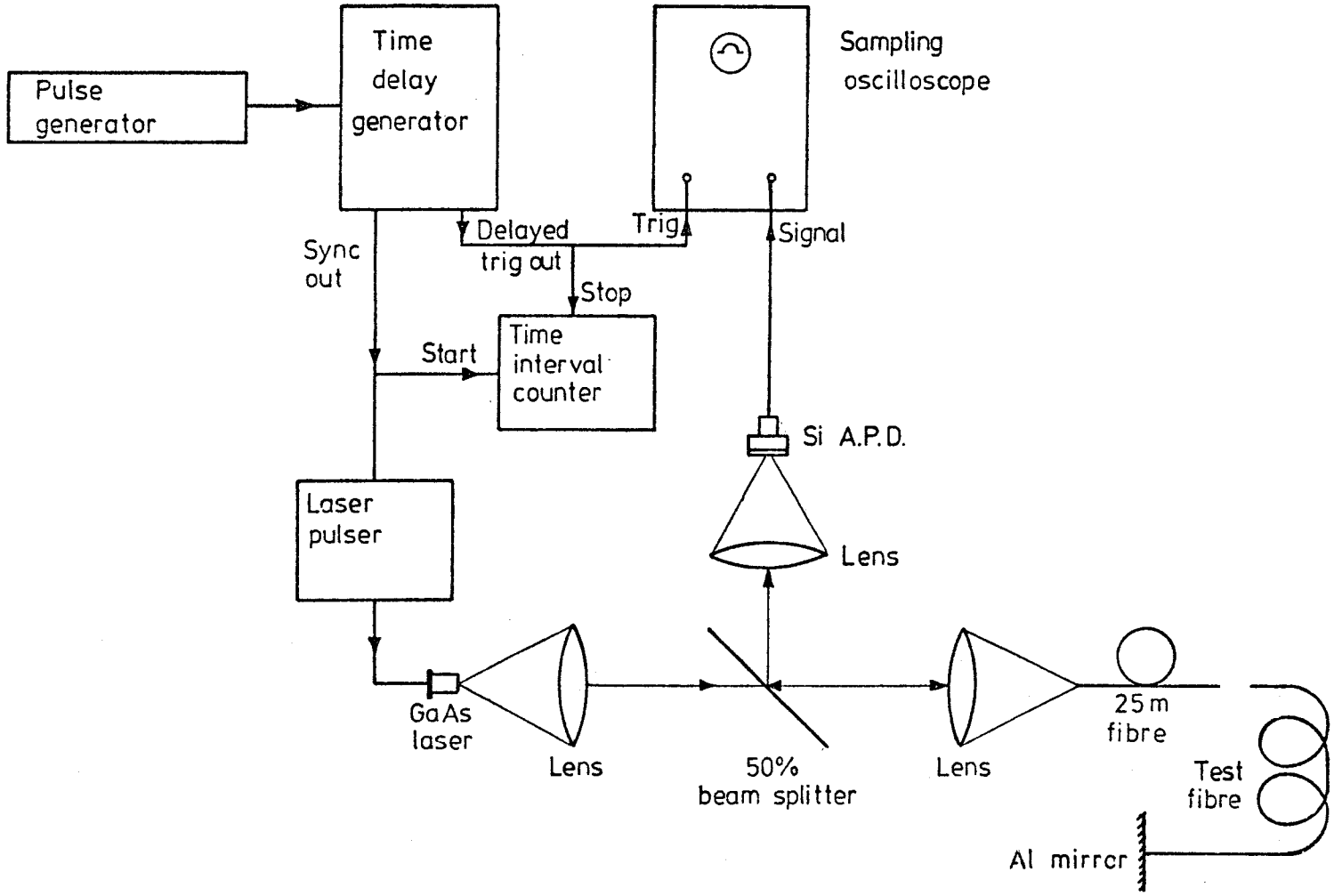

Figure 5.1 : Schematic diagram of optical pulse-delay measurement experiment.

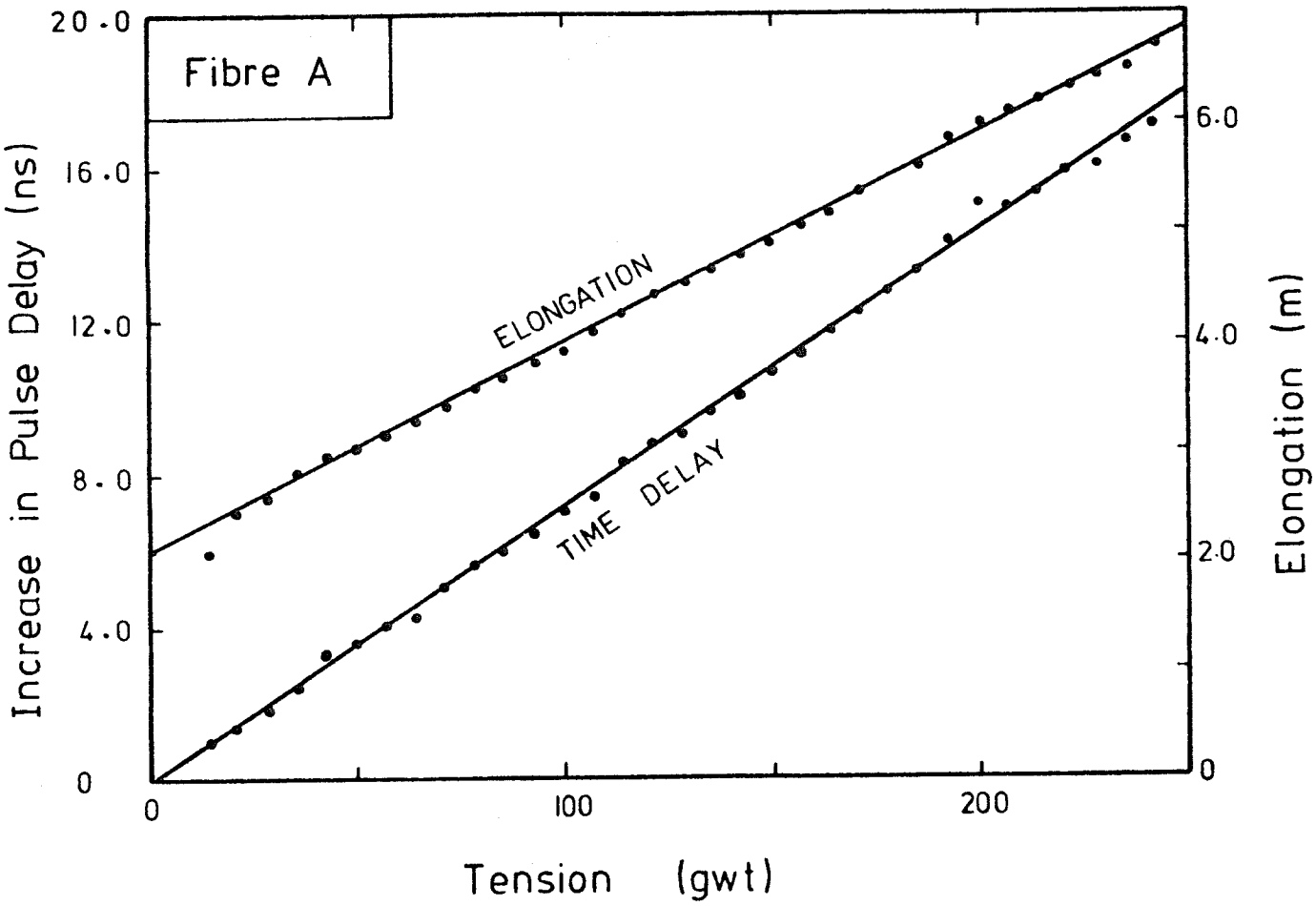

Figure 5.2 : Variation of pulse-delay and fibre extension with applied tension for Fibre A (Table 5.2). The fibre is unjacketed and has an effective length of 1.6km.

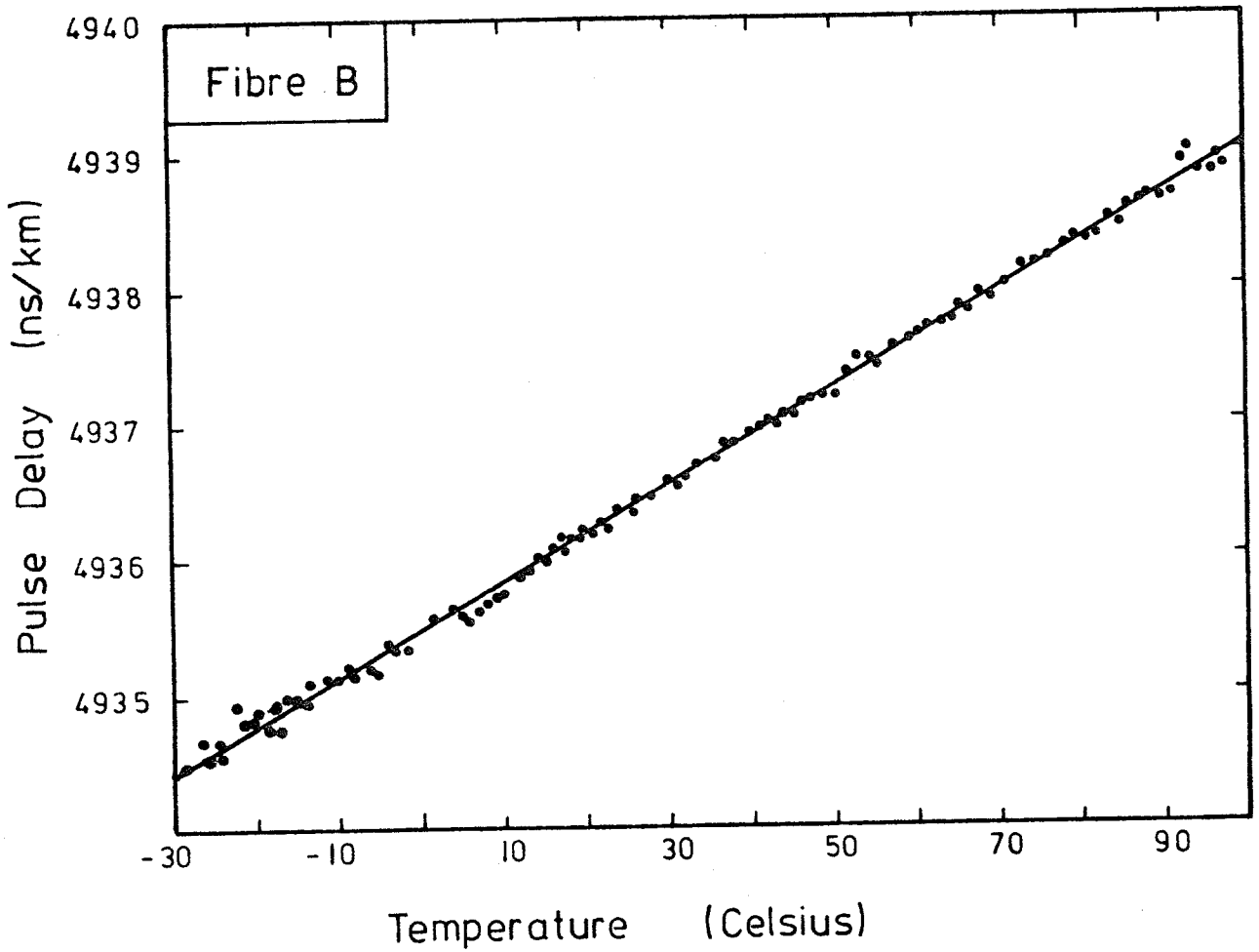

Figure 5.3 : Pulse-delay normalized to a length of 1km as a function of temperature for an unjacketed fibre, Fibre B. (Table 5.2)

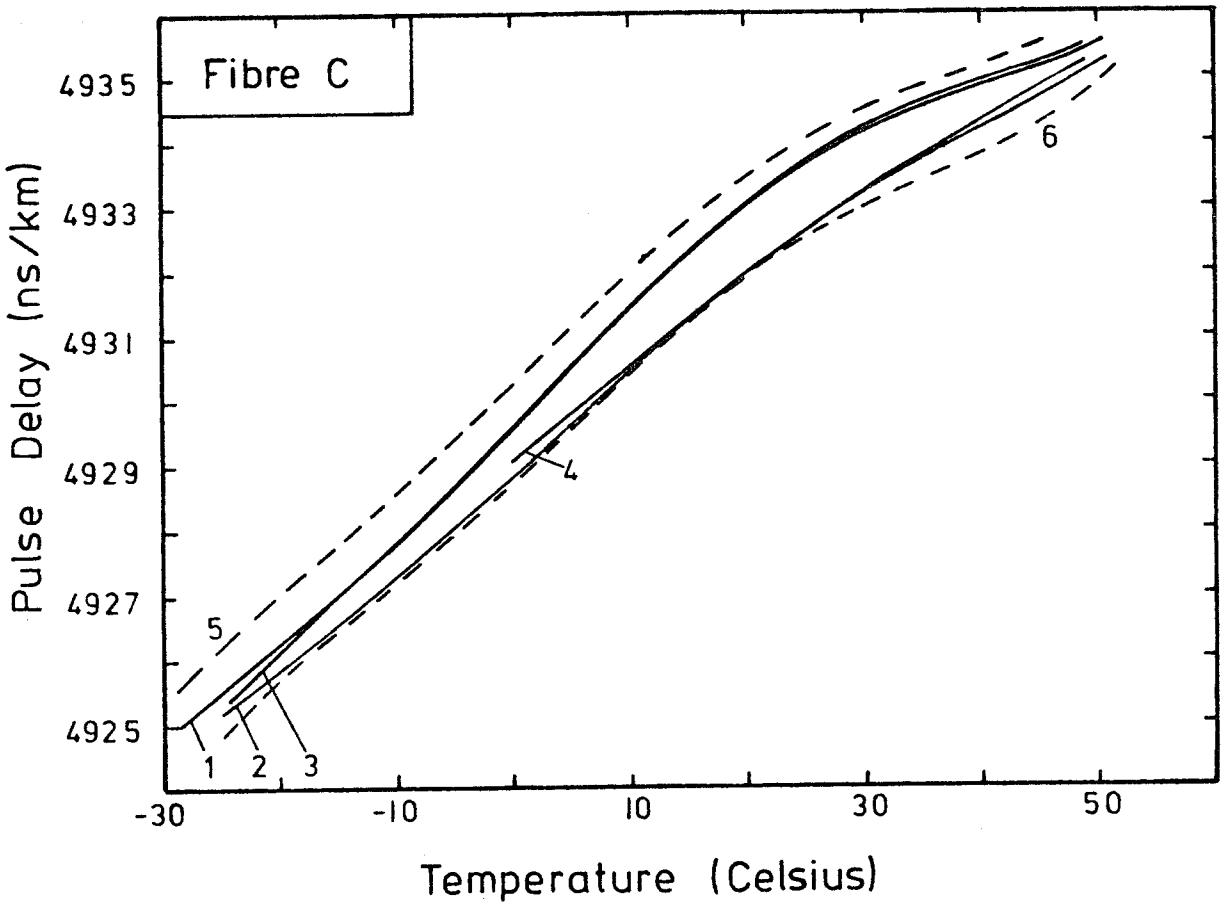

Figure 5.4 : Variation of pulse-delay with temperature for Fibre C jacketed with Nylon 6. The delay is normalised to a fibre length of 1km. Solid lines give the variation of delay measured when the temperature is cycled continuously (1 and 3 when temperature is increased, 2 and 4 as temperature is decreased). Broken lines, 5 and 6, show the effect of pausing at $-30^{o}C$ and $50^{o}C$, respectively.

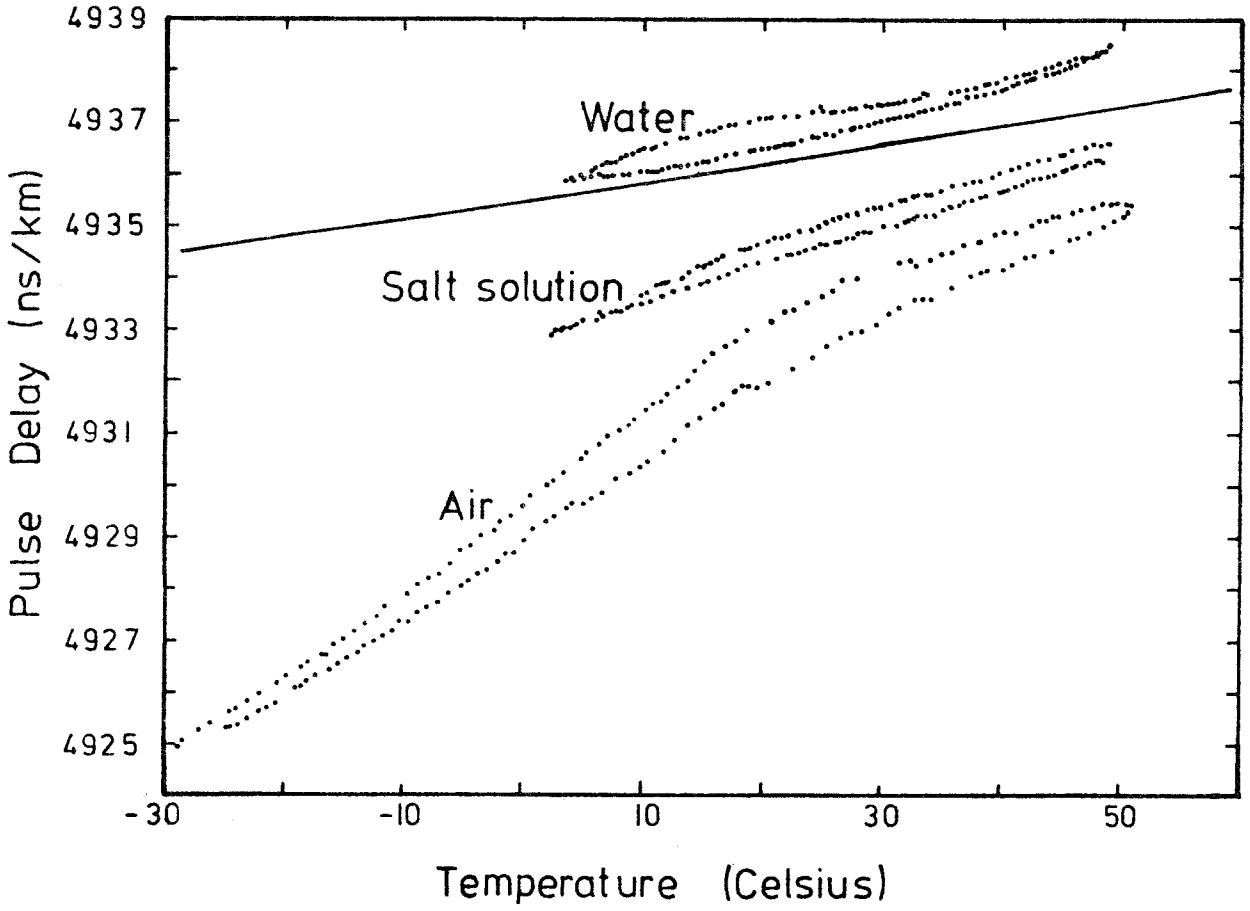

Figure 5.5 : Measured values of pulse-delay versus temperature for a nylon-jacketed fibre, Fibre C (Table 5.2), under various environmental conditions (dots). The solid curve gives time delay for unjacketed fibre, Fibre B (Table 5.2). All curves are normalised to 1km.

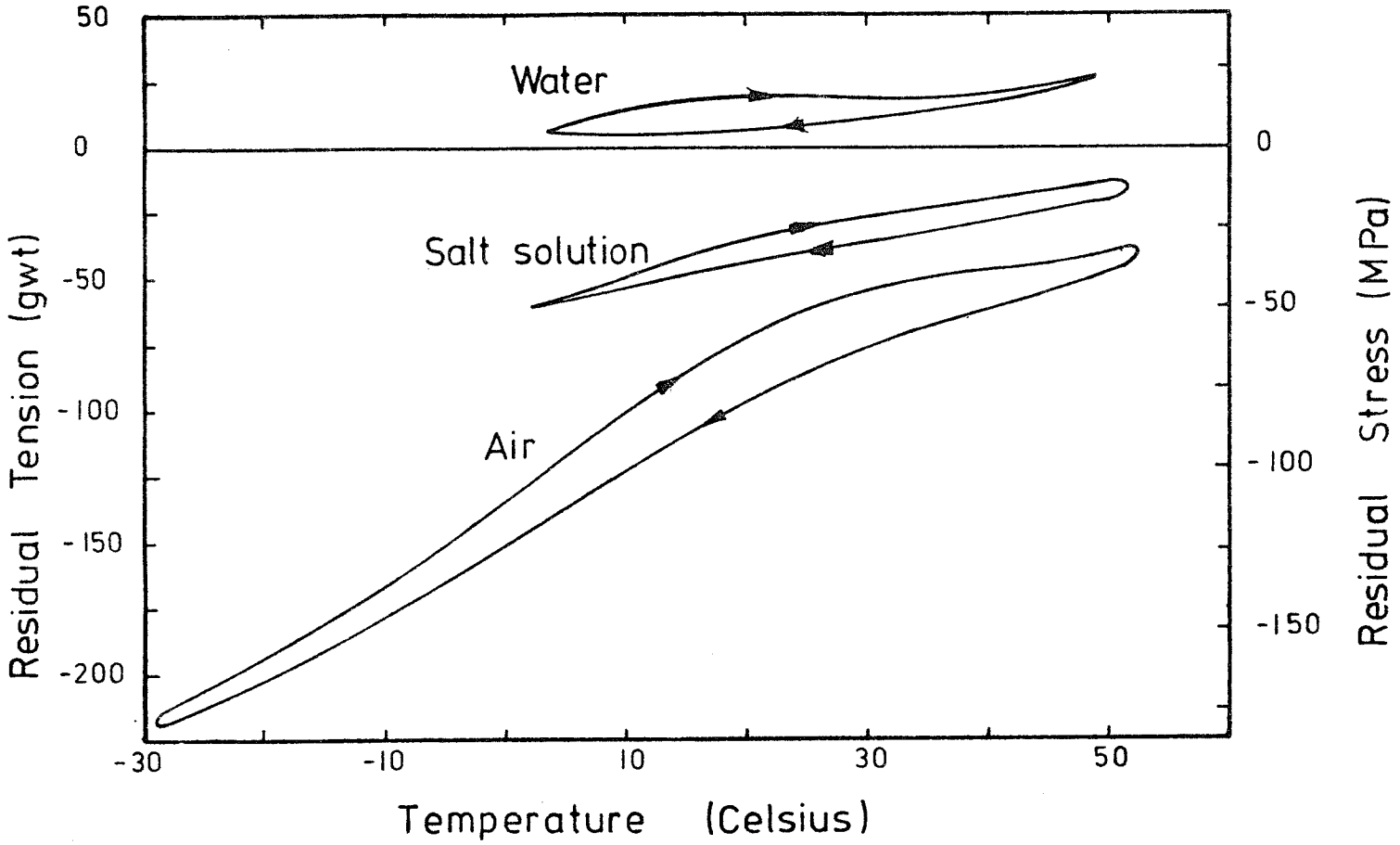

Figure 5.6 : Stress and force exerted on Fibre C by the nylon jacket for various environmental conditions.

CHAPTER 6 - WAVELENGTH-DEPENDENT MEASUREMENTS OF FIBRE ATTENUATION BY THE BACKSCATTER TECHNIQUE

6.1 INTRODUCTION

The use of backscattered power for attenuation measurements in optical fibres was proposed by Kapron et al[1] in 1972 and demonstrated by Barnoski et al[2] and Personick[3] in 1976. The backscattering technique is now well-established and has been the subject of a number of theoretical[4-7] and experimental[7-15] studies.

A pulse launched into an optical fibre loses power via a number of mechanisms, one of which is Rayleigh scattering resulting from small-scale inhomogeneities in the refractive index of the glass. A proportion of the power thus scattered is guided by the fibre back to the launching end where it may be detected. The resulting waveform takes the shape of a decaying pulse since the forward-travelling pulse and that portion of the light which is scattered backwards are both attenuated by propagation along the fibre. The derivative of the scatter return is thus a direct measure of the local attenuation at the scatter point.

One of the main attractions of the backscatter technique lies in its ability to measure variations of attenuation with distance. Thus sections of fibre of poor quality may be identified readily and breaks, or other point defects, may be located accurately. In addition, access to only one end of the fibre is required and this is a most desirable feature for field measurements.

The present chapter describes a part of a study of the backscatter technique conducted with Mr. A.J. Conduit and intended to test the validity of the method and to extend its range and applicability.

Attenuation measurements using the backscatter technique have, in the past, been restricted to a few selected wavelengths, since semiconductor-laser sources were normally used. The value of the

technique is considerably enhanced, in the present work by the use of the tunable laser system[12] described in Chapter 2. Thus the backscatter technique is employed, for the first time, to obtain the spectral attenuation of an optical fibre. Comparison of the results with more conventional attenuation measurements confirm that the backscatter technique can, in some cases at least, give a very accurate measure of fibre attenuation. In addition, with a tunable source, the method may be used to estimate the longitudinal variation of impurity content by comparison of length-dependent attenuation measurements on, and off, the peak wavelength of the absorption line.

A new sampling scheme[7] for the backscatter attenuation measurements was developed during the present study. Equipment employing the new, two-channel, sampling method is almost immune from drift and noise originating in the laser source.

6.2 THEORY

6.2.1 Two-channel Attenuation Measurements by the Backscattering Technique

An optical pulse propagating in a fibre scatters light and some of this is trapped by the fibre and returned to the source. The returned signal is observed as an exponentially decaying pulse, the rate of decay being determined by the attenuation of the fibre. Subject to the condition that the exciting pulse is sufficiently narrow for little attenuation to occur over its spatial width in the fibre, i.e.

$$W << \frac{1}{\alpha v_g} \tag{6.1}$$

the backscattered signal, p(t) is given by[3,4]

$$p(t) = \frac{P_o W S \alpha_s v_g}{2} \exp(-\alpha v_g t) \tag{6.2}$$

where the following symbols have been used:

P_o = peak power launched (W)

W = optical pulse width (s)

S = backscatter factor, i.e. the proportion of the scattered light collected by the fibre in the reverse direction.

α_s = Rayleigh scattering loss (np/m)

v_g = Average group velocity = c/N_1

α = $(\alpha' + \alpha'')/2$ with α' and α'' being the respective average attenuations of the forward travelling and backscattered pulses.

It has been shown[4] that the backscatter factor S for a step-index multimode fibre is

$$S = \frac{3(NA)^2}{8n_1^2} \tag{6.3a}$$

and for a graded-index fibre is

$$S = \frac{(NA)^2}{4n_1^2} \tag{6.3b}$$

where NA is the numerical aperture and n_1 is the refractive index at core centre.

Equation (6.2) can also be interpreted in spatial terms by the variable transformation

$$t = \frac{2\ell}{v_g} \tag{6.4}$$

where ℓ is the distance in metres to the scattering point.

With the standard point-by-point approach to attenuation measurement [8,11] an estimate of p(t), denoted $\hat{p}(t)$, is extracted from the receiver noise by a boxcar integrator which progressively samples and averages each point on the waveform. An average $\hat{\alpha}(\ell)$ is then derived from the slope of $\ln[\hat{p}(t)]$. When near maximum range,

the signal-to-noise ratio at the receiver is low and the scan time must be long to obtain adequate noise averaging. This imposes rigid limits on the stability of the source, detector and integrator if the measurement accuracy in α is to be maintained.

The configuration of the two-channel technique is shown in Figure 6.1. An optical pulse obtained from a semiconductor laser diode is launched into the fibre and the resulting backscattered power is detected by an avalanche photodiode and amplified for analysis. A fraction of the launched pulse is reflected from the beam splitter and detected to provide a timing reference for the time-delay generator. The latter provides trigger pulses to enable the sample and hold circuits, SH1 and SH2, to sample the amplified backscatter waveform at times t_1 and t_2 respectively. Note that the time-delay generator is synchronized to the optical pulse, so that jitter in the laser pulse does not result in uncertainty in the time position of the sampling windows. The analogue samples, $\hat{p}(t_1)$ and $\hat{p}(t_2)$, are converted into digital form (by an A/D converter) for processing. The results of many such samples may be numerically averaged to provide an estimate of the fibre attenuation

$$\hat{\alpha}(t_1,t_2) = \frac{\ln[\hat{p}(t_1)/\hat{p}(t_2)]}{v_g(t_2 - t_1)} \qquad (6.5)$$

where $\hat{\alpha}(t_1,t_2)$ represents the measured attenuation over the section of fibre in the region $t_1 \frac{v_g}{2} \leq \ell \leq t_2 \frac{v_g}{2}$. An advantage of the above scheme is that variations in the level of backscatter signal due to pulse amplitude fluctuations do not affect the accuracy of the calculation since the two sample sets are averaged over the same group of laser pulses. Accordingly, the stability of the laser-diode source, the avalanche photodetector and the amplifier is not critical and simple, economic, circuits may be employed. Furthermore, in order to eliminate any gain errors in the sampling and the conversion circuits the sample gates could, on alternate pulses, operate at times of t_1 and t_2 and then at times t_2 and t_1.

To obtain the attenuation characteristic of the whole fibre the

sample pair is scanned across p(t) and further application of equation (6.5) yields $\hat{\alpha}(t,t + \Delta T)$, where ΔT is the time separation of the samples, i.e. $\Delta T = t_2 - t_1$.

6.2.2 Optimisation of the Two-channel Sampling Method

If ε represents the worst-case error in the estimate of $p(t_1)$ and $p(t_2)$, the maximum error in the measured attenuation $\hat{\alpha}(t_1,t_2)$ occurs when

$$\frac{\hat{p}(t_1)}{\hat{p}(t_2)} = \frac{p(t_1) + \varepsilon}{p(t_2) - \varepsilon} \tag{6.6}$$

Defining δ as the maximum error in $\hat{\alpha}(t_1,t_2)$, i.e.

$$\delta = \left|\hat{\alpha}(t_1,t_2) - \alpha(t_1,t_2)\right|_{max} \tag{6.7}$$

it follows from equations (6.2), (6.5) and (6.6) that

$$\delta = \frac{1}{v_g \Delta T} \ln \left[\frac{1 + \varepsilon/p(t_1)}{1 - \varepsilon/p(t_2)}\right] \tag{6.8}$$

If the error ε is small in comparison to the samples $p(t_1)$ and $p(t_2)$ then equation (6.8) reduces to

$$\delta \simeq \frac{1}{v_g \Delta T} \left[\frac{\varepsilon}{p(t_1)} + \frac{\varepsilon}{p(t_2)}\right] \tag{6.9}$$

From equation (6.5)

$$\Delta T = \frac{1}{\alpha v_g} \ln \frac{p(t_1)}{p(t_2)} \tag{6.10}$$

From an instrumentation viewpoint the larger the sample error ε can be, the less stringent are the circuit requirements on such parameters as linearity, offsets and quantization error. The value of ε (expressed as a percentage of $p(t_1)$) which is tolerable in order to obtain a measurement to within δ of its true value α is shown

in figure 6.2. as a function of sample separation ΔT for fibres having attenuations of 3dB/km and 15dB/km. Consider, for example, the curve for the fibre having a loss of 3dB/km ($\alpha = 6.9 \times 10^{-4}$np/m); if the attenuation is to be measured to within 0.1 dB/km ($\delta = 2.3 \times 10^{-5}$np/m), then for sample separations ΔT of 0.1μs, 10μs and 30μs, the tolerable error ε is 0.02%, 1% and 0.22% of $p(t_1)$ respectively.

It is clear from the curve that there is an optimum sample separation, ΔT_{opt}, which maximizes the allowable ε and thereby minimizes the accuracy requirements of the instrumentation system. Thus for a fibre having an attenuation of 3dB/km the sample separation which maximises attenuation accuracy is approximately 10μs, corresponding to a 1km length of fibre between the two sample points; the use of other gate separations will necessarily invoke a penalty in measurement accuracy.

The power ratio $p(t_1)/p(t_2)$ which maximises attenuation accuracy may be found by differentiating eqn. (6.9). It is found that the optimum is independent of fibre attenuation α and has a value $\sim$ 5.6dB. Substituting this value into eqn. (6.10) results in the optimum sample separation

$$\Delta T_{opt} = \frac{1.28}{\alpha v_g} \qquad (6.11)$$

if α is expressed in np/m. Therefore, test equipment which is able to adjust the value of ΔT until the ratio of the samples is 5.6dB will automatically maximise attenuation accuracy.

The tolerable sampling error ε at optimum ΔT can be determined from equation (6.8) and is plotted in figure 6.3 with fibre attenuation α and required measurement accuracy δ as parameters.

It should be noted that the foregoing analysis assumes that the gain of the receiver is so adjusted that the first sample is at the maximum level acceptable by the measurement system. If this is not the case then the tolerable sample error ε is decreased proportionally. Note that the possibility of altering the amplifier gain at any time

during a backscatter scan gives a great flexibility to the design of two-channel instruments.

In some cases the optimum sample separation will be difficult to achieve. For example, it is inadvisable to site the two samples within different sections of a fibre link owing to the possible variation of the backscatter factor S between the sections[4]. In addition, the resolution of short-length attenuation variations requires a small gate separation. For non-optimal gate spacings the penalty P to be paid in the tolerable sample error ε in order to achieve a given attenuation accuracy is defined as

$$P = 10 \log_{10}(\varepsilon_{OPT}/\varepsilon) \qquad (6.12)$$

where ε_{OPT} is the sample accuracy required at the optimal gate separation. Curves giving the penalty P as a function of attenuation and ΔT are given in Figure 6.4. Note that the curve P = 0 represents optimal gate separation, as given by equation (6.11). As a further example, let us take a fibre having an attenuation of 3dB/km for which the optimum sample separation ΔT_{opt} is 10μs. The sample accuracy required for an attenuation error of $\delta = \pm 0.1$dB/km is $\varepsilon_{OPT} = 0.01 \times p(t_1)$ (figure 6.3). If, however, we require to inspect the fibre over a 250m section ($\Delta T = 2.5\mu s$), then figure 6.4 shows that, for the same error in attenuation, we now require a 3dB greater sample accuracy, i.e. $\varepsilon = 5 \times 10^{-3}\ p(t_1)$.

The implication of the foregoing is that a compromise is necessary between the attainment of overall attenuation accuracy and the resolution required for shortlength fluctuations. The latter requires small gate separations because of the difficulty in determining the slow decay in the backscatter signal when the difference between the power levels $p(t_1)$ and $p(t_2)$ is small. On the other hand, relatively large localised power variations are found at fault points and imperfections[8] leading to measurable differences in signal levels if the gates are positioned immediately before and after the point of interest. Thus relatively small gate separations are permitted and the accurate loss measurement of such discontinuities is not precluded.

A further consequence of the existence of an optimum gate separation is that greatest accuracy in the determination of overall link attenuation is obtained by summing the attenuation of individual fibre sections having lengths corresponding to ΔT_{opt}. This approach may well have a further advantage in that it should allow both sample points to be sited within the same fibre section in a jointed link, thus avoiding the problems which can result from variations in the backscatter factor S between fibre sections. The latter may be caused by changes in numerical aperture[5] or dopant level[4].

6.2.3 Noise Averaging

When the predominant source of noise at the processor input is due to signal quantisation, ε is governed by the accuracy of the A/D converter. Accordingly for an n-bit converter with $p(t_1)$ set at maximum level

$$\varepsilon = \frac{K}{2^n} \qquad (6.13)$$

where $\pm$ K is the dynamic range of the A/D converter.

When the amplifier thermal noise predominates, numerical sample averaging can be used to reduce ε to the level required. This is usually the case when distant sections of fibre are examined. Quantisation noise is not the dominant contribution to the measurement error ε in this situation. In addition source noise (i.e. variation in energy between successive pulses) normally causes the signal to vary by one quantisation level at least. Quantisation noise is thus normally eliminated in the subsequent signal averaging. The noise at the amplifier output may be assumed Gaussian, with variance σ^2. Averaging N samples reduces the variance to σ^2/N. Then taking ε as that error in $p(t_1)$ or $p(t_2)$ which is exceeded with a probability of 5% it follows, from the Gaussian distribution, that

$$\frac{\varepsilon}{\sigma/\sqrt{N}} = 1.96 \qquad (6.14)$$

Defining the signal-to-noise ratio (SNR) before averaging as

$$SNR = \left[\frac{p(t_1)}{\sigma}\right]^2 \tag{6.15}$$

we have from equations (6.14) and (6.15)

$$\frac{\varepsilon}{p(t_1)} = \frac{1.96}{\sqrt{N(SNR)}} \tag{6.16}$$

Figure 6.5 is a plot of $\frac{\varepsilon}{p(t_1)}$ against N and SNR. The graph of figure 6.3 indicates the value of $\frac{\varepsilon}{p(t_1)}$ required to obtain a given measurement accuracy in α. In combination with figure 6.5 the number of samples that must be averaged to obtain that ε can be found.

6.2.3.1 Receiver Amplifier Gain

When the signal-to-noise ratio is low the amplifier gain must not cause the magnitude of $p(t_1)$ to be so close to the range limit of the A/D converter as to truncate the noise distribution. This will cause a bias in the mean of the samples since the noise cannot average to zero, even after an infinite number of samples.

If $\pm K$ represents the dynamic-range limits of the A/D converter and σ^2 the variance of the noise $n(t_1)$ at the amplifier output, then for operation with low signal-to-noise ratios the bias produced in the mean of $p(t_1) + n(t_1)$ due to truncation is:

$$\begin{aligned} \text{bias} = {} & \left[K - p(t_1)\right] \int_{\frac{K-p/t_1)}{\sigma}}^{\infty} \frac{1}{\sqrt{2\pi}} e^{-\beta^2/2} \, d\beta \\ & - \left[K + p(t_1)\right] \int_{\frac{K+p(t_1)}{\sigma}}^{\infty} \frac{1}{\sqrt{2\pi}} e^{-\beta^2/2} \, d\beta \\ & - \sigma \int_{\frac{K-p(t_1)}{\sigma}}^{\frac{K+p(t_1)}{\sigma}} \beta \frac{1}{\sqrt{2\pi}} e^{-\beta^2/2} \, d\beta \end{aligned} \tag{6.17}$$

To keep this bias to an acceptable level of less than 10^{-5}K it is necessary that

$$\frac{K - p(t_1)}{\sigma} \geq 4 \qquad (6.18)$$

From equations 6.15 and 6.18 it follows that the A/D converter range utilization is

$$\frac{p(t_1)}{K} = \frac{\sqrt{SNR}}{4 + \sqrt{SNR}} \qquad (6.19)$$

Thus when the signal/noise ratio is low, as is the case when backscatter signals from sections of fibre remote from the launch point are measured, only the fraction of the dynamic range of the A/D convertor, given by equation (6.19), may be used. In this case the amplifier gain must be lowered to decrease the level of $p(t_1)$. The proportion by which the gain must be reduced is plotted in figure 6.6. It is apparent from the figure that this effect is very important for signal/noise ratios lower than 10 dB. Equation (6.9) shows that a reduction in $p(t_1)$ requires that the sample error ε be reduced proportionately in order to maintain the same attenuation accuracy. It is this effect that will ultimately determine the maximum attenuation range of any backscatter apparatus. Thus, although it is possible to continue to extract the backscatter trace from the noise when the SNR is very low, the amplitude of the signal is allowed to occupy only a very restricted portion of the dynamic range of the apparatus. The constraints which this imposes on the linearity and zero offsets of the data-acquisition system become rapidly more difficult to meet as the distance to the sample point is increased.

6.2.4 Timing Sensitivity

The uncertainty U in the Sample-and-Hold aperture (i.e. the timing jitter) produces an amplitude error when sampling fast slewing signals. During the sampling of $p(t_1)$ the error, ε_a, is equal to:

$$\frac{\varepsilon_a}{p(t_1)} = U.\alpha v_g \qquad (6.20)$$

where, from equation (6.2), $1/\alpha v_g$ is the time constant of p(t).

Figure 6.7 shows the variation of $\varepsilon_a/p(t_1)$ against U for a range of fibre attenuations. From these curves, and those of figure 6.3, it can be seen that if the aperture uncertainty is not to be the limiting factor, an uncertainty time of some 100ps is required. This fortunately is possible with current technology.

6.3.5 Measuring Range of Backscatter Test Equipment

6.3.5.1 The limiting factors

The sample accuracy required for local attenuation measurements is independent of the distance from the source to the fibre section under examination. As this distance is increased, however, it becomes more difficult to achieve a given sample accuracy, since the signal decays, while the noise of the receiver remains almost constant. The signal/noise ratio thus decreases with distance along the fibre and limits the accuracy with which samples may be acquired and hence the measuring range.

It is assumed here that the sampling gates have optimum separation. From equations (6.9) and (6.10) the sample accuracy required is therefore:

$$\frac{\varepsilon}{K} = \frac{\delta}{\alpha}\,\frac{p(t_1)}{K}\,\frac{\ell n\left[p(t_1)/p(t_2)\right]}{\left[1 + p(t_1)/p(t_2)\right]} \qquad (6.21)$$

Since $p(t_1)/p(t_2)$ is $\sim$ 5.6dB for optimum gate separation, equation 6.21 becomes:

$$\frac{\varepsilon_{OPT}}{K} \approx \frac{\delta}{\alpha} \times \frac{p(t_1)}{K} \times \frac{1}{3.6} \qquad (6.22)$$

where K is the dynamic range of the data-acquisition system.

Near the limit of the range the accuracy to which each sample is read is limited by the noise in the receiver and is given by equation (6.16). The minimum signal-to-noise ratio required in order to achieve a precision δ is therefore:

$$(SNR)_{min} = \left[\frac{1.96}{\sqrt{N}} \times \frac{\alpha}{\delta} \times 3.6\right]^2 \qquad (6.23)$$

The signal-to-noise ratio of the backscatter signal at the sampling gate may be written as:

$$SNR = \left[\frac{R.P_o.W.\alpha_s.S.v_g}{4\, i_n \sqrt{B}}\right]^2 \exp(-4\alpha\ell) \qquad (6.24)$$

where R is the responsivity of the avalanche photodetector, i_n is the spectral density of the input equivalent noise current, and B the bandwidth of amplifier. A factor of 2 has been introduced in equation (6.24) to account for the 3 dB loss of the beamsplitter in the optical path from the fibre to the detector.

The maximum distance, ℓ_{max}, from the launching end to sample gate 1 is reached when the signal-to-noise ratio, given by equation 6.24, has fallen to the smallest allowable value obtained from equation (6.23). Combining these equations, therefore, the range (defined as the maximum optical loss between the launching end and the position of gate 2 which allows a measurement precision δ) may be expressed as:

$$\alpha.\ell_{max} = \frac{\ell n}{2}\left[\frac{\alpha_s}{\alpha}\,\frac{\sqrt{N}\,\delta}{1.96\times3.6}\,\frac{P_o\,RWS\,v_g}{4\, i_n \sqrt{B}}\right] + \frac{1}{2}\alpha v_g \Delta T_{OPT} \qquad (6.25)$$

In the numerical example which follows, realistic values for the parameters of equation (6.25) are chosen and the range which might be achieved by two-channel backscatter equipment is then estimated.

6.5.3.2 Numerical example

The number of samples averaged is chosen to be 1000, so that for a pulse repetition rate of 1 k Hz the averaging time is 1 s for

each measurement. Typical values for the power launched into the fibre, and the pulse duration, are 1W and 100 ns, respectively, when the source is a single-heterostructure injection laser. Assuming that a graded-index fibre having a numerical aperture of 0.2 and a refractive index in the core of 1.5 is measured, it follows that $S = 4.4 \times 10^{-3}$ and $v_g = 2 \times 10^8$ ms^{-1}. At the emission wavelength of GaAs lasers the loss of good-quality fibres is dominated by Rayleigh scattering so that $\alpha = \alpha_s$.

The backscatter signal, $i_{p(t)}$, has a 3dB (electrical bandwidth which ranges from 22 to 110kHz for fibres having attenuations of 3 to 15dB/km. For the determination of attenuation the receiver bandwidth must be sufficient to pass p(t) without additional dispersion. A greater demand for receiver bandwidth arises when there is a need for accurate fault location for which the receiver must accommodate pulses of width W without dispersion. In either case it is advantageous to keep the receiver bandwidth as low as possible to maximize the signal/noise ratio. For the purposes of this example we choose a receiver with 10MHz bandwidth and an input equivalent noise current of 1pA/$\sqrt{\text{Hz}}$. It follows that the variance of the noise is

$$\sigma^2_{n(t)} = 10^{-17}(\text{Amps})^2$$

Using the above values, the first term of equation (6.25) which gives the maximum loss to sampling gate 1, is equal to 23.5dB for an accuracy δ of 0.1dB.km^{-1}. The final term represents the loss of the section of fibre under examination and is equal to 2.8dB when the gate separation is optimum. The range at which loss measurements can be made to within 0.1dB.km^{-1} is 26.3dB, for the parameters chosen .

From equation (6.24) it is found that the signal-to-noise ratio at time t_1 is $\sim$ 17dB, assuming that α_s is 3 dB/km. Equation (6.19) gives the maximum value of the ratio $\frac{p(t_1)}{K}$ as -2dB. This will not impose very stringent additional demands on the linearity of the sampling system. In fact, a 12-bit A/D converter would have,

typically, a linearity better than is required by a factor of 10.

The parameter values used here are for illustration only and, with suitable design choices, the predicted range can be extended. For instance, distance resolution can be sacrificed for a longer range. Thus, by increasing the pulse width and simultaneously narrowing the bandwidth of the amplifier, the range is extended at a rate of 7.5 dB (one-way) for each decade of distance resolution. Clearly, an increase in power and in detector responsivity, as well as a decrease in the receiver noise would also extend the range. The values given above are, however, representative of the performance given by presently-available components.

Further improvements can be obtained, in some circumstances, by increasing N, the number of samples averaged. If, however, the signal/noise ratio is lower than about 10dB, then the amplifier gain must be substantially reduced before averaging in order that the noise should not be truncated by the sampling system (usually in the A/D converter). The extent to which signal averaging may be used to enhance the range of backscatter test equipment is thus limited by the linearity of the sampling system.

6.3 IMPLEMENTATION OF THE TWO-CHANNEL TECHNIQUE USING THE DYE-LASER SYSTEM

The dye-laser system, described in Chapter 2, presents several advantages for backscatter measurements. For example, it has allowed, for the first time, backscatter attenuation measurements to be made as a function of wavelength. Secondly, the power available (200 - 500W in the 0.8 - 1.1 μm spectral region) is far higher than that given by semiconductor lasers. The backscatter signal is thus increased and the amplification and data-acquisition problems normally encountered in this experiment are alleviated to some extent.

Unfortunately, the dye-laser system also has a number of undesirable features, the most important of which are:

(a) variations of the energy contained in successive pulses,
(b) a gradual fall in output power in the first few minutes of operation,
(c) low repetition rate, and
(d) poor reliability of the spark-gap.

The two-channel technique is ideally suited for dealing with pulse-amplitude fluctuations, since these are automatically compensated for. The remaining problems have been solved by a careful design of the electronic instrumentation. In addition, the use of a mini-computer to control the entire experiment greatly improves the speed and accuracy of the measurement and provides great flexibility.

6.3.1 General Description of the Experiment

Pulses of 80ns duration are extracted from the output of the optical parametric oscillator, figure 6.8, by the pulse slicer. The light is transmitted by a beamsplitter and launched into the fibre. A mode-scrambler ensures that the fibre is excited under near-equilibrium conditions. The signal returning from the fibre is detected by a silicon avalanche photodiode and amplified. The resulting waveform is fed to two linear gates. The triggering signal for the gates is derived from the high-voltage pulse used to drive the Pockels cell and has no jitter with respect to the optical signal. A time-delay generator triggers the linear gates at times t_1 and t_2 on each waveform. The gates therefore acquire and average two samples from each scatter return. The averaged outputs of the gates are read many times by the digital voltmeter and the results are sent to the computer where further, numerical, averaging takes place. The ratio of the gate outputs gives the attenuation of the section of fibre corresponding to the sampling times t_1 and t_2. The source-compensation provided by this sampling scheme and the combination of analogue averaging in the gates and numerical averaging in the computer gives a reproducibility in the attenuation measurement of, typically, 0.05dB/km in a 50m section of fibre. This level of precision is achieved with only $\sim$ 1000 laser pulses.

The experiment arrangement is shown in more detail in figures

6.9 and 6.10.

6.3.2 Description of the Source

The CMX-4 dye-laser and parametric oscillator produce pulses of 1 μs duration in the wavelength range 0.82 - 1.07 μm. It is a great advantage, for signal averaging, to use a high pulse-repetition rate. The O.P.O. cannot, however, be operated safely at a rate of more than 15 pps. In addition, the repetition rate of the laser must be harmonically related to the mains frequency. To meet these requirements, the laser is triggered externally at a rate of 12.5Hz by a signal derived from the mains. The trigger circuit and hence the laser itself can be switched on and off remotely by the computer.

The pulse duration is not critical for most backscatter measurements. In the present experiments, a pulse width of 80ns was chosen as a reasonable compromise between length resolution (which improves with decreasing pulse width) and signal power (which is proportional to pulse width). In addition, the use of relatively long pulses relaxes the requirements for a very high extinction ratio in the electro-optic modulator.

The pulse-slicer, fig. 6.9, consists of a Pockels cell, polariser and high-voltage pulse-generator. In the absence of a high voltage across the Pockels cell, the output of the OPO is rejected by the prism-polariser. The modulator is therefore normally off. A clear pellicle beamsplitter (placed in front of the polariser) sends an 8% sample of the pulse to a photodiode which, in turn, triggers the high-voltage pulse-generator.

The spark-gap used here is the three-electrode device shown in fig. 2.2. It is biased to about 10kV through a 10MΩ charging resistor via a length of 50Ω coaxial transmission line. When triggered, the spark-gap discharges the coaxial cable and then switches itself off since the 10MΩ limiting resistor does not allow an arc discharge to be sustained. The duration of the high

voltage pulse emerging from the spark gap is therefore proportional to the length of the charged line. An 8 m section of RG 8A/U cable gives a pulse duration of 80 ns. A rectangular pulse is thus generated which reaches the Pockels cell and opens the optical gate. After passage through the Pockels cell, the electrical energy is absorbed by a 50Ω termination. The latter incorporates a potential divider to provide a trigger signal for the instrumentation.

The operation of a spark gap is statistical in nature so that it does not always fire in response to a trigger pulse and, in addition, it occasionally breaks down spontaneously. Neither of these occurences is of any consequence with equipment employing numerical averaging only and incorporating fast sample-and-hold circuits. In the present experiments, however, linear gates were used to provide a degree of analogue signal averaging. With these instruments, the failure of the spark gap to respond to a trigger pulse is not serious, provided that it does not occur too often. The spontaneous operation of the spark-gap is more troublesome, however, since the data acquisition system then attempts to sample the backscatter trace when no optical pulse is present. As a result, the linear gates are rapidly discharged, even with a large (10s) gate output time constant. Since the gate time constants are not exactly matched, this results in an error in the ratio measurements, if the gate outputs are read before they have recovered from the disturbance. The problem is overcome by inserting a simple logic circuit in the triggering line (see fig. 6.9). The circuit provides a trigger pulse in synchronism with the spark-gap breakdown only if an optical pulse is also present.

It is unavoidable that a small fraction of the OPO output is allowed through the optical gate when the latter is closed. The 80ns-wide output of the pulse slicer is thus accompanied by an unwanted small-amplitude pedestal. The latter has a relatively long duration, and it can contain a substantial proportion of the transmitted energy. Since the backscatter signal is proportional to the energy of the forward-travelling pulse (rather than to peak

power), the presence of a wide pedestal can seriously degrade the distance-resolution of the experiment. It is therefore important that the extinction ratio of the modulator should be very high.

A high extinction ratio is achieved by carefully aligning the Pockels cell and polariser and this usually means "iterating" between the various angular adjustments until the minimum transmission is reached with the gate closed. The quality of the polariser is also important (the extinction ratio was improved by a factor of 3 by selecting the best available prism polariser). The addition of a polariser before the Pockels cell was found to be of little use, since the output of the OPO is highly polarised. With careful adjustment of the pulse-slicer, a power extinction ratio better than 1000:1 was achieved reproducibly. This corresponds to an energy-ratio of about 80:1.

To preserve this extinction ratio throughout the experiment, the light scattered into the room must also be excluded from the receiver and this is achieved by enclosing almost the entire path of the beam inside cardboard tubing. Since the pump beam is the main source of scattered light, an absorption filter rejecting this wavelength is placed in front of, and very near to, the avalanche detector.

6.3.3 Launching Cell

The 4% Fresnel reflection produced when a pulse is launched into a fibre is several orders of magnitude greater than typical levels of the backscatter signal. To avoid overloading the detector or amplifier, it is usually desirable to reduce substantially the magnitude of this reflection in the backscatter return.

Directional couplers[2,11], gated photomultipliers[3] and polarisers[9] have been used elsewhere to eliminate the input-face

reflection. However, an angled index-matching cell (fig. 6.9) is perfectly satisfactory. The window of the cell is not perpendicular to the laser beam and the reflection from the air/glass interface does not fall within the acceptance cone of the launching lens. The transmitted beam is refracted at the interface and the fibre is therefore held at such an angle that its axis coincides with the direction of the laser beam in the cell. The latter is filled with paraffin oil and no further reflections occur either on the fibre face or at the inside surface of the cell window. The intensity of the reflection reaching the detector is reduced by at least 30dB.

6.3.4 Detection of the Backscatter Signal

An optical receiver designed and built by Mr. A.J. Conduit was used. The detector is an RCA C30817 avalanche photodiode. Further amplification is provided by a transimpedance preamplifier. A detailed description and a discussion of the circuit may be found in reference 14. The preamplifier has a passband from d.c. to 15MHz and can thus faithfully reproduce the temporal variations of the backscatter signal produced by an 80ns optical pulse. The transimpedance is 56kΩ.

The photodiode is capacitively coupled to the preamplifier in order to improve the long-term bias stability. The resulting low-frequency cut-off is less than 0.1Hz.

A further characteristic of the amplifier circuit is that it recovers extremely rapidly from overloads. The circuit comes out of saturation as soon as the signal level falls within the dynamic range of the amplifier. As a result, the gain and the optical power can be increased in order to utilise the full dynamic range of the sampling gates.

Finally, the d.c. offsets of the amplifier are very stable and can be finely adjusted to zero using a set of potentiometers.

6.3.5 Signal Acquisition

6.3.5.1 Linear gates

Although the general discussion of the two-channel technique in section 6.2 is based on an instrument incorporating two sample-and-hold circuits, a pair of Brookdeal 9415 linear gates have been used in the present experiment. This choice was made primarily because the linear gates were available and could, in principle, be incorporated in the experiment without difficulty. It has therefore been possible to test the two-channel technique without investing a large amount of time or money in the construction of a backscatter instrument using commercial high-speed sample-and-hold circuits and analog-to-digital converters. In addition, the linear gates each include two low-pass filters which attenuate the fluctuations of signal level and thus reduce the amount of subsequent numerical averaging needed to reach a given measurement accuracy.

A low-pass filter at the input of each gate charges exponentially with a time constant of 1μs when a trigger pulse is present. When signals with low repetition rates are sampled, it is desirable to charge this filter as rapidly as possible to avoid droop on the gates caused by leakage in the sample-and-hold circuits. On the other hand, if the sampling 'window' is large, the distance-resolution of the experiment is degraded, and in this case a 200ns trigger-pulse duration was chosen as a suitable compromise. At a pulse repetition rate of 12.5Hz, the gates thus appear to charge with an input time-constant of 0.4s. Since a large number of pulses are required to charge the input filter, the variation in optical power between successive pulses is smoothed to some extent.

Additional noise-reduction is provided by a second low-pass filter at the output of each gate. The time-constant of these filters, which is adjustable, is normally chosen to be a compromise between increased measurement time on the one hand and better elimination of signal amplitude fluctuation on the other. With long time-constants, the majority of the time taken to acquire the sample is spent waiting

for the output filter to charge. However, use of a novel technique reduced the charging time while retaining adequate signal averaging. It is based on the fact that the time constant of the gates can be controlled by an external capacitor. Thus a short initial time constant (0.3s) allows the gates to charge rapidly towards the mean signal level. Larger capacitors are then switched into the filter of each gate by reed-relays controlled remotely from the computer. As a result the time constant is increased to 6s and the signal fluctuations are greatly attenuated.

The output from each linear gate, once stabilised, is read about 75 times by the digital voltmeter (d.v.m.). The input to the d.v.m. is switched before each reading from one gate to the other. In this way, any remaining fluctuations of signal level affect both sets of readings in almost an identical manner and thus cancel.

The achievement of good distance resolution in this experiment required very small gate-separations $\Delta t = t_1 - t_2$. Section 6.2 shows that in order to measure the attenuation of a 50m section of fibre to within 0.1dB/km, samples $p(t_1)$ and $p(t_2)$ must be determined to within 0.01% of $p(t_1)$. Such a stringent requirement is only just within the specifications of the instruments and special precautions must be taken to avoid measurement errors. Thus the gain of the gates is only specified to within 1%. Before each attenuation measurement, therefore, a gain-calibration is performed by positioning both gates at time t_1 and measuring the ratio of their outputs. This ratio is a gain correction factor for the subsequent attenuation calculation.

The d.c. offsets of the gates must be carefully adjusted to zero. At low duty factors (i.e. the product of trigger pulse-width and pulse-repetition rate), however, the gate offsets tend to drift and a 10mV offset on each gate can lead to an error in the signal ratio of up to 0.18% of the dynamic range, i.e. substantially more than the desired resolution. The gate offsets are therefore monitored before and after each ratio measurement. A correction is then applied to the ratio and results in improvement of the accuracy by about one order of

magnitude. In addition, it is verified before each measurement that the offsets are less than 3mV.

The gate linearity was measured[15] and found to be better than 0.02% over the full dynamic range of both gates. However, only a fraction of the dynamic range of the instruments is used for the present measurements and the linearity is about 0.01% over the range of measured signal levels.

The shape and duration of the trigger pulses also affects the accuracy of the linear gates. This is especially important at very low duty factors and can cause substantial variations in offset voltage. To alleviate this problem, a gate separation generator has been designed to trigger both gates with pulses as nearly identical as possible, whether during attenuation measurements, gain correction measurements, or voltage-offset measurements.

The sampling window of the linear gates is sufficiently wide for a small, but significant, variation of power to occur across it. This leads to an error of about 2ns (for a fibre having a loss of 15dB km^{-1}) in the effective position of the samples. However, for constant attenuation, each gate is identically affected and there is no error in the estimated fibre-loss. Similarly little error will occur for small fluctuations of attenuation, or for low loss fibres.

6.3.5.2 Timing

The signal-acquisition equipment is triggered by the pulse slicer. A Hewlett-Packard 5398A time-synthesiser (or time-delay generator) gives a delayed pulse which determines the time-position t_1 of the first sample on the backscatter waveform. The 5398A has low jitter and excellent long-term stability. It is programmed by the computer via an IEEE-488 interface and can be used to scan the entire length of a fibre automatically.

After an appropriate delay, the time synthesiser triggers the gate separation generator which, in turn, triggers the linear gates,

either at times t_1 and t_2, or simultaneously at time t_1 for a gain calibration. The sample separation ($t_1 - t_2$) is determined by a coaxial delay-line (or, for very long delays, by a second digital delay generator) which ensures that the separation is stable and has little jitter. At the output of the delay line, the pulse is reshaped. A single monostable multivibrator sets the trigger pulse-width for both gates, so that the trigger pulses are nearly identical.

The sample-separation is calibrated with a time-interval counter. Similarly, the position of the first gate is deduced from the time-interval between the trigger-pulse and the reflection from the far end of the fibre. Naturally care must be taken to match the delays of the cables used in each channel to interconnect the instruments.

6.4 RESULTS

A few examples of the many results gathered illustrate the main features of the experimental technique.

6.4.1 Length-dependence of Attenuation

The variation of attenuation with lengths in 2.8km section of graded-index fibre (VD 230L) is shown in figure 6.11 for the operating wavelengths 0.87 and 1.00μm (thin lines). Note that the attenuation is given directly and does not need to be inferred from the slope of the backscatter characteristic.

The fibre was scanned at 20m intervals using a gate separation of 480ns (a distance resolution of $\sim$ 50m). This is far less than the optimum separation for a fibre having a loss of 2-3dB km^{-1}. Hence, in this case, attenuation accuracy has been sacrificed for improved positional resolution. Nevertheless (figure 6.11) a great deal of detail is obtained both in attenuation and in position. The correlation of the features of the two curves obtained at different wavelengths is a good indication of the reproducibility of the measurement. In fact, for these early scans, the results could be reproduced to within 0.05dB km^{-1}. Better reproducibility has since been achieved.

The backscatter measurement reveals that the fibre has a region of almost constant attenuation in the first 1.8km from the launching end, A. Very near to the launching end, however, there is a sharp increase in attenuation, probably caused by increased loss of higher-order, and leaky, modes. Beyond a few hundred metres, the modes subject to higher loss have largely disappeared and no longer cause a change in attenuation.

In the last kilometre of fibre, near end B, a series of fluctuations in attenuation, of amplitude $\pm$ 0.5dB km^{-1}, is observed. Although the scans reveal this fine structure very clearly, no information is provided directly as to the source of the fluctuations. In addition, the figure does not show whether the fluctuations would be observed in a single-pass measurement, such as the conventional cut-back technique, or whether they are merely a quirk of the backscatter method. Measurements were therefore made from end B (at 1.00μm) in an attempt to elucidate this question (heavy line in figure 6.11). The measurements from end B have been transformed to their mirror-image so that each abscissa value refers to the same point in the fibre for all curves. Care was taken, in this procedure, to account for all delays in the measurement system.

The fluctuations which are observed from end A also appear in the scan made from the other end. However, the curves are anti-correlated, i.e. a peak in one corresponds to a trough in the other. Longitudinal variations in scattering loss, in numerical aperture[5] or in fibre diameter[15] would give rise to anti-correlated backscatter attenuation characteristics. Fluctuations in absorption loss[15] or microbending loss would, on the other hand, lead to correlated attenuation features and cannot, therefore, cause the observed effects.

Diameter variations are the most likely cause of the anti-correlated attenuation fluctuations observed in c.v.d. fibres. The observed spatial frequency is too high for numerical aperture or scattering loss variations (which must originate in the fibre preform and whose spatial frequency is limited by the width of the hot zone

of the deposition system. On the other hand, diameter fluctuations having a wide range of spatial frequencies can be introduced during fibre-drawing[16]. This explanation was confirmed in a separate study[15] in which controlled diameter variations were deliberately induced during the fibre pulling.

A further consequence of the difference in the results measured from each end is that the attenuation of the scattered light is different from that of the forward-travelling pulse, although it is not possible to differentiate between the attenuation suffered by light propagating in the two directions. It is likely, however, that the backscattered light should be most sensitive to fluctuations in the fibre properties, since it is expected to excite the fibre more fully than the forward-travelling light. For example, a slight decrease in diameter from end A to end B may not affect significantly the loss of low-order modes in the direction A to B. On the other hand, the taper will convert backscattered power from high-order modes (and cladding modes) to low-order modes and may lead to a larger signal at the detector. Hence, although the power detected in a backscatter experiment has travelled along the fibre in both directions, the measured values of attenuation can be, and indeed, have been observed to be different when the fibre is reversed.

6.4.2 Length-dependence of OH^- Impurity Absorption

A graded-index fibre, having a GeO_2 - P_2O_5 - SiO_2 core and a numerical aperture of 0.20, was fabricated with a relatively thin B_2O_3/SiO_2 buffer layer in order to ensure significant absorption by OH^- ions which diffuse into the core from the substrate tube. The fibre was scanned at 25m intervals along its entire 1.5km length using a gate separation of 480ns. A mode scrambler at the launching end of the fibre simulated an equilibrium mode distribution.

Figure 6.12 shows the results of backscatter attenuation measurements made at wavelengths of 0.906, 0.946 and 1.006μm for the case of a pulse launched into the fibre end designated A. Similar

measurements were also made in the reverse direction, i.e. from end B, but for clarity only the curve for 0.946μm is shown since the other two were not significantly different from those obtained from end A.

The fibre attenuation at 0.906 and 1.006μm is reasonably independent of position. The small fluctuations, similar to those discussed earlier, are attributable to minor variations in diameter, numerical aperture or scattering coefficient. The height of the OH^- absorption peak at 0.946μm, however, shows a marked variation with length, indicating a reduction of OH^- concentration along the length from end A to end B. In confirmation the measurements from both ends of the fibre are in good agreement, except close to the launching end. The latter effect is not significant at the other wavelengths and can be attributed to differential mode attenuation, presumably caused by the diffusion profile of the absorbing OH^- ions which exists across the fibre core.

Possible causes of the variation in OH^- content along the fibre are the tapering of the deposited layer thickness which occurs at the beginning of each CVD pass with a consequent reduction in buffer layer thickness, or a possible temperature overshoot following burner flyback resulting in increased diffusion. Stereoscan studies, however, show no variation of buffer layer thickness, or core diameter, along the 1.5km section. The origin of the length-dependence of OH^- ion concentration thus remains obscure.

6.4.3 Spectral Attenuation Measurement using the Backscatter Technique

The spectral attenuation of optical fibres is most commonly measured using the cut-back method in which the output from a white-light source is filtered to a narrow spectral range (using an interference filter or a monochromator) and launched into the fibre. The output power is recorded over a range of wavelengths, the fibre then cut back to a length of a few metres and the measurement is repeated.

The ratio of the values obtained at each wavelength gives the attenuation of the section of fibre which has been removed. The method is well-established and gives accurate and reliable results provided that care is taken, particularly with regard to the launching conditions.

If values of attenuation given by backscatter measurements are to be trusted, it is important to demonstrate that they agree at all wavelengths of interest with the cut-back results. The dye-laser system provides an almost unique possibility of comparing the two methods. Furthermore, the sampling gates in the two-channel technique can be positioned across that section of fibre which is removed during the cut-back measurement; losses are thus compared on rigorously identical samples.

In order to compare the techniques under similar conditions only the last kilometre of a 1.5 km section of fibre (already described in 6.4.2) was measured. In this way, the first 500m of fibre gives a near-equilibrium distribution in the 1km section under inspection. A mode scrambler was used in the backscatter measurement and the linear gates were sited at times corresponding to 500m and 1500m from the launching end. For the cut-back measurement, light from a tungsten lamp was focused with a numerical aperture of 0.25 into the fibre (which is thus fully excited) and the output from 1500m compared with that obtained after cutting back to 500m.

The results are compared in figure 6.13 over the wavelength range 0.82 - 1.07 μm. It can be seen that the two techniques give very similar results, the difference between the curves being within experimental uncertainty at all wavelengths. Thus, for the present fibre at least, the two methods give equally valid results.

Any variation of the scattering loss with distance would result in a wavelength-dependent discrepancy between the two

measurements. Such a discrepancy might well be fortuitously concealed in a comparison made at a single wavelength. Thus, in spite of the large longitudinal variation of water content (see sub-section 6.4.2), the present, fairly typical, fibre has sufficient uniformity to give reliable backscatter attenuation measurements over a wide spectral range.

6.5 SUMMARY

A new, two-channel, sampling scheme has been developed for backscatter attenuation measurements. It eliminates errors caused by pulse amplitude fluctuations and allows great flexibility in the design and use of backscatter instruments. It has been shown that an optimum sampling-gate separation exists which minimises the measurement accuracy required to achieve a given precision in the estimate of attenuation. The range which can be achieved by an instrument employing the two-channel technique is estimated on the basis of components which are presently available.

The two-channel technique has been implemented of the dye-laser/OPO system for use over a range of wavelengths. Good agreement between cut back and backscatter measurements of spectral attenuation has been demonstrated. The backscatter technique has also been used to study the length-dependence of attenuation and OH^- ion concentration in multimode optical fibres.

REFERENCES TO CHAPTER 6

1 F.P. KAPRON, R.D. MAURER and M.P. TETER: 'Theory of backscattering effects in waveguides.' *Appl. Opt.*, 1972, *11*, pp. 1352-1356.

2 M.K. BARNOSKI and S.M. JENSEN: 'Fiber-waveguides: a novel technique for investigating attenuation characteristics.' *Appl. Opt.*, 1976, *15*, pp.2112-2115.

3 S.D. PERSONICK: 'Photon probe - an optical-fibre time domain reflectometer.' *Bell Syst. Tech. J.*, 1977, *56*, pp. 355-367.

4 E.G. Neumann: 'Theory of the backscattering method for testing optical fiber cables.' To be published.

5 P. Di VITA and U. ROSSI: 'The backscattering technique: its field of applicability in fibre diagnostics and attenuation measurements.' *Opt. & Quantum Electron.*, 1980, *11*, pp. 17-22.

6 B.L. DANIELSON: 'An assessment of the backscatter technique as a means for estimating loss in optical waveguides.' National Bureau of Standards (U.S.A.). Technical note 1018.

7 A.J. CONDUIT, J.L. HULLETT, A.H. HARTOG and D.N. PAYNE: 'An optimised technique for backscatter attenuation measurements in optical fibres.' *Opt. & Quantum Electron.*, 1980, *12*, pp. 169-178.

8 M.K. BARNOSKI, M.D. ROURKE, S.M. JENSEN and R.T. MELVILLE: 'Optical time domain reflectometer.' *Appl. Opt.*, 1977, *16*, pp. 2375-2379.

9 D.L. FRANZEN, B.L. DANIELSON and G.W. DAY: 'A simple first positive Nitrogen Laser system for use in optical fiber measurements.' *IEEE J. of Quantum Electron.*, 1978, *QE-6*, pp. 402-404.

10 B. COSTA, C. de BERNARDI and B. SORDO: 'Investigation of scattering characteristics and accuracy of the backscattering technique by wavelength dependent measurements.' Proceedings 4th European Conference on Optical Communication, Genoa 1978, pp. 140-145.

11 B. COSTA, B. SORDO: 'Experimental study of optical fibres attenuation by a modified back-scattering technique.' Proceedings. 3rd European Conference on Optical Communication, Munich 1977, pp. 69-71.

12 A.J. CONDUIT, A.H. HARTOG and D.N. PAYNE: 'Spectral- and length-dependent losses in optical fibres investigated by a two channel backscatter technique.' *Electron. Lett.*, 1980, *16*, pp. 77-78.

13 P. MATTHYSSE and C.M. de BLOK: 'Measurement of splice insertion loss using the backscattering method.' Proceedings 5th European Conference on Optical communication, Amsterdam 1979, pp. 9.5.1-9.5.4.

14 A.J. CONDUIT: 'Aspects of optical fibre communications.' Minithesis, Dept. of Electronics, University of Southampton, April 1979.

15 A.J. CONDUIT, D.N. PAYNE and A.H. HARTOG: 'Optical fibre backscatter-loss signatures: identification of features and correlation with known defects using the two-channel technique.' Proceedings of the 6th European Conference on Optical Communication, York, 1980, pp. 152-155.

16 M.R. HADLEY, D.N. PAYNE and R.J. MANSFIELD: 'Identification of sources of diameter fluctuations in smooth optical fibres by analysis of their spatial power spectrum.' Proceedings of the 6th European Conference on Optical Communication, York, 1980, pp. 53-56.

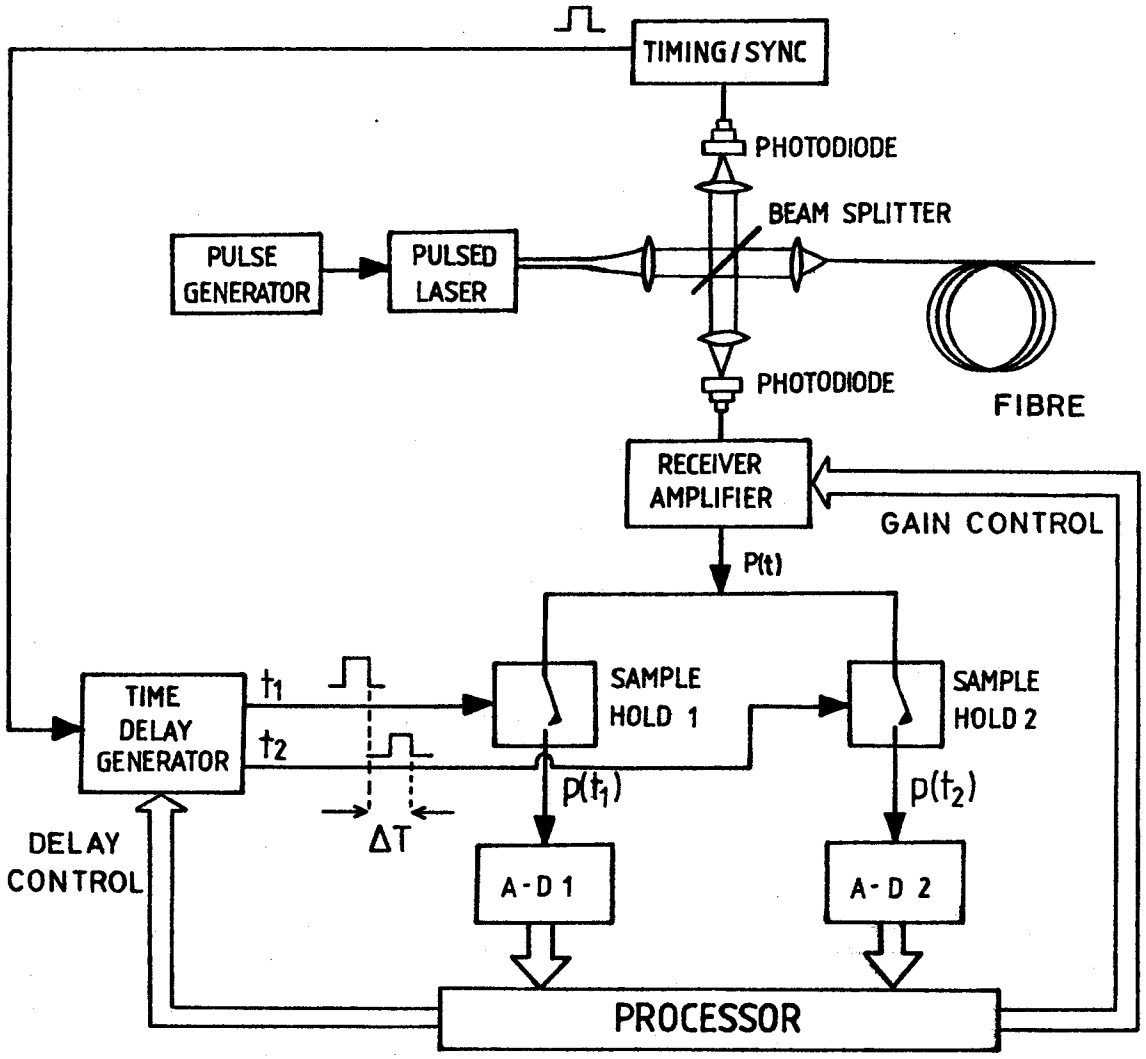

Figure 6.1 : Schematic diagram of a two-channel backscatter system.

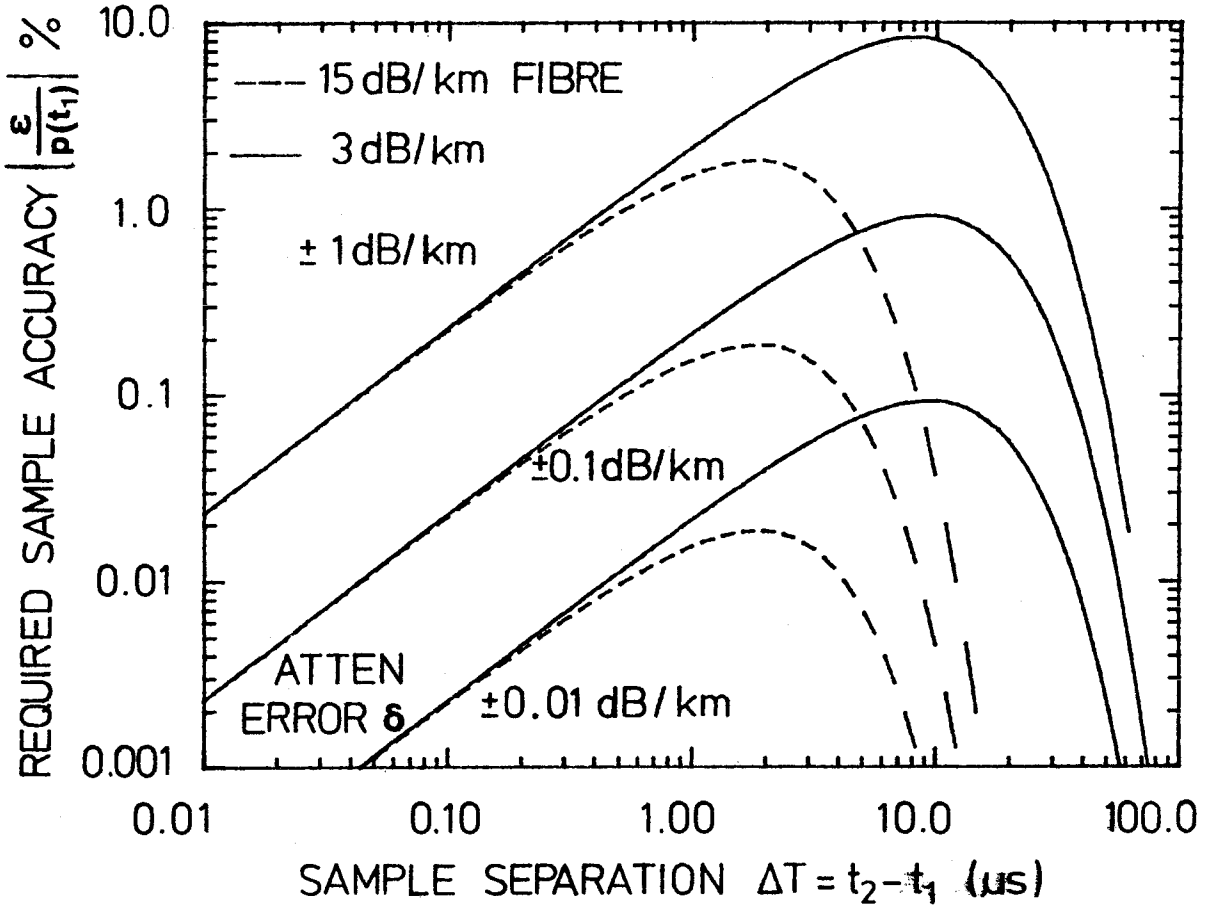

Figure 6.2 : Sample accuracy ε required to achieve an attenuation-measurement accuracy of 0.01, 0.1 and 1 dB km^{-1} as a function of sample separation. The sample accuracy is expressed as a percentage of the signal measured at sampling gate 1. Broken curves and solid lines are for fibres having losses of 15 db km^{-1} and 3 dB km^{-1}, respectively.

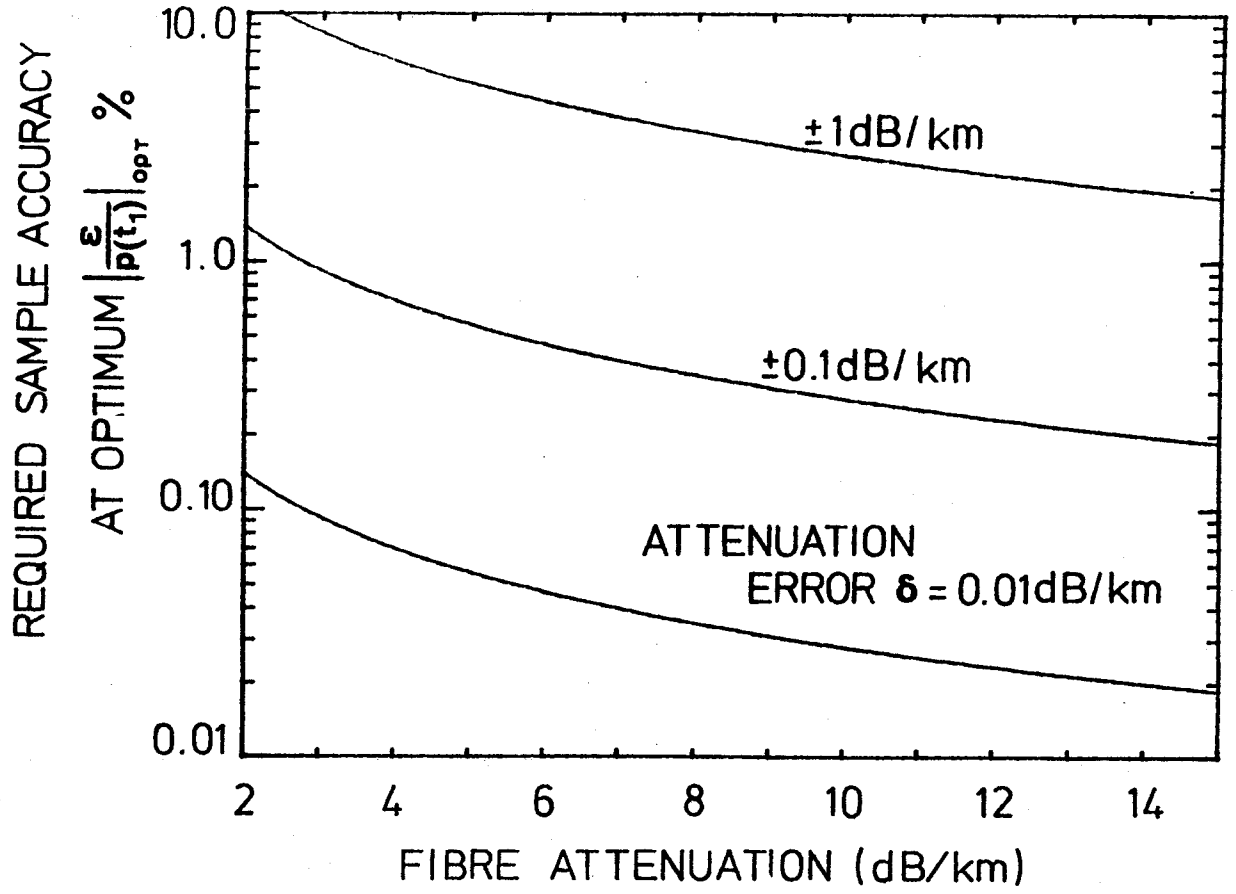

Figure 6.3 : Sampling accuracy (expressed as a percentage of the signal at gate 1) required at optimum sample separation ΔT_{opt} for attenuation measurement errors of ±0.01, 0.1 and 1 dB km^{-1}, plotted as a function of fibre attenuation.

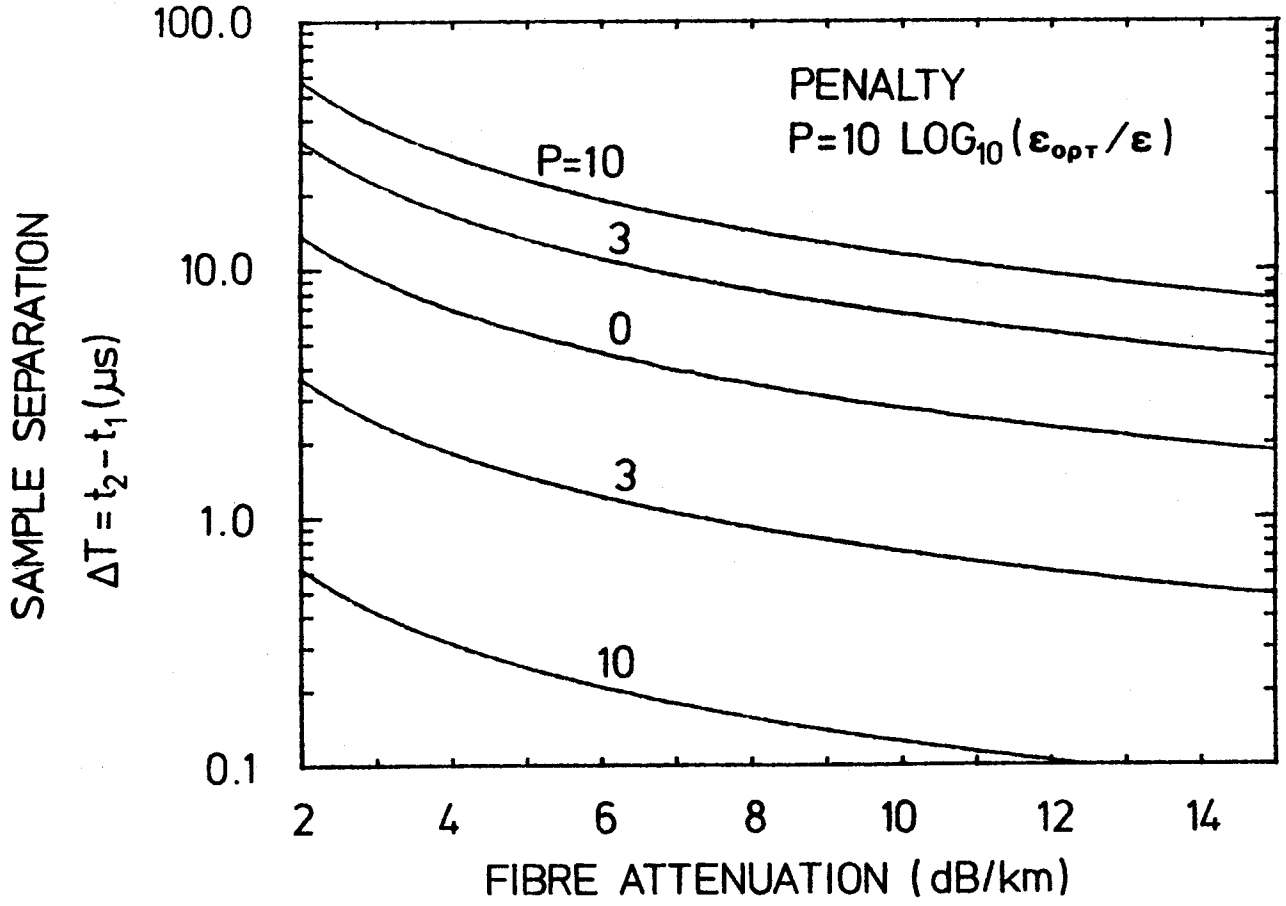

Figure 6.4 : Gate separations giving increased sampling accuracy requirement of 0, 3 and 10 dB (relative that needed at optimum spacing ΔT_{opt}) as a function of fibre attenuation.

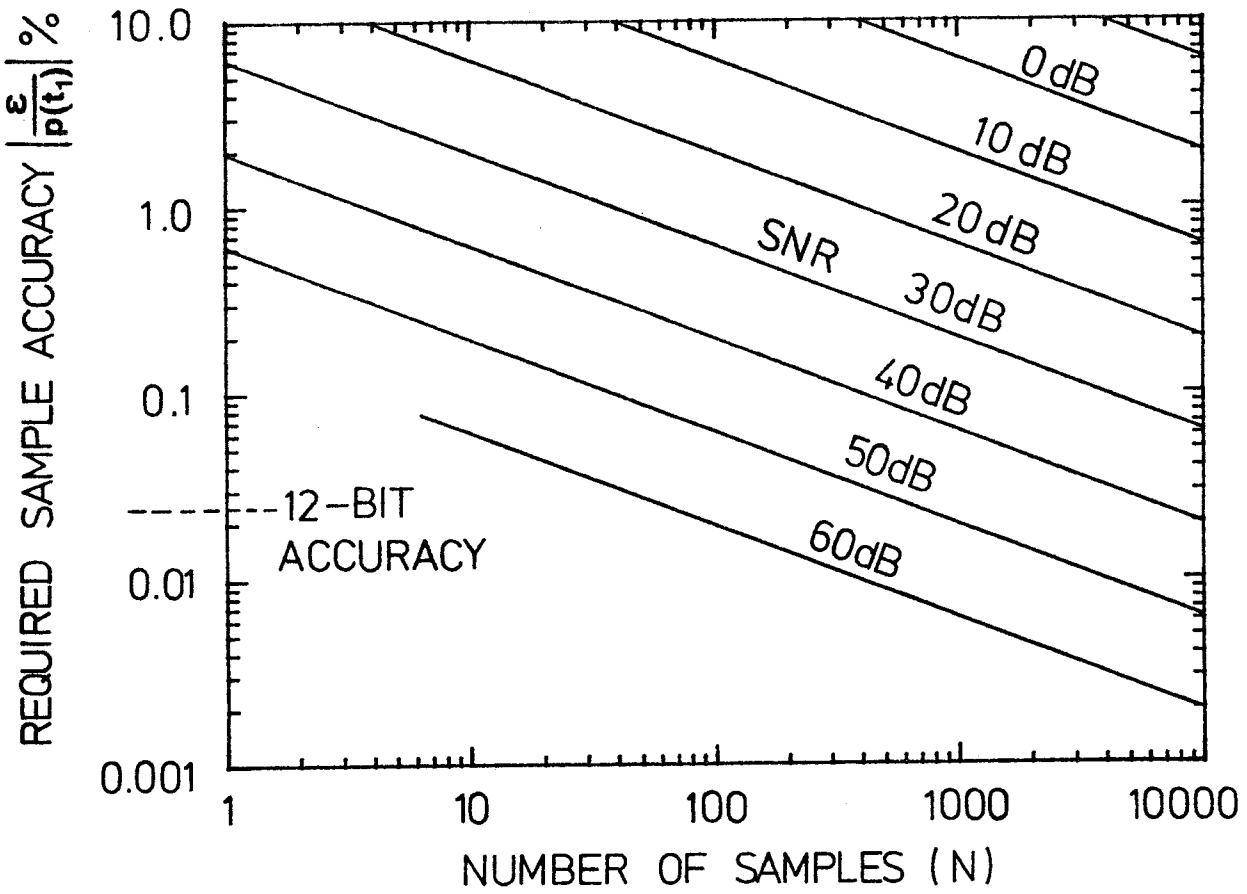

Figure 6.5 : Variation of ε (expressed as a percentage of the signal at gate 1) as a function of the number of samples for various signal-to-noise ratios before averaging. The broken line indicates the resolution of typical 12 bit A/D converters.

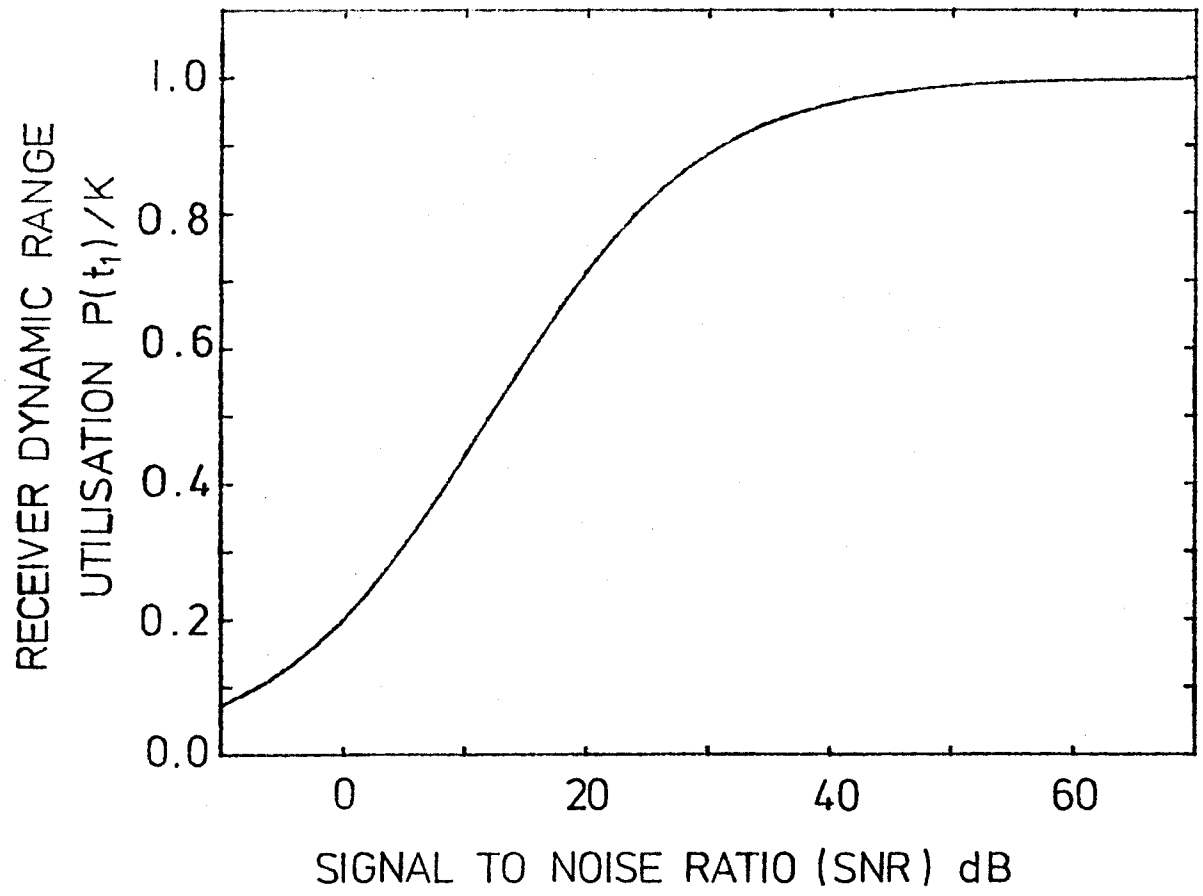

Figure 6.6 : Receiver range utilisation $p(t_1)/k$ as a function of signal-to-noise ratio. The proportion of the range which may be used must be reduced, if the SNR is low, to prevent a bias being introduced on the measured samples.

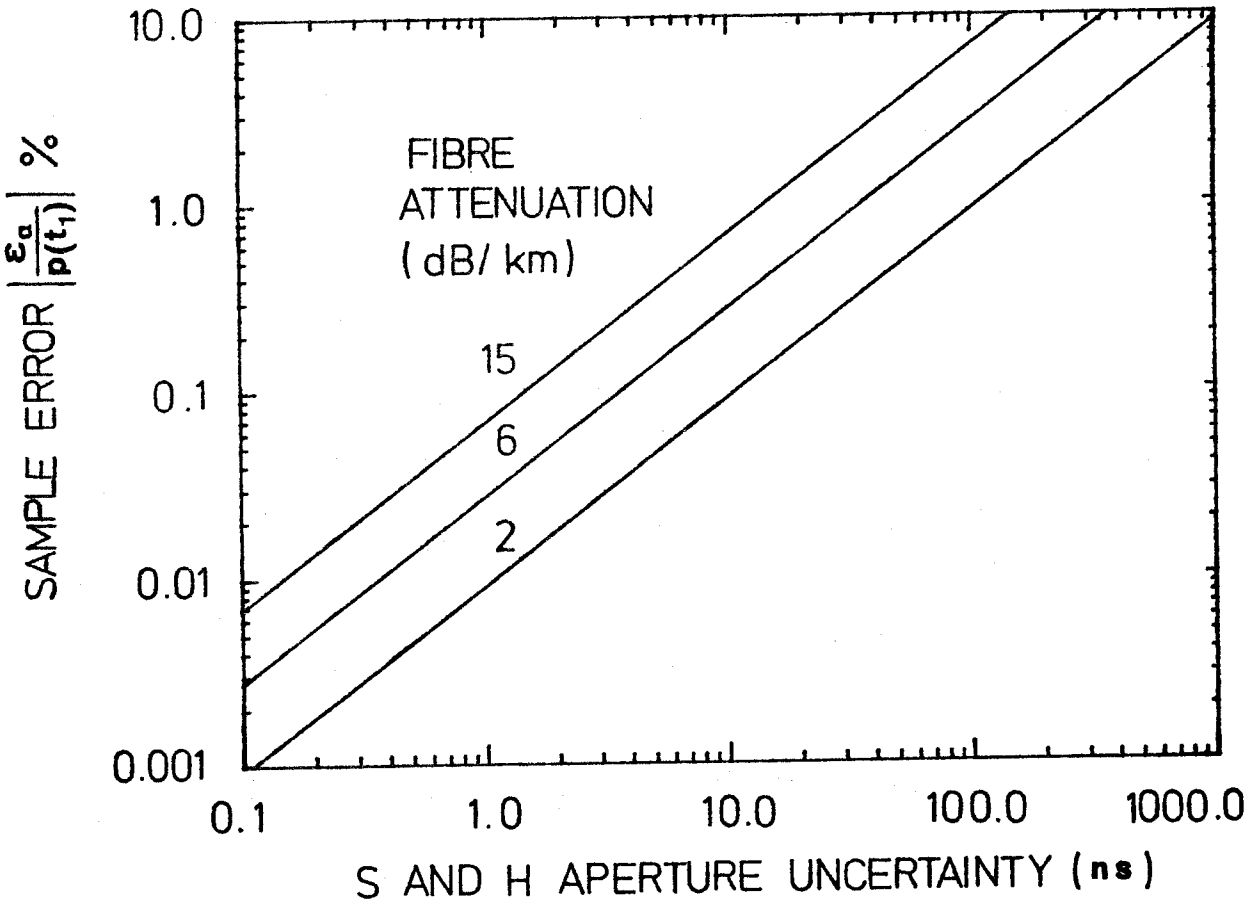

Figure 6.7 : Sample error ε_a (expressed as a percentage of $p(t_1)$) caused by jitter as a function of aperture timing uncertainty for fibre attenuations 2, 6 and 15 dB km^{-1}.

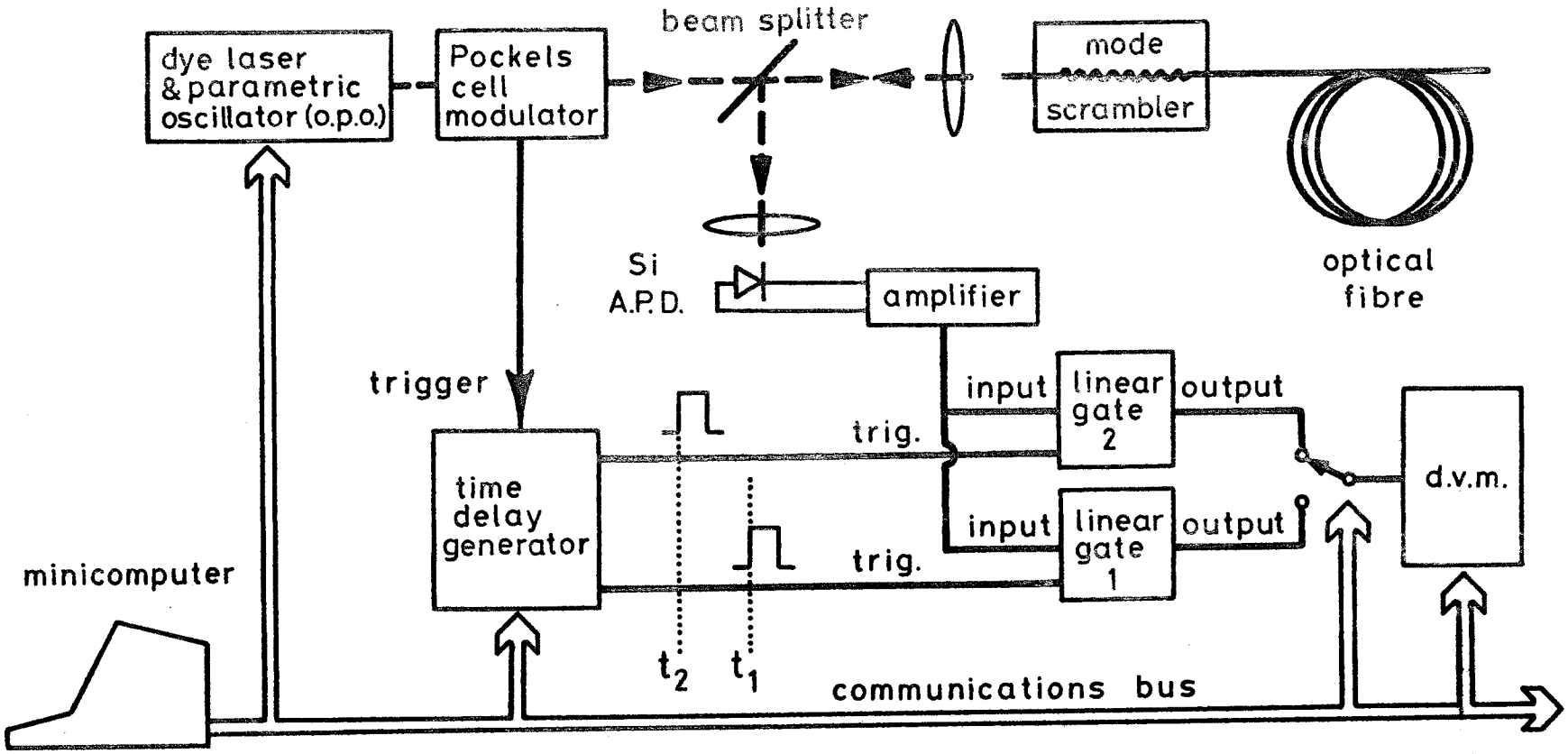

Figure 6.8 : Implementation of the two-channel backscatter technique on the dye-laser system.

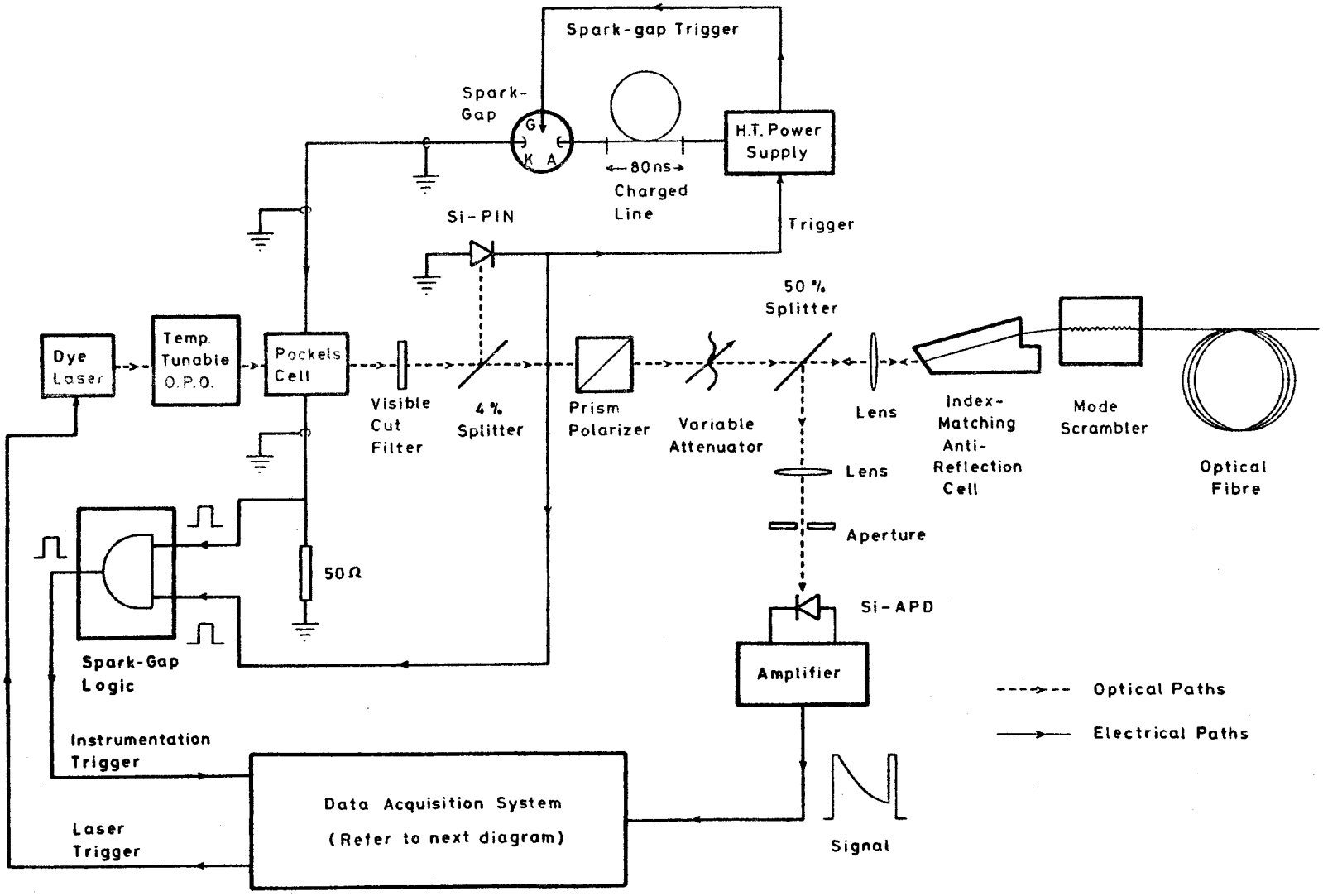

Figure 6.9 : Detailed optical arrangement of the dye-laser system for backscatter attenuation measurements.

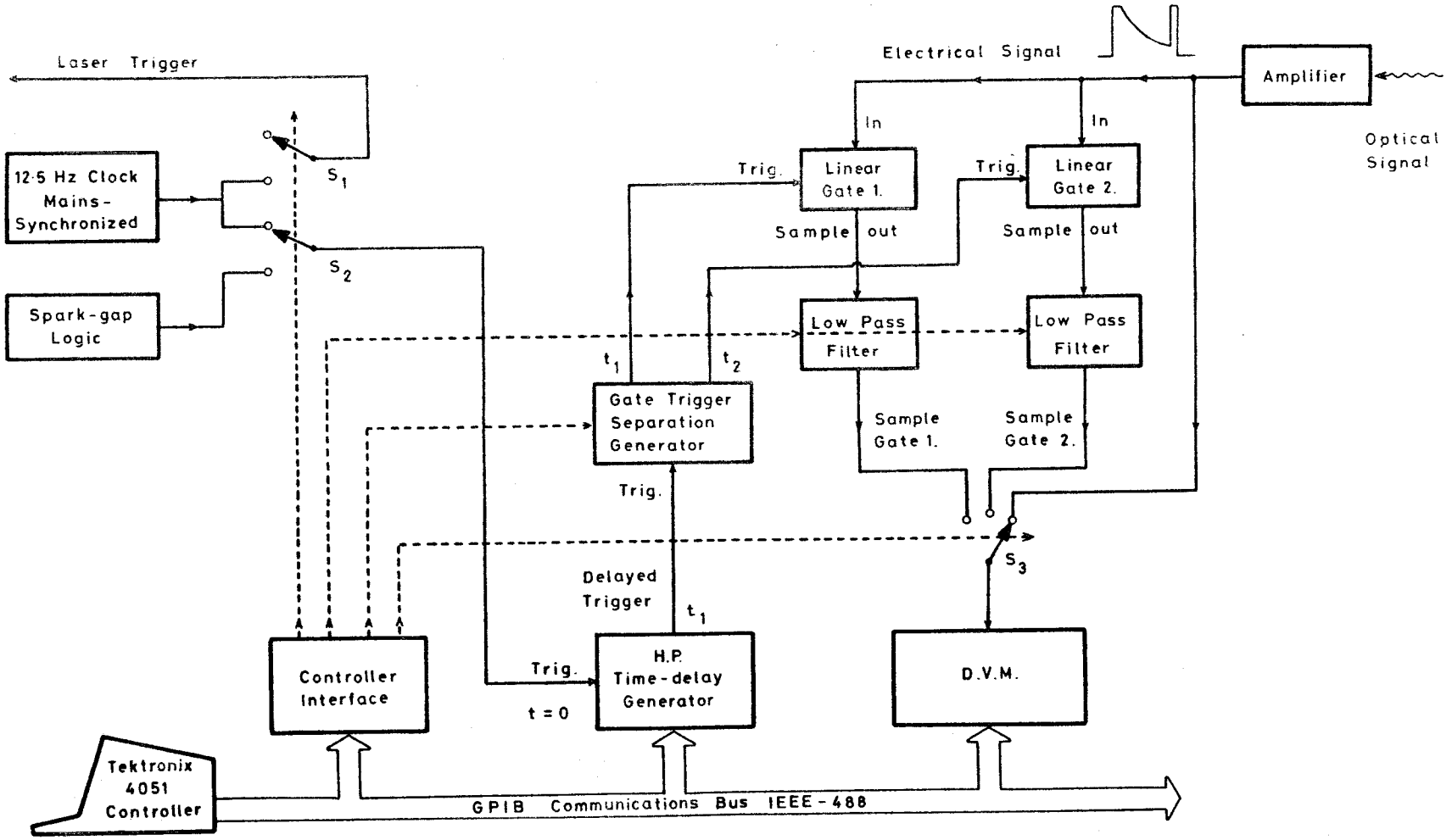

Figure 6.10 : Data acquisition system for two-channel backscatter attenuation measurements on the dye-laser system.

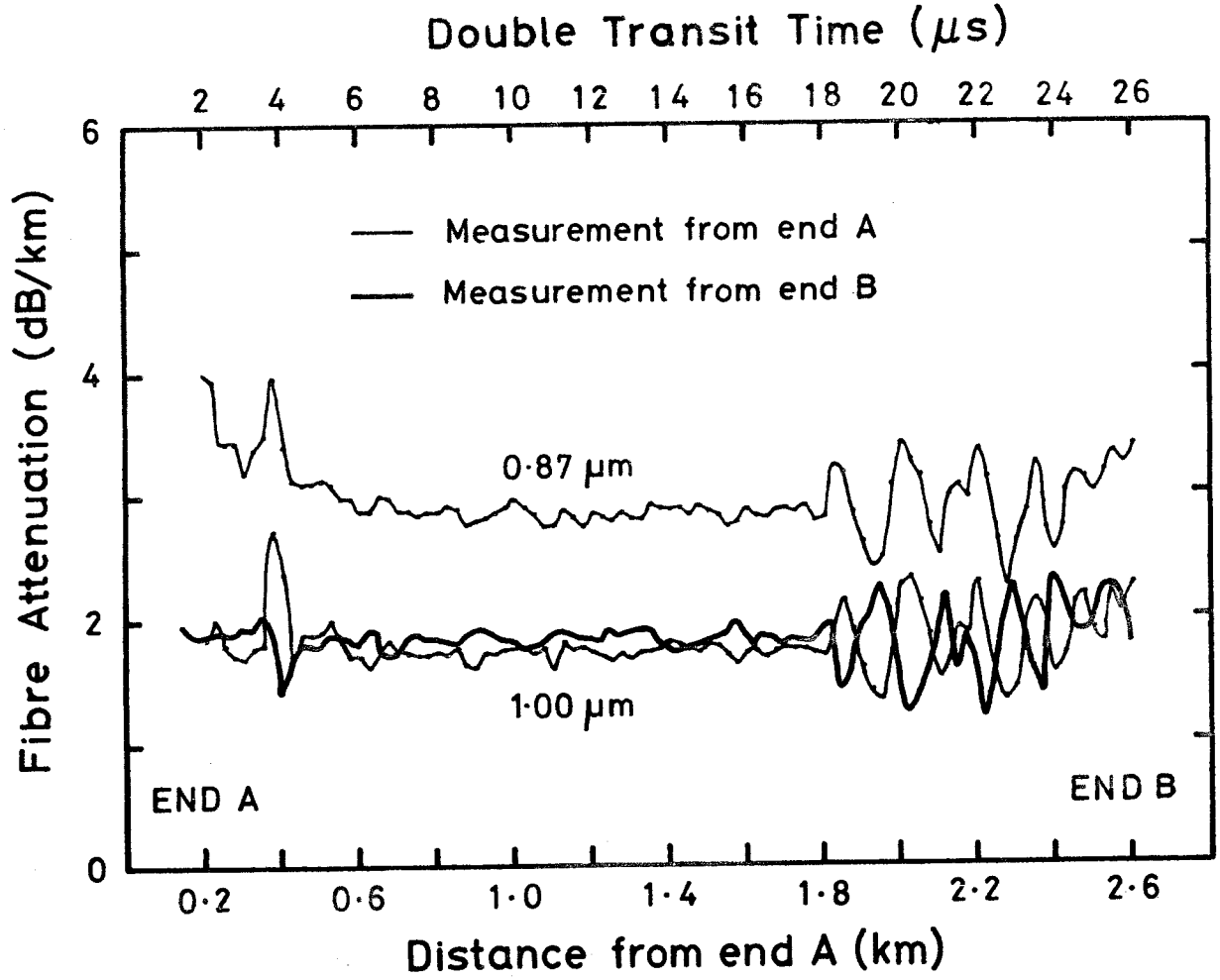

Figure 6.11 : Length-dependence of attenuation in fibre VD230L measured at the wavelengths 0.87 and 1.00μm. The light and heavy lines represent measurements made from ends A and B respectively.

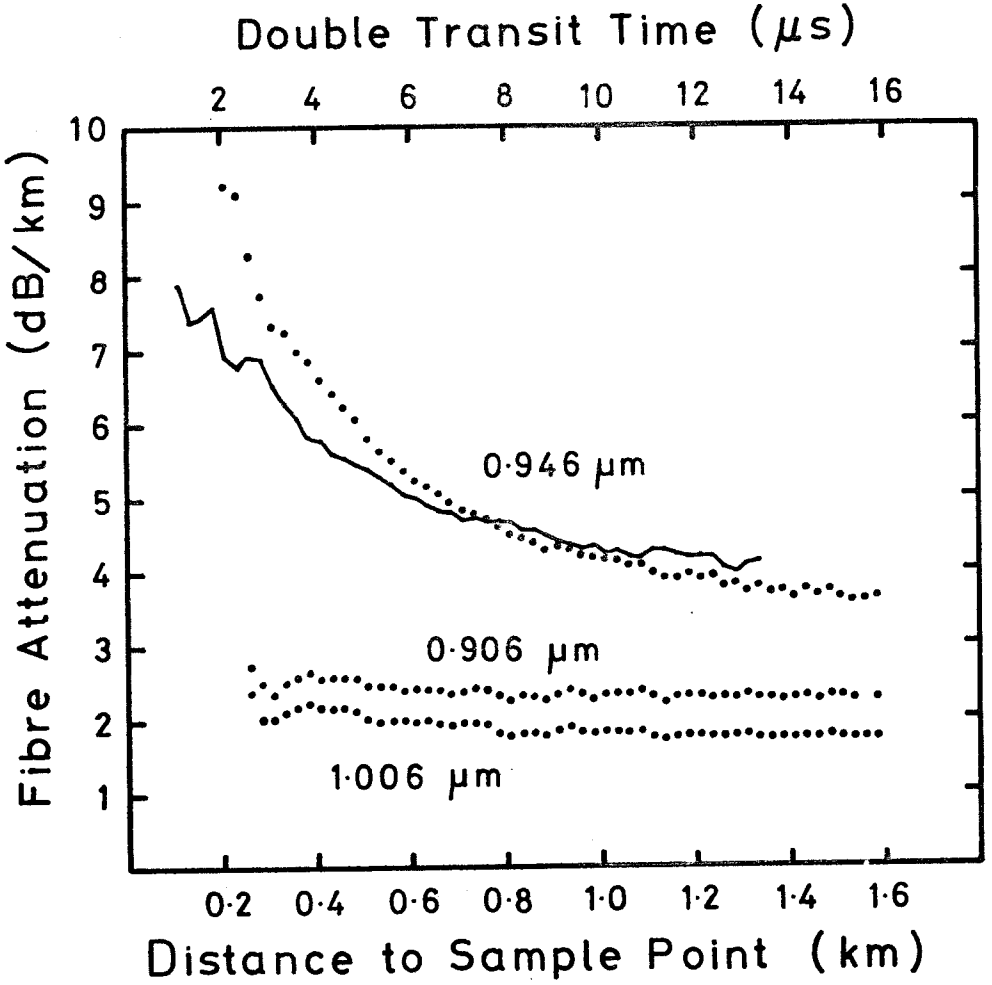

Figure 6.12 : Comparison of the length-dependence of attenuation measured at 0.906 μm, 0.946 μm and 1.006 μm in a graded-index germanophosilicate core fibre. Dotted curves refer to measurements from End A, the solid curve was measured from End B.

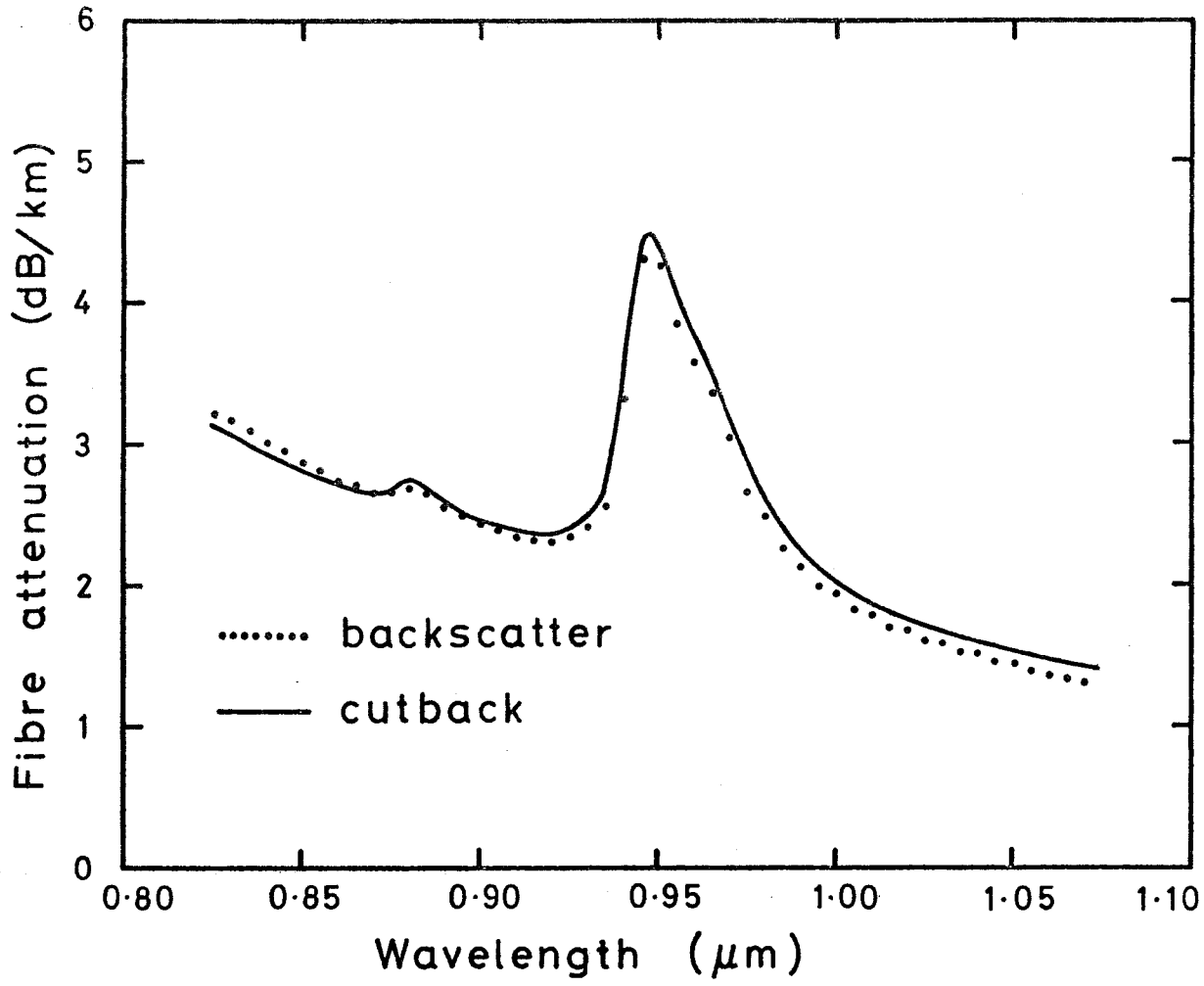

Figure 6.13 : Comparison of spectral attenuation measured using the backscatter and cut-back techniques on a graded-index germanophosphosilicate fibre.

CHAPTER 7 : CONCLUSIONS

A tunable source has been developed for the investigation of many wavelength-dependent propagation effects in optical fibre waveguides. This dye-laser/optical parametric oscillator system provides subnanosecond pulses of high power and almost monochromatic light at all wavelengths of interest for research into silica-based fibres.

With the aid of this source, the two major limitations on the bandwidth of multimode fibres, namely material dispersion and intermodal dispersion, have been investigated independently. It has also been demonstrated that the equipment and experimental techniques developed for the measurement of material dispersion can be used to determine, with a high degree of accuracy, the wavelength-dependence of chromatic dispersion in single-mode fibres. In addition, a new technique, based on similar measurements, has been proposed for assessing the level of stress applied by external forces to cabled fibres. Finally, the dye-laser system has allowed, for the first time, backscatter attenuation measurements to be made as a function of both positions in the fibre and wavelength of operation. The value of the backscatter technique as a diagnostic tool is thereby considerably enhanced.

7.1 LASER SYSTEM

The dye-laser/OPO system can be tuned over the wavelength range 0.4 - 2.6 μm and the peak power is at least 100W. The pulse-repetition rate may be varied up to 12.5 Hz and the pulse duration is approximately 1 μs. The linewidth can be maintained well below 1 nm throughout the wavelength range. Unfortunately the laser does not operate in the lowest-order transverse mode and the near-field contains several bright spots, the position and number of which can change in successive pulses. Similarly, the pulse amplitude can change by up to ±10% between successive pulses.

Short pulses, which are indispensable for most measurements on optical fibres are obtained from this source with an electro-optic modulator. A Germanium avalanche photodiode (which is sensitive to light at wavelengths shorter than about 1.9 μm) is used to detect the optical signals. The resulting waveforms are displayed on single-shot oscilloscope having a bandwidth of 500 MHz.

The performance of the dye-laser system is ideal in many respects. The main limitation to its value as a test source is insufficient time-resolution which is limited mainly by the bandwidth of the oscilloscope. A real-time oscilloscope with a 1GHz bandwidth and good sensitivity has become available commercially since the present work began and, with such an instrument, the time resolution would be limited by the speed of the detector and modulator. Again, recent developments have been made in the technology of high-speed modulators and of fast detectors for the 1.1 - 1.6 μm wavelength region. It is felt, however, that for radical improvements in bandwidth, a totally different system would have to be envisaged, based on a source which automatically produces ultra-short pulses, such as a synchronously-pumped down-converting device. A prime contender for this purpose is the colour-centre laser. Alternatively, synchronously-pumped optical parametric oscillators have been reported. It must be stressed that neither of these devices has yet been developed to the point where an equipment can be built and operated without difficulty. In addition, new detection methods, possibly based on auto-correlation techniques, would be required.

7.2 PULSE-DELAY MEASUREMENTS OF CHROMATIC DISPERSION

A pulse-delay technique has been developed for the measurement of material dispersion in optical fibres. The accuracy of the technique is very good and results covering a wide wavelength range have been obtained. Material dispersion has been investigated in a number of glass compositions as well as in fibres fabricated by various processes. Thus fibres with phosphosilicate, germano-silicate

and ternary germanophosphosilicate cores have been studied in order to assess the effect of the index-modifying additives on material dispersion. It has been shown, for example, that the addition of phosphoric oxide to silica has little effect on the material dispersion parameter which falls to zero at the wavelength of 1.272 μm. In contrast, the material dispersion parameter and the wavelenth of zero dispersion, in germanosilicate glasses increase with increasing concentration of additive. A similar effect has been observed in a ternary $GeO_2/P_2O_5/SiO_2$ glass. The wavelength of zero material dispersion therefore varies across the core of a graded-index, germanosilicate fibre. As a result, there is no wavelength where material dispersion vanishes, even to first order, in this type of fibre. The present results have, however, been used to show that an optimum operating wavelength exists, where intramodal broadening is primarily caused by second-order material dispersion.

A fibre with a silica core was also examined and the results show no significant differences with the material dispersion measured in bulk samples. It is concluded that the thermal history has little effect on the material dispersion parameter in optical fibres.

Finally a fibre with a $GeO_2/B_2O_3/SiO_2$ core and fibres made by the Phasil and Double Crucible processes have been studied. These fibres, together with those already mentioned, form a large sample of the glass compositions which are likely to be used as core materials in fibres for communications systems. For all compositions, the results indicate that material dispersion decreases as the operating wavelength is increased from the 0.8 - 0.9 μm region of emission of GaAs sources and falls to zero at some wavelength in the vicinity of 1.3 μm.

The accuracy of the measurement has been much improved since the work on phosphorus- and germanium-doped fibres was undertaken. Although these results are of sufficient precision for the design of systems using multimode fibres, more accurate and detailed measurements are desirable, and would have been performed had fibres been

available. Thus a more complete investigation of the dispersive properties of the P_2O_5/SiO_2 and GeO_2/SiO_2 systems is necessary. This would allow rules for the interpolation of results for various compositions to be established. A knowledge of the relationship between the numerical aperture (and hence, the core composition) and the material dispersion is of crucial importance in the design of single-mode fibres with specified dispersion characteristics. In addition, material dispersion is profoundly related to profile dispersion and it is important that measurements of these two quantities should give consistent results which, at present, is not the case.

The material dispersion of the $P_2O_5/GeO_2/SiO_2$, $GeO_2/B_2O_3/SiO_2$, $P_2O_5/GeO_2/B_2O_3/SiO_2$ and $P_2O_5/F/SiO_2$ multicomponent glass systems (which have great practical importance) is very poorly known. It is therefore necessary to investigate these glasses and establish the relationship between their composition and dispersion. Similarly the material dispersion of cladding glasses, for which very few measurements are available, is needed for the design of single-mode fibres. Although these materials cannot easily be investigated with the pulse-delay technique, a possible solution to use W fibres in which a lightly-doped core is surrounded by a heavily-doped cladding.

The measurement of chromatic dispersion in single mode fibres is also a natural extention of this work. High data rates and large repeater spacings are now envisaged for single-mode fibre systems and tight control of dispersion/wavelength characteristic of the fibres may be required, particularly for operation at 1.55 μm. Thus measurements of chromatic dispersion will be necessary, not only to assess the characteristics of the individual fibres, but also to correlate measured values of dispersion with calculations based on known dispersive properties of the materials and on measurements of the refractive-index profile. The results of such experiments should be of great assistance to the production of low-dispersion waveguides.

7.3 THE EFFECT OF STRESS AND TEMPERATURE ON PULSE DELAY

A series of experiments has been conducted in which multimode graded-index fibres were subjected to tensile stress and temperature cycling while the resulting change in transit-time was accurately monitored. The sensitivity of unjacketed germanophosphosilicate fibres to stress and temperature was found to be 53.7 ps km^{-1} MPa^{-1} and 35.7 ps km^{-1} k^{-1}, respectively. These values must be taken into account in those applications of optical fibres where extremely good delay-stability (e.g. in fibre delay-lines) is required.

Plastic jacketing materials are found to degrade considerably the temperature stability of optical fibres owing to the stress which develops during thermal expansion and contraction. It is possible to estimate the stress applied by a secondary jacket to an optical fibre by observing the change in pulse delay which occurs during the extrusion process. The stress applied by the coating can be obtained at any subsequent time by a simple pulse transit time measurement. Thus the variation of the stress applied to a fibre jacketed with Nylon 6 was monitored while the fibre was temperature-cycled in air, water and an aqueous solution of sea salt. These tests demonstrate both the ability of the pulse-delay technique to detect small changes in stress and the sensitivity of Nylon 6 to harsh surroundings. Pulse delay measurements thus provide an excellent means of assessing the suitability of particular coating materials to specific environmental conditions.

7.4 INTERMODAL DISPERSION

The intermodal dispersion of a series of high bandwidth fibres was measured over a wide wavelength range. A knowledge of the bandwidth/wavelength characteristics of these fibres allows the influence of profile dispersion and of profile errors on the dispersion to be distinguished. The measured values of bandwidth have been compared with calculations based on the refractive index distributions and the profile dispersion of the fibres.

The study reveals the considerable effect on the bandwidth of local deviations of the profile from the optimum. This fine structure of the profiles limits the maximum value of bandwidth to approximately 1.2 GHz in each of the fibres studied. In addition, the departure from circular symmetry and the length dependence of the profile are shown to affect severely the predictions of bandwidth, since a single profile measurement does not normally give a representative estimate of the index distribution along the whole fibre. Good agreement between theory and experiment was obtained, however for one fibre where profile measurements made at both ends of the fibre and along orthogonal diameters were available. In order to obtain accurate predictions of bandwidth from the refractive-index profile, it is clear that extremely detailed measurements of the index distribution are required.

7.5 ATTENUATION MEASUREMENTS BY THE BACKSCATTER TECHNIQUE

Wavelength-dependent measurements of attenuation by the back-scatter technique have been performed using a new experimental arrangement in which two samples are acquired from each return. The ratio of the light intensities thus measured gives directly the attentuation of the section of the fibre corresponding to the difference in the sampling times. The method automatically provides source-compensation for any fluctuations in pulse amplitude or for drift in the instrumentation. In addition, the technique is extremely flexible since the sampling-gate separation may be altered so that the most suitable compromise between distance resolution and accuracy in attenuation is reached. It is shown that there exists an optimum gate separation which maximises the allowable insertion loss from the source to the section of fibre under test. It is estimated that typical backscatter equipment using the two-channel technique could measure local attenuation to within 0.1 dB km^{-1} at a distance corresponding to a fibre loss of 26 dB.

The insensitivity of the technique to pulse amplitude fluctu-ations is demonstrated by measurements on the dye-laser system during

which a reproducibility of about 0.03 dB km^{-1} was achieved in 50m sections of fibre. These experiments were the first backscatter measurements to be made using a tunable source and the excellent agreement observed with the usual cut-back attenuation measurements has gone some way towards establishing the validity of the backscatter technique. The value of spectral backscatter loss measurements was further demonstrated in an experiment where the OH^- ion impurity absorption was measured as a function of position and was shown to vary substantially along the length of a fibre.

The backscatter method has proved to be an extremely useful means of determining the length-dependence of attenuation. It is hoped that with further development of the technique, and possibly with the aid of tunable sources, it will be possible to identify the exact nature of localised defects and relate them to their causes in the manufacture or handling of the fibre. Some questions do remain, however, as to the validity of the method, owing to the possibility of variations of the proportion of the forward-travelling power which is scattered and captured by the fibre. Further work is thus needed to clarify this point and allow a greater use to be made of the backscatter technique in a wide range of applications.

7.6 CLOSING REMARKS

When the work which has been described in this thesis began, the only fibre measurement commonly performed as a function of wavelength was that of attenuation. A large number of research laboratories are now equipped to measure over a wide wavelength range most parameters of importance to the performance of the fibres. Thus it is recognised that, although a number of parameters need only be measured at the operating wavelength, the knowledge of their wavelength-dependence often allows a much deeper understanding of the underlying reasons for the behaviour of the fibre. Wavelength-dependent measurements of loss, pulse dispersion and pulse delay are particularly important to the improvement of the transmission properties of optical fibres and the achievement of lower losses and

dispersion. In addition, since fibres are now being developed to operate over a wide spectral range, tunable or multiple-wavelength sources will in future be found in the test equipment used for quality-assurance.

It is hoped that the work presented here will be of some assistance to the progress of optical communications, either by the provision of new data concerning the properties of waveguide materials, or by the development of measurement techniques and the interpretation of the propagation effects which were observed.

CHAPTER 8 - APPENDIX: PUBLICATIONS, CONFERENCE PRESENTATIONS AND PRIZES

The work described in the thesis has led to the following publications, which are listed in order of submission. Conference presentations and prizes are listed separately.

8.1 PUBLICATIONS

[1] D.N. PAYNE and A.H. HARTOG: 'Determination of the wavelength of zero material dispersion in optical fibres by pulse-delay measurements'. *Electronics Letters* 1977, *13*, pp. 627-629.

[2] D.N. PAYNE and A.H. HARTOG: 'Pulse delay measurement of the zero wavelengths of material dispersion in optical fibres' n.t.z., 1978, *31* (2), pp. 130-132.

[3] M.J. ADAMS, D.N. PAYNE, F.M.E. SLADEN and A.H. HARTOG: 'Optimum operating wavelength for chromatic equalisation in multimode optical fibres'. *Electronics Letters* 1978, *14*, pp. 64-66.

[4] M.J. ADAMS, D.N. PAYNE, F.M.E. SLADEN and A.H. HARTOG: 'Wavelength-dispersive properties of glasses for optical fibres: The Germania Enigma'. *Electronics Letters* 1978,*14*, pp. 703-705.

[5] A.H. HARTOG, A.J. CONDUIT and D.N. PAYNE: 'Variation of pulse delay with stress and temperature in jacketed and unjacketed optical fibres'. *Optical and Quantum Electronics* 1979, *11*, pp. 265-273.

[6] A.H. HARTOG: 'Influence of waveguide effects on pulse-delay measurements of material dispersion in optical fibres'. *Electronics Letters* 1979, *15*, pp.632-634.

[7] A.J. CONDUIT, J.L. HULLETT, A.H. HARTOG and D.N. PAYNE: 'An optimised technique for backscatter attenuation measurements in optical fibres'. *Optical and Quantum Electronics* 1980, *12*, pp. 169-178.

[8] A.J. CONDUIT, A.H. HARTOG and D.N. PAYNE: 'Spectral- and length-dependent losses in optical fibres investigated by a two-channel backscatter technique'. *Electronics Letters* 1980, *16*, pp.77-78.

9 A.H. HARTOG, D.N. PAYNE and A.J. CONDUIT: 'Polarisation measurements on monomode fibres using optical time-domain reflectometry'. *I.E.E. Proceedings, Part H: Microwaves, Optics and Antennas* 1981 (to be published).

10 W.A. GAMBLING, A.H. HARTOG and C.M. RAGDALE: 'Optical fibre transmission lines'. *Proceedings I.E.R.E.* 1981 (to be published).

11 A.J. CONDUIT, D.N. PAYNE, A.H. HARTOG and M.P. GOLD: 'Optical fibre diameter vairations and their effect on backscatter loss measurements'. *Electronics Letters* 1981, *17*, pp. 307-308.

12 A.H. HARTOG, M.J. ADAMS, F.M.E. SLADEN, D.N. PAYNE and A. ANKIEWICZ: 'Comparison of measured and predicted bandwidth of graded-index multimode fibres'. Submitted to *I.E.E.E. Journal of Quantum Electronics.*

8.2 CONFERENCE PRESENTATIONS

1 M.J. ADAMS, D.N. PAYNE, F.M.E. SLADEN and A.H. HARTOG: 'Resolution limit of the near-field scanning technique'. *3rd European Conference on Optical Communication*, Munich, September, 1977.

2 D.N. PAYNE and A.H. HARTOG: 'Determination of the zero wavelength of material dispersion in optical fibres by pulse-delay measurements'. *3rd European Conference on Optical Communication* (post deadline session), Munich, September, 1977.

3 M. EVE, A.H. HARTOG, R. KASHYAP and D.N. PAYNE: 'Wavelength dependence of light propagation in long fibre links'. *4th European Conference on Optical Communication*, Genoa, September, 1978.

4 A.J. CONDUIT, A.H. HARTOG and D.N. PAYNE: 'Measurement of longitudinal stress in cabled fibres'. *I.E.E. Colloquium on Measurements in Optical Fibres*, London, May, 1979.

5 A.J. CONDUIT, A.H. HARTOG and D.N. PAYNE: 'Residual stress diagnosis in jacketed optical fibres by a pulse delay technique'. *5th European Conference on Optical Communication*, Amsterdam, September, 1979.

6 A.J. CONDUIT, D.N. PAYNE and A.H. HARTOG: 'Optical fibre back-scatter-loss signature: Identification of features and correlation with known defects using the two-channel technique' *6th European Conference on Optical Communication*, York, September, 1980.

7 A.H. HARTOG, D.N. PAYNE and A.J. CONDUIT: Polarisation optical time-domain reflectometry: Experimental results and application to loss and birefringence measurements in single-mode optical fibres'. *6th European Conference on Optical Communication* (post-deadline session), York, September, 1980.

8 A.J. CONDUIT, D.N. PAYNE and A.H. HARTOG: 'Fibre diameter variations and their effect on backscatter loss measurements'. *Third International Conference on Integrated Optics and Optical Fiber Communication*, San Francisco, April, 1981.

8.3 PRIZES

1 The author was awarded the 1979 John Logie Baird Travelling Scholarship by the Royal Television Society. The scholarship report, entitled 'Optical fibre waveguides'appeared in TELEVISION in May/June 1980.

2 The 1979 Electronics Letters Premium was awarded jointly to F.M.E. Sladen, M.J. Adams,D.N. Payne and myself by the Institution of Electrical Engineers.